12-23-2015

The Modulation of Non-steroidal Anti-inflammatory Toxicity as a Function of the Interplay between Uptake and Efflux Transporters

Renato J. Scialis
University of Connecticut, rsqh39@gmail.com

The Modulation of Non-steroidal Anti-inflammatory Toxicity as a Function of the Interplay between Uptake and Efflux Transporters

Renato J. Scialis, PhD

University of Connecticut, 2015

Diclofenac is a commonly used anti-inflammatory drug in the treatment of arthritis and pain. Although mechanisms of injury following diclofenac administration have been characterized, the roles that transporters have as modulators of exposure and toxicity remain unclear. To that end, *in vivo* transporter models were used to assess the toxicokinetics of diclofenac and its major metabolites. Whole body transporter knockout mice were administered diclofenac, and the dispositions of parent and metabolites were determined in bile, plasma, and liver. Diclofenac and its reactive acyl glucuronide were shown to be substrates for the efflux transporter Bcrp. Biliary excretion of diclofenac and its acyl glucuronide decreased in Bcrp knockout mice while only the plasma levels of the glucuronide increased compared to wild-type mice. Diclofenac acyl glucuronide was likewise determined to be a substrate for the basolateral efflux transporter Mrp3 evidenced by reduced plasma concentrations in Mrp3 knockout mice with no changes in biliary excretion. Toxic challenge by diclofenac resulted in increased intestinal injury in Mrp3 knockout mice compared to wild-types. *In vitro* assays revealed that human MRP3 also can transport diclofenac acyl glucuronide with apparent high affinity compared to human MRP2. The uptake of diclofenac acyl glucuronide was shown to be mediated by human OATPs in an *in vitro* system, specifically OATP2B1 exhibited concentration-dependent active uptake kinetics. As OATP2B1 and mouse Oatp2b1 are

expressed along the intestinal tract, the active uptake of the glucuronide metabolite may be contributory to the intestinal toxicity observed in animal models and human patients. Mechanistic studies indicated that diclofenac acyl glucuronide was able to induce oxidative stress through creation of reactive oxygen species and inhibition of superoxide dismutase. Furthermore, diclofenac acyl glucuronide was shown to be an inhibitor of both COX-1 and COX-2, which may also have contributed to intestinal injury. Lastly it was demonstrated that diclofenac acyl glucuronide can inhibit human MRP4 that is upregulated during oxidative stress. In summary, the data presented herein demonstrate the multifactorial pathways by which diclofenac acyl glucuronide is transported and contributes to tissue injury.

The Modulation of Non-steroidal Anti-inflammatory Toxicity as a Function of the Interplay between Uptake and Efflux Transporters

Renato J. Scialis

B.A., Hofstra University, 1996

A Dissertation

Submitted in Partial Fulfillment of the

Requirements for the Degree of

Doctor of Philosophy

at the

University of Connecticut

2015

APPROVAL PAGE

Doctor of Philosophy Dissertation

The Modulation of Non-steroidal Anti-inflammatory Toxicity as a Function of the Interplay between Uptake and Efflux Transporters

Presented by

Renato J. Scialis, B.A.

Major Advisor _____

Jose E. Manautou, Ph.D.

Associate Advisor _____

Xiao-bo Zhong, Ph.D.

Associate Advisor _____

Christopher L. Shaffer, Ph.D.

University of Connecticut

2015

DEDICATION

To my wonderful wife Ayako who gave me endless patience and support while I followed my dreams, and for my late father Renato G. Scialis who was so proud of all I accomplished.

ACKNOWLEDGEMENTS

First and foremost my extreme gratitude and eternal thanks go to my lovely wife Ayako and my two children, Nanako and Makoto. Without their love and encouragement, I could not have achieved this point in my life. They sacrificed much, yet they gave me much in return. All the hours toiled away in the lab or on the computer, either doing coursework or data analysis, I was able to do by drawing motivation from them. They made it all worthwhile, and I look forward to sharing in their successes as they have shared in mine. I love them dearly them. And to my parents, Mr. Renato and Emma Scialis, my in-laws, Mr. Gunji and Takako Kawamura, and my uncle Walter Pastore who shaped my past and gave so much support, I am truly thankful.

I am deeply grateful for having Dr. Jose Manautou as my advisor. When I explored doctoral graduate programs, Dr. Manautou was quick to reach out and bring me into his lab. I am amazed at his breadth of knowledge, and equally humbled by working under such a great person. His compassion, direction, and guidance were truly remarkable during this journey. I am honored to have studied under him, and thank him for helping me become a better scientist.

My research would not have been possible without the vital contribution of my collaborators. I am deeply appreciative for having worked with Dr. Ivan Csanaky who did much of the *in vivo* studies at the University of Kansas in Dr. Curtiss Klaassen's group. Dr. Csanaky's masterful surgeries made our disposition studies truly remarkable. I would like to thank Dr. Lauren Aleksunes who conducted the initial studies and gave critical feedback over the years. Dr. Mike Goedken, who provided valuable histopathology analysis, was also a key contributor to whom I owe immense gratitude.

I would like to thank my thesis committee members, both past and present. Dr. Chris Shaffer, who was my former supervisor at Pfizer, was unwavering in his support of me. Dr. Shaffer was instrumental in helping me overcome obstacles during my graduate studies, and I am in his debt. My thanks go to Dr. Xiao-bo Zhong who joined my thesis committee after the retirement of former member Dr. Urs Boelsterli. Dr. Zhong's feedback during seminars was engaging and insightful. And to Dr. Boelsterli who helped direct the research by offering his perspectives from his own diclofenac work, I am appreciative for his support and contribution to my work and investigative toxicology.

I would like to recognize the following graduate students, post-docs, and visiting scholars from the Pharm/Tox program: Dr. Sarah Campion, Ms. Meeghan O'Connor, Dr. Dan Ferreira, Dr. Xinsheng Gu, Mr. Phil Rohrer, Dr. Amy Bataille, Dr. Carolina Ghanem, and Mr. Kyle Saitta. My special thanks go to Dr. Swetha Rudraiah who endlessly helped me navigate the labs at UConn. I also thank Mr. Daniel Albaugh with whom I shared much coursework, laughs, and frustrations. His friendship was truly a blessing.

My thanks go to Mr. Jonathan Chupka and Ms. Shelly Mireles, my former colleagues at Pfizer, who both taught me much about cell culture and transporter studies that became critically important during my doctoral research. I also would like to thank my supervisor and managers at Pfizer, Dr. Chester Costales, Dr. Dave Rodrigues, and Dr. Larry Tremaine, for supporting my graduate studies while working full-time.

Lastly I would like to thank Ms. Ione Jackman and Ms. Denise Woodard from the UConn Histology group for their technical support. Ms. Woodard's expertise was crucial in getting the immunohistochemistry assay to yield such robust staining.

TABLE OF CONTENTS

LIST OF FIGURES

LIST OF TABLES

LIST OF ABBREVIATIONS

AA	arachidonic acid
ABCC	ATP-binding cassette transporter family C
ADR	adverse drug event
ALT	alanine aminotransferase
AMP	adenosine monophosphate
amu	atomic mass units
APAP	acetaminophen
APAP-CYS	acetaminophen cysteine
APAP-GLU	acetaminophen glucuronide
APAP-GSH	acetaminophen glutathione
APAP-NAC	acetaminophen *N*-acetylcysteine
APAP-SUL	acetaminophen sulfate
ATP	adenosine triphosphate
BCRP	breast cancer resistance protein
BUN	blood urea nitrogen
CAM	calcein acetomethoxy
CL_{int}	intrinsic uptake clearance
COX	cyclooxygenase
CYP	cytochrome P450
DCF	diclofenac
DCF-AG	diclofenac acyl glucuronide
DCFDA	5-(and-6)-carboxy-2′,7′-dichlorofluorescein diacetate
DMEM	Dulbecco’s modified Eagle’s medium
EDTA	ethylenediaminetetraacetic acid
EthD-1	ethidium homodimer 1
GI	gastrointestinal

GSH	glutathione
GST	glutathione S-transferase
HBSS	Hank’s balanced salt solution
HEK	human embryonic kidney
IA	intra-arterial
IL	interleukin
IP	intraperitoneal
IS	internal standard
K_m	substrate concentration at half the maximal velocity
KO	knockout
LC/MS/MS	liquid chromatography tandem mass spectrometry
LTC_4	leukotriene C4
MOPS	3-(N-morpholino)propanesulfonic acid
MRP	multidrug resistance-associated protein
m/z	mass to charge ratio
NADPH	β-Nicotinamide adenine dinucleotide 2'-phosphate
NAPQI	N-acetyl-*p*-benzoquinone imine
NSAID	non-steroidal anti-inflammatory drug
OATP	organic anion transporting polypeptide
OH-DCF	4′-hydroxy diclofenac
OH-DCF-AG	hydroxy diclofenac acyl glucuronide
P_{dif}	passive diffusion
PGE_2	prostaglandin E_2
PO	per os (oral)
RFU	relative fluorescence units
RT-PCR	reverse transcription polymerase chain reaction
SOD	superoxide dismutase

SNP	single nucleotide polymorphism
UDPGA	uridine 5'-diphosphoglucuronic acid
UGT	uridine 5′-diphospho-glucuronosyltransferase
V_{max}	maximal velocity
WT	wild-type

Chapter 1 REVIEW OF LITERATURE

1.1 Liver Overview

1.1.1 Structure and Function

The liver is the largest gland in the body and is responsible for a variety of important physiological functions. A depiction of the liver is shown in Figure 1.1. The human liver is divided into a right and left lobe, each of which is further organized into hepatic lobules with a hexagonal appearance. At the core of every lobule is a central vein. The corners of the lobule contain portal triads that are composed of a bile duct, hepatic artery, and a portal vein. About 60 to 70% of the blood supply to the liver originates from the portal vein while the remainder is provided by the hepatic artery (Richardson and Withrington, 1982). Blood coming from the portal veins can enter the sinusoids, which is an area that bathes the resident hepatic cells. Arterial blood is mixed with the partially deoxygenated portal blood in the sinusoidal space to provide oxygen. Sinusoidal blood traverses from the portal triad through the lobule and eventually collects into the central vein where it then gathers into the hepatic vein that ultimately drains into the inferior vena cava.

The lobule is divided into subregions referred to as centrilobular, midzonal, and periportal. In terms of functional units, the lobular regions are referred to as an acinus consisting of three zones wherein zone 1 is proximal to the portal triad, zone 2 is centrally located, and zone 3 is the area closest to the hepatic central vein. The periportal region (zone 1), being much closer to where oxygenated blood enters the sinusoids, is exposed to relatively high oxygen content. Oxygen levels continually decline through the midzonal (zone 2) and centrilobular (zone 3) regions. As a result,

the centrilobular zone is prone to hypoxia and injury due to low blood supply (Treinen-Moslen, 2001).

There are several cell types that can be found in the liver. Among the cells residing in the sinusoidal space are liver sinusoidal endothelial cells (LSEC) and Kupffer cells (KC). LSECs line the sinusoidal lumen and represent about 20% of the total liver cells (Maslak et al., 2015). They possess pores to permit the passing of material from the sinusoids into the space of Disse. KCs are the resident macrophages, making up over 80% of the total macrophages in the body. KCs play an integral role in the overall health of the liver as they are an important first line of defense against bacteria (Bilzer et al., 2006). Owing to their function as sentinels to hepatic well-being, the majority of KCs are found in the periportal region, which is the likely site of entry of microbes from portal blood circulation (Bouwens et al., 1986). KCs can be activated via microorganisms or hepatic injury with subsequent release of cytokines. Within the space of Disse are Ito cells (also known as stellate cells) that synthesize collagen and act as storage sites for vitamin A and fat (Stanciu et al., 2002).

The vast majority of hepatic cells are hepatocytes, which are the cells that carry out much of the metabolism in the liver. Hepatocytes take up about 80% of the total liver volume and constitute approximately 60% of all the liver cells (Malarkey et al., 2005). The liver is one of the primary sites for glycogen storage, which is converted to glucose during states of hypoglycemia. Hepatocytes carry out gluconeogenesis and are responsible for the synthesis of albumin, bile, and lipoproteins (Kutchai, 2004b). There is an estimated 139 million cells per gram of human liver yielding an approximate total

number of 217 billion hepatocytes in an adult liver (Sohlenius-Sternbeck, 2006; Molina and DiMaio, 2012).

1.1.2 Metabolic Enzymes and Transporters

Hepatocytes are metabolically active and possess the full array of enzymes that participate in Phase I (hydrolysis, reduction, and oxidation) as well as Phase II biotransformation (acylation, amino acid conjugation, glucuronidation, glutathione conjugation, methylation, and sulfation). Phase I metabolism occurs predominantly through cytochrome (CYP) P450 enzymes of which the main subtypes are CYP1A2, CYP2A6, CYP2B6, CYP2C8, CYP2C9, CYP2C19, CYP2D6, CYP2E1, and CYP3A4/5. In general the CYPs preferentially act upon the following substrates: 1) CYP1A2 – planar hydrophobic compounds with high logP that may be basic or neutral (e.g., phenacetin and theophylline), 2) CYP2C9 – acidic compounds or neutrals with high level of hydrogen bonding that have both hydrophobic and lipophilic regions (e.g., diclofenac and warfarin), 3) CYP2D6 – basic amines that are lipophilic and possess a nitrogen that is protonated at physiological pH (e.g., atomoxetine and dextromethorphan), 4) CYP2E1 – lipophilic compounds that are small with low logP (e.g., aniline and chlorzoxazone), and 5) CYP3A4 – basic or neutral compounds that are lipophilic (e.g., filodipine and midazolam) (Smith et al., 1998b; Lewis, 1999; Smith, 2003; Zhou et al., 2009; FDA, 2014).

Of the Phase II enzymes, uridine 5'-diphospho-glucuronosyltransferases (UGTs) have a significant role as an elimination mechanism for non-steroidal anti-inflammatory drugs (NSAIDs). There are three subfamilies, UGT1, UGT2A, and UGT2B with each subfamily consisting of multiple enzymes many of which are expressed in the liver

(Ohno and Nakajin, 2009; Harbourt et al., 2012). UGTs catalyze the transfer of uridine 5'-diphosphoglucuronic acid to a nucleophilic region of substrate thereby facilitating the biliary or urinary excretion of the conjugated metabolite (Coughtrie and Fisher, 2003). A review by Williams et al. (2004) indicated that of the top 200 marketed drugs that undergo glucuronidation, approximately 35% of the conjugation is mediated by UGT2B7 while UGT1A4 and UGT1A1 accounted for 20% and 15%, respectively (Williams et al., 2004). Glucuronidation does not always result in permanence of conjugation as glucuronides can be degraded back to an aglycone parent and glucuronate by the actions of β-glucuronidase (Sperker et al., 1997). UGTs can form an acyl glucuronide (R-COO-), ether glucuronide (R-O-), or nitrogen glucuronide (R-N-).

Returning to the structural layout of the hepatic lobule, work by Jungermann and Katz (1989) demonstrated that the periportal region (zone 1) was higher in glutathione (GSH) and lower in CYP abundance while the centrilobular region (zone 3) exhibited higher CYP levels along with lower intracellular glutathione. As glutathione has a critical role to sequester reactive intermediates, the reduced glutathione supply makes the centrilobular region more prone to certain types of injury. The gradient distribution of CYPs and GSH throughout the lobule renders a phenotypic pattern for which the periportal region is susceptible to injury from allyl alcohol and cocaine, from different mechanisms that involve generation of reactive metabolites (also higher oxygen levels may be contributory for oxygen-dependent reactions), while the centrilobular zone is sensitive to damage from carbon tetrachloride and acetaminophen as a result of depletion of GSH (Harisch and Meyer, 1985; Badr et al., 1986; Powell et al., 1994; Lim et al., 1995).

Of the aforementioned CYPs, CYP3A4 accounts for roughly 30% of total hepatic CYP content, yet CYP3A4 is responsible for nearly 50% of the overall metabolism that occurs in the liver (Shimada et al., 1994; Rodrigues, 1999; Williams et al., 2002). One of the reasons for the wide-ranging activity of CYP3A4 is due in part by a large binding pocket that can accommodate substrates of different sizes (Beaumont et al., 2010). Phase I metabolism by CYPs is dependent on β-Nicotinamide adenine dinucleotide 2'-phosphate (NADPH) to provide a source of electrons while Phase II reactions rely on cofactors that must be continually replenished. Generally, biotransformation is thought of as a detoxifying process that converts xenobiotics into more water-soluble forms that can subsequently excreted via biliary efflux or elimination in urine, however this is not always the case. Hepatocytes in the centrilobular region are responsible for metabolism of acetaminophen, making this region more susceptible to injury due to the generation of reactive intermediates such as NAPQI that are partially sequestered by GSH (Parkinson, 2001; Hinson et al., 2010).

The hepatocyte, which is essentially cuboidal in nature, is a polarized cell that is specifically oriented with respect to functionally active surfaces. The surface exposed to sinusoidal blood and the space of Disse is the basolateral membrane while the opposing side is the apical membrane. It is via the apical membrane that the hepatocyte excretes substances in the bile canaliculi which coalesce into bile ducts. The flow of bile in the lobule runs counter to that of sinusoidal blood flow, going from the centrilobular region toward the portal triad. The bile ducts merge into the common bile duct that terminates into the duodenal region of the small intestine. The basolateral membrane of hepatocytes has a number of transporters that facilitate the uptake of

substrates from sinusoidal space into the cell. Among the uptake transporters are equilibrative nucleoside transporters (ENTs, *SLC29*s), organic anion transporters (OATs, *SLC22A*s), organic anion transporting polypeptides (OATPs, *SLCO*s), organic cation transporters (OCTs, *SLC22A*s), and sodium-taurocholate co-transporting polypeptide (NTCP, *SLC10A1*) (Giacomini et al., 2010).

Also on the basolateral membrane are multidrug resistance-associated proteins (MRPs) that are efflux transporters from the ATP-binding cassette family C (*ABCC*s). A listing of the major uptake and efflux transporters along with their corresponding intra-family protein homologies is shown in Table 1.1. The bile canalicular membranes likewise host a number of efflux transporters belonging to several different transporter gene families (*ABCB*s, *ABCC*s, *ABCG*s, *SLC29*s, and *SLC47A*s). Many of the aforementioned uptake and efflux transporters are involved in the hepatobiliary disposition of endogenous substances as well as xenobiotics and their metabolites emphasizing the importance of understanding their roles in modulating the systemic exposure and elimination of compounds (Zamek-Gliszczynski et al., 2012). Physiologically, the interplay of uptake and efflux transporters is responsible for the recirculation of bile as 20% of the total bile pool is eliminated from the body on a daily basis (Heaton, 1969). The recirculation is primarily dependent upon NTCP (basolateral uptake) and BSEP (canalicular efflux) along with secondary uptake by the OATPs and basolateral as well as canalicular efflux by MRPs (Kullak-Ublick et al., 2000).

1.1.3 Gene Regulation

The expression of CYPs, UGTs, and transporters can be modulated via several mechanisms. CYP1A2 for instance is inducible via activation of the aryl hydrocarbon

receptor (AhR) (Nebert et al., 2004). Cigarette smoke has been shown to increase CYP1A2 expression via AhR, a result that may be causally linked to the increased tumorigenesis due to metabolism of procarcinogens present in cigarette smoke (Dertinger et al., 2001). Activation of the pregnane X receptor (PXR) leads to induction multiple genes such as CYP2C9, CYP3A4, and the efflux transporters MDR1 (*ABCB1*) as well as MRP2 (*ABCC2*). PXR belongs to a class of orphan nuclear receptors for which the endogenous substrate has yet to be identified. PXR has a ligand binding domain as well as a DNA-binding domain, enabling it to both recognize circulating substrates and bind to regulatory regions in target genes (Kliewer et al., 1998). After a ligand binds to PXR, the PXR-ligand complex enters the nucleus and forms a heterodimer with retinoid X receptor (RXR). The heterodimer is stabilized by additional cofactors allowing the complex to bind to response elements in the target genes and promote transcriptional upregulation. Shukla et al. (2011) reported that out of 2,816 clinically relevant compounds, 310 (11% of the total) were found to be activators of PXR. UGTs are regulated by a wide array of transcriptions factors such as AhR, constitutive androstane receptor (CAR), farnesoid X receptor (FXR), nuclear factor erythroid-related factor 2 (Nrf2), peroxisome proliferator-activated receptors (PPAR α & γ), PXR, and RXR (Hu et al., 2014).

Activation of PXR has physiological ramifications. For instance, elevation in bile salts stimulates PXR to modulate both CYP activity as well as transporter expression resulting in a reduction of toxic bile salts, which if left unchecked could induce cholestasis and ultimately lead to hepatic injury (Staudinger et al., 2001; He et al., 2011). Induction of the efflux transporter MRP3 (*ABCC3*) has been demonstrated to occur via

pathways involving CAR and PXR while MRP4 (*ABCC4*) is upregulated by activation of CAR (Cherrington et al., 2002; Teng et al., 2003; Zollner et al., 2006). The induction of MRP3 and MRP4 as a compensatory defense mechanism during cholestasis is indicative of the important role that basolateral efflux transporters have in attenuating cell injury (Claudel et al., 2011). Aleksunes et al. (2008b) reported induction of Mrp3 and Mrp4 in mice following toxic challenge by acetaminophen, and the induction was mediated through Nrf2. Further material on transporters will be detailed in subsequent sections.

1.2 Small Intestine Overview

1.2.1 Structure and Function

The small intestine is a contiguous structure, with an average length of 6.5 meters in adults (Hounnou et al., 2002). A representation of the small intestine structure is shown in Figure 1.2. The small intestine is functionally separated into three areas: duodenum, jejunum, and ileum. The duodenum represents the first part of the small intestine and is physically joined to the pyloric region of the stomach. The duodenum is the shortest region of the small intestine with a length of approximately 25 cm. The next portion of the small intestine is the jejunum, which is about 2.5 meters in length in adults. The ileum is the last section of the small intestine and accounts for the remaining length before the gastrointestinal tract transitions into the large intestine.

It is in the duodenum where gastric chyme is mixed with secretions from the liver, gall bladder, pancreas, and small intestine. Bile, which elmusifies lipids to permit absorption of fats, is released into the small intestine though the action of cholecystokinin, a hormone that stimulates the gall bladder to release bile through the common bile duct.

The duodenum neutralizes the acidic contents emanating from the stomach by secreting bicarbonate (Campbell, 1993). The jejunum also secretes digestive enzymes and moves luminal contents via peristaltic contractions to the ileum. The ileum is the segment where nutritional absorption is greatest. Bile acids are reabsorbed via active uptake in the ileum (Kutchai, 2004a). There is a pH gradient along the small intestine with a duodenal pH range of 6 to 6.6 while the terminal ileum pH is approximately 7.4 (Evans et al., 1988; Fallingborg, 1999).

The structure of the small intestine can be regarded as an elongated tube, and the cavity within the small intestine is referred to as the lumen. Taken as a whole, the small intestine has an absorptive surface area of 32 square meters (Helander and Fandriks, 2014). The effective surface area exceeds that of a standard cylinder due to the presence of plicae circulares, which are folds along the entirety of the small intestine. The plicae circulares are comprised of projections called villi, and each villus has a layer of enterocytes that are the absorptive cells of the intestinal tract. The enterocytes have microvilli that further increase surface area of the cells. Goblet cells are also present in the villi, though to a far less degree than enterocytes. The function of goblet cells is to secrete mucus. Within the villus is a network of blood capillaries and lymph vessels known as the lacteal. The capillaries take up amino acids and sugars while lipids are absorbed into the lacteal. The flow of nutrients into the intestinal capillaries is directed to the hepatic portal vein that eventually goes to the liver (Campbell, 1993). In addition to nutrients, the small intestine has a role in the absorption of critical electrolytes and buffers such as sodium, potassium, chloride, and bicarbonate.

1.2.2 Metabolic Enzymes and Transporters

Similar to the liver, the small intestine possesses both Phase I and Phase II metabolic enzymes (Prueksaritanont et al., 1996). In contrast to the liver for which CYP3A4 constitutes 30% of the total CYP content, the allotment of CYP3A4 makes up nearly 82% of all the CYPs expressed in the intestine with CYP2C9 accounting for 14% (Paine et al., 2006). Despite the relatively high expression of intestinal CYP3A, the absolute amount of CYP3A4 present in the small intestine is only 1% of the CYP3A amount in the liver (Yang et al., 2004). Nonetheless, the metabolic enzymes in the small intestine are able to modulate the overall bioavailability of substances. In pharmacokinetic terms, the extent of bioavailability after oral dosing is determined using the relationship:

Equation 1.1

$$F = F_a \times F_g \times F_h$$

where F is the oral bioavailability, F_a is the fraction of dose absorbed from the intestinal lumen, F_g is the fraction of dose escaping the intestine (gut), and F_h is the fraction of dose escaping the liver. The sedative agent midazolam is a compound that has high passive uptake and can easily enter enterocytes yielding an apparent F_a value of 1. Metabolism in the enterocytes diminishes the amount of midazolam presented to the intestinal capillaries due to activity of CYP3A4 (Paine et al., 1996) resulting in a F_g of 0.54. Furthermore, the loss of midazolam from intestinal metabolism was found to be comparable to the liver F_h value of 0.56 (Thummel et al., 1996). Thus the oral bioavailability of midazolam is about 30% given that F = 1 × 0.54 × 0.56 = 0.30, and this value was also observed by other researchers (Akabane et al., 2009). In addition to CYP3A4, other major CYPs found along the small intestine are CYP1A1, CYP2C9, CYP2C19, and CYP2D6. The distribution of CYPs is not uniform as expression is

relatively high in the duodenum and reaches maximal expression in the proximal jejunum followed by sustained decreases through the medial and distal jejunal regions with low or non-existent CYP protein in the ileum (Paine and Thummel, 2003). Regarding Phase II enzymes, the small intestine has expression of UGTs throughout each of the respective intestinal regions (Ritter, 2007). It was recently shown that of the major UGTs, UGT1A1 was present in the jejunum and ileum at levels comparable to CYP3A4 (Busch et al., 2015). Additionally, UGT1A3 and UGT2B7 were detected at protein levels greater than or equal to other major Phase I enzymes such as CYP2C9, CYP2C19, and CYP2D6. For the UGTs quantified, protein amounts were highest in the jejunum. Intestinal UGTs can be regulated by the same transcription factors previously mentioned as well as caudal-related homeodomain protein 2 (Cdx2), which is specific to the intestine and modulates several UGTs (Gregory et al., 2004; Gregory et al., 2006).

Just as the hepatocyte is polarized, enterocytes too possess a polarized orientation. The apical membranes of enterocytes face the intestinal lumen and express a number of uptake and efflux transporters. Recently, proteomic work by Groer et al. (2013) and Drozdzik et al. (2014) demonstrated that transporter expression in the small intestine is dominated by PEPT1 (*SLC15A1*), which is involved in the transport of peptides (Adibi, 2003). PEPT1 accounted for approximately half of the quantified transporters in a small pool of healthy subjects. Also detected were the sodium dependent bile transporter ASBT (*SLC10A2*), organic cation transporters, OATP2B1 (*SLCO2B1*), MDR1, MRP2, MRP3, and breast cancer resistance protein (BCRP, *ABCG2*). MDR1 and CYP3A4 are in close proximity to each at the apical membrane, creating a synergistic mechanism by which substrates that elude CYP-mediated metabolism are excreted back into the

lumen after which reuptake into the cell may eventually result in substrate biotransformation (Christians, 2004). Though the large intestine lies beyond the scope of this thesis, a significant finding from Drozdzik's work was the relatively high MRP3 expression in the colon, accounting for 36% of the total quantified transporter proteins. The extent of MRP3 expression along the intestinal tract, and its role as a protective mechanism, is an important concept as it relates to the research detailed in subsequent chapters.

Metabolic enzymes and transporters in the small intestine are regulated via similar mechanisms as those present in the liver. Additionally, Phase I and II enzymes as well as transporters are also subjected to modulation by components that are in food. For instance, grapefruit juice has been shown to inhibit the activities of both CYPs and transporters (Kantola et al., 1998; Kivisto et al., 1999; Fukazawa et al., 2004; Glaeser et al., 2007; Scialis et al., 2011). It is well known that bergamottin, a component of grapefruit juice, incapacitates CYP by a mechanism colloquially referred to as suicide inactivation (Eagling et al., 1999; Goosen et al., 2004). The impact of grapefruit juice on small intestine function is multivariate ranging from reduced bioavailability of fexofenadine due to inhibition of intestinal OATPs that mediate uptake into enterocytes or alternatively increased plasma concentrations of cholesterol lowering 3-hydroxy-3-methylglutaryl coenzyme A reductase inhibitors (henceforth referred to as statins) due to blockade of CYP metabolism.

Analysis of the constituents in grapefruit juice revealed that the contributors of the observed inhibition (e.g., bergmamottin, naringin, and quercetin) were present in µM to mM concentrations depending on whether the juice or pulp were assayed (Ross et al.,

2000; De Castro et al., 2006). Intestinal transporter inhibition was reported to also occur with other fruit juices such as apple, grape, and orange (Dresser et al., 2002). Owing to the inhibition potential grapefruit juice possesses, clinicians need to be mindful of potential drug interactions that may result in toxicity as demonstrated in a patient taking verapamil while consuming grapefruit juice (Pillai et al., 2009). In that case, the intake of grapefruit juice along with the recommended dosage of verapamil led to a marked increase in plasma verapamil concentrations. The cause for the increased exposure was two-fold: 1) the constituents in grapefruit juice inhibited CYP3A4 that is the primary enzyme involved in verapamil metabolism, and 2) the transporter-mediated elimination of verapamil via MDR1 was likewise inhibited by grapefruit juice.

1.3 Transporters

1.3.1 Structure and Function

The movement of materials into and out of cells may occur through passive diffusion or carrier-mediated transport. In a carrier-mediated process, transporter proteins function to translocate substrates, and this process may or not involve an energy input component. Some gene families are responsible for excretion of substrates from the cell to extracellular space while other gene families function as uptake transporters. Of the entirety of transporters in the genome, several families of transporter genes are responsible for the disposition of therapeutic agents and/or their metabolites, and three of the major subtypes that are relevant to the work presented herein are listed in Table 1.1 along with their respective intra-family protein sequence homologies.

The first major class of transporters belongs to the ATP-binding cassette (ABC) family which is further divided into seven subfamilies (ABCCA to ABBCG). Most of the focus

of this review will be on members of the ABC subfamily C. As suggested by their name, the ABC transporters use ATP to energize transport activity. Although the overall structure of ABC transporters can vary, there are several conserved features. ABCC proteins, of which there are thirteen identified genes, have the following general arrangement: 1) extracellular N-terminus linked to a membrane spanning domain (MSD0) with five transmembrane helices followed by a cytoplasmic loop 2) MSD1 with six transmembrane helices, 3) cytosolic nucleotide binding domain (NBD1), 4) MSD2 with six transmembrane helices, and 5) cytosolic NBD2 with C-terminus. The above indicated structure is reflective of the longer ABCCs 1, 2, 3, 6, 8, 9, and 10 whereas the shorter ABCCs 4, 5, 7, 11, and 12 have a cytosolic N-terminus-MSD1-NBD1-MSD2-NBD2 arrangement (Gottesman et al., 2002). MSD0 is important for trafficking of the proteins to their respective locations and for retention of the protein to the plasma membrane (Westlake et al., 2005; Bandler et al., 2008). The NBD regions carry out the binding of ATP and subsequent hydrolysis to ADP. The two MSDs with their twelve helices form a channel that closes on the cytoplasmic side upon presentation of substrate and ATP. The substrate is then released into the extracellular space, and ATP is hydrolyzed to ADP re-initializing the transporter to accept substrate from the cytoplasm (Linton, 2007). Each transport cycle requires two ATP molecules. The presence of glutathione has been shown to promote the activity of ABCCs *in vitro* (Qian et al., 2001).

Most of the ABCC proteins are expressed at the basolateral membrane while ABBC2 (alias MRP2) is unique in that it is exclusively expressed on the apical membrane. There is broad overlap of substrates for the various ABCCs. Common substrates of the

longer ABCC proteins are organic anions, glucuronide conjugates, glutathione as well as glutathione conjugates, and sulfated compounds (Deeley et al., 2006). The shorter ABCCs transport glucuronide conjugates as well as bile salts, nucleosides, prostaglandins, and sulfates. ABCC7 (alias cystic fibrosis transmembrane conductance regulator [CFTR]) is an atypical ABCC in that it functions as a chloride ion channel and was identified as being the protein that is defective in cystic fibrosis (Rommens et al., 1989). ABCCs 8 and 9 serve as sulfonylurea receptors (alias SURs) and have a role in modulating insulin (Thomas et al., 1995; Aguilar-Bryan et al., 1998). ABCCs 11 and 12 are thought to be duplicates with closest homology to ABCC5 (Tammur et al., 2001). ABCC11 can efflux anions, glucuronides, nucleotides, and is a determinant for ear wax type (wet vs. dry) while ABCC12 is expressed in breast cancer (Bera et al., 2002; Chen et al., 2005; Yoshiura et al., 2006). The consequence of the wet ear wax phenotype is an increased risk of breast cancer in Japanese but not Caucasian women (Ota et al., 2010; Lang et al., 2011). ABCC13 does not appear to be a functional protein as it contains only one fully formed NBD, hence it cannot properly bind ATP (Annilo and Dean, 2004).

The members of the ABCG subfamily of transporters are much smaller and consist of a cytosolic N-terminus coupled to a NBD and a single MSD with six helices and cytosolic C-terminus. The proteins are considered half-transporters in that they dimerize to form a functional unit (Ozvegy et al., 2001). ABCG1 is the human homologue to a protein in *Drosophila* that produces a white eye color due to the efflux of brown and red pigments (Chen et al., 1996). ABCG1 and ABCG4 are thought to modulate the efflux of sterols and have high expression the brain (Wang et al., 2008). ABCG2 (alias BCRP) has a

major role in the disposition of xenobiotics and can mediate the efflux of anti-cancer drugs, statins, and Phase II conjugates (Robey et al., 2007). BCRP is responsible for the basolateral efflux of substrates from the central nervous system and is also located along the canalicular domains in the hepatocyte and the apical domain of the intestines (Berge et al., 2000). ABCG5 and ABCG8 form a heterodimer and are located at the apical membrane in hepatocytes where they excrete cholesterol and other sterols into the bile (Lu et al., 2001).

The last major transporter family that will be covered is the solute-carrier (SLC) that is comprised of more than fifty subfamilies. As it pertains to the research in the thesis, focus will be on the SLCO subfamily. There are thirteen distinct transporter proteins encoded by the *SLCO* genes, and the SLCOs are referred to as organic anion transporters or more colloquially as organic anion transporting polypeptides (OATPs). The SCLOs have a typical structure of cytosolic N-terminus, a MSD with eight to nine helices, an extracellular loop, a second MSD with three helices, and finally a cytosolic C-terminus. In contrast to the ABC transporters, SLCOs are not energized by ATP and may use bidirectional transport as a driving mechanism. The exact mechanism of SLCO transport has not been clearly defined, though it is generally thought that the 2 MSDs form a pore having an internal positive charge with multiple substrate binding sites (Han et al., 2010; Niemi et al., 2011). SLCO2B1 activity can be modulated by extracellular pH in that acidic conditions increase the inward transport of substrates, however other SLCOs do not necessarily share this trait (Tirona and Kim, 2007).

The SLCOs are distributed throughout the body and with diverse orientation, i.e. apical vs. basolateral localization (Roth et al., 2012). Among those expressed in the brain are

SLCO1A2, SLCO2B1, SLCO1C1, and SCLO3A1. The liver has SLCO1B1 and SLCO1B3, which are hepatoselective, as well as SLCO1A2 and SLCO2B1. Intestinal expression of SLCOs consists of SLCO1A2 and SLCO2B1 that are both facing the intestinal lumen. The kidneys possess SLCO1A2 and SLCO4C1 on opposing membranes. Finally, SLCO2B1 is expressed constitutively in skeletal muscle. Muscle tissue is sensitive to a type of injury called rhabdomyolysis, which is a syndrome characterized by muscle pain and myopathy. During rhabdomyolysis, muscle tissue is destroyed, and the degradants are released into the blood potentially leading to renal failure as the kidneys become inundated with the muscle protein myoglobin that cannot be cleared properly (Sauret et al., 2002; Polderman, 2004). A causative factor for rhabdomyolysis is the accumulation of statins via uptake by SLCO2B1 into muscle tissue. As the intracellular statin concentrations increase beyond the muscle's ability to metabolize the substances, toxicity begins to occur resulting in myopathy of muscle (Knauer et al., 2010). Inhibition of SLCO-mediated statin uptake by the clinically relevant antibiotic rifampicin was shown to attenuate statin-induced cytotoxicity using an *in vitro* model (Zhang et al., 2013). Among the other SLCOs substrates are antibiotics (β-lactams), bile salts, glucuronide conjugates, peptides, prostaglandins, sulfated compounds, and thyroid hormones (Tirona and Kim, 2007; Roth et al., 2012).

1.3.2 Pharmacogenomics

As is the case for many genes, transporters can have a variety of polymorphisms that can affect protein functionality with clinical ramifications. For instance, a SNP for ABCC2 in which the amino acid at position 412 changes from an arginine to a glycine (R412G) resulted in a loss of methotrexate efflux, as measured in an *in vitro* system,

compared to wild type ABCC2 (Hulot et al., 2005). The arginine at 412 is conserved in the Abcc2 sequence of other animals and is thought to be involved in substrate recognition. Clinically, the R412G mutation was linked to a 3-fold increase in the elimination half-life of methotrexate resulting in an overdose that may have contributed to nephrotoxicity. Another SNP for ABCC2, this time in the promoter region hence having a no impact on the protein sequence, was correlated with a statistically significant 25% increase in the plasma concentrations of mycophenolic acid acyl glucuronide (AcMPAG) in healthy subjects compared to homozygous wild-type carriers (Levesque et al., 2008). AcMPAG has immunosuppressive pharmacology similar to its parent compound, thus a rise in plasma concentration of the pharmacologically active metabolite in carriers of mutant ABCC2 may result in pharmacodynamic effects (Schutz et al., 1999; Shipkova et al., 2002).

Mutations in ABCC2 are associated with pathogenesis of Dubin-Johnson Syndrome (DJS) as a result of impaired expression and functionality. The phenotype of affected subjects is characterized by hyperbilirubinemia, jaundice, and darkened livers (Dubin and Johnson, 1954; Shani et al., 1970). The mutations in the *ABCC2* gene are a combination of alternate deletion, splicing, or substitution (Chen and Tiwari, 2011). Several SNPs were shown to have reduced activity suggested to be the result of misfolded protein structure (Mor-Cohen et al., 2001). Other explanations for loss of activity were attributed to SNPs in the NBDs that might limit the binding of ATP to energize transport (Tsujii et al., 1999). In addition to functional loss, trafficking of ABCC2 was shown to be impaired with localization of protein directed to the endoplasmic reticulum rather than the plasma membrane (Arlanov et al., 2012). The

Eisai hyperbilirubinuria rats, which lack Mrp2 as a result of a stop codon insertion, are used as a rodent model of DJS (Ito et al., 1997; Johnson et al., 2006).

To date, there has been little focus on the clinical significance of ABCC3 polymorphisms. Nonetheless, research from multiple groups demonstrated that polymorphisms of ABCC3 are numerous. Saito et al. (2002) initially reported 30 ABCC3 SNPs, however the functional significances were not investigated. Work by Lang et al. (2004) indentified 51 mutations, and a SNP in the promoter region was correlated with a reduction in both hepatic mRNA and protein though only the mRNA reduction was statistically significant. A comprehensive analysis of ABCC3 SNPs was performed by Kobayashi et al. (2008) who characterized eleven SNPs with all polymorphisms occurring in the protein coding regions. Eight of the polymorphisms that were found in MSD0, NBD1, and NBD2 were determined to have normal function as well as expression and had proper localization to the plasma membrane. A SNP in NBD2, in which arginine was changed to serine at position 1381 (R1381S), caused the protein to accumulate within the cell and remain bound to the endoplasmic reticulum.

The remaining two SNPs in Kobayashi's research were determined to have reduced functional activity. The first of these SNPs is located on the extracellular side of MSD1 at position 346 where serine is replaced with a phenylalanine (S346F). The second SNP is localized near NBD1 at position 607 and consists of an asparagine substitution in place of serine (S607N). The transport activity was measured using estradiol-17β-glucuronide as a probe and compared to the wild-type ABCC3 sequence. Transport activity for the two SNPs was between 67 to 77% lower compared to the wild-type. Moreover, the previously mentioned eight SNPs yielded transport activity that was

greater than or similar to that of wild-type. The S346F mutation is estimated to occur in 2.5% of Caucasians while the S607N SNP has a prevalence of approximately 2.8% in African-Americans. More recently, a report by Pussegoda et al. (2013) indicated that a SNP near the N-terminus at position 1503 was significantly correlated with ototoxicity in children receiving cisplatin during chemotherapy treatment. Considering that cisplatin is a substrate for ABCC3, the correlation may be due to altered protein function, though the authors of the study did not investigate ABCC3 protein activity.

Polymorphisms have likewise been discovered for uptake transporters. Nozawa et al. (2002) reported that 10% of Japanese subjects were homozygous for a SNP at position 392 where isoleucine is changed to threonine (I392T) for SLCO2B1, and that the prevalence of I392T SNP, known colloquially as the *3 allele, occurred in approximately 31% of the subject pool. Using an *in vitro* cell-based system, the I392T SNP was found to have reduced transport kinetics compared to homozygous wild-type (*1 allele) of the known OATP2B1 substrate estrone-3-sulfate. Substrate affinity, in terms of K_m, was the same between *1 and *3 alleles though the *3 V_{max} was reduced by over 50%. Results from *in vivo* studies indicate that the reduction in *3 transport capacity has clinical significance. In a report by Akamine et al. (2010), Japanese subjects with the *3 allele had a 51% increase in fexofenadine plasma concentrations compared to *1 carriers. Experiments with *in vitro* cell-based systems indicated that fexofenadine is an OATP2B1 substrate (Nozawa et al., 2004; Ming et al., 2011). However, not all OATP2B1 SNPs result in loss of activity as substrates aliskiren and glyburide did not have altered activity compared to the wild-type allele (Ieiri et al., 2012; Tapaninen et al., 2013).

Given the importance transporters have in modulating the uptake and efflux of critical endogenous substances as well as their respective roles in mediating the clearance of xenobiotics, further investigation into transporter loss of function is warranted. Transporter knockout models afford a mechanistic means by which dispositional changes can be uncovered. As it applies to the field of toxicology, transporter knockout models can serve as surrogates to human polymorphisms whereby the ramifications of diminished transporter function can be quantified. To this end, a major goal of the present work is to use animal knockouts to study the disposition of toxicants.

1.4 Cyclooxygenases

1.4.1 Structure and Function

There are two genes that are responsible for the coding of enzymes involved in arachidonic acid metabolism, prostaglandin-endoperoxide synthase 1 (COX-1, *PTGS1*) and 2 (COX-2, *PTGS2*). Following initial characterization of COX-1 enzyme in sheep (DeWitt and Smith, 1988), the structure and sequence of human COX-1 was elucidated by Yokoyama and Tanabe (1989) and found to be 599 amino acids in length. Work by Funk et al. (1991) showed that mutation of a serine (Ser) to asparagine at position 529 abolished activity of the enzyme. COX-2 was characterized by Hla and Neilson (1992) and reported to have 604 total amino acids. Kim et al. (2005) discovered that mutation of a cysteine (Cys) residue at position 555 to a serine eliminated enzyme activity. Furthermore, mutation of the Cys526 site to a serine prevented the binding of inducible nitrous oxide synthase (iNOS, *NOS2*). The binding of iNOS to Cys526 causes it to be S-nitrosylated resulting in increased enzymatic activity. S-nitrosylation is regarded as an important post-translational event that can modulate the intrinsic activity of targeted

proteins (Hess et al., 2005). Of the thirteen cysteine residues on COX-2, only Cys526 can be activated by iNOS.

The two encoded COX proteins share about 65% identity for their native amino acid sequence (Altschul et al., 1997). Structurally, the two COX enzymes share similar features. The COX protein structure has a membrane bound domain at the amino-terminus, a proton acceptor site between residues 190 to 210, a substrate recognition region is located near position 350, there is a site for cyclooxygenase activity between amino acids 370-390, a heme binding motif is located three amino acid residues from the catalytic site, and there is a serine site between positions 510 to 530 near the carboxyl-terminus that is involved in aspirin pharmacology (Magrane and Consortium, 2011; UniProt, 2015). COX-1 has ubiquitous expression in most tissues and is constitutively active thus functioning as a housekeeping gene (Dewitt and Meade, 1993; Smith and Dewitt, 1996). COX-2, in contrast, is not detectable under homeostatic conditions, though its expression can be inducible and sustained for short durations (Evett et al., 1993). COX proteins are monotopically membrane bound as homodimers within the endoplasmic reticulum (Mbonye et al., 2006). Despite the differences in expression and modulation of activity, the two COX enzymes share similar enzyme kinetics (Smith et al., 1996).

Both COX proteins perform the same enzymatic reaction of converting arachidonic acid (AA) to prostaglandin G_2, which is subsequently converted to prostaglandin H_2 by hydroperoxidase activity in the COX enzyme. PGH_2, being unstable, is then further metabolized into prostacyclins, prostaglandins, or thromboxanes by a number of synthases that are tissue specific (Nicolaou et al., 2014). The products of these

reactions have varying pharmacologies ranging from induction of inflammation, inhibition of platelet function, immunosuppression, vasodilation, and inhibition of T-cell production (Moncada et al., 1976; Sravan Kumar and Das, 1994; Zhou et al., 2007; Kalinski, 2011).

1.4.2 COX Inhibition

The inhibition of COX enzymes as the pharmacological basis of anti-inflammatory drugs was first postulated in 1971 (Ferreira et al., 1971; Vane, 1971). Compounds that inhibit COX are sorted into four structural classes: 1) salicylic acids, 2) anthranilic acids, 3) acetic acids, and 4) propionic acids. Examples of each structural class are aspirin (salicylic), mefenamic acid (anthranilic), diclofenac (acetic), and ibuprofen (propionic) (Kalgutkar and Daniels, 2010). Inhibitors of the COX enzymes fall into one of three categories: selective 1) COX-1 selective inhibitor, 2) non-selective inhibitor of COX-1/2, or 3) COX-2 selective inhibitor.

Early therapeutic agents were generally non-selective COX inhibitors. Discovery and characterization of the COX-2 protein shifted efforts of medicinal chemists to develop therapeutic agents that had greater COX-2 antagonism so as to minimize the deleterious effects associated with suppression of COX-1 function (Borne et al., 2013). Inhibition of COX occurs as a result of competitive inhibition, tight binding of inhibitors, or covalent modification. Mefenamic acid and ibuprofen are examples of competitive inhibitors that interfere with the binding of AA to the COX catalytic site (Catella-Lawson et al., 2001).

Tight binders are not covalently bound, rather the inhibitor-enzyme complex dissociates relatively slowly (Rome and Lands, 1975). Formation of the tightly bound complex has been described as a two step process, initial binding followed by a conformational change permitting closer association of inhibitor and enzyme wherein the second step is time dependent (Copeland et al., 1994). Compounds such as indomethacin, a non-selective COX inhibitor in the same structural category as diclofenac, need to bind to one of the COX-2 homodimer units to block AA metabolism. (Prusakiewicz et al., 2009). Ibuprofen and mefenamic acid need to occupy the substrate binding sites in both COX-2 subunits to inhibit the catalytic conversion of AA into PGH_2. The mechanism of action for COX inhibitors has been linked to interaction with the arginine (Arg) residue at position 120. Under normal conditions, Arg120 interacts with the carboxylate moiety of arachidonic acid (Marnett et al., 1999). COX inhibitors occupy the substrate binding site with an orientation such that the negatively charged carboxylate region of the inhibitor is ion-paired with Arg120 due to the positively charged arginine. Mutation of Arg120 to other amino acids diminished the inhibition potency of diclofenac, indomethacin, ketoprofen, and meclofenamic acid (Mancini et al., 1995).

Selective COX-2 inhibitors do not possess carboxylic acid moieties, rather they contain sulfonamides or sulfones. The mechanism for selective COX-2 inhibition is such that the sulfonamide or sulfone of the inhibitor interacts with other regions of the enzyme rather than orient towards Arg120 as the traditional COX inhibitors do. The changes in COX-2 amino acids compared to the COX-1 sequence, specifically a valine at positions 434 and 523, create a larger binding pocket allowing the inhibitor to access a secondary

region in the COX-2 enzyme that is otherwise inaccessible in COX-1 (Zarghi and Arfaei, 2011).

The final category of COX inhibitors is the covalent modifier. Despite the long history of anti-inflammatory drug research, only one therapeutic agent has been developed and subsequently identified as a covalent modifier, aspirin. The site of covalent modification differs for each enzyme with a serine at position 530 and 516 for COX-1 and COX-2, respectively, that is acetylated by aspirin (Shimokawa and Smith, 1992; Lecomte et al., 1994). The mechanism of action for aspirin relative to other COX inhibitors is distinct in that the blockade by competitive inhibitors or tight binders is eventually reversible, taking more time for the tight binders, while covalent modification is irreversible. COX enzymes exposed to aspirin must be newly synthesized for cells to regain COX metabolism of AA. The effect of aspirin on COX-1 in platelets is a loss of ability to produce thromboxane, a required component in the blood clotting process (Schror, 1997). Though aspirin can acetylate both COX enzymes, its potency for COX-1 is far greater than that for COX-2 (Awtry and Loscalzo, 2000).

1.4.3 COX Pharmacology

The metabolism of AA by the COX enzymes yields a number of prostaglandin derivatives. In the context of the work presented in this thesis, the formation of prostaglandin E_2 (PGE_2) is of significance. Formation of PGE_2 occurs through the metabolism of PGH_2 by prostaglandin E synthase (*PTGES*). PTGES was reported to be dependent on glutathione and found to be inducible by the proinflammatory cytokine interleukin 1 beta (IL-1β) (Jakobsson et al., 1999). COX-2 was similarly reported by Mitchell et al. (1994) to be inducible by cytokines such as IL-1β and tumor necrosis

factor alpha (TNFα). PGE_2 acts as a ligand for several receptors known as EP1, EP2, EP3, and EP4 (Coleman et al., 1994). The rank order affinity of PGE_2 for its receptors are EP3 > EP4 >> EP2 > EP1 (Abramovitz et al., 2000; Mohan et al., 2012).

Activation of EP1 and EP3 by PGE_2 results in an increase of intracellular calcium, or alternatively, for EP3 activation reduces cyclic adenosine monophosphate (cAMP) formation. In contrast, EP2 and EP4 activation stimulates production of cAMP. Hoshino et al. (2003) reported the involvement of EP2 and EP4 activation as a mechanism for PGE_2-mediated protection of the gastrointestinal tract. Using ethanol as a model toxicant, PGE_2 was able to inhibit apoptosis of cultured gastric mucosal cells (Hoshino et al., 2002). Use of specific agonists for EP2 and EP4 led to a decrease in ethanol-induced toxicity. Furthermore, EP2 and EP4 agonists also suppressed activation of several caspases. In consideration that caspases are involved in mediating apoptosis (McIlwain et al., 2013), suppression of caspase activity via EP2 and EP4 activation promotes cell viability. Neither EP1 nor EP3 agonists maintained cell viability in gastric cells exposed to ethanol suggesting that EP1 and EP3 do not have a role with regards to caspase inhibition and suppression of apoptosis. Nonetheless, EP1 activation by PGE_2 is a protective mechanism as it results in an increase in the release of bicarbonate, a critical buffer for the intestinal tract to neutralize the acidity of gastric chyme (Takeuchi et al., 1997).

Yokotani et al. (1996) published a report detailing the role that EP3 activation has in reducing the secretion of gastric acid. Using a gastric epithelial cell line that expressed EP4, but not EP1 or EP3, the addition of PGE_2 to the cells resulted in production of hexosamine (Hassan et al., 1996). The formation of hexosamine occurs during

synthesis of gastric mucous (Gindzienski et al., 2003), hence EP4 activation represents yet another pathway by which PGE_2 maintains the overall health and integrity of the gastrointestinal tract. Overall, the outcome of PGE_2 synthesis and subsequent binding to its native receptors is an apparent resistance to damage from toxicants through several distinct but physiologically relevant and complementary pathways.

The role that COX-1 has in maintaining health of the gastrointestinal tract was demonstrated using mice that were exposed to radiation. Cox-1 but not Cox-2 was induced in mice exposed to radiation (Cohn et al., 1997). In that same study, mice were then challenged with indomethacin which has greater potency against COX-1 compared to COX-2 (Blanco et al., 1999). The administration of indomethacin reduced both PGE_2 synthesis as well as the number of surviving intestinal stem cells. Treatment with a PGE_2 analogue was able to counter the indomethacin effect on the stem cells. The authors conclude that PGE_2 generated from Cox-1 had a protective effect in their mouse model.

The cytoprotective effects of COX-2 are evidenced by its apparent induction in neoplastic tissue (Eberhart et al., 1994). As an example, PGE_2 stimulated colon tumors in a rat model wherein PGE_2 was administered over multiple weeks (Kawamori et al., 2003). The authors of that study reported transcriptional expression of all EP receptors. PGE_2 administration also decreased the level of apoptosis compared to control. The authors concluded that PGE_2 stimulated cellular proliferation in addition to inhibiting apoptosis. The potential for PGE_2 to induce cellular growth in models of tumor growth created interest in pursuing COX-2 inhibition as a potential treatment for metastases of the colon (Ferrandez et al., 2003; Koehne and Dubois, 2004; Fujimura et al., 2007).

As mentioned previously, COX-2 is inducible, and its expression increases during inflammation or injury (Mizuno et al., 1997). A rat model was used to demonstrate that inhibition of COX-2 was associated with a delay in repair of ulcers as well as reduction of angiogenesis (Ma et al., 2002). A separate study reported that activation of EP4 but not EP1, EP2, or EP3 accelerated wound healing in a rodent model of intestinal ulceration (Hatazawa et al., 2007). Ulceration in the animals was induced by application of heat that led to a marked increase of intestinal PGE_2. The involvement of EP4 in wound repair was confirmed by administration of an EP4 agonist. Administration of a selective EP4 antagonist caused a delay in healing. Furthermore, rats and mice that received indomethacin and rofecoxib (a selective COX-2 inhibitor), experienced delays in ulcer repair in contrast to animals given SC-560 (a selective COX-1 inhibitor). Furthermore, the latency in healing was observed in Cox-2 knockout mice but not Cox-1 knockout mice. Thus it can be inferred from the Hatazawa study that COX-2 was operative in healing of ulcers through generation of PGE_2 that acted on EP4 receptors.

Given the importance of COX-1 and COX-2 for protection of the gastrointestinal tract as well as involvement on cellular regeneration, inhibition of both pathways would be contributory toward exacerbation of gastrointestinal injury. One of the critical components of COX inhibition is the production of PGE_2 from AA metabolism. In this framework, the research presented in subsequent chapters will focus on the role that DCF and its metabolites have in causing injury to the intestinal tract.

1.5 Diclofenac

1.5.1 Pharmacokinetics and Metabolism

Diclofenac is an NSAID that was developed by Ciba Geigy and patented in Europe and the United States in 1965 and 1971, respectively (Sallmann and Pfister, 1971). In the United States, diclofenac is available only by prescription and is commonly given in 100 mg doses though its therapeutic benefit can be achieved with dosing of 50 to 200 mg per day (Novartis, 2011; Depomed, 2014). Diclofenac is also prescribed as a gel for topical applications. Low dose diclofenac was made available as an over-the-counter (OTC) remedy in a number of countries (Hinz et al., 2005). As recently as 2015, diclofenac was removed from OTC status by the Medicines and Healthcare products Regulatory Agency (MHRA) in the United Kingdom due to concerns of cardiac toxicity (MHRA, 2015). Consequently, diclofenac became available as a prescription only medicine similar to its status in the United States.

The pharmacokinetics of diclofenac has been characterized in animals and man. Approximately 60% of diclofenac is eliminated in feces in the dog and rat with the remaining 40% excreted in the urine (Riess et al., 1978). The elimination pathway is reversed in monkey whereby approximately 80% of the dose is eliminated in urine with 20% excretion in feces. Similar to monkey, 60% of the dose was excreted in the urine of healthy human subjects with the remainder directed to biliary excretion (Stierlin and Faigle, 1979). The bioavailability of diclofenac in human subjects given a single 50 mg dose was reported to be 54% (Willis et al., 1979). In healthy human subjects receiving an oral dose, the maximum plasma concentration (C_{max}) was calculated to be 2.0 µg/mL (6.75 µM) occurring approximately 2.5 hours after dosing with a terminal half-life of 1.8

hours. A food effect was observed in humans in that the time to maximum plasma concentration was increased however the overall exposure of diclofenac, as measured by integration of plasma-concentration time profiles, was similar between fasting and non-fasting subjects (Willis et al., 1981).

Diclofenac undergoes extensive metabolism, and less than 1% of the dose is excreted in the urine as parent compound. Major Phase I metabolites are 3'-hydroxy-, 4'-hydroxy-, 5-hydroxy, 3',4'-dihydroxy-, and 4',5-dyhyroxy-diclofenac as the result of catalysis by CYP2C8, CYP2C9 (for 4'-hydroxy), and CYP3A4 (for 5-hydroxy) (Riess et al., 1978; Stierlin and Faigle, 1979; Bort et al., 1999a). Approximately 30% of the total diclofenac dose is excreted in urine as the 4'-hydroxy metabolite while biliary excretion of 4'-hydroxy accounts for up to 20% of the dose (Davies and Anderson, 1997). Phase II metabolites are taurine and acyl glucuronide conjugates of diclofenac (Pickup et al., 2012; Sarda et al., 2012). Glucuronide conjugates can subsequently be hydroxylated. Regarding glucuronide formation, the predominant enzyme is UGT2B7 (*UGT2B7*). In addition to UGT2B1, Nakamori et al. (2012) reported that diclofenac can be glucuronidated by UGT2B15, UGT2B17, and UGT1A9.

Diclofenac has excellent absorption as characterized in the Caco-2 colorectal adenocarcinoma cell line. Caco-2 cells are often used to test compound permeability and determine if there is transport by MDR1 as the cells express this efflux transporter (Marino et al., 2005). Owing to the polarization of Caco-2 cells, test compounds are assayed in an Apical→Basolateral (A→B) and Basolateral→Apical (B→A) format, and the flux or movement of compound is reported as a two dimensional parameter with units of cm/sec. The A→B and B→A values for diclofenac are 20 and 21 × 10^{-6} cm/sec,

respectively (Yazdanian et al., 2004). The B→A/A→B ratio of 1.1 signifies diclofenac is not a MDR1 substrate as ratios > 2 indicate MDR1 efflux. The cell assay was confirmed with a parallel artificial membrane permeability assay (PAMPA), which is a non-cell based assay that uses lipids to mimic a physiologic barrier (Nakamori et al., 2012). Diclofenac's permeability classifies it as highly permeable and similar to compounds such as caffeine, midazolam, and verapamil. Using Equation 1.1, the bioavailability of diclofenac can be broken down as follows:

$$F = F_a \times F_g \times F_h = 1 \times 0.64 \times 0.85 = 0.54 = 54\%$$

The above relationship indicates that: 1) absorption of diclofenac is complete as a consequence of high permeability, 2) intestinal enzymes significantly contribute to overall diclofenac metabolism, and 3) hepatic metabolism is less than intestinal metabolism following an oral dose (Varma et al., 2010).

1.5.2 Reactive Metabolites

The metabolism of diclofenac results in reactive metabolites. Both the 4'- and 5-hydroxy metabolites (refer to Figure 2.8) can form quinone imines due to the hydroxy groups being *para* to nitrogen (Shen et al., 1999). A simplified reaction is shown below:

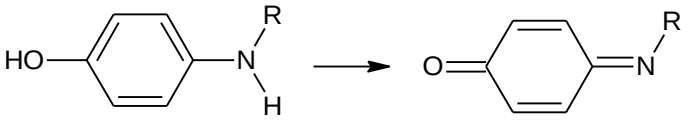

Exposure to diclofenac has been linked to bone marrow toxicity. Studies with neutrophils provided evidence that a quinone imine derivative of diclofenac was detected in neutrophils (Miyamoto et al., 1997). Neutrophils are white blood cells that protect the body against microorganisms.

One the ways in which neutrophils carry out their antimicrobial function is to generate reactive oxygen species from the release of myeloperoxidase (Monteseirin et al., 2001). Myeloperoxidase (*MPO*) generates hypochlorous acid (HOCl) from chloride ions using hydrogen peroxide, which is reduced to water (Arnhold, 2004). HOCl then reacts with a number of agents to produce reactive oxygen and nitrogen species. Regarding diclofenac-associated bone marrow toxicity, Miyamoto and colleagues demonstrated that myeloperoxidase, through the synthesis of HOCl, generated diclofenac quinone imine reactive species. Though the authors admit that quinone imine formation by MPO is slow, they argue that such a reaction could occur *in vivo* and be a contributory factor to the bone marrow toxicity that can occur during treatment with diclofenac (Sell et al., 1999; Aydogdu et al., 2006).

In addition to diclofenac, a number of marketed agents are metabolized into acyl glucuronides including clofibric acid, diflunisal, fenoprofen, furosemide, ibuprofen, ketoprofen, mycophenolic acid, suprofen, tolmetin, valproic acid, and zomepirac (Bailey and Dickinson, 1996; Bolze et al., 2002). Ferosemide acyl glucuronide has very low reactivity as a result of its benzoic acid structure providing a stabilizing force through resonance of the aryl π bonds (Sawamura et al., 2010). Though ibuprofen is converted to an acyl glucuronide that can covalently bind albumin, it has an excellent safety profile in that reports of adverse drug reactions (ADRs) were less than or equal to placebo (Fries et al., 1991; Kellstein et al., 1999). In the case of ketoprofen, its reactive glucuronide was shown to covalently bind to the UGT enzyme that generated it (Terrier et al., 1999). Despite the UGT modification by ketoprofen acyl glucuronide, ketoprofen usage for pain relief did not result in any ADRs during an 18 month study designed to

test its overall safety in 402 patients (Kneer et al., 2009). Valproic acid was found to form covalent adducts, via its acyl glucuronide, in patients taking the drug for epilepsy treatment. Yet in those patients that tested positive for valproic acid antibodies, the antibody titer was reportedly low (Williams et al., 1992). Factoring the incidence of covalent adduct formation and antibody generation in response to the adducts, valproic acid usage is not likely to result in hypersensitivity reactions. That said, valproic acid itself has been linked to nonalcoholic fatty liver disease that is characterized by mixed hepatocellular injury thought to have an immune component (Farinelli et al., 2015). Of the more reactive acyl glucuronides listed above, the rank order of reactivity is tolmetin > zomepirac > diclofenac. Zomepirac was withdrawn from marketed status due to fatal hypersensitivity reactions (FDA, 1998). Interestingly, Cannell et al. (2001) reported that incubation of colon cancer cells with the acyl glucuronides of diclofenac, diflunisal, and zomepirac attenuated the cellular division of the cells perhaps as a result of their covalent adduction to factors involved in proliferation.

1.5.3 Liver Toxicity

Liver injury can be determined through the use of serum markers, specifically alanine aminotransferase (ALT), aspartate aminotransferase (AST), alkaline phosphatase (ALkP), and bilirubin. ALT and AST are indicators of hepatocellular damage while ALkP and bilirubin are used to indicate biliary obstruction or cholestasis (Green and Flamm, 2002). ALT is more exclusive to the liver cells and is found in the cytosol while AST is localized in both in the cytosol and mitochondria. Elevations of ALT and AST in the blood may indicate that a degree of liver injury or necrosis has occurred. ALkP is useful as an indicator of cholestasis due to its localization along the bile canalicular domain.

Bilirubin is formed during the breakdown of heme, and its elimination is dependent upon glucuronidation before excretion into the bile. The pattern of liver injury is contingent upon the extent of elevations in the serum markers. For reference, the upper limit of normal (ULN) for ALT, ALkP, and bilirubin are 40 U/L, 115 U/L, and 1.2 mg/dL, respectively (livertox.nih.gov). A comparative score, R value, is used to categorize the type of injury and is determined as follows:

Equation 1.2

$$R = [ALT/ULN_{ALT}]/[ALkP/ULN_{ALkP}]$$

As a general guideline, an R value $\geq$ 5 indicates hepatocellular injury, an R of $\leq$2 represents cholestatic injury, and R values between 2 to 5 signify a mixture of cholestatic and hepatocellular injury (Chalasani et al., 2014).

According to diclofenac prescribing information, hepatotoxicity from diclofenac can manifest within one to two months of therapeutic use (Novartis, 2011). A composite of reported diclofenac hepatotoxicity cases is shown in Table 1.3. The calculated R values for the cases cited appear to indicate that the liver injury attributable to diclofenac usage exhibited a pattern of hepatocellular damage while one of the cited cases seems to have been a mixed cholestatic and hepatocellular phenotype. Presentation of jaundice, which can occur during cholestasis, was positively correlated with severe liver injury though several subjects with jaundice recovered once diclofenac treatment was stopped. Manifestation of high ALT values did not reliably predict that mortality would necessarily follow. As an example, Chalasani et al. (2015) followed 899 subjects for drug-induced liver injury for which twelve subjects were identified as taking diclofenac. Of the twelve subjects, one exhibited a peak ALT of 1,895 U/L before ultimately dying. The diclofenac group as a whole had a mean ALT of 1,266 ± 680 U/L, a value that is approximately 30-

fold greater than the ALT ULN. Five of the diclofenac subjects were classified as having mild injury (increased ALTs & bilirubin <2.5 mg/dL) while six were deemed to have severe injury (bilirubin >2.5 mg/dL, hospitalization, jaundice, and organ failure). Liver injury from diclofenac accounted for nearly 36% of the entire cohort of subjects taking analgesics (12 of 33 total subjects) suggesting that diclofenac usage carries greater risk of hepatic injury compared to other anti-inflammatory drugs.

One key feature of diclofenac patients who develop liver injury is the dosing regimen. When liver injuries do occur, more often than not the patients are adherent to the prescribed dosage indicating that the liver injury is likely not a function of diclofenac overdose. This is in stark contrast to acetaminophen for which overdose is more common. An analysis by Larson et al. (2005) revealed that acetaminophen accidental overdoses and suicide attempts accounted for 133 and 122 cases, respectively, out of 662 acute liver failures over a six year period. The majority of subjects overdosing on acetaminophen survived, however 27% died and 8% needed liver transplants for which 29% of transplant patients did not survive beyond three weeks after surgery. Lastly, the median acetaminophen dose was 24 g despite product labeling warnings not to exceed 4 g per day. The high incidence of acetaminophen is linked to ease of access as an over-the-counter medication (Sheen et al., 2002).

Reports of diclofenac overdose are rare, however once such case was published by Netter et al. (1984) in which a 19-year old man intentionally overdosed on 1.5 g of diclofenac, which is 7.5-fold greater than the maximum recommended therapeutic dose (MRTD). Diclofenac plasma concentration seven hours after ingestion was 60.1 µg/mL (189 µM), which is 30-fold higher than the plasma C_{max} after a 50 mg therapeutic dose.

Despite the overdose and subsequent high diclofenac plasma concentrations, the subject recovered after two days with no apparent injury to liver or kidneys. Diclofenac overdose has been associated with renal dysfunction after an accidental overdose (Kulling et al., 1995). In that case a 29-year old man consumed 2 g of diclofenac (10-fold MRTD) and survived. No information regarding liver injury was given, however renal function was affected as evidenced by peak serum creatinine levels of 2.6 mg/dL compared to the normal range of 0.7 to 1.5 mg/dL (Lee, 2013). Tolerance of diclofenac during an overdose is not consistent as seen in a case whereby a 30-year old woman took 1 g of diclofenac (5-fold MRTD) and died two weeks after the overdose (Montiel et al., 2010). Hepatic and renal injury were apparent, leading to organ failures for both, with maximal ALT and serum creatinine levels of 4,710 U/L and 3.7 mg/dL, respectively. The role that diclofenac may have had in that case is unclear due to ingestion of several other medications including 8 g ibuprofen. In a study of 1,572 German subjects taking analgesics, approximately 25% were found to be using diclofenac with ibuprofen usage second-most at 21% (Freytag et al., 2014). In 426 subjects taking multiple analgesics, diclofenac was consumed with ibuprofen in 8.9% of the cases with polypharmacy also observed with acetaminophen (6.6%), metamizole (6.3%), and tramadol (4.9%). Despite the fact that subjects took more than the recommended dosage of diclofenac or consumed multiple analgesics, the most common risk was gastrointestinal bleeding.

The exact mechanisms of liver injury following diclofenac usage are not wholly clear. In the examples cited above and Table 1.3, injury ranged from mild to severe/fatal without clear distinction of the injury phenotype. For instance, all fatalities presented with jaundice, yet not all patients who developed jaundice died. Additionally, ALT values

were minimally 20-fold higher than ULN in the cases where fatality was reported. Subjects that eventually recovered had ALTs that were comparable to the fatalities. Several of the cases showed evidence of hypersensitivity that was determined by the presence of antinuclear antibodies. Furthermore, accumulation of eosinophils was found in livers of diclofenac subjects with hepatotoxicity supporting the hypersensitivity hypothesis. Eosinophils are part of the immune system and are involved in the development of delayed-type hypersensitivity reactions (Akahira-Azuma et al., 2004).

Dunk et al. (1982) reported their finding of a 52-year old man who had been taking diclofenac for the treatment of pain. After four months of usage, the individual developed jaundice with AST and bilirubin levels of 1,375 U/L and 7.4 mg/dL, respectively. Upon cessation of diclofenac treatment, the jaundice gradually subsided during the following week. The patient subsequently continued diclofenac treatment a month later, and within several weeks the jaundice reappeared. A liver biopsy was performed, and the presence of eosinophils as well as Kupffer cell proliferation was detected in the liver signifying activation of the immune system. Such activation may also result in production of anti-diclofenac antibodies, a point illustrated by Aithal et al. (2004) who reported that subjects with hepatotoxicity due to diclofenac treatment had anti-diclofenac antibodies.

Further evidence for immune modulation is provided by the work of Yano et al. (2012) for which plasma IL-17 was induced in mice given an 80 mg/kg dose of diclofenac. Hepatotoxicity in the mice was diminished when IL-17 was sequestered by an anti-IL-17 antibody indicating that IL-17 may have promoted injury through pro-inflammatory pathways (Jin and Dong, 2013). A recently published study characterized immune

activation by diclofenac in an *in vitro assay* with human hepatoma cell lines wherein the pro-inflammatory mediators IL-1, IL-8, and TNF as well as monocyte chemoattractant protein and immune mediator S100 calcium-binding protein A9 were upregulated by 50 µM diclofenac (Oda et al., 2015). Yet antibody presence does not appear to be a specific indicator of liver injury as antibodies were detected in 60% of subjects on diclofenac who did not have liver injury. Presumably, the anti-diclofenac antibodies are likely directed against the covalent adducts that were described in the preceding section. Nonetheless, hypersensitivity to diclofenac is cause for concern in that there is the possibility of adverse reaction to other structurally similar anti-inflammatory drugs (del Pozo et al., 2000; Picaud et al., 2014).

Non-immune hepatotoxicity may be linked to formation of metabolites and blockade of critical organelle function. For example, research by Castell et al. (1997) demonstrated that generation of *N*,5-dihyroxy diclofenac was associated with hepatocellular injury. Base on the results in a follow-up study, the authors postulated that continual generation of the *N*,5-dihydroxy diclofenac from 5-hydroxy diclofenac by CYPs depletes the cell of NADPH (Bort et al., 1999b). Furthermore, both diclofenac and *N*,5-dihydroxy diclofenac were shown to deplete ATP. The loss of both ATP and NADPH is detrimental to the cell since ATP is needed to generate NADPH as well as to drive a number of cellular functions. Under normal conditions, cells can replenish ATP in the mitochondria, however diclofenac disrupts mitochondrial function. It has been shown that diclofenac interferes with the mitochondrial permeability transition pore, allowing the pore to remain open for a longer duration leading to mitochondrial swelling and cell death (Gomez-Lechon et al., 2003b; Lim et al., 2006).

1.5.3 Intestinal Toxicity

It has been well established that therapeutic usage of NSAIDs is correlated with gastrointestinal injury. In a study of 1,800 subjects being treated for arthritis, ulceration and gastrointestinal lesions occurred in 24% and 37%, respectively, of the patient population (Geis et al., 1991). Just as for other NSAIDs, treatment with diclofenac is associated with gastrointestinal ADRs such as abdominal pain, bleeding, perforation, and ulceration (Novartis, 2011). Thomas et al. (2012) monitored 943 patients receiving diclofenac by prescription and noted that of the 561 ADRs, 267 (48%) were gastrointestinal in nature. Abdominal pain accounted for 19% with ulceration making up 6% of reported ADRs.

As a consequence of intestinal injury and to promote patient compliance, diclofenac can be prescribed as a combination treatment with misoprostol (Pfizer, 2014). Misoprostol is a synthetic PGE_1 analogue, and its therapeutic benefit is a result of activating EP receptors to stimulate the gastrointestinal secretion of bicarbonate and mucous (Karim and Gels, 1995). Administration of 0.2 mg misoprostol one to three times daily was effective in reducing the incidence of gastrointestinal ulcers after a twelve week treatment period (ulceration in 4.4% of patients receiving combination therapy vs. ulceration in 11% of subjects receiving diclofenac monotherapy (Verdickt et al., 1992). Another therapeutic benefit of misoprostol co-administration with diclofenac was a marked reduction in the number of patients experiencing abdominal pain, 19% vs. 70% for monotherapy (Agrawal et al., 1995). Thus, as a PGE_1 analogue, misoprostol is able to partially restore the prostaglandin-mediated protection that is otherwise attenuated following exposure to diclofenac.

The intestinal injury during diclofenac treatment is linked to the inhibition of COX enzymes by diclofenac. That diclofenac inhibits both COX enzymes is part of the pathogenesis in gastrointestinal ulcers (Tanaka et al., 2001; Sigthorsson et al., 2002). Emery et al. (1999) conducted a study in which patients with arthritis received either diclofenac or the selective COX-2 inhibitor celecoxib. Patients were followed for six months, and a subset was analyzed for gastrointestinal injury via endoscopy. Pharmacologically, both agents were effective in ameliorating inflammation and pain. A higher percentage of patients taking diclofenac experienced abdominal pain (21%) and developed gastrointestinal ulcers and/or erosions (45%) compared to the celecoxib group (11% for pain and 23% for ulcers/erosions). The higher incidence of diclofenac-induced gastrointestinal injury resulted in a withdrawal rate from therapy that was more than twice the withdrawal for celebrex (16% vs. 6%, respectively). Reanalysis of a separate study was somewhat contradictory in that celecoxib and diclofenac appeared to be comparable with respect to gastrointestinal injury (Silverstein et al., 2000; Juni et al., 2002). A possible explanation for the parity may be attributable to a higher dosage of celecoxib (800 mg) in the report by Silverstein et al. relative to the dose used in the study by Emery and colleagues (200 mg twice a day).

The degree of intestinal injury following exposure to diclofenac is partially dependent on the route of administration. For instance, in a study wherein diclofenac was administered either orally or via application to skin by gel, oral dosing resulted in 39% of subjects developing gastrointestinal ADRs whereas 25% of patients with topical skin application manifested gastrointestinal injury (Roth and Fuller, 2011). The withdrawal rate in the oral dosing group was 2.5-fold greater than the rate observed in the skin

application group. That gastrointestinal injury also occurred during topical application of diclofenac is indicative of a systemic effect for which the magnitude was enhanced after oral dosing due to the higher systemic concentration of diclofenac. As per the prescribing information for diclofenac topical gel, standard application of the gel (4 g gel, 4 times/day) results in a total daily dose of 160 mg with an average maximum plasma concentration of 0.015 ng/mL (0.051 µM) while an oral daily regimen of 150 mg (50 mg, 3 times/day) yields an average maximum plasma concentration of 2.27 µg/mL (7.67 µM) (Novartis, 2014). The lower maximum plasma concentration from topical application is consistent with what was determined for ketoprofen for which plasma concentrations following topical administration were 1% of the plasma concentrations following the nominal oral dose of 200 mg (Kneer et al., 2009).

Gastrointestinal injury following diclofenac administration has been demonstrated to occur in animal models of acute exposure. Rats given a single dose of diclofenac developed intestinal ulcers within 24 hours of administration (Atchison et al., 2000a; Atchison et al., 2000b). Sequestration of diclofenac with cholestryramine, which is therapeutically used to reduce bile reabsorption, decreased the incidence of gastric injury but not intestinal damage compared to diclofenac monotherapy in rats (Ramírez-Alcántara et al., 2005). It has been suggested that the reactive metabolites of diclofenac, specifically the acyl glucuronide, may be linked to induction of intestinal ulceration (Seitz and Boelsterli, 1998; Ware et al., 1998). The theory is that the glucuronide conjugate may compromise the integrity of the intestinal tract via covalent modification to enterocytes. An alternate hypothesis is that the acyl glucuronide undergoes cleavage to the aglycone parent compound, which is then able to induce

enteropathy. LoGuidice et al. (2012) demonstrated that chemical inhibition of β-glucuronidase decreased the number and size of ulcers in mice treated with diclofenac and inhibitor compared to mice that received only diclofenac. The intestinal injury observed both in animal models and human patients most likely involves contribution from both diclofenac and its acyl glucuronide. As such, one of the key themes of the research presented in this thesis is to further expand the probable mechanisms causing intestinal injury.

1.6 Summary

The work presented throughout this thesis focuses on the roles that BCRP, MRP3, and OATP2B1 may have in modulating the exposure of diclofenac and its primary metabolites. BCRP, OATP2B1, and MRP2 have been extensively studied for substrates evidenced by 247, 84, and 141 studies, respectively, as listed in the University of Washington (UW) *in vitro* Drug Interaction Database (UW, 1999-2015). In comparison, MRP3 is underrepresented with respect to literature reports having 23 unique citations in that same database (see Table 1.2). Though the UW repository may not contain all reported studies, its frequent update and breadth of data capture help to underscore the relative obscurity of MRP3 findings. In consideration of the lack of data regarding DCF elimination by transporters other than Mrp2, our initial investigations included Bcrp and Mrp3 as potential canalicular and basolateral mediators of DCF transporter-mediated clearance.

Our hypothesis was that deletion of Bcrp or Mrp3 would result in altered disposition of DCF or its metabolites. To assess the contribution of efflux transporters in DCF disposition, we utilized whole-body *in vivo* transporter knockout animal models and

administered a single low dose to mice. The doses used were presumed to be below the threshold that would induce tissue damage. Regardless of dose selection, a potential consequence of gene deletion is an upregulation of other genes as a compensatory response, a condition that may have potential ramifications for the overall design and anticipated outcome of our studies. For instance, rats that are missing Mrp2 via a spontaneous mutation were demonstrated to have induction of Mdr1 in brain but not liver (Hoffmann and Loscher, 2007). A similar situation can occur in humans. For example, in a subset of patients with acute myeloid leukemia there is deletion of one or both copies of MRP1, yet the overall MRP activity was found to be comparable to normal hematopoietic cells taken from healthy patients (van Der Kolk et al., 2000). The authors of that study speculate that upregulation of other efflux transporters was the reason. As it pertains to our study design, the mice used in our studies were not reported to have alterations in other efflux transporters such as Mrp2 (Manautou et al., 2005; Zelcer et al., 2005). Thus the results detailed in Chapter 2 reflect bona fide hepatic canalicular efflux of DCF and DCF-AG by Bcrp as well as basolateral efflux of DCF-AG by Mrp3.

Based on the results observed in Chapter 2, we focused our efforts on Mrp3 and further hypothesized that loss of Mrp3 would have a deleterious effect such that mice lacking Mrp3 would be more susceptible to liver and/or intestinal injury after a single toxic administration of DCF. The data in Chapter 3 support the claim that Mrp3 functions as an important protective mechanism against injury. Indeed, the presence of Mrp3 was able to attenuate the extent of intestinal injury after an acute toxic dose of DCF. Mice that lacked Mrp3 exhibited an increase in the incidence of injury, in terms of number of

erosions and ulcers, as well as severity of damage compared to wild-type mice. Strikingly, there was no evidence of hepatic injury in either wild-type mice or Mrp3 knockout mice. Although DCF is implicated in liver injury in humans, the potential for DCF-mediated hepatotoxicity was not readily apparent on an acute basis with the mouse models implemented in our studies. It is possible that hepatotoxicity caused by diclofenac manifests only after repeated dosing. Despite the null finding in liver, the intestinal toxicity was unequivocal and emphasizes the importance of Mrp3 as a vital clearance mechanism in the intestine.

Acyl glucuronides have low passive uptake (Zhou et al., 2005; Shackleford et al., 2006; Patel et al., 2013; Kimoto et al., 2015), therefore the uptake of DCF-AG into enterocytes would likely occur through active transport. Since glucuronide conjugates have been reported to be substrates of OATP2B1, a major intestinal uptake transporter, the uptake of DCF-AG was postulated to occur via OATP2B1. To test this theory, an *in vitro* system wherein OATP2B1 was stably transfected into human embryonic kidney (HEK) cells was utilized. HEK cells provide an advantage to study transporter activity in an overexpressed system as these cells have low to non-existent expression of many of the uptake and efflux transporters shown in Table 1.1 (Ahlin et al., 2009). The uptake of DCF-AG via OATP2B1 was quantified and determined to be saturable. A mouse homologue, Oatp2b1 (*Slco2b1*), likewise is expressed along the intestinal tract allowing for a reasonable argument that DCF-AG intestinal uptake in the mouse studies was mediated by Oatp2b1.

In prior sections, the intrinsic toxicity of DCF was detailed as was the reactivity of DCF-AG. Given the high biliary DCF-AG concentrations detected in the acute toxicokinetic

study, along with the apparent injury characterized in the Mrp3 knockout mice in the toxicodynamic study, it seemed plausible that DCF-AG was a direct mediator of the observed toxicity. Nonetheless, the manner by which DCF-AG causes toxicity is not wholly clear. Rather than focus on immunologic pathways, as suggested by those supporting a hapten hypothesis, that may or may not manifest in a mouse model, investigation into other causal mechanisms was considered. Furthermore, immune hypersensitivity would require multiple doses, which is not the case in our acute injury model.

We theorized that DCF-AG was cytotoxic, and used HEK cells to measure the extent of DCF-AG has on cell viability. The data in Chapter 4 provide evidence that DCF-AG is indeed cytotoxic, and that DCF-AG can induce cell death more so than DCF. The mechanism of the cytotoxicity was thought to occur through oxidative stress. Rationale for the oxidative stress hypothesis stems from the report that suprofen acyl glucuronide inhibited superoxide dismutase, an important component of antioxidant defense (Kakkar et al., 1984; Chiou et al., 1999; Fukui and Zhu, 2010). Subsequently, DCF-AG was analyzed for induction of oxidative stress by means of two distinct pathways. Not only was DCF-AG able to generate reactive oxygen species, but it also exhibited a dose-dependent inhibition of superoxide dismutase. Furthermore, DCF-AG was tested for inhibition of cyclooxygenase enzymes and found to inhibit both COX-1 and COX-2. As mentioned in the prior section, perturbation of COX metabolism of arachidonic acid renders the intestinal tract more susceptible to injury and diminishes the capacity for regeneration.

Inhibition of efflux of either cytoprotective or danger signals from stressed cells can interfere with cellular signaling and limit adaptive response to toxicants. PGE_2 is an important cytoprotective agent that was reported to be a substrate for MRP4 in addition to other MRP4 cellular signaling substrates such as cyclic nucleotides and steroid hormones (Reid et al., 2003b; Russel et al., 2008). Thus the final objective of current work was to assess the effect of analgesics and their respective metabolites on the function of MRP4. Further impetus for conducting MRP4 inhibition stems from two findings: 1) MRP4 protein expression is inducible following challenge by hepatotoxicants, and 2) the high concentrations of parent compound and metabolites after a toxic challenge. A listing of reported inhibitors of MRP4 can be found in Table 1.4 (Morrissey et al., 2012). Inhibition of MRP4, using leukotriene C4 as the substrate, was detected for DCF, DC-OH, and DCF-AG. Inhibition failed to surpass 50% up to 300 µM, therefore IC_{50} values could not be determined. Whereas DCF had low inhibition potency for MRP4 efflux of methotrexate, its inhibition potency for MRP4 efflux of leukotriene was decidedly weaker. The full significance of MRP4 inhibition as it pertains to a clinical setting remains to be determined.

In summary, the research presented throughout the thesis provides evidence on the complex interaction between efflux and uptake transporters. Specifically, OATP2B1 mediates the uptake of DCF-AG in an *in vitro* system, while the efflux of DCF-AG was characterized both *in vitro* using MRP3 vesicles as well as *in vivo* with a Mrp3 knockout mouse model. Perturbation of transporter activity, in the form of Mrp3 deletion, results in increased susceptibility to intestinal injury following a toxic DCF dose. *In vitro* assays showed that DCF-AG may have directly contributed to the intestinal enteropathy by

causing a state of oxidative stress vis-à-vis induction of reaction oxygen species in addition to inhibition of superoxide dismutase. Furthermore the pharmacological activity of DCF-AG against COX-1 and COX-2 may have promoted injury by attenuating the levels of cytoprotective prostaglandins. As it relates to the human condition, patients taking DCF who possess polymorphic MRP3 may be at risk for greater intestinal injury. At the very least, these data justify investigation of human MRP3 polymorphisms during the course of treatment with DCF or similar therapeutic agents that have reactive acyl glucuronides.

Figure 1.1 Structure and organization of human liver

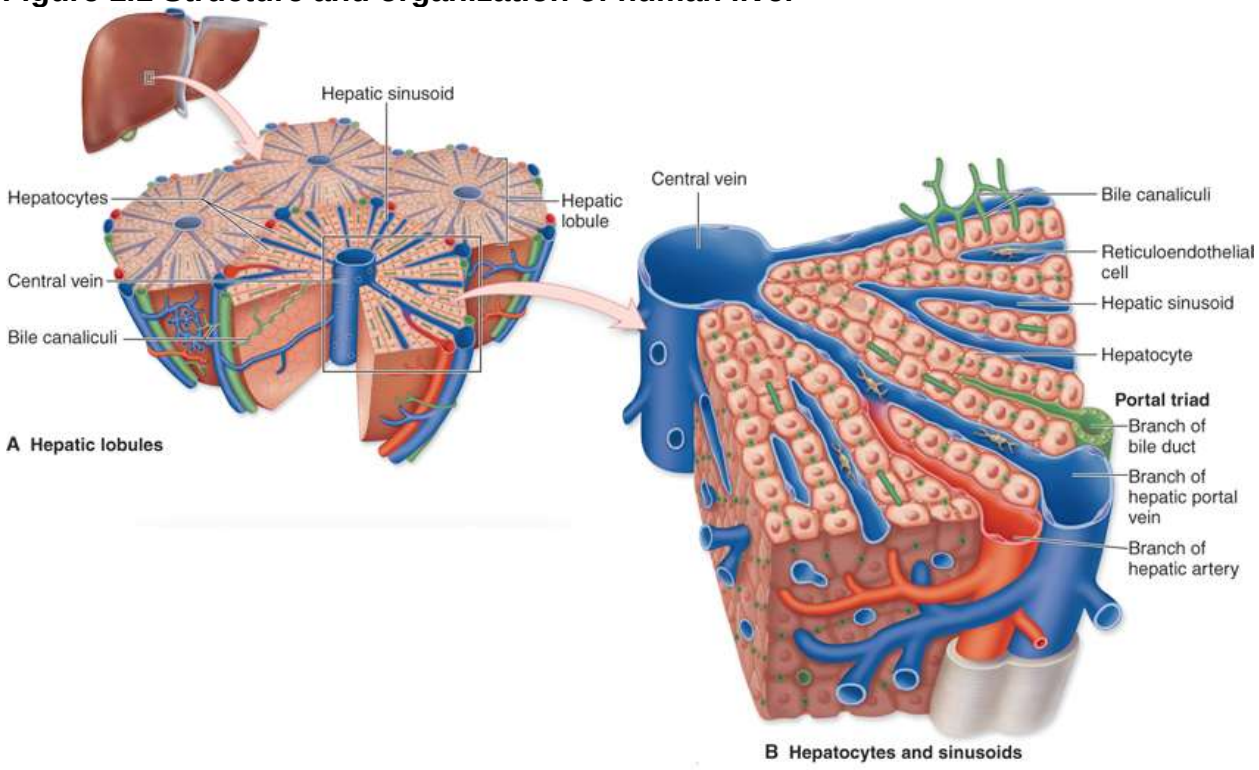

Source: Howard M. Reisner: *Pathology: A Modern Case Study.* 2015. McGraw-Hill Education. Reproduced with permission of McGraw-Hill Education.

Figure 1.1 Structure and organization of human liver.

Each lobe of the liver consists of lobules with a hexagonal appearance. The lobules are anatomically structured such that blood flows from portal triads at the periphery of the lobule toward the central vein in the middle of the lobule. In contrast bile flows from the central vein towards bile ducts in the portal triad. The majority of the lobule is populated with hepatocytes that are metabolically active.

Figure 1.2 Structure and organization of human small intestine

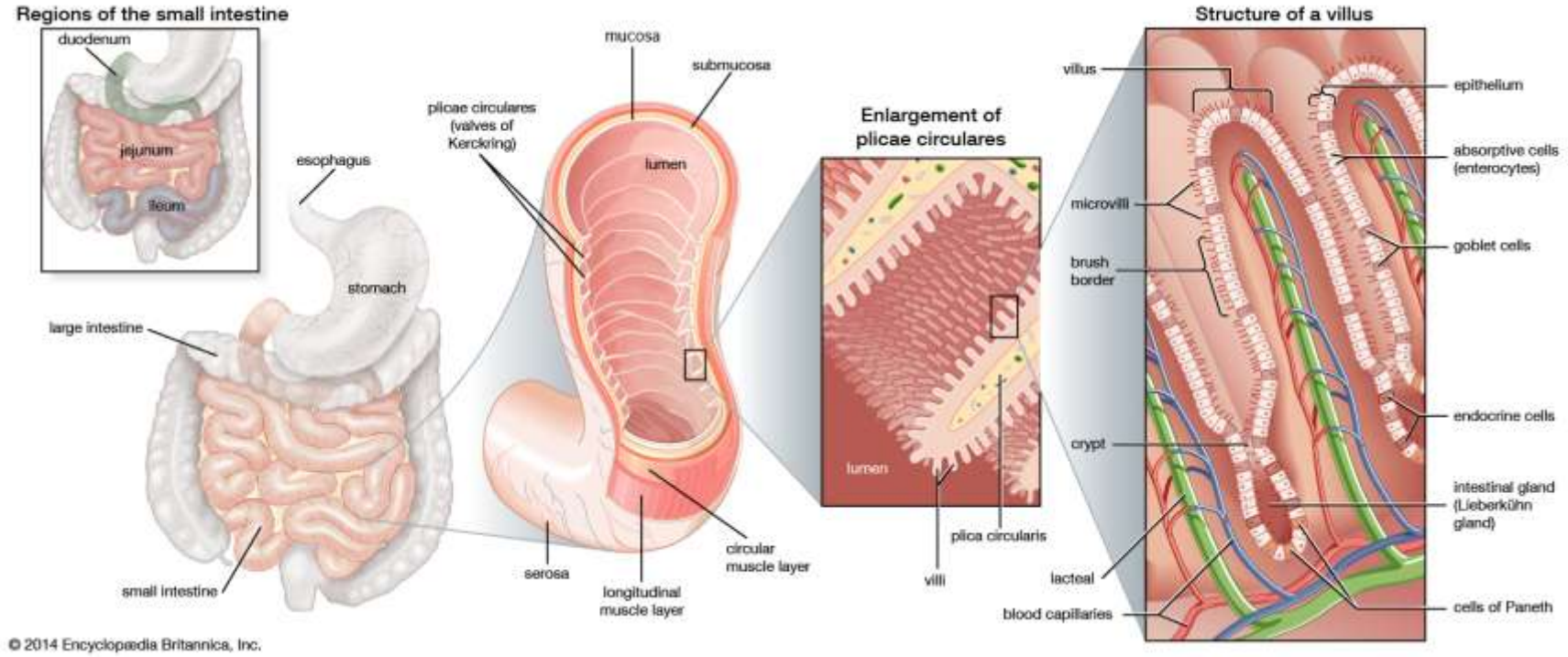

"small intestine: regions and structures". Art. Encyclopædia Britannica Online. Web. 27 Oct. 2015.

http://www.britannica.com/science/duodenum/images-videos/Structures-of-the-small-intestine-The-inner-wall-of-the/68637

Figure 1.2 Structure and organization of human small intestine.

The small intestine consists of three physically contiguous segments. Each segment has a hallow cavity called the lumen. The effective surface area within the lumen and magnified by folds termed plicae circulars that have fingerlike protrusions denoted as villi. The villi are comprised of a single layer of enterocytes. Substances that are taken up by the enterocytes from the lumen can be metabolized, transported back into the lumen, or excreted into the villus.

Table 1.1 Protein sequence homology of human efflux and uptake transporters involved in xenobiotic disposition

Gene (alias)	ABCC1 (MRP1)	ABCC2 (MRP2)	ABCC3 (MRP3)	ABCC4 (MRP4)	ABCC5 (MRP5)	ABCC6 (MRP6)	ABCC7 (CFTR)	ABCC8 (SUR1)	ABCC9 (SUR2)	ABCC10 (MRP7)	ABCC11 (MRP8)	ABCC12 (MRP9)	ABCC13 (MRP10)
ABCC1	100	48	57	38	42	45	31	33	34	35	33	33	35
ABCC2		100	46	36	43	38	31	31	32	34	33	34	32
ABCC3			100	35	39	43	30	33	34	36	33	32	34
ABCC4				100	42	33	37	32	32	33	34	34	25
ABCC5					100	37	30	31	31	39	41	45	-
ABCC6						100	31	31	30	33	30	31	30
ABCC7							100	32	31	30	28	30	-
ABCC8								100	67	31	29	29	-
ABCC9									100	31	29	28	-
ABCC10										100	31	34	-
ABCC11											100	48	-
ABCC12												100	-
ABCC13													100

Gene (alias)	ABCG1 (WHITE1)	ABCG2 (BCRP)	ABCG4 (WHITE2)	ABCG5 (Sterolin-1)	ABCG8 (Sterolin-2)
ABCG1	100	31	72	26	25
ABCG2		100	30	30	29
ABCG4			100	27	25
ABCG5				100	32
ABCG8					100

Gene (alias)	SLCO1A2 (OATP1A2)	SLCO1B1 (OATP1B1)	SLCO1B3 (OATP1B3)	SLCO1B7 (LST-3)	SLCO1C1 (OATP-F)	SLCO2A1 (PGT)	SLCO2B1 (OATP2B1)	SLCO3A1 (OATP-D)	SLCO4A1 (OATP-E)	SLCO4C1 (OATP-H)	SLCO5A1 (OATP-J)	SLCO6A1 (GST)
SLCO1A2	100	42	41	41	46	36	30	34	30	29	31	22
SLCO1B1		100	80	73	45	34	31	34	29	30	33	25
SLCO1B3			100	78	47	33	32	35	30	30	33	24
SLCO1B7				100	42	34	32	34	29	28	33	24
SLCO1C1					100	33	31	34	31	28	30	23
SLCO2A1						100	42	36	31	32	32	26
SLCO2B1							100	34	29	30	32	24
SLCO3A1								100	35	35	35	26
SLCO4A1									100	44	37	33
SLCO4C1										100	34	44
SLCO5A1											100	27
SLCO6A1												100

Table 1.1 Protein sequence homology of human efflux and uptake transporters involved in xenobiotic disposition. Homology of transporter proteins for each gene was determined with the online basic local alignment search tool (BLAST) using the wild-type amino acid sequence for every gene (http://blast.ncbi.nlm.nih.gov/Blast.cgi). Each number reflects the percentage of positive identification between two amino acid sequences. A "-" indicates homology could not be determined by the BLAST algorithm.

Table 1.2 Literature reports for MRP3 substrates using *in vitro* assays

Substrate	Therapeutic Category	K_m (μM)	V_{max} (pmol/min/mg)	V_{max}/K_m (μL/min/mg)	Comments	PubMed ID
7-hydroxycoumarin glucuronide	None (natural product)	187	460	2.46	-	22415933
Cefadroxil	Antibiotics	2500	600	0.24	-	22166395
Dehydroepiandrosterone sulfate	Androgens	46.3	281	6.07	MRP3 wild-type	15083066
Dehydroepiandrosterone sulfate	Androgens	34.6	269	7.77	MRP3 R1297H	15083066
E3040 glucuronide	None (metabolite of thromboxane inhibitor)	-	-	-	Substrate	19628752
Erythromycin	Antibiotics	-	-	-	Substrate	21451505
Estradiol-17β-glucuronide (E17βG)	Estrogens	9.1	116	12.7	-	24154606
E17βG	Estrogens	-	-	-	-	18698235
E17βG	Estrogens	24.2	71.5	2.95	MRP3 wild-type	15083066
E17βG	Estrogens	16	72.3	4.52	MRP3 R1297H	15083066
E17βG	Estrogens	-	-	-	Substrate	19628752
E17βG	Estrogens	-	-	-	Substrate	18245269
E17βG	Estrogens	-	-	-	Substrate	20360302
E17βG	Estrogens	56	2,220	39.6	-	21511945
Fexofenadine	H-1 Receptor Antagonists	-	-	-	Substrate	18245269
Gadolinium-ethoxybenzyl-diethylenetriamine pentaacetic acid	Diagnostic Agents	1800	116	0.1	-	24056116
Gemfibrozil glucuronide	Fibric Acid Derivatives	-	-	-	Substrate	19628752
Glutathione methylfluorescein	None (dye)	-	-	-	Substrate	17172311
Isoscutellarin	Food Products	-	-	-	Substrate	22822035
Leucovorin	Antidotes	-	-	-	Substrate	12874005
Leukotriene C4	None (metabolite of arachidonic acid)	-	-	-	MRP3 wild-type	15083066
Scutellarin	Herbal Medications	-	-	-	Substrate	22822035
Troglitazone glucuronide	Thiazolidinediones	-	-	-	Substrate	19628752

R1297H: arginine substituted for histidine at amino acid position 1297

Table adapted from http://didb.druginteractioninfo.org

Table 1.3 Case studies of hepatotoxicity from diclofenac usage

Gender	Age (years)	Dose Regimen Duration	ALT (U/L)	ALkP (U/L)	R value	Status	Reference
F	55	N/A N/A 2 weeks	937	466	6	Jaundice, Death	(Lascar et al., 1984)
M	56	100 mg QD 5 weeks	2,110	321	20	Jaundice, Death	(Breen et al., 1986)
F	21	200 mg QD 14 days	1,113	269	12	Jaundice, Death	(Snijder et al., 1987)
M	45	75 mg BID 3 months	922	213	12	Recovery (DCF stopped)	(Helfgott et al., 1990)
F	54	75 mg BID 6 weeks	763	186	12	Recovery (DCF stopped)	(Helfgott et al., 1990)
F	83	50 mg TID 9 days	314	230	4	Jaundice, Recovery (DCF stopped)	(Nezic et al., 2012)
F	60	50 mg TID 88 days	1,829	168	31	Jaundice, Recovery (DCF stopped)	(LiverTox, 2015)
F	60	N/A N/A 46 days	1,895	303	18	Jaundice, Death[1]	(Chalasani et al., 2015)
10F/2M	50 (15)	N/A N/A 83 days	1,266 (680)	222 (100)	16 est.	11 recoveries, 1 death[1]	Chalasani et al., 2015)

Abbreviations: BID – two times a day, est – estimate, F – female, M – male, N/A – not available, QD – once a day, TID – three times a day. Values in parentheses represent standard deviation
[1]: indicates same subject

Table 1.4 Reported *in vitro* inhibition of MRP4 using inside-out vesicles

Inhibitor	Substrate	IC_{50} (μM)	PubMed ID
Benzbromarone	9-(2-phosphonomethoxyethyl)adenine (PMEA)	150	12695538
Candesartan	Uric acid	16	17674156
Celecoxib	Methotrexate	35	17005917
Diclofenac	Methotrexate	0.006	17005917
Dilazep	PMEA	20	12695538
Dipyridamole	PMEA	2	12695538
Dipyridamole	Cholyltaurine	<20	12883481
Indomethacin	Methotrexate	6.1	17005917
Ketoprofen	Methotrexate	11.9	17005917
Losartan	Uric acid	1.5	17674156
MK-571	PMEA	10	12695538
MK-571	Cholyltaurine	~2	12695538
Nitrobenzylmercaptopurine riboside	PMEA	75	12695538
Probenecid	PMEA	2,300	12695538
Probenecid	Cholyltaurine	~100	12695538
Probenecid	Cyclic GMP	<100	11856762
Sildenafil	PMEA	20	12695538
Sulfinpyrazone	PMEA	420	12695538
Sulindac	Methotrexate	2.11	17005917
Telmisartan	Uric acid	11	17674156
Trequinsin	PMEA	10	12695538
Zaprinast	PMEA	250	12695538

Table adapted from http://dbts.ucsf.edu/fdatransportal

Chapter 2 IDENTIFICATION AND CHARACTERIZATION OF EFFLUX TRANSPORTERS THAT MODULATE THE DISPOSITION OF DICLOFENAC AND ITS METABOLITES AT SUBTOXIC DOSES USING WHOLE-BODY TRANSPORTER KNOCKOUT MODELS

2.1 Abstract

In the present work, *in vivo* transporter knockout (KO) mouse models were used to characterize the pharmacokinetics of diclofenac (DCF) and the disposition of its primary metabolites following a single sub-toxic dose. Mice that were lacking breast cancer resistance protein (Bcrp) or multidrug resistance-associated protein (Mrp)3 were administered 3 or 10 mg DCF by intraarterial injection and compared to a wild-type (WT) strain of similar background. The results indicated that Bcrp acts a canalicular efflux mediator for DCF as WT mice had biliary excretion values that were 2.2- to 2.6-fold greater than Bcrp KO mice. Bcrp deletion did not affect the basolateral efflux of DCF. Furthermore, diclofenac acyl glucuronide (DCF-AG) was found to be a substrate of Bcrp, and the loss of Bcrp caused DCF-AG plasma levels to increase 1.8- to 3.2-fold in KO animals compared to WT. In addition, the biliary excretion of DCF-AG increased by 1.4-fold in WT versus KO. Furthermore, Mrp3 was found to mediate the basolateral transport of DCF-AG, but not DCF nor 4'-hydroxy diclofenac (OH-DCF). WT mice had DCF-AG plasma concentrations that were 7.0- to 8.6-fold greater compared to Mrp3 KO animals, however no change in DCF-AG biliary excretion was observed. The *in vivo* mouse data were further supported by *in vitro* studies. Vesicular transport experiments with human MRP3 demonstrated that MRP3 is able to transport DCF-AG. The data suggest that MRP3 has both a low and high affinity binding site. The low affinity MRP3

transport had a V_{max} and K_m of 170 pmol/min/mg and 98.2 µM, respectively. The high affinity MRP3 V_{max} and K_m parameters were estimated to be 71.9 pmol/min/mg and 1.78 µM, respectively. In summary, we offer evidence that the disposition of DCF-AG can be affected by both Bcrp and Mrp3, and these findings may be applicable to humans.

2.2 Introduction

The non-steroidal anti-inflammatory drug diclofenac (DCF) has been used for a number of years to treat arthritis and for pain management. Its primary mechanism of action is to block the metabolism of arachidonic acid by cyclooxygenase enzymes (COX) into pro-inflammatory mediators, and it is known that DCF can inhibit both COX-1 and COX-2 (Menasse et al., 1978). The pharmacokinetics of DCF has been extensively characterized in animal and human models. In humans receiving either an intravenous or oral dose, DCF administration resulted in 65% of dosage excretion in the urine with the remaining 35% eliminated in feces (Riess et al., 1978). Conversely, elimination of DCF in dogs and rats was reversed with 65% elimination in feces and 35% in urine. The percentage contributions were determined using radiometric analysis, a sensitive method that permits accurate mass balance assessment.

The metabolic profile of DCF has likewise been carefully profiled, and only a small portion of DCF is eliminated as unchanged parent compound (Stierlin and Faigle, 1979; Stierlin et al., 1979). DCF is metabolized *in vivo* into a variety of hydroxylated and conjugated metabolites (Bort et al., 1999a; Tang et al., 1999; King et al., 2001; Kenny et al., 2004). Using *in vitro* assays, a multitude of major and minor metabolites have also been detected, and most of their structures have been elucidated (Pickup et al., 2012; Sarda et al., 2012). Though DCF is normally given orally, it has excellent physicochemical qualities resulting in nearly 100% dose absorption. This is due in part to the high passive uptake that DCF possess, categorizing it as an ECCS class 1B compound (Varma et al., 2015). The complete absorption leads to a large fraction of the dose entering portal circulation from which there is extensive partitioning of DCF into

the liver. Upon entering hepatic cells, primarily hepatocytes, DCF is subjected to multiple clearance pathways. Since the Phase I and Phase II enzymes that metabolize DCF have been characterized, there is a need to better understand which transporters contribute to DCF clearance.

The liver is host to a variety uptake and efflux transporters, many of which are exclusively localized to either the basolateral membrane or the (apical) canalicular domain (Giacomini et al., 2010). Uptake transporters are expressed on the basolateral membrane and modulate the transport of endogenous as well as xenobiotic compounds from blood into the liver. Furthermore, the basolateral membrane is host to an array of efflux transporters that translocate intracellular substrates into hepatic sinusoidal space. Efflux transporters are also expressed on the canalicular domains and serve to excrete their substrates into the bile canaliculi whereupon biliary flow carries the substrates into the common bile duct, which ultimately terminates into the duodenal region of the small intestine. The interplay of these transporters can result in extensive elimination and reuptake of substances, prolonging their residence time in the body (Roberts et al., 2002).

The efflux transporters have broad substrate affinity. The multidrug resistance-associated proteins (MRPs, encoded by *ABCC* genes) transport endogenous substances such as organic anions, bile salts, glutathione, and steroids as well as xenobiotics and their conjugated metabolites. For example, MRP3 (*ABCC3*) was observed to transport acetaminophen glucuronide, estradiol-17β-glucuronide, leukotriene C4, and morphine-3-glucuronide (Hirohashi et al., 1999; Manautou et al., 2005; Zelcer et al., 2005). BCRP (*ABCG2*) has substrates such as estrone-3-sulfate,

methotrexate, and SN-38 that is the pharmacologically active metabolite of irinotecan (Kawabata et al., 2001; Vlaming et al., 2009a). MRP2 (*ABCC2*) overlaps with the aforementioned transporters and can mediate the excretion of pravastatin, carboxydichlorofluorescein as well as 4-methylumbelliferone conjugated metabolites (Zamek-Gliszczynski et al., 2006a; Elsby et al., 2011).

The rat homologue of MRP2 was determined, using mutant rats that lack Mrp2, to modulate the elimination of DCF-AG from the liver into bile (Seitz et al., 1998). The finding was particularly impactful as it was one of the first reports to ascribe the importance of transporters in mediating toxicity from DCF exposure. In that study, rats lacking Mrp2 had significantly lower intestinal injury compared to rats with functional Mrp2. Thus, exploration of other efflux transporters that may have affinity for DCF or its metabolites is warranted in order to enhance understanding of how transporter clearance can modulate toxicity after DCF administration.

The purpose of the current work was to identify other efflux transporters that are responsible for mediating the disposition of either DCF or its primary metabolites. To accomplish this goal, mouse transporter knockout models in which either Bcrp or Mrp3 were genetically deleted were utilized. The selection of Bcrp and Mrp3 would allow insight into how a major canalicular (in addition to Mrp2) or basolateral transporter, respectively, can potentially impact the dispositional profile of DCF or its conjugated metabolites. Furthermore, the affinity of DCF and its metabolites for human MRP3 was also investigated via *in vitro* assays with commercial vesicles.

2.3 Materials and Methods

Chemicals and Reagents. Alamethecin, AMP, ATP, DCF, formic acid, indomethacin (used as the IS), KCl, $MgCl_2$, MOPS, NADPH, OH-DCF, Tris-HCl, and UDPGA were purchased from Sigma-Aldrich Corporation (St. Louis, MO). DCF-AG was purchased from Toronto Research Chemicals Incorporated (Toronto, Canada). Solutol® HS 15 was provided by the BASF Corporation (Florham Park, NJ). MRP2 and MRP3 vesicles were purchased from GenoMembrane Corporation (Kanazawa, Japan). All LC/MS/MS solvents were of high analytical grade and were purchased from Burdick & Jackson (Muskegon, MI).

Animals. Mrp3-null mice of FVB 129/Ola background were provided by Dr. Piet Borst (Netherlands Cancer Institute, Amsterdam, Netherlands). Bcrp-null mice having C57BL/6 background were generated at the University of Kansas Medical Center. Mice were housed in an American Animal Associations Laboratory Animal Care accredited facility of University of Kansas Medical Center under a standard temperature-, light-, and humidity-controlled environment. Mice had free access to Laboratory Rodent Chow 8604 (Harlan, Madison, WI) and drinking water. All animal studies were performed in accordance with the Guide for the Care and Use of Laboratory Animals using protocols reviewed and approved by the local Institutional Animal Care and Use Committee of University of Kansas Medical Center (Kansas City, KS).

***In Vivo* Studies.** Male 2-4 month old FVB 129/Ola WT, FVB 129/Ola Mrp3 KO, C57BL/6 WT, and C57BL/6 Bcrp KO mice were anesthetized intraperitoneally with a ketamine/midazolam mixture (100 and 5 mg/kg, respectively), and both the right carotid artery and the common bile duct were cannulated for sample collection. The mice

received a single intraarterial dose of 3 or 10 mg/kg DCF in 10:90 (v/v) Solutol HS 15:0.9% saline at a dosing volume of 10 mL/kg. Bile flow was monitored, and bile fractions were collected in fifteen minute intervals from -15 to 0, 0 to 15, 15 to 30, 30 to 45, 45 to 60, 60 to 75, and 75 to 90 minutes post administration. Blood samples were collected into heparinized tubes at 2, 7.5, 22.5, 37.5, 52.5, 67.5, and 90 minutes after administration, and the blood was subsequently centrifuged to yield plasma. The volumes of bile were determined gravimetrically, using 1.0 for specific gravity. Both bile and plasma were stored at -20 °C until analysis. At the conclusion of the study (90 min post-administration), animals were sacrificed by overdose with ketamine and midazolam. Livers were harvested and quickly frozen in liquid nitrogen prior to storage at -80 °C.

Bioanalytical Analysis. Bile and plasma were diluted with 0.1% formic acid in water (Solvent A) for LC/MS/MS detection as well as to stabilize DCF-AG. Liver samples were homogenized by bead milling using Solvent A. A 50 µL aliquot of diluted biological matrix was then precipitated with 400 µL of 0.1% formic acid in acetonitrile (Solvent B) containing IS. Standard curves using naïve matrices were prepared in a similar fashion. Samples and standards were vigorously vortex-mixed and centrifuged at 1000 × *g* for 15 min and 5 °C. A 200 µL aliquot of supernatant was removed and evaporated under Nitrogen gas at 45 °C. The resulting residue was reconstituted with 200 µL of 90:10 (v/v) A:B, vigorously vortex-mixed, and centrifuged prior to injection onto LC/MS/MS. The injection volume for all sample types was 10 µL.

***In Vitro* Metabolism.** Untreated livers from three male FVB (WT & KO) and C57 (WT & KO) mice were homogenized using a Dounce Teflon homogenizer in ice-cold Tris-HCL buffer (50 mM Tris, 15.4 mM KCl, 2 mM EDTA) in a ratio of 4 parts buffer to 1 part liver.

The homogenate was centrifuged at 9,000 × *g* for 30 min and 4 °C, and the S9 supernatant fraction was removed, separated into aliquots, and kept frozen at -80°C. The S9 fraction was analyzed for protein content using a Pierce BCA kit (Thermo Fisher Scientific Inc., Grand Island, NY) following the manufacturer's recommendations. Incubation reactions were conducted in duplicate in the presence of increasing DCF concentrations. The reaction mixture consisted of DCF, 0.1 M phosphate buffer pH 7.4 at 37 °C, 1 mg/mL S9 protein, 10 µg/mL Alamethacin, 1 mM GSH, 5 mM $MgCl_2$, 1 mM NADPH, and 1 mM UDPGA. Incubations without cofactors ($MgCl_2$, NADPH, UDPGA) served as the control. The total incubation volume was 300 µL, and the reaction mixture was open to air. Aliquots of 50 µL were taken at 0, 7.5, 15, 30, and 45 min, immediately quenched with 200 µL ice-cold Solvent B, and kept on ice. At the end of the experiment, samples were mixed with 50 µL IS, and 200 µL of the mixture was removed to be evaporated to dryness under N_2 at 40 °C. The resulting residue was reconstituted in 200 µL of 90:10 (v/v) solvents A:B, vigorously vortex-mixed, and injected onto the LC/MS/MS. The samples were monitored for the disappearance of DCF. The LC/MS/MS response (DCF peak area/IS peak area) was converted to percentage remaining with 0 min serving as 100%. All percentage values were log transformed and plotted against incubation time to yield an elimination rate (k) that was derived from the slope of the resulting line. The elimination rate was converted into an apparent half-life using the formula:

Equation 2.1

$$t_{1/2} = \frac{ln(2)}{-k}$$

The initial enzyme velocity was calculated using the equation:

Equation 2.2

$$v_0 = ln(2) \times \frac{1}{t_{1/2}(min)} \times [S] \times \frac{mL\ incubation}{mg\ of\ S9\ protein}$$

where v_0 is expressed as pmol/min/min and [S] is the DCF substrate concentration in µM. The kinetic parameters of K_m and V_{max} were then calculated by plotting v_0 as a function of [S].

***In Vitro* Transport.** Commercially available MRP2 and MRP3 inside-out vesicles were quickly thawed from storage and placed on ice. Incubation reactions consisted of uptake buffer at pH 7.0 (50 mM MOPS-Tris, 70 mM KCl, and 7.5 mM $MgCl_2$), 25 µg vesicle protein, 5 mm of AMP or ATP, and 2.5 mM GSH. After a 5 min pre-incubation period of reaction mixture, incubations were commenced by addition of increasing concentrations of DCF-AG. Incubations were conducted at 37 °C in a total volume of 75 µL. Reactions were quenched by the addition of 100 µL ice-cold stopping buffer (40 mM MOPS-Tris and 70 mM KCl), and the quenched mixtures were quickly transferred to a 96-well glass-fiber filter plate (EMD Millipore, Billerica, MA). The filter plate was subjected to vacuum filtration followed by 5 rapid washes of 100 µL/well ice-cold stopping buffer. The filter plate was allowed to completely dry before extraction of samples. DCF-AG was extracted by filling each well of the filter plate with 200 µL of 80:20 (v/v) methanol:0.1% formic acid in water. Plates were shaken for 15 min on ice, and the filtrate was collected via centrifugation at 3,000 × *g* for 10 min and 4 °C. The filtrate was evaporated to dryness under warm N_2 at 40 °C. The resulting residue was reconstituted with 200 µL of 90:10 (v/v) solvents A:B, vigorously vortex-mixed, and injected onto the LC/MS/MS. The accumulation of DCF-AG was quantified against a

standard curve, and the uptake data were expressed as pmol normalized to mg vesicle protein.

LC/MS/MS Method. Chromatographic separation of analytes was performed on a Synergi™ 4 µm Max-RP 50 × 2 mm column (Phenomenex Incorporated, Torrance, CA). The system front end consisted of a HTC PAL Autosampler (LEAP Technologies Incorporated, Carrboro, NC), a SCL-10Avp system controller, two LC10ADvp pumps, and a DGU-14A degasser (Shimadzu Scientific Instruments, Columbia, MD). Analytes of interest were eluted using a gradient profile that began with 10% solvent B for the first 1.0 min, which was then increased to 90% solvent B at 3.5 min using a linear gradient and held at this mixture for 0.5 min before reverting back to initial solvent conditions for 1.0 min to re-equilibrate the column. The flow rate was 0.4 mL/min, and the column effluent was directed to waste for the initial 1.5 min before switching to the mass spectrometer. Analytes were detected using an AB Sciex API™ 4000 LC/MS/MS triple quad mass-spectrometer with a TurboIonSpray® probe and Analyst version 1.4.2 software (AB Sciex, Framingham, MA) that was operated in multiple reaction monitoring mode. Ion spray voltage was -4250 V, and the source temperature was set to 400 °C. The mass transitions in negative ion mode for monitoring DCF, OH-DCF, DCF-AG, and indomethacin were *m/z* 294.0→249.9, 309.9→265.9, 470.1→192.9, and 356.0→311.8, respectively. The retention times of DCF, OH-DCF, DCF-AG, and indomethacin were 3.25, 2.84, 2.69, and 3.20 min, respectively. Concentrations of analytes in the samples were determined by comparing the peak area ratios (analyte/IS) to those in the standard curve using a linear regression model. The criterion of acceptance for standards was defined to be ±20% of nominal concentration.

Statistical Analysis. Data are expressed as mean ± standard error of the mean. *P* values $\leq$ 0.05 were considered as statistically significant. Statistical analysis of data was performed using R version 3.2.1 (R Core Team, 2015). Two groups were compared by Student's *t* test, and multiple groups were compared by an analysis of variance followed by Tukey's *post hoc* test. GraphPad Prism version 6.0 (GraphPad Software Incorporated, La Jolla, CA) was used to calculate kinetic parameters (V_{max} and K_m).

2.4 Results

***In Vivo* Studies**. Plasma concentrations of DCF and OH-DCF in C57 WT and C57 Bcrp KO mice receiving 3 mg/kg DCF were nearly equal (Figure 2.1A-B), whereas KO animals had on average 1.8-fold higher DCF-AG plasma levels compared to WT (Figure 2.1C). Biliary excretion for DCF was 2.2-fold higher in WT animals relative to KO (Figure 2.1D) with statistical significance observed at each time interval. OH-DCF biliary levels were relatively unchanged between WT and KO (Figure 2.1E) though DCF-AG biliary WT concentrations were 1.4-fold greater than KO at 90 min, and the difference was statistically significant (Figure 2.1F). The trends observed at the 3 mg/kg dose were also evident following 10 mg/kg DCF administration. DCF and OH-DCF plasma concentrations were approximately equal in WT and KO (Figure 2.2A-B), while DCF-AG KO plasma levels were increased 3.2-fold compared to WT (Figure 2.3C). DCF WT biliary excretion was higher by 2.6-fold compared to KO (Figure 2.2D). From 60 min and beyond, biliary OH-DCF and DCF-AG WT levels were elevated by 1.3- and 1.4-fold, respectively, versus KO animals. Analysis of whole liver collected 90 min after 3 or 10 mg/kg DCF showed no significant differences between WT and KO for DCF or OH-DCF while DCF-AG was not detected in the samples (Figure 2.3A-C).

The plasma concentrations of DCF and its metabolites in FVB WT and FVB Mrp3 KO animals are shown in Figure 2.4 and Figure 2.5. At the 3 mg/kg dose, the overall data showed little statistical significance between WT and KO plasma concentrations for DCF and OH-DCF (Figure 2.4A-B). Strikingly, there was nearly an 8.6-fold increase in DCF-AG WT plasma levels versus that of KO animals (Figure 2.4C). With regards to biliary excretion, all three analytes had similar concentrations between WT and KO

subjects (Figure 2.4D-F). The 10 mg/kg data for the FVB mice exhibited comparable trends for the plasma profiles of DCF and OH-DCF (Figure 2.4A-B). WT plasma DCF-AG was greater than KO by 7.0-fold (Figure 2.4C). Biliary levels of DCF, OH-DCF, and DCF-AG were unremarkable between WT and KO after a 10 mg/kg dose (Figure 2.4D-F) though OH-DF began to show a slight increase in KO biliary output relative to WT. Liver concentrations were determined 90 min post-administration and were not found to be statistically different between genotypes for each analyte, which was true for both the 3 mg/kg and 10 mg/kg doses (Figure 2.5A-B).

The pharmacokinetics of DCF at each dose for all genotypes is summarized in Table 2.1. The parameters listed in the table were calculated using non-compartmental analysis. The data show that the relative half-lives of DCF at each dose for each genotype were comparable with the exception of the 10 mg/kg Mrp3 KO mice that had a $t_{1/2}$ of 52.9 ± 9.8 min, which was slightly elevated compared to the rest of the dosing groups. The overall exposure of DCF, as assessed by $AUC_{0\text{-tlast}}$ normalized by dose, further demonstrated that the absorption and distribution of DCF were fairly alike.

Metabolite Identification. In order to account for metabolism of DCF that extended beyond generation of OH-DCF and DCF-AG, WT and Mrp3 KO bile were pooled from a number of animals, extracted with organic solvent, and infused onto the LC/MS. Spectra from 100 amu to 1000 amu were acquired in both positive ion and negative ion mode and compared between genotypes. The WT spectra were subtracted from KO spectra, and the resulting signals were analyzed for traces of DCF metabolites. As shown in Figure 2.7, several metabolites possessing an isotopic distribution similar to DCF were identified (for reference, DCF-AG is shown in Figure 2.7C). The masses of

the primary peaks were compared using MetabolitePilot software (Framingham, MA, CA). Structures of the proposed biliary metabolites are shown in Figure 2.8. M1 and M2 are the hydroxylated metabolites, while M3 is DCF-AG. M4 is positively identified, based on product ion fragmentation, as OH-DCF-AG (Figure 2.7D). M6, a taurine conjugate, corresponds to the peak shown in Figure 2.7A. M7, an S-cysteine conjugate, matches the profile observed in Figure 2.7B. M9, a dihydroxylated glutathione adduct, is putatively identified as the peak shown in Figure 2.7F. The structure of M9, for which the profile is indicated by Figure 2.7E, is uncertain as its mass does not match up to typical combinations.

In Vitro **Metabolism**. To determine if the different strains of mice have similar metabolic capacity, S9 fraction was generated by pooling naïve liver homogenates from several WT or KO mice. S9 was chosen for metabolic studies to afford a system capable of multiple biotransformation pathways (Wu and McKown, 2004). The range of DCF was selected to cover the plasma concentrations that were observed in the *in vivo* studies. Conditions for the assay were based on the work by Fisher et al. (2000) in order to promote Phase II metabolism. Incubations conducted in the presence of cofactors (e.g., GSH and UPDGA) required for Phase II metabolism showed that the background-matched strains (e.g., C57 WT and C57 Bcrp KO) had indistinguishable profiles (Figure 2.9A-B). The metabolic data were analyzed to determine relevant kinetic parameters, and these values are summarized in Table 2.2. C57 WT and Bcrp KO mice had apparent V_{max} values of 846 ± 31 and 882 ± 26 pmol/min/mg, respectively, while the K_m values were 69.3 ± 4.3 and 82.4 ± 1.1 µM, respectively. Likewise, the V_{max} data for FVB WT and Mrp3 KO mice were 734 ± 32 and 696 ± 79 pmol/min/mg,

respectively, and the K_m parameters were determined to be 44.3 ± 3.5 and 43.3 ± 9.0 µM, respectively. From the V_{max} and K_m data, the intrinsic metabolic clearances were calculated with the equation:

Equation 2.3

$$CL_{int} = \frac{V_{max}}{K_m}$$

The resulting CL_{int} for C57 WT and Bcrp KO were 12.2 and 10.7 µL/min/kg, respectively, while those for FVB WT and Mrp3 KO were 16.7 and 16.4 µL/min/mg, respectively.

***In Vitro* Transport**. With the mouse models showing evidence that Mrp3 can mediate the efflux of DCF-AG *in vivo*, the next objective was to determine the extent by which DCF-AG interacts with human MRP3. As rodent Mrp2 was previously shown to modulate DCF-AG toxicity (Seitz et al., 1998), human MRP2 was also examined for DCF-AG affinity. MRP2 and MRP3 inside-out vesicles were assessed for DCF-AG transport, and it was determined that uptake was linear for several minutes before reaching an apparent plateau (Figure 2.10A-B). The uptake of DCF-AG with MRP2 and MRP3 was found to be ATP- and time-dependent. Having established an optimal incubation time for further studies, vesicles were incubated for 5 min in the presence of increasing DCF-AG concentrations. The concentration-dependent uptake by MRP2 and MRP3 was determined to be saturable (Figure 2.11A-B). The Eadie-Hofstee plot for MRP2 uptake suggests an allosteric sigmoidal interaction, hence the ATP-dependent data were fit using this model. MRP3 uptake of DCF-AG, when graphed using an Eadie-Hofstee plot, indicated a biphasic profile. Therefore, MRP3 data was fit using a two K_m model. The results of the model outputs for MRP2 and MRP3 are summarized in Table 2.3. The V_{max} and K_m for MRP2 vesicular uptake of DCF-AG were determined

to be 130 pmol/min/mg and 50.5 µM, respectively, yielding a transporter intrinsic clearance (using Equation 2.3) of 2.58 µL/min/mg. Analysis of MRP3 kinetics led to identification of a possible low affinity and high affinity binding site for DCF-AG transport. The low affinity V_{max} and K_m for MRP3 were 170 pmol/min/mg and 98.2 µM, respectively, with a transporter clearance of 2.37 µL/min/mg for the low affinity site. The high affinity V_{max} and K_m parameters were estimated to be 71.9 pmol/min/mg and 1.78 µM, respectively, and the high affinity transporter clearance was calculated to be 40.3 µL/min/mg.

Figure 2.1 Plasma and biliary concentration versus time profiles of DCF, OH-DCF, and DCF-AG in C57 WT and C57 Bcrp KO mice after 3 mg/kg DCF dose

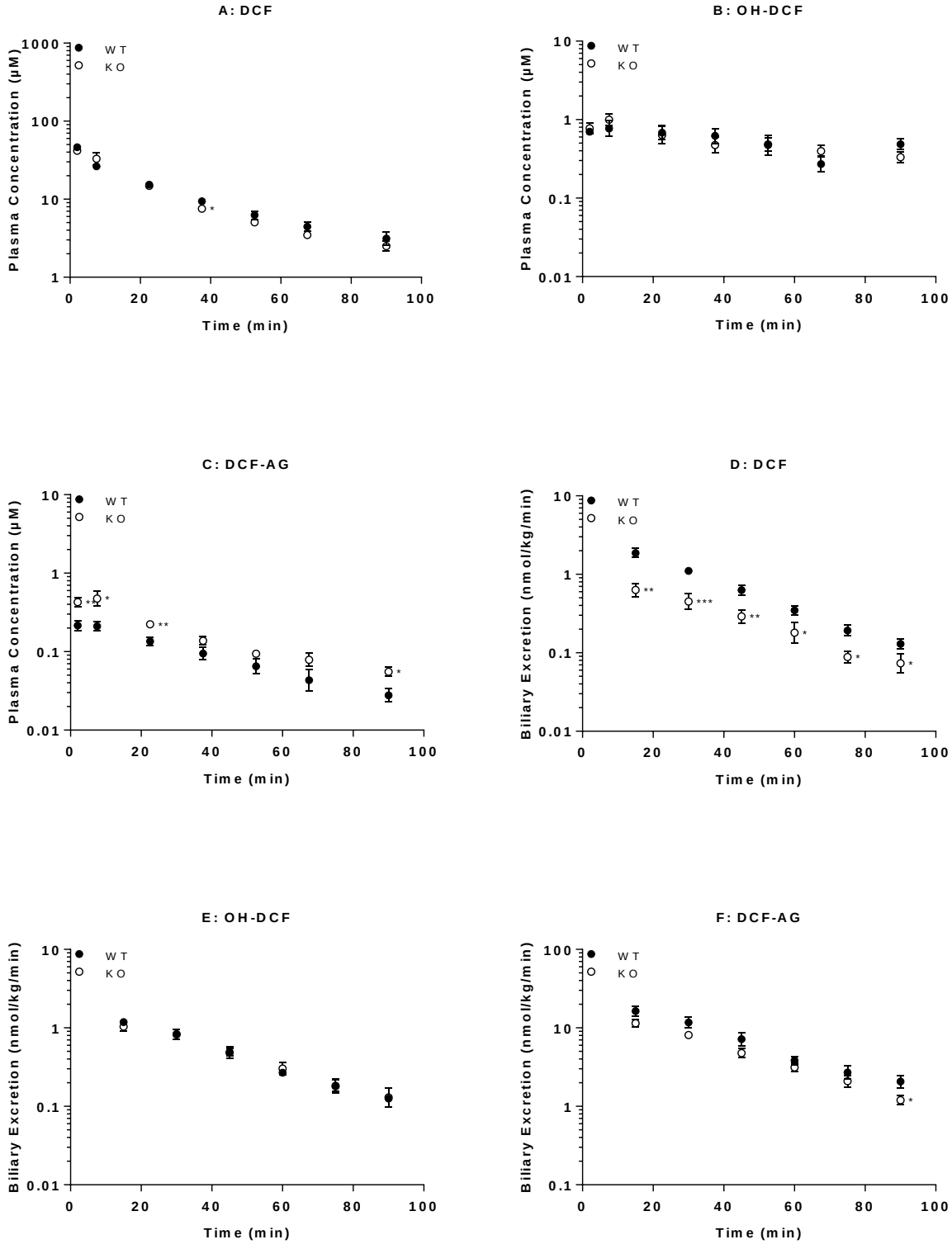

Figure 2.1 Plasma and biliary concentration versus time profiles of DCF, OH-DCF, and DCF-AG in C57 WT and C57 Bcrp KO mice after 3 mg/kg DCF dose. Pharmacokinetics of DCF and its metabolites in WT (○) and Bcrp KO (●) mice after a single intraarterial dose of 3 mg/kg DCF. (A-C) Plasma concentration profiles for (A) DCF, (B) OH-DCF, and (C) DCF-AG at discrete time points. (D-F) Biliary excretion profiles for (D) DCF, (E) OH-DCF, and (F) DCF-AG. Time points represent accumulation of biliary flow during successive 15 min intervals (0-15, 15-30, 30-45, 45-60, 60-75, and 75-90 min). All data are expressed as mean ± standard error of the mean for 5-6 subjects/group. * $P < 0.05$; ** $P < 0.01$; *** $P < 0.001$ versus WT.

Figure 2.2 Plasma and biliary concentration versus time profiles of DCF, OH-DCF, and DCF-AG in C57 WT and C57 Bcrp KO mice after 10 mg/kg DCF dose

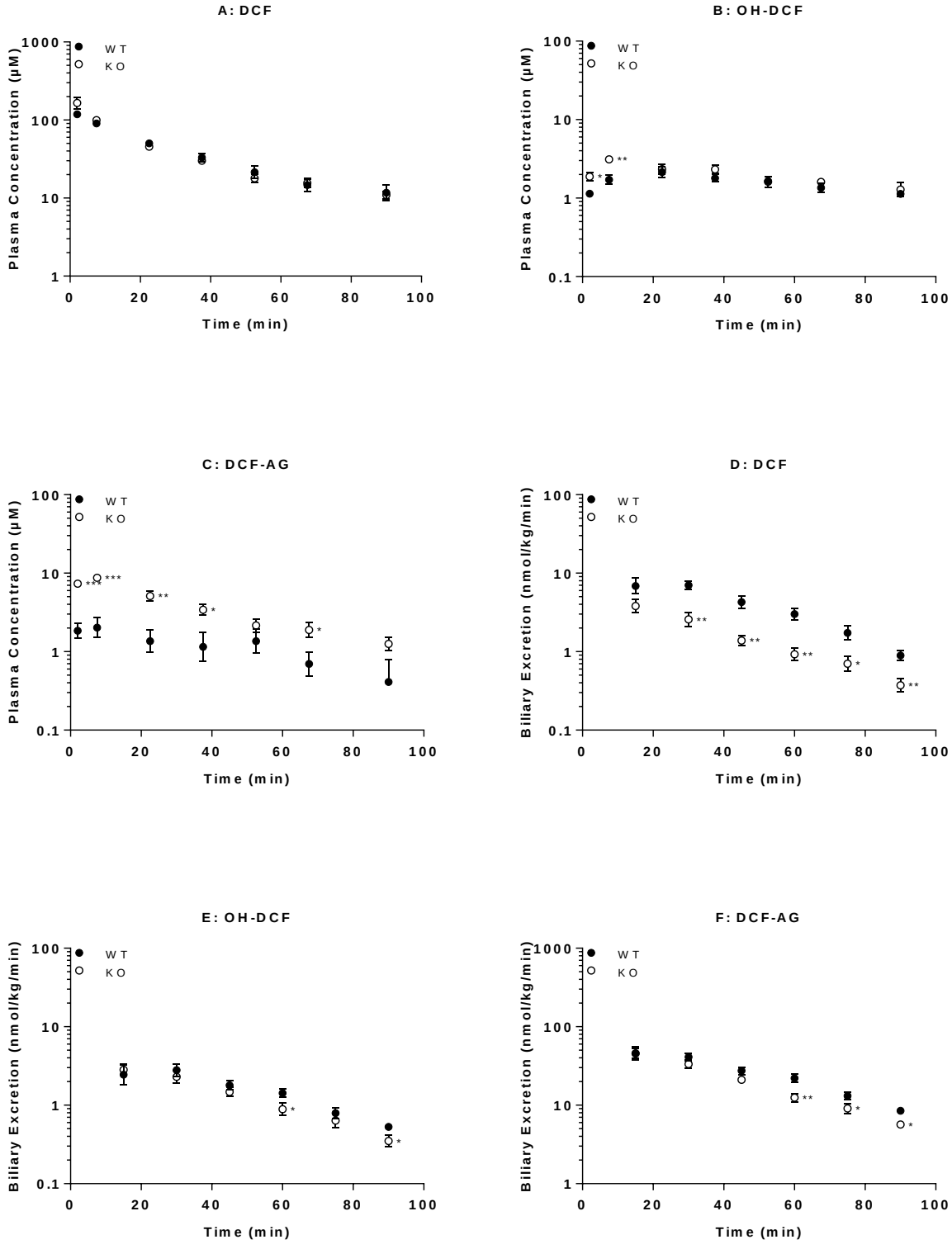

Figure 2.2 Plasma and biliary concentration versus time profiles of DCF, OH-DCF, and DCF-AG in C57 WT and C57 Bcrp KO mice after 10 mg/kg DCF dose. Pharmacokinetics of DCF and its metabolites in WT (○) and Bcrp KO (●) mice after a single intraarterial dose of 10 mg/kg DCF. (A-C) Plasma concentration profiles for (A) DCF, (B) OH-DCF, and (C) DCF-AG at discrete time points. (D-F) Biliary excretion profiles for (D) DCF, (E) OH-DCF, and (F) DCF-AG. Time points represent accumulation of biliary flow during successive 15 min intervals (0-15, 15-30, 30-45, 45-60, 60-75, and 75-90 min). All data are expressed as mean ± standard error of the mean for 5-6 subjects/group. * $P < 0.05$; ** $P < 0.01$; *** $P < 0.001$ versus WT.

Figure 2.3 Terminal liver concentrations of DCF, OH-DCF, and DCF-AG in C57 WT and C57 Bcrp KO mice after 3 or 10 mg/kg DCF dose

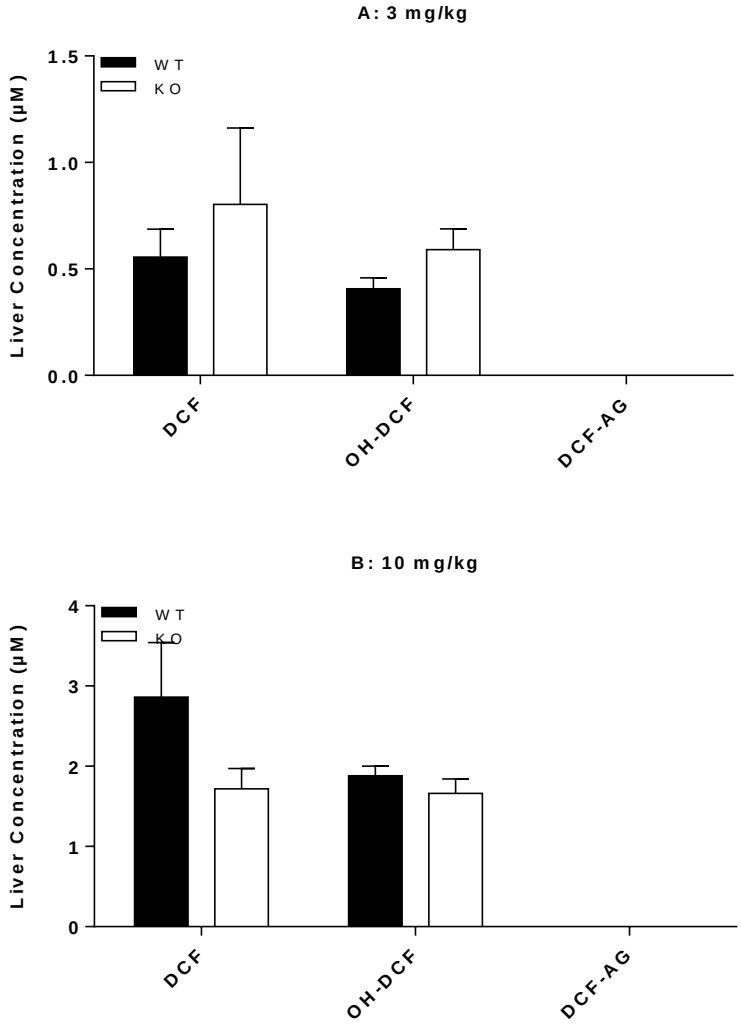

Figure 2.3 Terminal liver concentrations of DCF, OH-DCF, and DCF-AG in C57 WT and C57 Bcrp KO mice after 3 or 10 mg/kg DCF dose. Hepatic concentrations of DCF, OH-DCF, and DCF-AG in WT (□) and KO (■) mice were determined 90 min after DCF administration. Data are expressed as mean ± standard error of the mean for 5-6 subjects/group.

Figure 2.4 Plasma and biliary concentration versus time profiles of DCF, OH-DCF, and DCF-AG in FVB WT and FVB Mrp3 KO mice after 3 mg/kg DCF dose

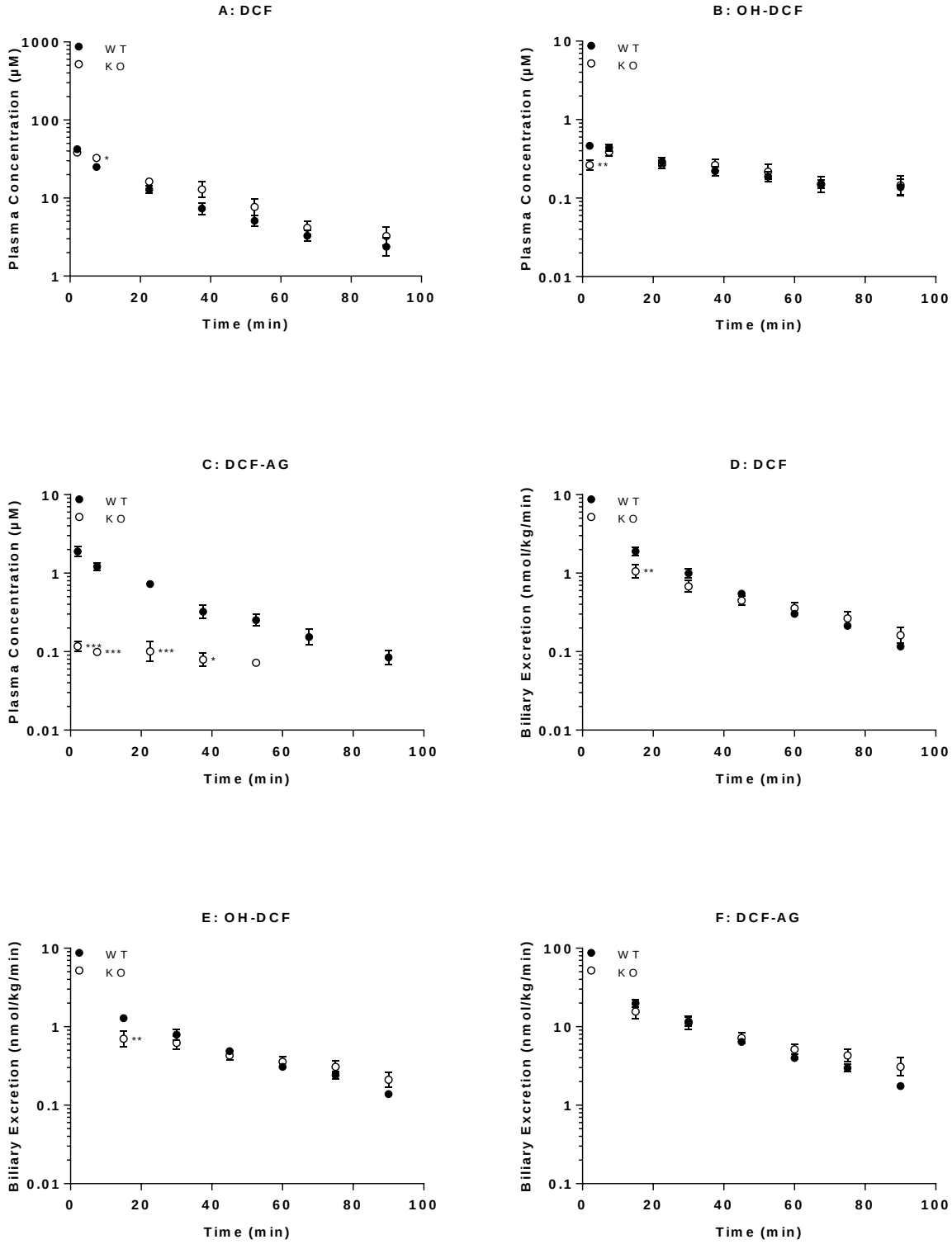

Figure 2.4 Plasma and biliary concentration versus time profiles of DCF, OH-DCF, and DCF-AG in FVB WT and FVB Mrp3 KO mice after 3 mg/kg DCF dose. Pharmacokinetics of DCF and its metabolites in WT (○) and Mrp3 KO (●) mice after a single intraarterial dose of 3 mg/kg DCF. (A-C) Plasma concentration profiles for (A) DCF, (B) OH-DCF, and (C) DCF-AG at discrete time points. (D-F) Biliary excretion profiles for (D) DCF, (E) OH-DCF, and (F) DCF-AG. Time points represent accumulation of biliary flow during successive 15 min intervals (0-15, 15-30, 30-45, 45-60, 60-75, and 75-90 min). All data are expressed as mean ± standard error of the mean for 7 subjects/group. * $P < 0.05$; ** $P < 0.01$; *** $P < 0.001$ versus WT.

Figure 2.5 Plasma and biliary concentration versus time profiles of DCF, OH-DCF, and DCF-AG in Mrp3 WT and KO mice after 10 mg/kg DCF dose

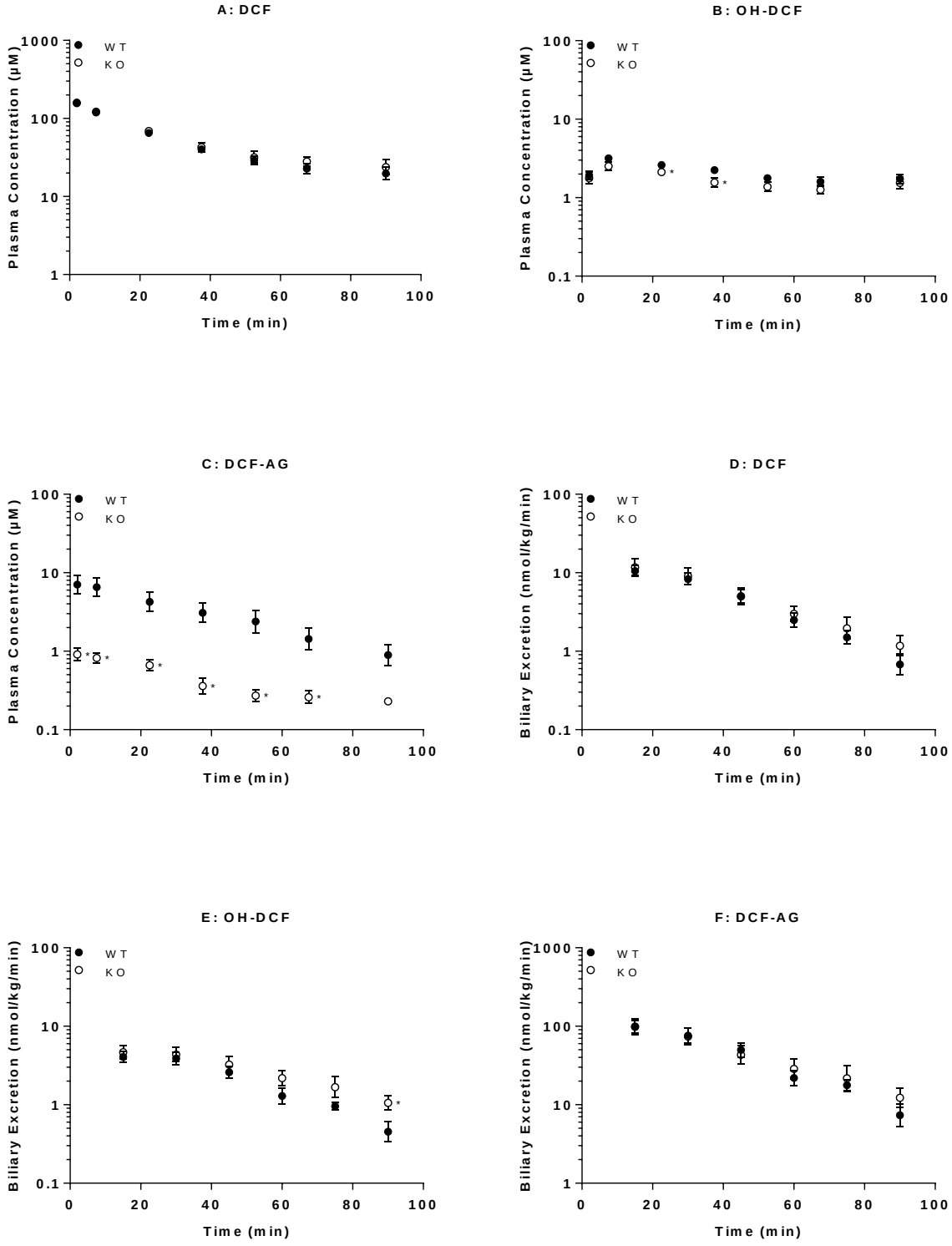

Figure 2.5 Plasma and biliary concentration versus time profiles of DCF, OH-DCF, and DCF-AG in FVB WT and FVB Mrp3 KO mice after 10 mg/kg DCF dose. Pharmacokinetics of DCF and its metabolites in WT (○) and Mrp3 KO (●) mice after a single intraarterial dose of 10 mg/kg DCF. (A-C) Plasma concentration profiles for (A) DCF, (B) OH-DCF, and (C) DCF-AG at discrete time points. (D-F) Biliary excretion profiles for (D) DCF, (E) OH-DCF, and (F) DCF-AG. Time points represent accumulation of biliary flow during successive 15 min intervals (0-15, 15-30, 30-45, 45-60, 60-75, and 75-90 min). All data are expressed as mean ± standard error of the mean for 7 subjects/group. * $P < 0.05$; ** $P < 0.01$; *** $P < 0.001$ versus WT.

Figure 2.6 Terminal liver concentrations of DCF, OH-DCF, and DCF-AG in FVB WT and FVB Mrp3 KO mice after 3 or 10 mg/kg DCF dose

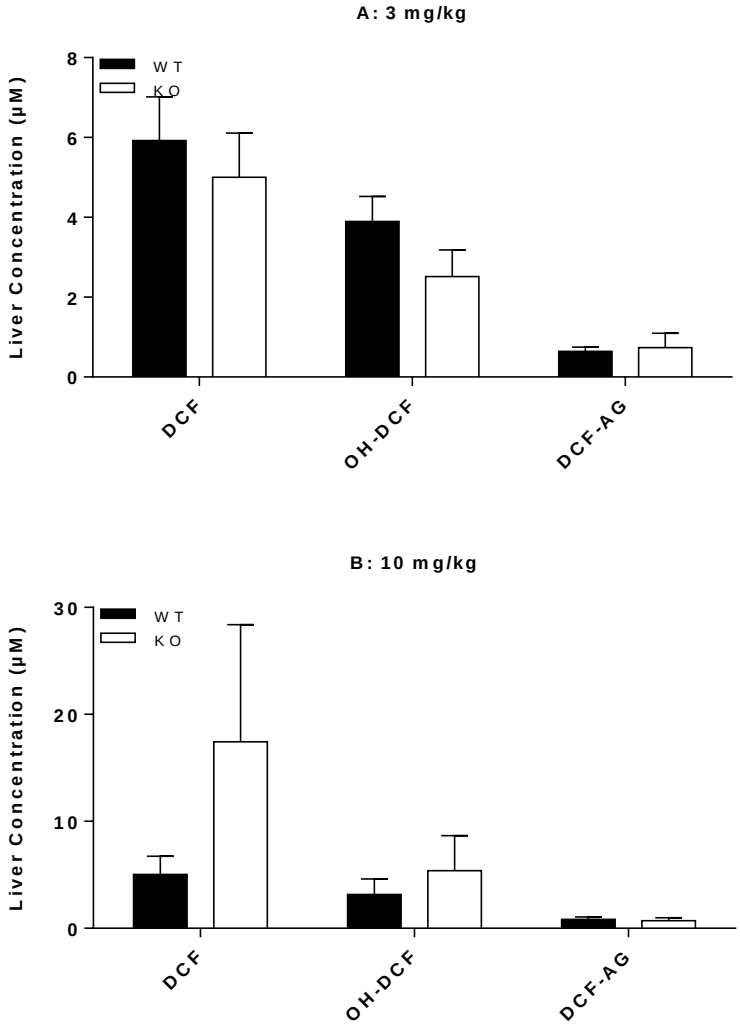

Figure 2.6 Terminal liver concentrations of DCF, OH-DCF, and DCF-AG in FVB WT and FVB Mrp3 KO mice after 3 or 10 mg/kg DCF dose. Hepatic concentrations of DCF, OH-DCF, and DCF-AG in WT (□) and KO (■) mice were determined 90 min after DCF administration. Data are expressed as mean ± standard error of the mean for 6-7 subjects/group.

Table 2.1 Summary of DCF pharmacokinetic parameters in plasma of WT and KO mice after a single 3 or 10 mg/kg DCF dose

Dose	Genotype	C_0 (μM)	$t_{1/2}$ (min)	$AUC_{0\text{-tlast}}$ (μM × min)
3 mg/kg	C57 WT	57.8 ± 6.0	31.2 ± 4.0	1,050 ± 50
	C57 BCRP KO	46.0 ± 5.1	27.8 ± 3.6	1,020 ± 80
10 mg/kg	C57 WT	132 ± 8	30.5 ± 3.1	3,420 ± 290
	C57 BCRP KO	201 ± 44	33.5 ± 2.5	3,570 ± 340
3 mg/kg	FVB WT	51.4 ± 5.1	24.0 ± 4.1	862 ± 86
	FVB Mrp3 KO	41.2 ± 3.3	37.5 ± 9.2	1,110 ± 130
10 mg/kg	FVB WT	178 ± 16	37.8 ± 5.6	4,220 ± 420
	FVB Mrp3 KO	172 ± 13	52.9 ± 9.8	4,770 ± 280

Table 2.1 Summary of DCF pharmacokinetic parameters in plasma of WT and KO mice after a single 3 or 10 mg/kg DCF dose. C_0 indicates the estimated DCF plasma concentration at time zero, $t_{1/2}$ is the DCF elimination half-life, and $AUC_{0\text{-tlast}}$ is the area under the plasma concentration versus time curve for DCF from time zero to the last collected time point. Parameters were calculated using non-compartmental analysis. Each value represents the mean ± standard error of the mean of 5-7subjects/group.

Figure 2.7 Mass spectral identification of major DCF conjugated metabolites excreted in bile

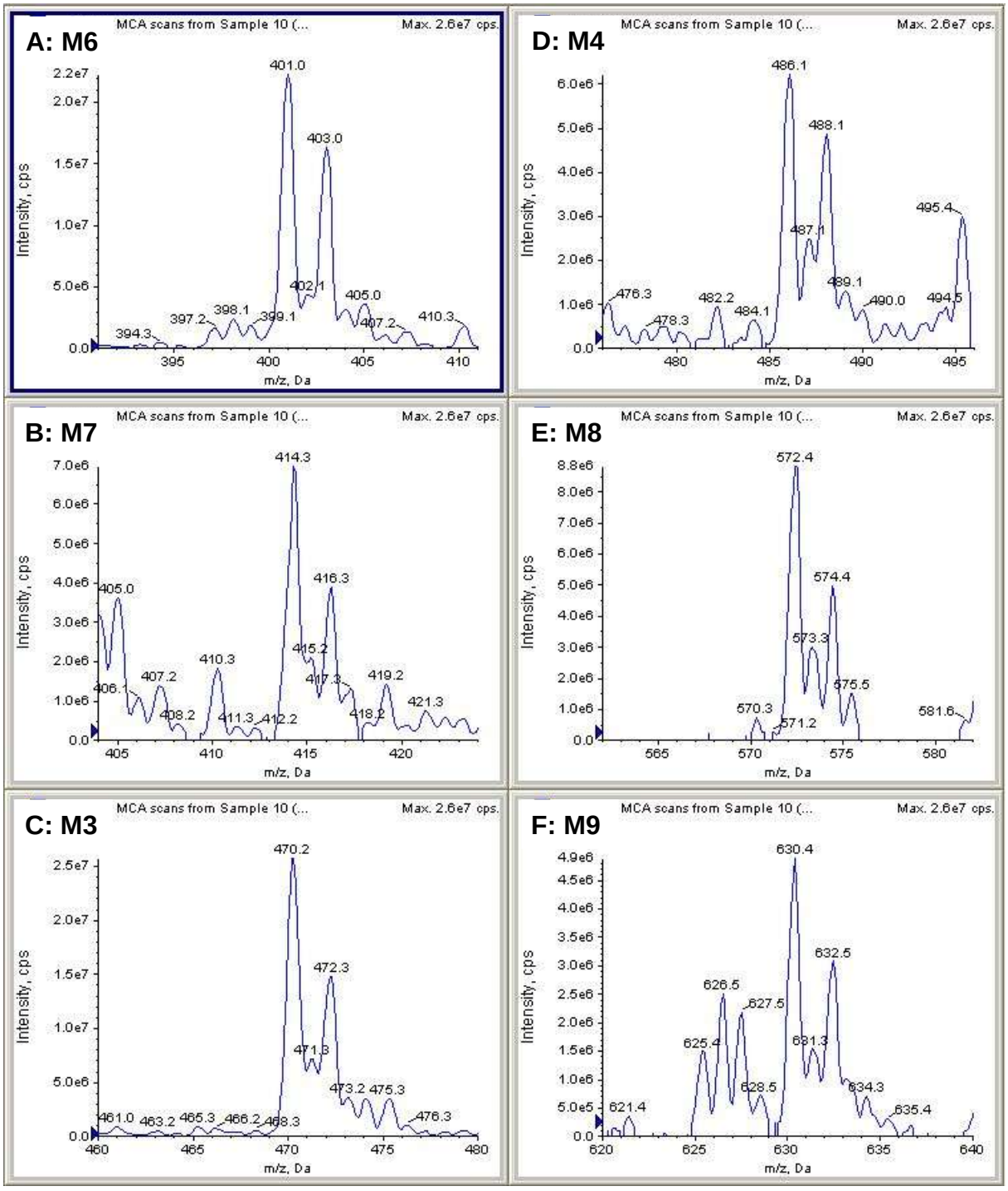

Figure 2.7 Mass spectral identification of major DCF conjugated metabolites excreted in bile. Bile from WT and Mrp3 KO mice were pooled, extracted with organic solvent, and infused onto a mass spectrometer. The infusion was then scanned across a range of masses for which multiple acquisitions were made to determine masses of putative metabolites. The WT spectral profile was subtracted from the KO profile resulting in a range of masses (i.e., metabolites) that can be considered to be in excess in KO compared to WT. (A) DCF taurine conjugate, (B) DCF cysteine conjugate, (C) DCF-AG, (D) either 4'- or 5-OH-DCF-AG, (E) unknown DCF conjugate, and (F) di-hydroxy-DCF glutathione.

Figure 2.8 Structures of DCF metabolites based on biliary MS/MS infusion data

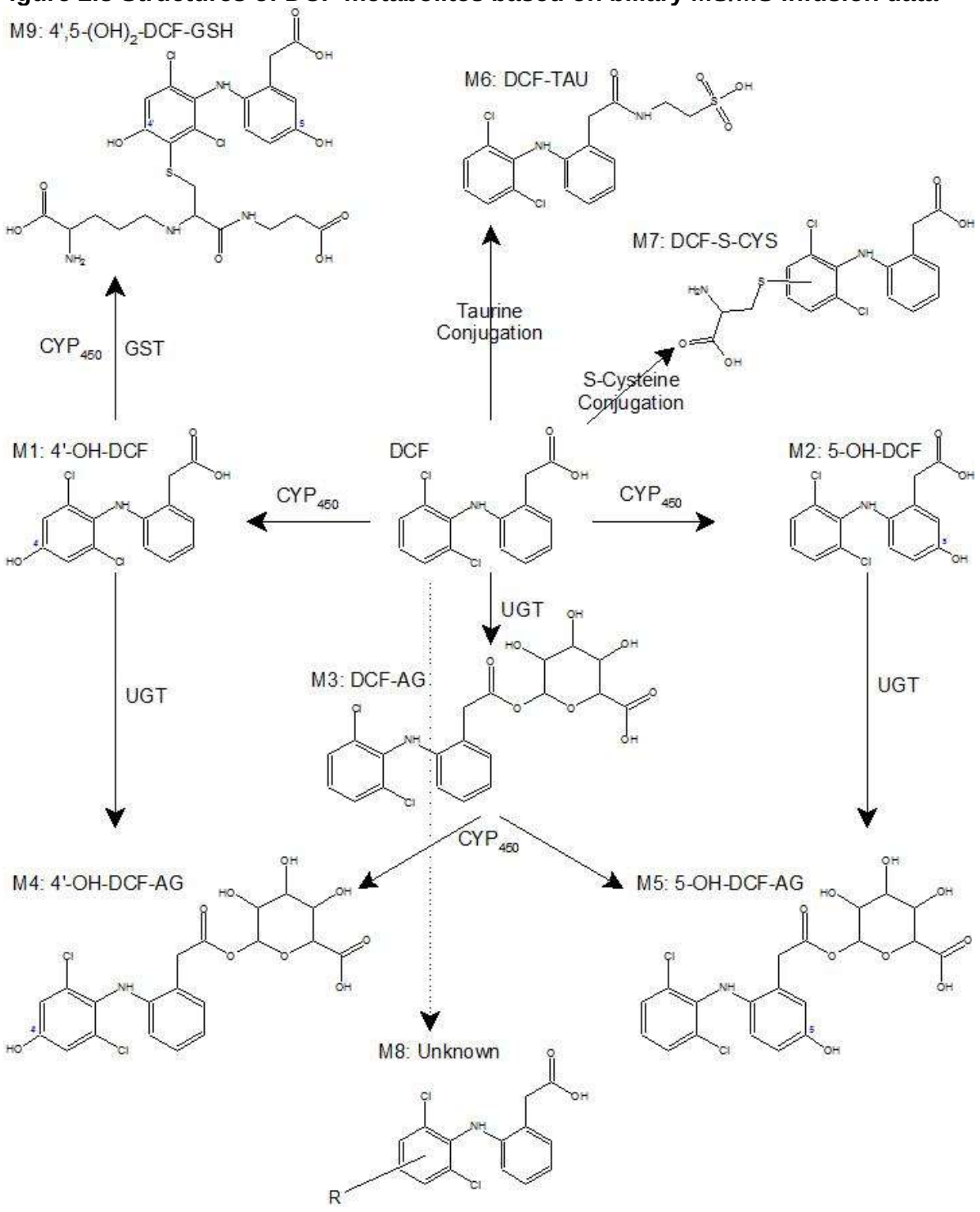

Figure 2.8 Structures of DCF metabolites based on biliary MS/MS infusion data. M1 and M2 are hydroxylated metabolites (OH-DCF) that have the same parental mass as do M4 and M5 (OH-DCF-AG) which can be generated from M1, M2, or M3 (DCF-AG). DCF can also be conjugated to M6 (taurine conjugate), M7 (cysteine conjugate), and M9 (di-hydroxy glutathione conjugate) which were identified in spectral scans. The structure of M8 has not been elucidated, however is appears to have a negative ion mode mass (m/z) of 572.

Figure 2.9 *In vitro* metabolism of DCF using hepatic S9 fraction from C57 and FVB mice

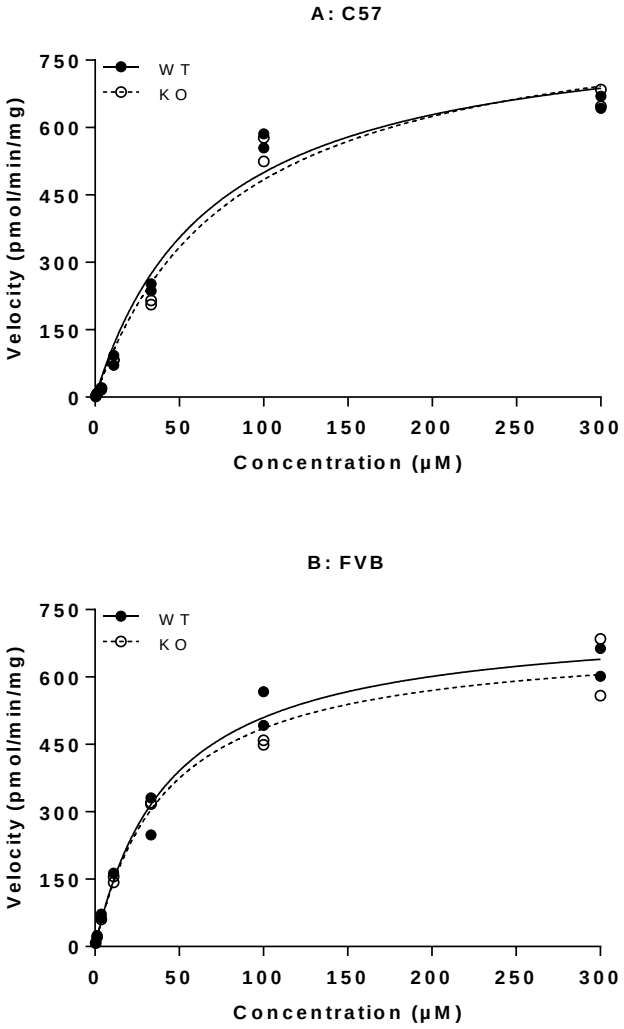

Figure 2.9 *In vitro* metabolism of DCF using hepatic S9 fraction from C57 and FVB mice. Pooled S9 fraction was prepared from (A) C57 WT and C57 Bcrp KO and (B) FVB WT and FVB Mrp3 KO mice. Incubations consisted of 1 mg/mL S9 protein and were conducted at 37 °C. Cofactors (e.g., GSH and UDPGA) were added to permit Phase II metabolism. Initial incubations were conducted in duplicate at 0, 7.5, 15, 30, and 45 min, and the responses at each concentration were used to generate a velocity for the corresponding concentration. The results indicate the two WT and KO pairings (i.e., FVB and C57) have nearly equal intrinsic metabolic capacity. Each data point represents the velocity for a given concentration from 2 separate studies.

Table 2.2 Summary of *in vitro* DCF metabolism in mouse models

Genotype	V_{max} (pmol/min/mg)	K_m (μM)	Metabolic CL_{int} (μL/min/mg)
C57 WT	846 ± 31	69.3 ± 4.3	12.2
C57 KO	882 ± 26	82.4 ± 1.1	10.7
FVB WT	734 ± 32	44.3 ± 3.5	16.7
FVB KO	696 ± 79	43.3 ± 9.0	16.4

Table 2.2 Summary of *in vitro* DCF metabolism in mouse models. Metabolic parameters were determined using S9 fraction from FVB and C57 strains of mice that were WT or KO for Bcrp or Mrp3. Data represent the mean ± standard error of the mean from 2 separate studies.

Figure 2.10 Time-dependent transport of DCF-AG by MRP2 and MRP3 using inside-out vesicles

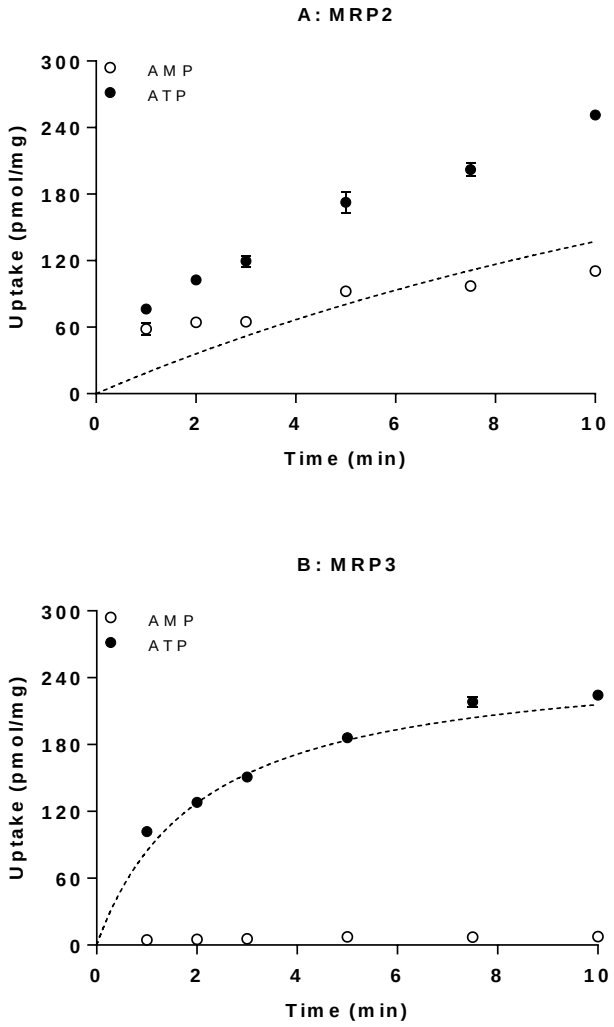

Figure 2.10 Time-dependent transport of DCF-AG by MRP2 and MRP3 using inside-out vesicles. DCF-AG was incubated with vesicles in the presence of 5 mM AMP (○) or 5 mM ATP (●) at 37 °C. (A) Uptake of 10 µM DCF-AG by MRP2. (B) Uptake of 1 µM DCF-AG by MRP3. The dotted lines in both plots represent the nonlinear fit of DCF-AG active uptake and were determined by subtracting the AMP values (background and passive uptake) from the ATP response. Each data point reflects the mean ± the standard error of the mean for n=3 measurements per time point.

Figure 2.11 Determination of the concentration-dependent transporter kinetics of MRP2 and MRP3 for DCF-AG

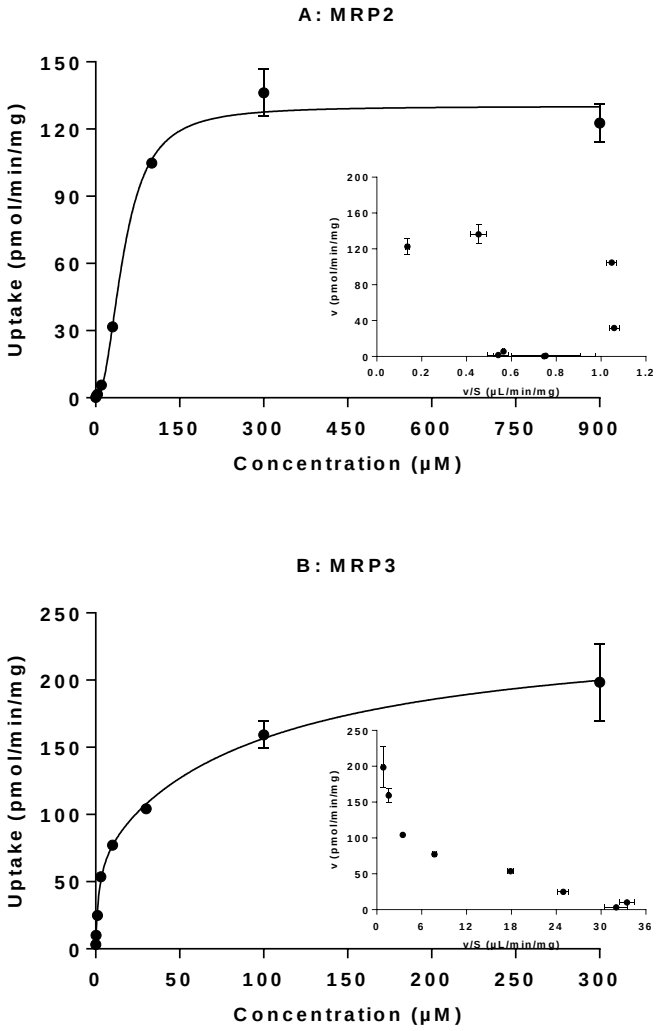

Figure 2.11 Determination of the concentration-dependent transporter kinetics of MRP2 and MRP3 for DCF-AG. MRP2 and MRP3 vesicles were incubated with increasing concentrations of DCF-AG in the presence of 5 mM AMP or ATP for 5 min at 37 °C. AMP response was subtracted from ATP, and the resulting data was fit to determine kinetic parameters. (A) MRP2 data was fit according to an allosteric sigmoidal model that yielded an apparent Hill slope of 2.2. Insert: Eadie-Hofstee plot. (B) MRP3 data was fit according to a two-K_m indicating the presence of high affinity and low affinity binding sites. Insert: Eadie-Hofstee plot. Each data point reflects the mean ± the standard error of the mean for n=3 measurements per concentration.

Table 2.3 Summary of MRP2 and MRP3 vesicle kinetic studies for DCF-AG

Transporter	V_{max} (pmol/min/mg)	K_m (μM)	Transport CL_{int} (μL/min/mg)
MRP2	130	50.5	2.58
MRP3 (low affinity)	170	98.2	2.37
MRP3 (high affinity)	71.9	1.78	40.3

Table 2.3 Summary of MRP2 and MRP3 vesicle kinetic studies for DCF-AG. MRP2 had single K_m transport affinity for DCF-AG whereas MRP3 demonstrated biphasic kinetics. Intrinsic transporter clearance (V_{max}/K_m) for MRP2 and the low affinity MRP3 clearance were comparable. In contrast, the high affinity MRP3 efflux clearance was over an order of magnitude greater than that of MRP2.

2.5 Discussion

Currently, more is known about which transporters are inhibited by DCF rather than which transporters mediate the disposition of DCF and its primary metabolites. Thus the intention of the present work was to investigate the impact of efflux transporters on DCF disposition. Studies in TR- rats, which are of a Wistar background and have a spontaneous mutation for the *Abcc2* gene thereby lacking functional expression of Mrp2 (Kitamura et al., 1990), demonstrated that the those mutants are resistant to intestinal injury compared to non-mutant Wistar rats (Seitz et al., 1998). Though intestinal injury in the TR- rats was significantly lower compared to non-mutants, GI damage was not completely abolished. The mechanism of the decreased injury stems from the reduced biliary translocation of reactive intermediates, such as DCF-AG, from the hepatocyte into the bile canaliculi. That seminal work laid the foundation for further investigation into transporter-mediated modulation of DCF-associated toxicity.

The results presented herein demonstrate the involvement of other efflux transporters to modulate disposition of not only reactive metabolites, but also of DCF itself. Data from two subtoxic doses of DCF indicate that Bcrp, which is expressed on the canalicular domain along with Mrp2, is partially responsible for the active transport of DCF. This discovery was supported by the observations that C57 Bcrp WT animals had statistically higher DCF biliary excretion compared to KO after a dose of 3 or 10 mg/kg DCF (Figure 2.1D and Figure 2.2D). The reduction in DCF biliary output in the KO did not result in any increase in the KO DCF plasma concentration. KO mice exhibited a statistically significant increase in DCF-AG plasma concentrations compared to WT (Figure 2.1C and Figure 2.2C), and this increase was paralleled in KO by a decrease in DCF-AG

biliary excretion (Figure 2.1F and Figure 2.2F). Taken together the results indicate that Bcrp is operative, *in vivo*, with respect to modulation of DCF and DCF-AG transport activity.

Lagas et al. (2009) reported the involvement of Bcrp to transport DCF, though this was conducted using a transfected cell system with polarized MDCK cells in a transwell format. For that study, murine Bcrp exhibited greater transport of DCF compared to human BCRP (transport was assessed by comparing A→B to B→A vectorial transport). Curiously, a follow-up study by Lagas et al. (2010) with an *in vivo* Bcrp knockout mouse model from a FVB background contradicted their earlier findings. Whereas we report that C57 WT had DCF biliary excretion 2.2- to 2.6-fold greater compared to that of C57 Bcrp KO, the Lagas Bcrp KO mice had 1.2-fold more biliary DCF compared to WT though this difference was not statistically significant. The authors acknowledge the disconnect between their *in vitro* and *in vivo* data, yet there was no rationale given for the divergent results. DCF-AG WT plasma levels in the Lagas *in vivo* study were modestly higher without statistical significance in contrast to the present data that reflect 1.8- and 3.2-fold greater KO plasma concentrations relative to WT (Figure 2.1C and Figure 2.2C). That said, the Lagas study did indicate biliary DCF-AG levels were 2.1-fold greater in WT compared to KO. There is some limitation to the Lagas report, primarily the selection of a single time point, 60 min post-administration, from which to make comparisons between genotypes. In contrast, we report plasma and bile profiles over a span of time giving greater power to make dispositional characterizations. We also assessed the pharmacokinetics from two doses compared to a single 5 mg/kg IV dose for the Lagas work.

In addition to demonstrating the interplay of Bcrp activity, we also report that Mrp3 is responsible for the *in vivo* translocation of DCF-AG. This key outcome was observed in the plasma profiles at each sub-toxic dose for which C57 WT mice had 7.0- to 8.6-fold greater DCF-AG plasma concentrations compared to C57 Mrp3 KO (Figure 2.4C and Figure 2.5D). In the same 2010 Lagas publication referenced previously, FVB WT mice had approximately 2-fold greater DCF-AG plasma concentrations (at 60 min) compared to FVB Mrp3 KO, hence our data are confirmatory. Considering the degree of separation between WT and KO, it is evident Mrp3 plays a major role in the disposition of DCF-AG. Whereas Bcrp deletion led to altered disposition of plasma and biliary profiles for DCF and DCF-AG, deletion of Mrp3 only affected basolateral excretion of DCF-AG. There were no changes to DCF-AG biliary output (Figure 2.4F and Figure 2.5F) nor were there changes in hepatic levels of DCF-AG (Figure 2.6A-B). The lack of elevated biliary DCF-AG was unexpected given the published reports of increased biliary excretion of 4-methylumbelliferyl glucuronide and acetaminophen glucuronide in Mrp3 KO mice (Manautou et al., 2005; Zamek-Gliszczynski et al., 2006b).

All mouse strains were evaluated for their intrinsic metabolic capacity using S9 fraction. S9 was chosen as the modality for this assessment due to the presence of an array of metabolic enzymes (Lu, 2014). The results from *in vitro* metabolism studies suggest that mice of C57 and FVB backgrounds have similar metabolic capacity (Figure 2.9A-B). From these data, it can be inferred that deletion of transporters did not result in any compensatory changes to enzymatic (Phase I and Phase II) expression or activity. Therefore, changes in the biliary excretion or plasma dispositional profiles are reflective

of diminished transporter capacity, due to selective genetic deletion, rather than innate differences in metabolic competency.

Upon consideration that the FVB strain of mice had such a large differential regarding WT and KO plasma DCF-AG concentrations without concomitant changes in biliary output, the bile from WT and KO were infused into a LC/MS/MS system to permit rudimentary metabolite identification. The WT spectra was subtracted from the KO spectra and analyzed for likely candidates that could account for the fraction of DCF-AG not present in KO plasma. The spectral scans revealed several important findings. Firstly, of the three quantified analytes, DCF-AG biliary levels were 10-fold greater than DCF and OH-DCF, and the DCF-AG excreted in bile accounted for nearly 12% of the total DCF dose. Secondly, a diclofenac taurine conjugate (designated as M6 in Figure 2.8) was also detected and found to have a signal intensity (Figure 2.7A) nearly equal to DCF-AG (Figure 2.7C). The DCF-TAU response is suggestive that taurine conjugation may be as dominant of a metabolic process as glucuronidation. Taurine conjugates of DCF in mice were likewise reported by Sarda et al. (2012) and Pickup et al. (2012). In fact, both Sarda's and Pickup's respective works provided evidence that multiple taurine conjugates were detectable furthering the notion that taurine conjugation constitutes a significant clearance mechanism. Taurine conjugation is an important detoxification step since the amide that is formed results in less reactive compared to the ester bond that is present in DCF-AG (Montalbetti and Falque, 2005). The significance of the spectral scans and identification of other conjugated metabolites implies that the portion of DCF-AG which was not excreted into plasma was putatively converted into other metabolites that were ultimately transported into bile. Another biliary metabolite of high

intensity observed at *m/z* of 572 was categorized as M7 (Figure 2.8). The structure of M7 remains to be elucidated, however it may be similar to a metabolite, which was detected using human liver microsomes, that was described as being 4'-OH-2'-glutathion-deschloro-diclofenac (Yu et al., 2005).

Bearing in mind that these data and that of the TR- rat study provided conclusive evidence of DCF-AG *in vivo* transport, the last component of the work was to assess the affinity of DCF-AG to be transported by human MRP2 and MRP3. The purpose of the investigation was to gauge if human MRPs had similar potential to interact with DCF-AG. To that end, studies with commercial inside-out vesicles were carried out. In keeping with the TR- rat data, our results indicated that DCF-AG is a substrate of MRP2 (Figure 2.10A) and that transport by MRP2 was saturable (Figure 2.11A). The affinity of DCF-AG for MRP2 was relatively weak in that the ATP incubation responses ranged from 1.5- to 2.0-fold greater than the AMP responses. Furthermore, the activity of MRP2 for DCF-AG appears to have an element of allosteric modulation, evident by a Hill slope estimate of 2.2. The Eadie-Hofstee plot for MRP2 is in agreement with an allosteric effect (Hutzler and Tracy, 2002). The allosterism is a function of MRP2 having multiple binding sites (Zelcer et al., 2003a). Like DCF-AG, estradiol-17β-glucuronide was demonstrated to be transported with cooperative binding by human MRP2 vesicles as it had a Hill slope of 2.4 (Elsby et al., 2011; Li et al., 2011). MRP3-mediated transport of DCF-AG was determined be biphasic with a high affinity and low affinity binding site (Figure 2.11B). Whereas the dynamic response by MRP2 was low, MRP3 had a maximal fold-ratio (ATP/AMP) of 37 at the low end of the concentration range while the minimal ratio was 1.5-fold at the highest tested concentration. The intrinsic transporter

clearance of the high affinity site indicated that DCF-AG can be transported by MRP3 to a greater degree at low DCF-AG concentrations compared to MRP2 (Table 2.3).

Overall these data offer insight on the disposition of DCF and its metabolites. We offer proof that Bcrp can mediate DCF translocation from the hepatocyte into bile, and that DCF-AG can also be transported by Bcrp. The deletion of Bcrp not only diminished biliary DCF-AG efflux, but it also resulted in an increase in plasma DCF-AG concentrations. In contrast, Mrp3 was involved in the basolateral excretion of DCF-AG from the liver into blood. Despite the profound differences between WT and KO for DCF-AF levels, there was no effect on DCF-AG biliary excretion suggesting only basolateral disposition was affected. Finally, we report that human MRP3, through the means of an *in vitro* assay, appeared able to transport DCF-AG. Based on the *in vitro* MRP3 vesicle assay and the *in vivo* Mrp3 KO study, it is highly likely that MRP3 is an operative transporter of DCF-AG *in vivo* for humans. As such investigations into human MRP3 polymorphisms are warranted to ascertain the extent to which patients may experience dispositional changes to MRP3 substrates.

Chapter 3 MULTIDRUG RESISTANCE-ASSOCIATED PROTEIN 3 (MRP3) PLAYS AN IMPORTANT ROLE IN PROTECTION AGAINST ACUTE TOXICITY OF DICLOFENAC

3.1 Abstract

Diclofenac (DCF) is a non-steroidal anti-inflammatory drug commonly prescribed to reduce pain in acute and chronic inflammatory diseases. One of the main DCF metabolites is a reactive diclofenac acyl glucuronide (DCF-AG) that covalently binds to biological targets and may contribute to adverse drug reactions arising from DCF use. Cellular efflux of DCF-AG is partially mediated by multidrug resistance-associated proteins (Mrp). The importance of Mrp2 during DCF-induced toxicity has been established, yet the role of Mrp3 remains largely unexplored. In the present work, Mrp3 knockout (KO) mice were used to study the toxicokinetics and toxicodynamics of DCF and its metabolites. DCF-AG plasma concentrations were 90% lower in KO mice than in wild-type (WT) mice, indicating that Mrp3 mediates DCF-AG basolateral efflux. In contrast, there were no differences in DCF-AG biliary excretion between WT and KO suggesting that only DCF-AG basolateral efflux is compromised by Mrp3 deletion. Susceptibility to toxicity was also evaluated after a single high DCF dose. No signs of injury were detected in livers and kidneys, however ulcers were found in the small intestines. Furthermore, the observed intestinal injuries were consistently more severe in KO compared to WT. DCF covalent adducts were observed in liver and small intestines, however staining intensity did not correlate with the severity of injuries implying that tissues respond differently to covalent modification. Overall, the data provides strong evidence that (1) *in vivo* Mrp3 plays an important role in DCF-AG

disposition and (2) compromised Mrp3 function can enhance injury in the gastrointestinal tract after DCF treatment.

3.2 Introduction

Diclofenac (DCF) is a non-steroidal anti-inflammatory drug (NSAID) that is prescribed to alleviate symptoms associated with ankylosing spondylitis, osteoarthritis, rheumatoid arthritis, and migraine (McNeely and Goa, 1999; Novartis, 2011; Depomed, 2014). DCF is generally well tolerated although long term usage has been implicated with a variety of adverse drug events (ADR) in a subset of patients. The most common side effects of DCF are discomfort, ulceration, and bleeding in the gastrointestinal (GI) tract. These ADRs are related to DCF pharmacodynamics, namely chronic inhibition of cyclooxygenase (COX) enzymes causing a decrease of prostaglandins that protect the GI mucosa (Menasse et al., 1978; Wallace, 2008). NSAIDs as a group have a mean liver injury rate of 1 per 100,000 users. However, chronic DCF administration increases the risk of liver injury to 6 per 100,000 users (de Abajo et al., 2004). More recently, a meta-analysis of cardiovascular safety implicated DCF with a higher risk of cardiovascular death and stroke among a group of seven NSAIDs (Trelle et al., 2011).

DCF undergoes extensive first-pass metabolism in humans, and approximately 50% of the dose is systemically available (Willis et al., 1979). The majority of DCF is converted into metabolites of which 65% are eliminated in urine with the remainder excreted in bile (Riess et al., 1978; Novartis, 2011). Among the main products are hydroxylated metabolites, the predominant being 4′-hydroxy diclofenac (OH-DCF), that can form reactive quinone imines that adduct and deplete glutathione causing a state of oxidative stress (Tang et al., 1999). Another key metabolite is the highly reactive diclofenac acyl glucuronide (DCF-AG), which is primarily catalyzed in humans by uridine 5′-diphospho-glucuronosyltransferase (UGT) 2B7 (King et al., 2001). It has been shown that

inheritance of one or two copies of the UGT2B7*2 allele was associated with an increased risk of DCF-induced hepatotoxicity compared to UGT2B7*1 homozygotes as the *2 variant possesses higher catalytic activity (Daly et al., 2007).

DCF-AG is initially formed as a β-1-*O*-acyl glucuronide (β-anomer) which can be cleaved by β-glucuronidase into DCF and glucuronic acid. β-anomers spontaneously isomerize into β-glucuronidase-resistant 2-, 3-, and 4-*O*-acyl isomers (Sallustio et al., 2000). DCF-AG undergoes these rearrangements as the pH changes from acidic to physiologic conditions such as those that occur in the GI tract (Ebner et al., 1999; Kenny et al., 2004). DCF-AG can form adducts with multiple proteins in the liver and GI tract, and dipeptidyl peptidase IV was identified as a DCF-AG target in rat liver where adduction resulted in decreased activity (Hargus et al., 1995). Furthermore, it was found that broad-acting UGT inhibitors can significantly diminish the covalent binding of DCF metabolite to hepatocellular proteins *in vitro* (Kretz-Rommel and Boelsterli, 1993). There is consensus that repeated exposure to DCF-AG contributes to the idiosyncratic drug reaction seen with clinical usage, however the exact nature of how DCF-AG contributes to the etiology of these reactions remains unclear.

The potential for DCF-AG to cause extrahepatic covalent binding modifications is contingent upon active transport. For instance, DCF-AG was not detected in the bile of rats lacking canalicular multidrug resistance-associated protein 2 (Mrp2, *Abcc2*) (Seitz et al., 1998). A follow-up study revealed that Mrp2 mutant rats also had reduced intestinal ulceration compared to wild-type (WT) rats (Seitz and Boelsterli, 1998). These findings are important as they suggest that Mrp2 is at least partially responsible for

DCF-AG excretion from hepatocytes into bile. The mechanism by which DCF-AG is transported from hepatocytes into blood remains less understood.

Among the MRPs that are expressed along the basolateral membrane, MRP3 (*ABCC3*) has been demonstrated to export glucuronide conjugates of other compounds (Zelcer et al., 2001; Zelcer et al., 2006). In a Caucasian sample pool, fifty-one single nucleotide polymorphisms (SNP) in MRP3 were found (Lang et al., 2004). A pharmacogenomic study of healthy Japanese subjects identified twenty-one novel SNPs, with two resulting in immature transcript due to insertion of a stop codon (Fukushima-Uesaka et al., 2007). Functional significance of MRP3 SNPs was demonstrated whereby several MRP3 SNPs expressed in an *in vitro* system had impaired transporter function either by reductions in transporter activity or disruption of intracellular transporter trafficking to the cell membrane (Kobayashi et al., 2008).

Because MRP3 has been shown to transport both endogenous and exogenous glucuronide conjugates, it can be hypothesized that perturbation of MRP3 expression or function may affect the disposition and toxicity of DCF-AG *in vivo*. To investigate the role of MRP3 in the disposition and toxicity of DCF, a mouse Mrp3 knockout (KO) model is used to assess the disposition of DCF-AG and whether Mrp3 deletion increases likelihood of injury.

3.3 Materials and Methods

Chemicals and Reagents. DCF, OH-DCF, Dulbecco's phosphate buffered saline (DPBS), formic acid, indomethacin (as the IS), and sodium citrate were purchased from Sigma-Aldrich Corporation. (St. Louis, MO). DCF-AG was purchased from Toronto Research Chemicals Incorporated (Toronto, ON, Canada). Solutol® HS 15 was provided by the BASF Corporation (Florham Park, NJ). DCF antiserum was graciously donated by Dr. Dietmar Knopp (Technische Universität München, München, Germany).

Animals. Mrp3-null mice of FVB 129/Ola background were provided by Dr. Piet Borst (Netherlands Cancer Institute, Amsterdam, Netherlands). An additional set of Mrp3 KO mice having C57BL/6J background were generated at the University of Kansas Medical Center. Mice were housed in an American Animal Associations Laboratory Animal Care accredited facility of University of Kansas Medical Center under a standard temperature-, light-, and humidity-controlled environment. Mice had free access to Laboratory Rodent Chow 8604 (Harlan, Madison, WI) and drinking water. All animal studies were performed in accordance with the Guide for the Care and Use of Laboratory Animals using protocols reviewed and approved by the local Institutional Animal Care and Use Committee of University of Kansas Medical Center (Kansas City, KS).

***In Vivo* Studies.** *Toxicokinetics*. Male 2-3 month old FVB 129/Ola WT and FVB 129/Ola KO mice were anesthetized intraperitoneally with a ketamine/midazolam mixture (100 and 5 mg/kg, respectively), and both the right carotid artery and the common bile duct were cannulated for sample collection. The mice received a single intraarterial dose of 75 mg/kg DCF in 10:90 (v/v) Solutol HS 15:DPBS at a dosing

volume of 5 mL/kg. Bile flow was monitored, and bile fractions were collected in fifteen minute intervals from -15 to 0, 0 to 15, 15 to 30, 30 to 45, 45 to 60, 60 to 75, and 75 to 90 minutes post administration. Blood samples were collected into heparinized tubes at 2, 7.5, 22.5, 37.5, 52.5, 67.5, and 90 minutes after administration, and the blood was subsequently centrifuged to yield plasma. The volumes of bile were determined gravimetrically, using 1.0 for specific gravity. Both bile and plasma were stored at -20 °C until analysis. At the conclusion of the study (90 min post-administration), animals were sacrificed by overdose with ketamine and midazolam. Livers were harvested and quickly frozen in liquid nitrogen prior to storage at -80 °C.

Toxicodynamics. 2-3 month old male WT and KO (C57BL/6 background) were injected a single intraperitoneal dose of either vehicle, 10:90 (v/v) Solutol HS15: DPBS, or 90 mg/kg DCF in vehicle at a dosing volume of 5 mL/kg. The mice were then allowed access to food and water *ad libitum*. Twenty four hours after dosing, the mice were anesthetized for sacrifice with an intraperitoneal injection of 50 to 70 mg/kg pentobarbital. Blood was collected and centrifuged to yield plasma and kept frozen at -20 °C. Kidneys, liver, and small intestines were harvested, fixed in buffered formalin for 24 hours with gentle shaking at room temperature, and then transferred into 70% ethanol. Tissues were subsequently paraffin embedded and sectioned onto glass slides for histopathology and immunohistochemistry.

Bioanalytical Analysis. Bile and plasma were diluted with 0.1% formic acid in water (Solvent A) for LC/MS/MS detection as well as to stabilize DCF-AG. Liver samples were homogenized by bead milling using Solvent A. A 50 µL aliquot of diluted biological matrix was then precipitated with 450 µL of 0.1% formic acid in acetonitrile (Solvent B)

containing IS. Standard curves using naïve matrices were prepared in a similar fashion. Samples and standards were vigorously vortex-mixed and centrifuged at 1350 × *g* for 10 min and 4 °C. A 200 µL aliquot of supernatant was removed and evaporated under Nitrogen gas at 45 °C. The resulting residue was reconstituted with 200 µL of 90:10 (v/v) A:B, vigorously vortex-mixed, and centrifuged prior to injection onto LC/MS/MS. The injection volume for all sample types was 10 µL.

LC/MS/MS Method. Chromatographic separation of analytes was performed on a Synergi™ 4 µm Max-RP 50 × 2 mm column (Phenomenex Incorporated, Torrance, CA). The system front end consisted of a HTC PAL Autosampler outfitted with a Coolstack set to 4 °C (LEAP Technologies Incorporated, Carrboro, NC), a SCL-10Avp system controller, two LC10ADvp pumps, and a DGU-14A degasser (Shimadzu Scientific Instruments, Columbia, MD). Analytes of interest were eluted using a gradient profile that began with 10% solvent B for the first 1.0 min, which was then increased to 90% solvent B at 3.5 min using a linear gradient and held at this mixture for 0.5 min before reverting back to initial solvent conditions for 1.0 min to re-equilibrate the column. The flow rate was 0.4 mL/min, and the column effluent was directed to waste for the initial 1.5 min before switching to the mass spectrometer. Analytes were detected using an AB Sciex API™ 4000 LC/MS/MS triple quad mass-spectrometer with a TurboIonSpray® probe and Analyst version 1.4.2 software (AB Sciex, Framingham, MA) that was operated in multiple reaction monitoring mode. Ion spray voltage was -4250 V, and the source temperature was set to 400 °C. The mass transitions in negative ion mode for monitoring DCF, OH-DCF, DCF-AG, and indomethacin were *m/z* 294.0→249.9, 309.9→265.9, 470.1→192.9, and 356.0→311.8, respectively. The retention times of

DCF, OH-DCF, DCF-AG, and indomethacin were 3.25, 2.84, 2.69, and 3.20 min, respectively. Concentrations of analytes in the samples were determined by comparing the peak area ratios (analyte/IS) to those in the standard curve using a linear regression model. The dynamic range was 10 to 5,000 ng/mL for bile, liver homogenate, and plasma samples. The criterion of acceptance for standards was defined to be ±20% of nominal concentration.

Immunohistochemistry. Slides for immunohistochemistry were deparaffinized by xylene, and the xylene was removed by sequentially decreasing concentrations of ethanol followed by hydration in water. After a 30 min heat induced epitope retrieval in sodium citrate buffer, endogenous peroxidase activity was blocked with 3% hydrogen peroxide for 15 min. Slides were subsequently treated with an Avidin/Biotin Blocking Kit (Vector Laboratories Incorporated, Burlingame, CA) as per the manufacturer's recommendations and incubated with a Dako Serum-free Protein Block (Dako Incorporated, Carpinteria, CA) for 30 min. A rabbit polyclonal primary antibody against DCF at a 1:5000 (v/v) dilution was applied for 60 min at room temperature after which slides were incubated for 30 min with a 1:300 dilution of a Dako biotinylated swine anti-rabbit secondary antibody. The slides were then exposed to streptavidin-horseradish peroxidase (BD Biosciences, San Jose, CA) for 30 min. To develop the chromagen, a 30 min treatment with a Vector® NovaRED^{TM} Substrate Kit was utilized, and slides were counterstained with Mayer's Hematoxylin (Thermo Fisher Scientific Inc., Grand Island, NY). Finally, slides were dehydrated with ethanol and xylene and cover-slipped using Histomount Mounting Solution (Life Technologies). For negative controls, samples from the vehicle-only groups were treated in the same manner as subjects dosed with DCF.

Clinical Chemistry. Plasma samples from the toxicodynamic study were analyzed for alanine transaminase (ALT) and blood urea nitrogen (BUN) using kits purchased from Thermo Fisher Scientific Incorporated (Grand Island, NY) as per the manufacturer's recommendations. Positive and negative controls were utilized to assess assay functionality. A BioTek UV/Vis microplate spectrophotometer (BioTek Instruments Incorporated, Winooski, VT) was used to measure assay endpoints.

Histopathology. *Liver & Kidney*. Liver and kidney samples were fixed in 10% neutral-buffered zinc formalin prior to processing and paraffin embedding. Tissue sections (5 µm) were stained with hematoxylin and eosin. Sections were examined by light microscopy for the presence and severity of necrosis and degeneration using an established grading system (Ishiguro et al., 2008).

Gastrointestinal Tract. The gastrointestinal tract was examined histologically with multiple transverse sections of the stomach and large intestine and Swiss Roll sections of the small intestine (Moolenbeek and Ruitenberg, 1981). Histological examination used a scoring system adapted from a method described by Krieglstein et al. (2007). Briefly, 3 independent parameters were measured for a combined semi quantitative injury score; the degree of villus/crypt damage, the severity of inflammation (none, minimal, mild, moderate, marked, and severe), and the depth of injury (mucosa with epithelium and lamina propria, submucosa, muscularis, and serosa).

Statistical Analysis. Data are expressed as mean ± standard error of the mean. *P* values $\leq$ 0.05 were considered as statistically significant. Statistical analysis of data was performed using R version 3.2.1 (R Core Team, 2015). Two groups were

compared by Student's *t* test, and multiple groups were compared by an analysis of variance followed by Tukey's *post hoc* test.

3.4 Results

Toxicokinetic Study. In animals that remained anesthetized for surgical exposure of the abdominal cavity and bile duct cannulation, the maximal tolerated dose without morbidity was 75 mg/kg. Plasma concentrations for 75 mg/kg DCF (Figure 3.1A) were significantly higher in KO compared to WT, and the increases were generally less than 40%. Conversely, OH-DCF concentrations in plasma (Figure 3.1B) were significantly higher in WT with a 90% increase observed at 37.5 min. There was a dramatic disparity in plasma concentrations between WT and KO for DCF-AG (Figure 3.1C) with WT having nearly 9-fold higher concentrations in plasma compared to KO. A summary of pertinent toxicokinetic parameters is presented in Table 3.1 Both genotypes had similar estimated DCF plasma concentrations at time zero (C_0). Though there was a difference in the DCF elimination half-life ($t_{1/2}$) between the 2 genotypes, the DCF plasma exposure ($AUC_{0\text{-}tlast}$) for WT and KO was comparable.

To determine whether the loss of Mrp3 affected the biliary disposition of DCF and the two metabolites under consideration, the biliary excretion of DCF and its metabolites were quantified. There was no difference in bile flow between WT and KO (data not shown). The biliary excretion of DCF and its metabolites were equivalent between the two genotypes (Figure 3.1D, E, and F). Of the three analytes, DCF-AG was most predominant in bile constituting nearly 10% of the total DCF dose for each genotype, whereas DCF and OH-DCF biliary concentrations accounted for 0.2 and 0.1% of total DCF dose, respectively, irrespective of genotype. The limited availability of KO mice permitted assessing hepatic concentrations of DCF and its metabolites only at the terminal time point of 90 min post-administration. The KO livers had more DCF though

the difference was not statistically significant. OH-DCF and DCF-AG concentrations in KO livers were statistically lower compared to WT (Figure 3.2). In contrast to bile for which the major detected analyte was DCF-AG, unchanged DCF in both genotypes was most abundant compared to OH-DCF and DCF-AG.

Clinical Chemistry. Having established a role for Mrp3 to modulate systemic exposure of DCF-AG *in vivo*, the next objective was to evaluate to susceptibility of KO to DCF-induced injury. For these studies, the DCF dose was increased to 90 mg/kg as that was the maximal non-lethal dose in animals that were non-surgerized and freely moving. Rather than oral gavage, intraperitoneal administration was used to maximize dose absorption and delivery of DCF via portal circulation for immediate uptake into the liver. ALT concentrations (Figure 3.3A) were not significantly different between WT and KO suggesting no injuries in the liver. Furthermore, ALT values in all vehicle control and DCF-treated groups were less than 40 U/L, which is the upper limit of normal range for ALT. BUN levels (Figure 3.3B) were statistically higher in KO mice compared to WT, however the lack of difference between vehicle and DCF treated groups in KO mice suggest there was no DCF-induced renal injury.

Histopathology. Histopathological examination of liver and kidneys showed no obvious injuries at the administered dose confirming the clinical chemistry results (data not shown). The small intestines were also examined and scored according to three categories of injury. WT which received DCF showed a trend of higher injury compared to vehicle treated subjects (Figure 3.4), though these differences were not statistically significant. In addition, KO dosed with DCF had significantly greater incidence and severity of erosions and ulcers compared to treatment-matched WT mice. For both WT

and KO, ulcers were observed in the jejunal and ileal but not duodenal regions of the small intestine. Thus, the data suggest that the loss of Mrp3 increased the susceptibility to intestinal injury from an acute dose of DCF.

Immunohistochemistry. Sections of livers, kidneys, and small intestines were subjected to immunohistochemistry in order to determine the extent of DCF adduction. The rationale for conducting this assay was that reactive intermediates or metabolites of DCF are known to covalently bind to proteins. Thus the goal was to establish possible links between covalent binding of reactive DCF products and tissue injury. Kidneys were entirely devoid of DCF adduct staining implying that reactive DCF metabolites were not likely to be generated or accumulated by transit in kidneys (data not shown). In contrast, WT and KO livers showed strong evidence of DCF adduction after DCF administration compared to vehicle controls. The staining was robust and was observed in centrilobular, midzonal, and periportal regions (Figure 3.5B, C, E, and F). Vehicle controls did not exhibit staining suggesting that the primary antibody was specific for diclofenac adducts (Figure 3.5A and C). Interestingly, the livers showed intense staining for DCF adduct yet this organ did not manifest any apparent signs of injury either through clinical chemistry or histopathology. Lastly, compared to small intestines from vehicle controls which were unremarkable (Figure 3.5G and J), the small intestines from WT and KO also exhibited positive staining of DCF adducts (Figure 3.5H, I, K, L). The level of adduct staining in the small intestine was notably weaker than that observed in the liver as qualitatively assessed by chromagen intensity and the degree of scatter. Adduct formation was detected along the brush border of villi and extended inwards towards the basement membrane. In terms of regiospecificity, staining was

scattered throughout the small intestine and did not appear to be confined to any particular location.

Figure 3.1 Toxicokinetics of DCF and its metabolites in FVB WT and FVB Mrp3-KO mice after a single intraarterial dose of 75 mg/kg DCF

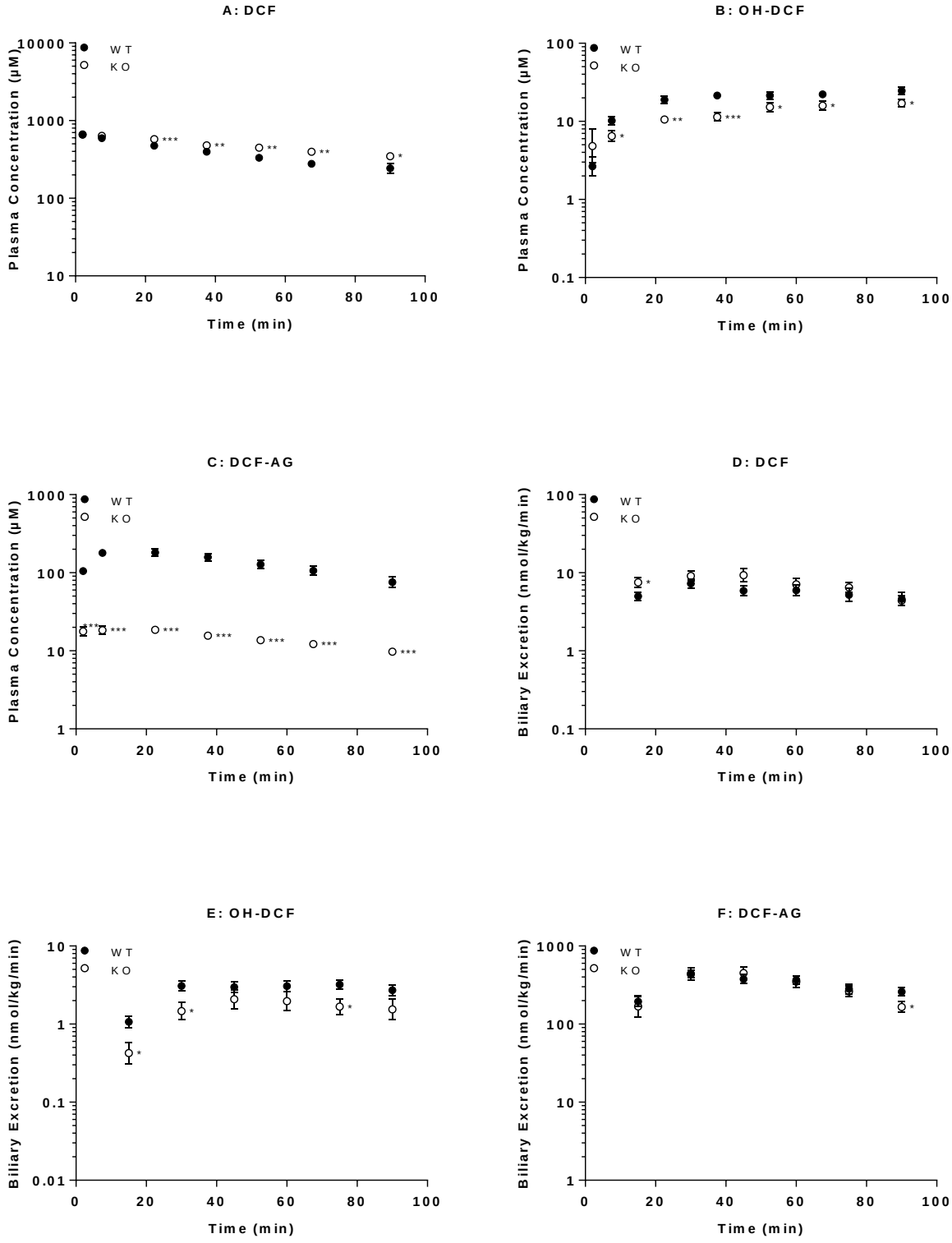

Figure 3.1 Toxicokinetics of DCF and its metabolites in FVB WT (●) and FVB Mrp3 KO (○) mice after a single intraarterial dose of 75 mg/kg DCF. (A-C) Plasma concentration profiles for (A) DCF, (B) OH-DCF, and (C) DCF-AG at discrete time points. (D-F) Biliary excretion profiles for (D) DCF, (E) OH-DCF, and (F) DCF-AG. Time points represent accumulation of biliary flow during successive 15 min intervals (0-15, 15-30, 30-45, 45-60, 60-75, and 75-90 min). All data are expressed as mean ± standard error of the mean for 10-12 subjects/group. * $P < 0.05$; ** $P < 0.01$; *** $P < 0.001$ versus WT.

Table 3.1 Summary of DCF toxicokinetic parameters in plasma of FVB WT and FVB Mrp3 KO after a single 75 mg/kg DCF dose

Genotype	C_0 (μM)	$t_{1/2}$ (min)	$AUC_{0\text{-tlast}}$ (μM × min)
WT	699 ± 31	74.1 ± 12.8	34,600 ± 2,100
KO	701 ± 38	108 ± 10	35,900 ± 2,500

Table 3.1 Summary of DCF toxicokinetic parameters in plasma of FVB WT and FVB Mrp3 KO after a single 75 mg/kg DCF dose. C_0 indicates the estimated DCF plasma concentration at time zero, $t_{1/2}$ is the DCF elimination half-life, and $AUC_{0\text{-tlast}}$ is the area under the plasma concentration versus time curve for DCF from time zero to the last collected time point. Data are expressed as mean ± standard error of the mean for 10-12 subjects/group.

Figure 3.2 Hepatic concentrations of DCF, OH-DCF, and DCF-AG in FVB WT and FVB Mrp3 KO mice

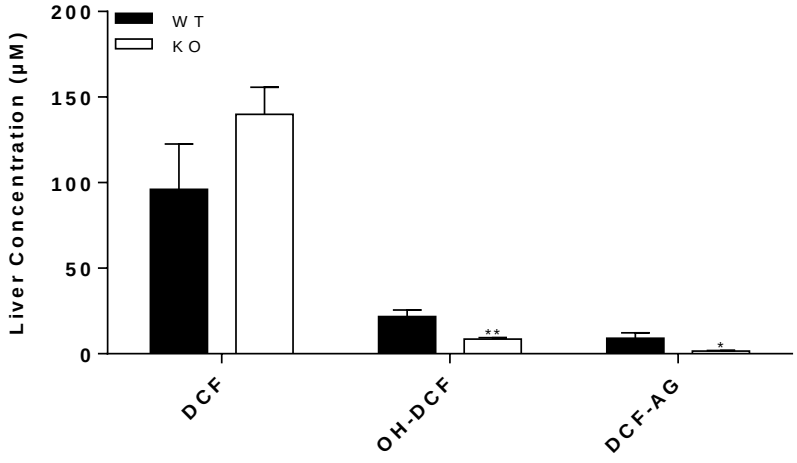

Figure 3.2 Hepatic concentrations of DCF, OH-DCF, and DCF-AG in FVB WT (■) and FVB Mrp3 KO (□) mice. Mice were injected with 75 mg/kg DCF. Livers were harvested 90 min following administration of vehicle or DCF. Data are expressed as mean ± standard error of the mean for 10-12 subjects/group. * $P < 0.05$; ** $P < 0.01$ versus WT.

Figure 3.3 Clinical chemistry of WT and KO mice 24 hours after a single dose of 90 mg/kg DCF

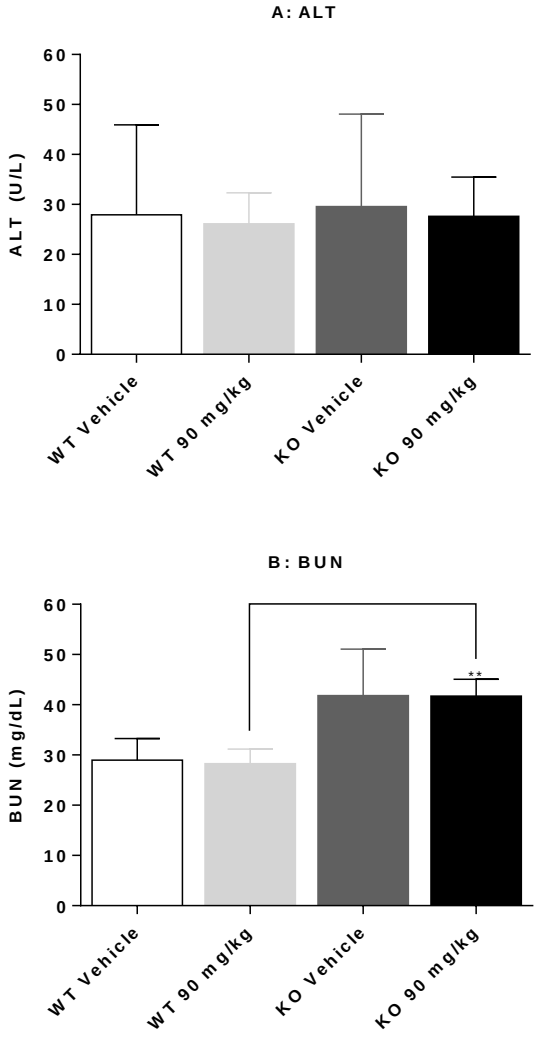

Figure 3.3 Clinical chemistry of C57 WT and C57 Mrp3 KO mice 24 hours after a single dose of 90 mg/kg DCF. (A) Plasma alanine aminotransferase (ALT). (B) Plasma blood urea nitrogen (BUN). Results are expressed as mean ± standard error of the mean for 3-7 subjects/group. ** $P < 0.01$ versus WT.

Figure 3.4 Summary of histopathology of small intestines from C57 WT and C57 Mrp3 KO mice 24 hours after administration of vehicle or 90 mg/kg DCF

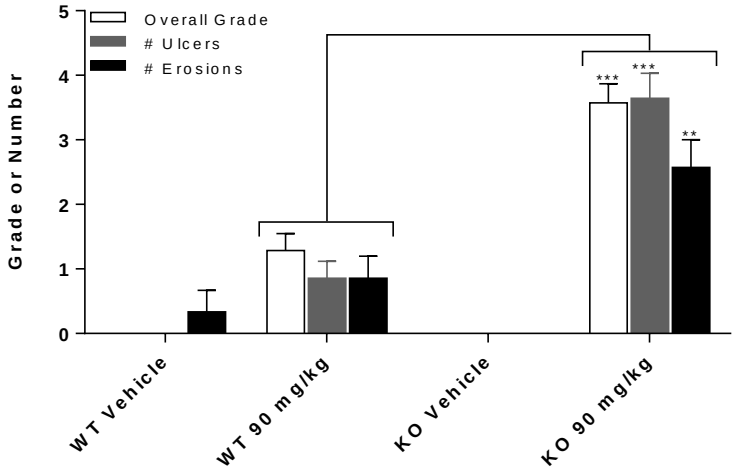

Figure 3.4 Summary of histopathology of small intestines from C57 WT and C57 Mrp3 KO mice 24 hours after administration of vehicle or 90 mg/kg DCF. Results are expressed as mean ± standard error of the mean for 3-7 subjects/group. The overall grade was based on the following scheme: 0 = none, 1= minimal, 2 = mild, 3 = moderate, 4 = marked, and 5 = severe. Ulcers and erosions reflect the number of findings that were indentified on an entire tissue section. ** $P < 0.01$; *** $P < 0.001$ versus treatment-matched WT.

Figure 3.5 Immunohistochemistry of tissues taken from C57 WT and C57 Mrp3 KO mice treated with vehicle or 90 mg/kg DCF

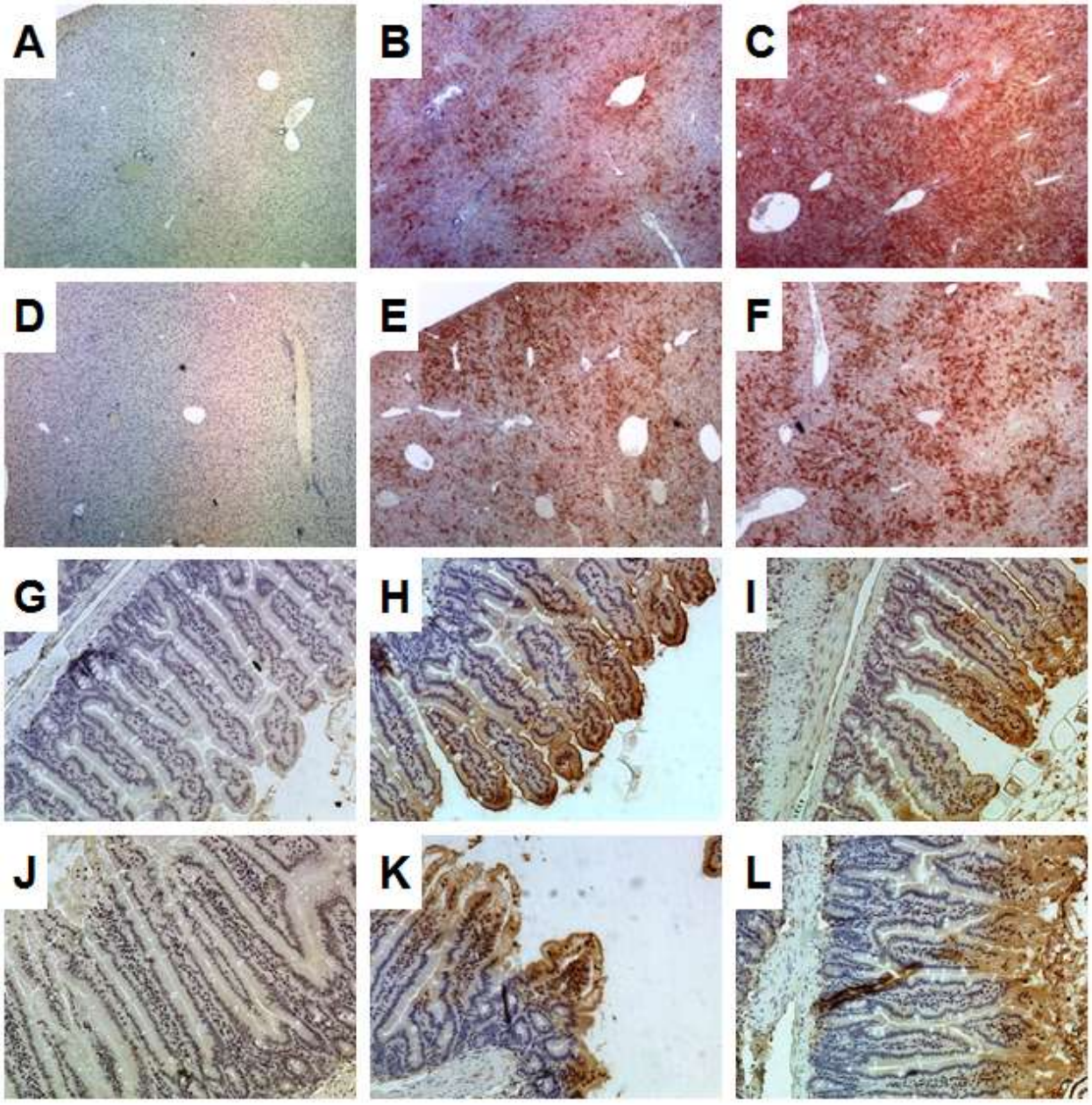

Figure 3.5 Immunohistochemistry of tissues taken from C57 WT and C57 Mrp3 KO mice treated with vehicle or 90 mg/kg DCF (immunoperoxidase with hematoxylin counterstain). Tissues were harvested 24 hours after administration. (A-C) Liver sections at 4× magnification. (A) Representative liver section from vehicle treated WT. (B and C) WT liver from subjects 3 and 6 after 90 mg/kg. (D) Liver from vehicle treated KO. (E and F) KO liver from subjects 4 and 7 after 90 mg/kg. (G-L) Small intestine sections at 15× magnification. (D) Representative small intestine from vehicle treated WT. (H and I) WT small intestine from subjects 4 and 6 after 90 mg/kg. (J) Small intestine from vehicle treated KO. (K and L) KO small intestine from subjects 2 and 4 after 90 mg/kg. The presence of DCF adducts is visualized by the presence of red/brown staining.

3.5 Discussion

This work explores the role of Mrp3 on the disposition and acute toxicity of DCF. DCF has high passive permeability, therefore its uptake into tissues should not be limited by active transport processes (Huang et al., 2010). The elevated DCF and lower OH-DCF plasma concentrations in KO compared to WT (Figure 3.1A-B) may indicate metabolic saturation. *In vitro* studies using mouse hepatic S9 fraction did not show differences in DCF metabolism as the WT and KO K_m values were comparable (Chapter 2 Figure 2.9). Further evidence of metabolic saturation comes from the OH-DCF plasma concentration-time profile which was relatively flat at 75 mg/kg DCF whereas at lower doses plasma OH-DCF was initially high before decreasing by first-order kinetics (Chapter 2 Figure 2.4).

The present DCF-AG data are consistent with low dose studies and demonstrate Mrp3-mediated DCF-AG efflux (Figure 3.1C). Our data confirm the observation reported by Lagas et al. (2010) that DCF-AG is an *in vivo* substrate of mouse Mrp3. KO had DCF-AG plasma concentrations that were nearly 90% lower compared to WT. Plasma concentrations of several glucuronide metabolites have been reported to be lower in Mrp3 KO compared to WT mice (Manautou et al., 2005; Zamek-Gliszczynski et al., 2006b). As KO mice were comparable to WT in terms of overall transporter expression except for Mrp3, the results indicate that Mrp3 mediates DCF-AG basolateral efflux *in vivo*.

DCF, OH-DCF, and DCF-AG biliary excretion showed no evident distinction between WT and KO. Because Mrp3 acts as a basolateral efflux pump for bile acids (Zelcer et al., 2003c), the bile flow in WT and KO was measured and found to be equal suggesting

that Mrp3 deletion and DCF treatment did not affect bile flow. That DCF-AG biliary excretion was similar between WT and KO was unexpected considering the pronounced plasma differences. Other studies in KO mice reported that low plasma or perfusate concentrations of glucuronides were inversely correlated with increased glucuronide biliary concentrations compared to WT (Manautou et al., 2005; Zamek-Gliszczynski et al., 2006b). Similar to rats, canalicular DCF-AG excretion would likely have been mediated by Mrp2 given the 88% protein sequence homology between mouse and rat Mrp2 (Altschul et al., 2005). Another canalicular transporter, breast cancer resistance protein (Bcrp, *Abcg2*), has been also demonstrated to transport DCF (Lagas et al., 2009). Exploratory studies in our laboratory with Bcrp-KO mice resulted in slight reductions of DCF-AG biliary excretion compared to WT (Chapter 2 Figure 2.1 and Figure 2.2).

To account for other possible DCF metabolites, bile fractions were pooled and infused onto the LC/MS/MS for qualitative metabolite profiling. Peaks corresponding to DCF taurine conjugate and diclofenac acyl glucuronide (OH-DCF-AG) were detected in prior exploratory studies (Chapter 2 Figure 2.7). Identification of these metabolites is consistent with their formation in rodent (Kenny et al., 2004; Sarda et al., 2012). Nonetheless, the OH-DCF-AG signal in KO bile would not have wholly accounted for the DCF-AG fraction that was diverted from entering the blood. Despite the DCF-AG mass balance inequity between WT and KO, there are instances in which Mrp3 ablation affects basolateral but not canalicular efflux. Zelcer et al. (2006) noted that hyodeoxycholate glucuronide perfusate concentrations were 4-fold greater in WT compared to KO while bile concentrations were similar between genotypes. Moreover,

fexofenadine plasma concentrations decreased 50% in Mrp3-KO mice relative to WT, yet biliary and hepatic fexofenadine concentrations between the genotypes were the same (Tian et al., 2008). Thus, Mrp3 deletion solely affected DCF-AG basolateral efflux.

The other aim of this study was to assess the susceptibility of Mrp3-null subjects to DCF-induced injury. Initial studies in FVB 129/Ola mice at a 90 mg/kg DCF dose resulted in KO, but not WT, exhibiting greater intestinal injury (data not shown). As FVB 129/Ola KO mice were unavailable, further studies were conducted in C57BL/6 KO mice. Neither the liver nor kidneys showed any evidence of damage by serum biomarker analysis (Figure 3.3). DCF has been shown to induce nephrotoxicity in ICR mice evidenced by a 2.5-fold increase in BUN concentrations 24 hours following an oral 100 mg/kg dose (Hickey et al., 2001). The finding in ICR mice likely reflects that strain's higher sensitivity to renal injury since C57BL/6 mice (Figure 3.3B) had no changes in BUN concentrations compared to vehicle treatment 24 hours after 90 mg/kg intraperitoneal administration. Regarding the liver, Lagas et al. (2010) reported that a 25 mg/kg intraperitoneal DCF injection caused ALT concentrations to increase 2-fold compared to WT leading the authors to conclude that slight liver toxicity occurred. However, the mice used in that study were triple knockouts for Bcrp, Mrp2, and Mrp3 making it difficult to ascribe which transporter was truly responsible for enhancing the toxic effect. Additionally, ALT, bilirubin, liver weights, and triglycerides were also slightly elevated in the triple KO versus WT suggesting that the mice may be more susceptible to challenge by a toxicant (Vlaming et al., 2009b). Though liver and kidney were devoid of injury for the present study, the small intestines in both genotypes exhibited damage with KO mice sustaining greater injury (Figure 3.4). The intestinal injury is consistent

with published reports on DCF ulcerogenicity (Atchison et al., 2000b; Ramirez-Alcantara et al., 2009).

Reactive DCF metabolites form adducts with a number of hepatic proteins (Seitz et al., 1998; Sallustio and Holbrook, 2001; Kenny et al., 2004). Immunohistochemistry revealed widespread covalent binding in the liver and small intestine but not in kidneys of both WT and KO (Figure 3.5). Qualitative assessment of the extent of staining did not provide meaningful distinction between the two genotypes (data not shown). DCF adduct staining was most intense in the liver, yet this organ did not appear to have any obvious histopathological damage. DCF-AG synthesis would be high in the liver, and it is plausible that DCF-AG adducted albumin, which is synthesized in the liver, and/or sequestered by thiols (protein and non-protein) that are not critical cellular targets. Though staining in small intestines was less robust, histopathology revealed significant damage (Figure 3.4). DCF-AG adduction to enterocytes potentially compromised enterocyte function and viability and possibly induced an immune-mediated response. Modulation of the immune function within 24 hours of toxicant exposure has previously been demonstrated for drugs such as acetaminophen (APAP). Administration of a toxic APAP dose activates hepatic macrophages (i.e., Kupffer cells) to release proinflammatory cytokines (Blazka et al., 1995b). This in turn stimulates the migration and infiltration of immune cells into the liver, influencing the ultimate toxic outcome. The role of the immune system in intestinal toxicity following DCF administration was beyond the scope of the present work and will be a focus of future studies.

DCF-AG could adduct enterocyte proteins on the extracellular surface or alternatively adduct from within after uptake by various transporters. Glucuronide conjugates can be

transported by organic anion transporting polypeptides (OATPs) of which OATP2B1 (*SLCO2B1*) is the predominant isoform in the human intestine (Ishiguro et al., 2008; Drozdzik et al., 2014). It is likely through the mouse Oatp2b1 homologue, which is also expressed in the intestines, that DCF-AG uptake occurs (Cheng et al., 2005). Nonetheless, the fact that the liver had intense adduct formation without apparent injury compared to the intestine which had extensive damage but moderate adduction may indicate that protein adducts of DCF metabolite(s) do not necessarily contribute to or cause toxicity.

DCF administration resulted in two diverse outcomes: 1) rapid generation of DCF-AG that was excreted into bile or plasma and 2) COX inhibition that decreased local and/or systemic prostaglandins that protect the GI mucosa. Based on the data, we propose the following series of events to occur in our model of DCF-induced toxicity. DCF-AG is taken up and covalently binds to targets (plasma membrane, intracellular proteins, etc.) compromising the integrity of the enterocyte. In KO, the DCF-AG basolateral efflux is attenuated potentially leading to higher accumulation of intracellular DCF-AG within enterocytes compared to WT. Meanwhile, intestinal mucosal protection is weakened due to DCF's pharmacological inhibition of both COX-1 and COX-2 (Menasse et al., 1978) causing a decrease in protective prostaglandins. Simultaneously, the highly permeable DCF enters enterocytes and exerts further injury through mitochondrial dysfunction leading to apoptosis (Gomez-Lechon et al., 2003a; Lim et al., 2006). Unbound DCF-AG may also dissociate into DCF and glucuronic acid intensifying diclofenac-induced mitochondrial dysfunction. Mrp2, which normally confers a measure of protection via DCF-AG efflux, could be affected as Mrp2 translocates intracellularly

from its apical membrane localization during oxidative stress (Sekine et al., 2006). The proposed events would, in theory, breakdown the overall intactness of the GI tract.

There are several issues that remain to be addressed: (1) the relationship between DCF-AG exposure and developing injury is unclear, (2) determining the DCF-AG concentrations in the small intestine that can cause damage, and (3) assessing why the small intestines but not liver or kidneys were affected. It will be necessary to devise experiments wherein the mechanism of injury by DCF-AG can be studied with minimal interference from its parent or hydroxylated metabolites. The degree of intestinal COX inhibition also warrants examination as a contributing cause for the GI injury observed following DCF administration.

In conclusion, the present work demonstrates that (1) Mrp3 is responsible for DCF-AG basolateral efflux during a toxic DCF challenge, (2) hepatic canalicular efflux is not perturbed by Mrp3 deletion, (3) KO mice have greater gastrointestinal damage compared to WT, and (4) appearance of adducts does not necessarily signify the occurrence of injury as certain organs are more sensitive to injury than others.

Chapter 4 ELUCIDATION OF THE MECHANISMS THROUGH WHICH THE REACTIVE METABOLITE DICLOFENAC ACYL GLUCURONIDE CAN MEDIATE TOXICITY

4.1 Abstract

We have previously investigated the toxicity of diclofenac (DCF) following a single high dose and reported significant intestinal injury in mice lacking the efflux transporter Mrp3. One proposed mechanism was that diclofenac acyl glucuronide (DCF-AG), as a substrate of Mrp3, played a part in mediating injury. Thus the goal of the current work was to determine the role that DCF-AG had in the observed enteropathy. Since both humans and mice express the uptake transporter OATP2B1 (*SCLO2B1*) in the intestines, this transporter was characterized for DCF-AG uptake. *In vitro* assays using HEK-OATP2B1 cells demonstrated that DCF-AG was a substrate with a V_{max} and K_m of 17.6 ± 1.5 pmol/min/mg and 14.3 ± 0.1 µM, respectively. It was also determined that DCF-AG has low passive diffusion, thus its uptake into cells would be highly dependent on active uptake. Another key finding from our *in vitro* assays was that DCF-AG was not only cytotoxic, but that its cytotoxicity was greater compared to DCF and occurred within 1 to 3 hours of exposure. The potential for DCF-AG to induce reactive oxygen species (ROS) was also addressed. We report that 1 mM DCF-AG caused a 6-fold increase in ROS by 3 hours. Further investigation focused on induction of oxidative stress through inhibition of superoxide dismutase (SOD). We observed that whereas DCF increased SOD activity, DCF-AG had 100% inhibition of SOD at the highest tested dose of 1 mM. Taken together, the cytotoxicity, SOD, and ROS results strongly suggest DCF-AG induced oxidative stress in our *in vitro* models. Lastly, DCF-AG was screened

for pharmacologic activity against COX-1 and COX-2 and was found to have IC_{50} values of 0.620 ± 0.105 and 2.91 ± 0.36 μM, respectively. Despite the weaker potency compared to its parent compound, that DCF-AG was able to inhibit the COX enzymes constituted a novel finding. Since COX inhibition can lead to intestinal ulceration, it is plausible that DCF-AG can also contribute to enteropathy via COX inhibition. Taken into context, the work presented herein demonstrated the multifactorial pathways by which DCF-AG can act as a direct contributor to toxicity following DCF administration.

4.2 Introduction

Prior work on DCF focused on its disposition and the contribution of efflux transporters in modulating toxic outcomes. In one notable report using rats that lacked the efflux transporter Mrp2 (*Abcc2*), these mutant rats exhibited resistance to intestinal injury after DCF administration (Seitz and Boelsterli, 1998). This discovery was followed up by the observation that DCF-AG administration led to increased GI ulceration compared to DCF administration. Our own work with efflux transporters demonstrated that Bcrp (*Abcg2*) and Mrp3 (*Abcc3*) had functional roles with respect to the disposition of DCF and DCF-AG (Chapter 2). Furthermore, toxicodynamic studies conducted in Mrp3 KO mice showed conclusively that KO mice developed increased intestinal damage compared to WT (Scialis et al., 2015). Despite the susceptibility differences between genotypes, the mechanisms involved in the increased injury remain unclear.

Our work, as well as that of others, demonstrated that administration of DCF leads to the formation of covalent adducts along the intestinal epithelia (Ware et al., 1998; Atchison et al., 2000b). In these instances, adduct formation was detected not only along the brush border of the intestinal villi, but was also observed within the enterocyte as well. It is reasonable to assume that adduction on the extracellular surface of plasma membrane was followed by internalization of the adducted protein (Boelsterli, 2003). Another pathway may involve the active transport of DCF-AG by intestinal uptake transporters followed by intracellular adduction. Indeed, the GI tract expresses a number of transporters that have recently been quantified by proteomic analysis using LC/MS/MS (Groer et al., 2013). One of the major uptake transporters is OATP2B1 (*SCLO2B1*), a known carrier for conjugated substances (Gao et al., 2012).

There exists then a distinct possibility that uptake of DCF-AG by OATP was contributory to the enteropathy observed in the aforementioned animal models. Evidence for uptake transporter activity, as a causative means towards injury, has gained recent attention. For instance, stably transfected HEK-OATP cells were used to explore toxicity due to transporter-mediated uptake of statins in a report by Zhang and colleagues (2013). For that work, active uptake of several compounds in the statin class of drugs by OATP1B1 (*SCLO1B1*) was shown to cause a left-shift in cytotoxicity potency compared to the toxicity observed in HEK-WT cells. The Zhang study takes on meaningful significance upon consideration that OATP1B1 is a major hepatoselective transporter. Since OATP2B1 intestinal expression is also correlated with uptake activity in the intestines (Sai et al., 2006), understanding the relationship between uptake and toxicity should be pursued.

Toxicity from DCF-AG cannot purely arise through its active uptake or decreased excretion. Other processes must occur to account for the increased GI injury attributed to DCF-AG compared to parental compound. A possible modality is involvement of the immune system either by activation of liver-specific Kupffer cells or immune response caused by covalent adduct recognition (Yano et al., 2012). The covalent adduct immune response hypothesis is difficult to test on an acute basis since the presence of antibodies due to covalent adducts does not always result in injury (Vojdani et al., 2015). Case in point, there was intense hepatic adduct formation in our DCF toxicodynamic study, yet despite the presence of resident macrophages which are known to be activated during a cytotoxic challenge, no hepatotoxicity was apparent (Chapter 3).

The findings in the liver strongly suggest that DCF-mediated enteropathy is not mediated by protein adduction in enterocytes. Nevertheless, there are alternative explanations for how DCF-AG is directly causing injury after DCF administration. A possibility is oxidative stress through inhibition of superoxide dismutase (SOD). SOD is a critical cellular defense mechanism for coping with reactive oxygen species (ROS) (Fridovich, 1978). Precedent of SOD inhibition by xenobiotic metabolites comes from a study by Chiou et al. (1999) in which suprofen acyl glucuronide inhibited SOD. Given the structural class similarity between DCF-AG and suprofen acyl glucuronide, DCF-AG inhibition of SOD becomes a distinct prospect. In addition to SOD perturbation, DCF-AG may induce oxidative stress by generation of ROS just as DCF has been shown to incite (Lim et al., 2006).

Gastrointestinal injury after DCF administration can occur through its pharmacologic effects, namely inhibition of cyclooxygenase (COX) enzymes. COX metabolism of arachidonic acid gives rise to a number of physiologically important derivatives such as prostaglandin E_2 (PGE_2) which functions to protect the GI mucosa (Kotani et al., 2006). DCF, a non-selective inhibitor of COX-1 and COX-2, promotes GI injury though decreased PGE_2 signaling. Inhibition of both COX isoforms is necessary for injury to develop. Toxicity studies wherein a selective COX-1 or COX-2 inhibitor was administered to mice failed to show significant GI damage (Tanaka et al., 2001). Yet, when a cocktail of a selective COX-1 and COX-2 inhibitors was given, profound injury became evident. DCF potency for COX-1 and COX-2 is weaker compared to selective inhibitors such as SC-560 and DuP-697 (Seibert et al., 1996; Smith et al., 1998a), so its ability to provoke injury is a reflection that promiscuity for general COX inhibition, rather

than potency against a single COX isoform, is a determining factor. In that context and considering that some DCF metabolites have shown pharmacological activity against COX, the capability of DCF-AG to inhibit COX enzymes presents an intriguing avenue to explore. Though conjugated metabolites are normally thought to be devoid of pharmacological activity compared to parent compounds, examples exist to the contrary. Such cases include morphine-6-glucuronide and mycophenolic acyl glucuronide (Osborne et al., 1992; Schutz et al., 1999). The pharmacologic potencies of those two glucuronide metabolites are equivalent to their parent compounds. In light of this, DCF-AG may possess enough COX inhibition pharmacology to promote injury.

Thus the goal of the current work was to identify the various mechanisms that DCF-AG can promote injury. This was accomplished through analysis of uptake by OATPs to determine if active uptake of DCF-AG can occur, and by conducting *in vitro* assays to quantify the extent of cytotoxicity as a result of ROS generation or inhibition of COX and SOD enzymes.

4.3 Materials and Methods

Chemicals and Reagents. DCF, DCFDA, DMEM, formic acid, hydrogen peroxide, HEPES, indomethacin (used as the IS), MOPS, and SC-560 were purchased from Sigma-Aldrich Corporation. (St. Louis, MO). DCF-AG was purchased from Toronto Research Chemicals Incorporated (Toronto, Canada). AA, COX-1, COX-2, Dup-697, and SOD were purchased from Cayman Chemical (Ann Arbor, MI). Calcein-AM was purchased from Thermo Fisher Incorporated (Waltham, MA). Ethidium homodimer-1 was purchased from Biotium Inc. (Hayward, CA). Stably-transfected HEK-OATP2B1 cells were created at Pfizer Inc (Sandwich, UK) and were previously described (Kalgutkar et al., 2013). All LC/MS/MS solvents were of high analytical grade and were purchased from Burdick & Jackson (Muskegon, MI).

***In Vitro* Transport.** HEK-WT and HEK-OATP2B1 cells were seeded at 60,000 and 90,000 cells/well, respectively, in 96-well poly-D-lysine coated microplates. Cells were grown in DMEM containing 10% heat-inactivated fetal bovine serum and 5 mM sodium pyrutate. Plates were kept in an incubator set to 95% relative humidity, 5% CO_2, and 37 °C. Upon reaching confluency 48 hours after seeding, the growth media was discarded, and cells were washed three times with 100 µL uptake buffer at 37 °C. Two types of buffer were used for the studies: 1) HBSS supplemented with 20 mM HEPES and titrated to pH 7.4, and 2) HBSS fortified with 20 mM MOPS and titrated to pH 6.0. The last wash was left on the cells for 15 min to equilibrate the cells before dosing commenced. After the equilibration period had passed, the last wash was removed and cells were dosed with 50 µL uptake buffer containing increasing DCF-AG concentrations. Plates were quickly placed on a shaker set to 150 rpm and 37 °C and incubated for 0.1,

0.5, 1, and 2 min. Termination of uptake was performed by quickly removing the uptake buffer, and the cells were washed 4 times with 200 µL ice-cold uptake buffer. Intracellular DCF-AG was extracted by adding IS in 100 µL ice-cold methanol and shaking the cell plates for 15 min at 4 °C. Cellular extracts were transferred into a clean 1 mL deep-well microplate and mixed with 100 µL solvent A. Sample plates were vigorously vortex-mixed and injected onto the LC/MS/MS. A DCF-AG standard curve was prepared using naïve cells and extracted using the same process described for samples. The injection volume for all sample types was 10 µL. Total DCF-AG uptake was quantified using the standard curve, and the data were reported as pmol. Cell counts and cell size were measured using a Millipore Scepter device (EMD Millipore, Billerica, MA), and total protein was determined using a Pierce BCA kit following the manufacturer's recommendations (Thermo Fisher Scientific Incorporated, Waltham, MA). Concentrations were then normalized to pmol per µL of total cell volume in each well.

Kinetic Modeling. The DCF-AG uptake data was subsequently analyzed using a 2-compartamental model previously described for OATP-mediated uptake (Poirier et al., 2008; Poirier et al., 2009). Essentially the model is governed by three processes: 1) $P_{dif,in}$ defined as passive diffusion from the media into the cell, 2) K_{active} which is active transport from the media into the cell, and 3) $P_{dif,out}$ representing passive diffusion from the cell into the media. A schematic of the model is shown in Figure 4.1. Each process is described using the following equations:

Equation 4.1

$$P_{dif,in} = P_{dif} \times C_{media}$$

Equation 4.2

$$K_{active} = \frac{V_{max} \times C_{media}}{K_m + C_{media}}$$

Equation 4.3

$$P_{dif,out} = P_{dif} \times C_{cell}$$

where P_{dif} was a passive diffusion constant (µL/min), C_{media} was the DCF-AG concentration of the media (µM), K_{active} is the saturable OATP2B1-mediated active transport that follows Michaelis-Menten kinetics, V_{max} is the maximal transport velocity (pmol/min), K_m is the substrate affinity (µM) at half the V_{max}, and C_{cell} is the intracellular DCF-AG concentration (µM). The P_{dif} and V_{max} parameters noted above were normalized by the total cellular protein per well to yield units of µL/min/mg and pmol/min/mg, respectively. The amount of DCF-AG in each compartment was defined by:

Equation 4.4

$$A_{media} = C_{media} \times V_{media}$$

Equation 4.5

$$A_{cell} = C_{media} \times V_{cell}$$

where A_{media} and A_{cell} were the DCF-AG amounts (pmol), V_{media} was the volume of the dosing buffer (50 µL), and V_{cell} was the total cellular volume per well (µL) that was determined during the cell counting procedure using total cell counts and cell diameter. Utilizing the previously described relationships, the temporal uptake of DCF-AG into cells was based on the following differential equation:

Equation 4.6

$$\frac{dA_{cell}}{dt} = K_{active} + P_{dif,in} - P_{dif,out}$$

The concentrations from the uptake studies were imported into Berkeley Madonna software v8.3.18 (Macey et al., 2000). A fourth order Runge-Kutta integration algorithm

was implemented using a proportional error model in which the time course data were log transformed. The software was used to fit the data and determine values for K_m, P_{dif}, and V_{max}. Each modeling run consisted of 6 concentrations, 4 time points in duplicate, and 2 cell types (HEK-WT and HEK-OATP2B1) giving 96 total data points. Model performance in Berkeley Madonna was assessed by selection of initial guesses and parameter ranges that resulted in the lowest root mean square error.

Cytotoxicity Assay. HEK-OATP2B1 cells were seeded at 100,000 cells/well in 96-well Optilux microplates (BD Gentest, Waltham, MA). Cells were grown in DMEM containing 10% heat-inactivated fetal bovine serum and 5 mM sodium pyrutate. Plates were kept overnight in an incubator set to 95% relative humidity, 5% CO_2, and 37 °C. The following day, the growth media was discarded, and cells were washed twice with 100 µL uptake buffer at 37 °C (HBSS, 20 mM HEPES, pH 7.4). After washing, cells were dosed in triplicate with 100 µL vehicle (uptake buffer with organic solvent), DCF, or DCF-AG and incubated for 3, 6, or 12 hours at 37°C. Thirty minutes before the incubation period ended, the cells were briefly removed from the incubator, overlaid with 100 µL of a cocktail containing 2 µM Calcein-AM (CAM) and 4 µM Ethidium Homodimer-1 (EthD-1), and placed back in the incubator for a final 30 minutes. Plates were then removed, and fluorescence was measured on a SpectraMax Gemini XPS reader (Molecular Devices, Sunnyvale, CA). The excitation/emission wavelengths for CAM were 490/520 nm while the excitation/emission wavelengths for EthD-1 were 530/620 nm. Responses for CAM and EthD-1 were normalized against the vehicle control cells.

ROS Assay. HEK-OATP2B1 cells were seeded, grown, and washed as detailed in the preceding section. After washing, the cells were dosed in triplicate with 100 µL vehicle or increasing concentrations of hydrogen peroxide, DCF, or DCF-AG and incubated for 1, 2, or 3 hours at 37 °C. At the end of the incubation period, the cells were removed from the incubator, the dosing media carefully aspirated, and the cells were gently washed once with 100 µL uptake buffer. Cells were overlaid with 100 µL of 1 µM CAM or 20 µM Dichlorofluorescein diacetate (DCFDA) and were placed back in the incubator for an additional 30 minutes at 37 °C. At the end of the incubation period, plates were removed, and fluorescence of the cells was measured on a SpectraMax Gemini XPS reader (Molecular Devices, Sunnyvale, CA). The excitation/emission wavelengths for both CAM and DCFDA were 490/530 nm. Responses for CAM and DCFDA were normalized against the vehicle control cells.

SOD Inhibition Assay. The SOD assay was conducted using a Cayman Chemical SOD kit with minor modifications to the recommended protocol. Briefly, SOD incubations consisted of 198 µL radical detector, 10 µL of copper/zinc SOD, and 2.3 µL vehicle or increasing concentration of inhibitor. Reactions commenced upon the addition of 20 µL xanthine oxidase, and the mixtures were shaken at 60 rpm in the dark for 30 min at room temperature. Samples were then read on a BioTek UV/Vis microplate spectrophotometer (BioTek Instruments Incorporated, Winooski, VT) at a wavelength of 450 nm. The SOD activity in all samples was compared against a SOD standard curve. Absorption responses were background subtracted, and the percentage SOD inhibition was determined by normalizing the inhibitor response to vehicle controls.

COX Inhibition Assay. The COX assay was performed using a Cayman Chemical COX kit with minor modifications to the recommended protocol. Briefly, COX incubations consisted of 194 µL reaction buffer, 2 µL heme, 2 µL COX (1 or 2) enzyme, 2 µL of arachidonic acid (AA), and 4 µL of vehicle or increasing concentration of inhibitor. Reactions were conducted for 2 min in duplicate at 37 °C and were quenched by the addition of 10 µL 1 M HCl. A 200 µL aliquot of the quenched reaction was transferred into a 1 mL deep-well microplate and diluted with 200 µL ice-cold methanol. From the diluted mixture, a 100 µL aliquot was mixed with 100 µL IS in ice-cold methanol, vigorously vortex-mixed, and injected onto the LC/MS/MS. Methodology for detecting analytes of interest were modified from Shinde et al. (2012). The injection volume for all sample types was 10 µL. Rather than merely follow AA depletion, COX inhibition was determined by monitoring the appearance of PGE_2 (PGE_2/IS peak area ratio) in all samples and normalizing the inhibitor response to vehicle controls.

LC/MS/MS Method. Chromatographic separation of analytes was performed on a 2.6 µm Kinetex XB-C18 30 × 2 mm column (Phenomenex Incorporated, Torrance, CA). The system front end consisted of a HTC PAL Autosampler (LEAP Technologies Incorporated, Carrboro, NC), a CBM-20A system controller, two LC20ADvp pumps, and a DGU-14A degasser (Shimadzu Scientific Instruments, Columbia, MD). Analytes of interest were eluted using one of two gradient profiles: method 1 (for DCF-AG) began with 10% solvent B for the first 0.5 min, which was then increased to 90% solvent B at 1.25 min using a linear gradient and held at this mixture for 0.25 min before reverting back to initial solvent conditions for 0.5 min to re-equilibrate the column, and method 2 (for PGE_2) began with 10% solvent B for the first 0.5 min, which was then increased to

95% solvent B at 2.00 min using a linear gradient and held at this mixture for 0.5 min before reverting back to initial solvent conditions for 0.5 min to re-equilibrate the column. The flow rate for both methods was 0.3 mL/min, and the column effluent was directed to waste for the initial 0.5 min before switching to the mass spectrometer. Analytes were detected using an AB Sciex API™ 4000 LC/MS/MS triple quad mass-spectrometer with a TurboIonSpray® probe and Analyst version 1.5.2 software (AB Sciex, Framingham, MA) that was operated in multiple reaction monitoring mode. Ion spray voltage was -4250 V, and the source temperature was set to 400 °C. The mass transitions in negative ion mode for monitoring AA, DCF-AG, PGE_2, and indomethacin were *m/z* 303.3→259.0, 470.1→192.9, 351.1→271.0, and 356.0→311.8, respectively. The retention times of AA, DCF-AG, PGE_2, and indomethacin were 2.46, 1.32, 1.55, and 1.47 (1.85 for method 2) min, respectively. Concentrations of analytes in the samples were determined by comparing the peak area ratios (analyte/IS) to those in the standard curve using a linear regression model. The criterion of acceptance for standards was defined to be ±20% of nominal concentration.

Statistical Analysis. Data are expressed as mean ± standard error of the mean. *P* values $\leq$ 0.05 were considered as statistically significant. Statistical analysis of data was performed using R version 3.2.1 (R Core Team, 2015). Two groups were compared by Student's *t* test, and multiple groups were compared by an analysis of variance followed by Tukey's *post hoc* test. GraphPad Prism version 6.0 (GraphPad Software Incorporated, La Jolla, CA) was used to calculate the IC_{50} for COX inhibition assays.

4.4 Results

***In Vitro* Transport**. The uptake of DCF-AG by a major intestinal transporter was measured using stably transfected HEK-OATP2B1 cells. DCF-AG kinetic uptake by OATP2B1 was measured at pH 6.0 and 7.4 to reflect the physiological conditions that OATP2B1 is exposed to in the intestine and liver, respectively (Fallingborg, 1999). DCF-AG was incubated at six concentrations ranging from 1 to 300 µM with time points taken at 0.1, 0.5, 1, and 2 min. The uptake of DCF-AG was both time- and concentration-dependent (Figure 4.2). Concentration versus time data were then analyzed using a 2-compartmental model as shown in Figure 4.1. The model was used to estimate transporter kinetic parameters that are summarized in Table 4.1. The kinetic parameters of V_{max}, K_m, and P_{dif} at pH 6.0 were 27.8 ± 4.1 pmol/min/mg, 15.2 ± 0.8 µM, and 0.0522 ± 0.0120 pmol/min/mg, respectively. It was determined that at pH 7.4, DCF-AG has V_{max}, K_m, and P_{dif} values of 17.6 ± 1.5 pmol/min/mg, 14.3 ± 0.1 µM, and 0.0245 ± 0.0030 pmol/min/mg, respectively. The higher V_{max} and P_{dif} values at pH 6.0 were found to be statistically significant compared to the parameter estimates at pH 7.4.

Cytotoxicity Assay. Having established a role for OATP2B1-mediated uptake of DCF-AG, HEK-OATP2B1 cells were incubated with DCF or DCF-AG and monitored over time. Cell viability was assessed using two fluorescent dyes that offer different modalities and are complementary to each other. Cell viability measured by CAM, which detects intact cells through esterase activity, indicated that as early as 3 hours, cell death by DCF was apparent at the 1 mM dose and by 12 hours 29% of the total cells were dead (Figure 4.3A). The cell viability was confirmed by EthD-1 that detects cell death by binding to

DNA once the nuclear envelope becomes compromised, and EthD-1 response increased by a maximum of 1.3-fold for the 12 hour 1 mM incubation (Figure 4.3C). Compared to DCF, DCF-AG induced greater cell death. After 3 hours, approximately 61% of cells were dead at the 1 mM dose, and the number of dead cells increased to 85% by 12 hours for the 1 mM condition. (Figure 4.3B). EthD-1 in DCF-AG incubations corroborated the CAM results. The EthD-1 response for a 12 hour incubation with 1 mM DCF increased over 2-fold compared to vehicle control (Figure 4.3D).

ROS Assay. Taking into account that DCF had been shown to promote generation of reactive oxygen species, we investigated if DCF-AG had a similar potential. As for the cytotoxicity assay, HEK-OATP2B1 cells were exposed to DCF or DCF-AG and observed for ROS generation. Since cytotoxicity was evident by 3 hours, the ROS assay was conducted from one to three hours to determine if ROS preceded cell death. ROS production was measured with the fluorescent probe DCFDA. Hydrogen peroxide, a known ROS producer, was used as positive control and exhibited an increase in DCFDA signal in a dose-dependent manner (Figure 4.4A). All hydrogen peroxide incubations achieved statistical significance compared to vehicle controls. ROS production by DCF was relatively modest by comparison resulting in a statistically significant 1-2 fold increase at 3 hours for the 1 mM dose (Figure 4.4B). DCF ROS induction appeared to indicate a dose response at 3 hours. DCF-AG demonstrated a clearer time-dependent ROS production culminating with a 5.5-fold increase at 3 hours for the 1 mM dose (Figure 4.4C). The 500 µM DCF-AG showed trends of increased ROS generation, though only for the 3 hour incubation, which yielded a 1.8-fold increase versus vehicle that was statistically significant.

SOD Inhibition Assay. The SOD inhibition assay was utilized to explore whether DCF or DCF-AG could inhibit SOD enzymatic activity. SOD incubations were non-cell based and consisted of a mixture of substrate, enzymes, inhibitor, and detection reagent. Rather than inhibiting SOD activity over the concentration range, DCF caused an apparent stimulation with the stimulus becoming statistically significant at the 250 µM dose and beyond (Figure 4.5). DCF-AG had an opposite effect and was associated with a dose-dependent decrease in SOD activity such that there was a striking 100% inhibition of SOD at the 1 mM dose (Figure 4.5). Furthermore, a statistically significant inhibition of 27% was observed at the 250 µM DCF-AG dose.

COX Inhibition Assay. The pharmacology of DCF for COX enzymes has been thoroughly evaluated, yet the pharmacology for DCF-AG has not been characterized. Hence, the final aspect of our work was to explore DCF-AG inhibition of COX enzymes. COX inhibition assays were non-cell based and used isolated COX enzymes that were mixed with substrate, co-factor, and inhibitor. Selective inhibitors of COX-1 and COX-2 were used as controls. Inhibition was assessed by measuring the decreased synthesis of PGE_2 from AA. A summary of the findings is listed in Table 4.2. SC-560 and DuP-691, as selective COX-1 and COX-2 inhibitors, had IC_{50} values of 0.00166 ± 0.00022 µM and 0.00714 ± 0.0007 µM, respectively (Figure 4.6A and Figure 4.7A). DCF, as a non-selective COX inhibitor had COX-1 and COX-2 IC_{50} concentrations of 0.0206 ± 0.0037 µM and 0.103 ± 0.005 µM, respectively (Figure 4.6B and Figure 4.7B). OH-DCF was more potent against COX-1 than COX-2 and reached an apparent plateau for COX-2 inhibition. The OH-DCF IC_{50} values were estimated to be 0.375 ± 0.075 µM and 21.2 ± 0.3 µM for COX-1 and COX-2, respectively (Figure 4.6C and Figure 4.7C).

Lastly, DCF-AG was demonstrated to inhibit PGE_2 synthesis with COX-1 and COX-2 IC_{50} estimates of 0.620 ± 0.105 μM and 2.91 ± 0.36 μM, respectively (Figure 4.6D and Figure 4.7D). COX-1 inhibition potency of DCF-AG was weaker compared to OH-DCF, however COX-2 inhibition potency by DCF-AG was more intermediate with respect to DCF and OH-DCF.

Figure 4.1 Visual representation of a mechanistic 2-compartmental transporter model

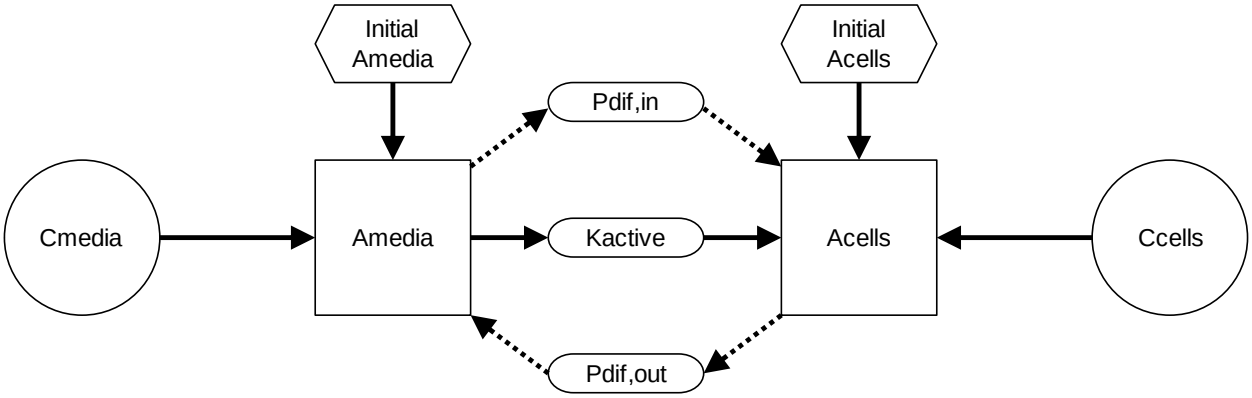

Figure 4.1 Visual representation of a mechanistic 2-compartmental transporter model. The movement of DCF-AG in the proposed model is described by three vectorial processes: 1) passive diffusion from the buffer into the cell, 2) active transport from the buffer into the cell, and 3) passive diffusion from the cell into the buffer. Active transport for this model applies for the OATP2B1-mediated uptake of DCF-AG.

Figure 4.2 Concentration versus time profiles of DCF-AG uptake by OATP2B1

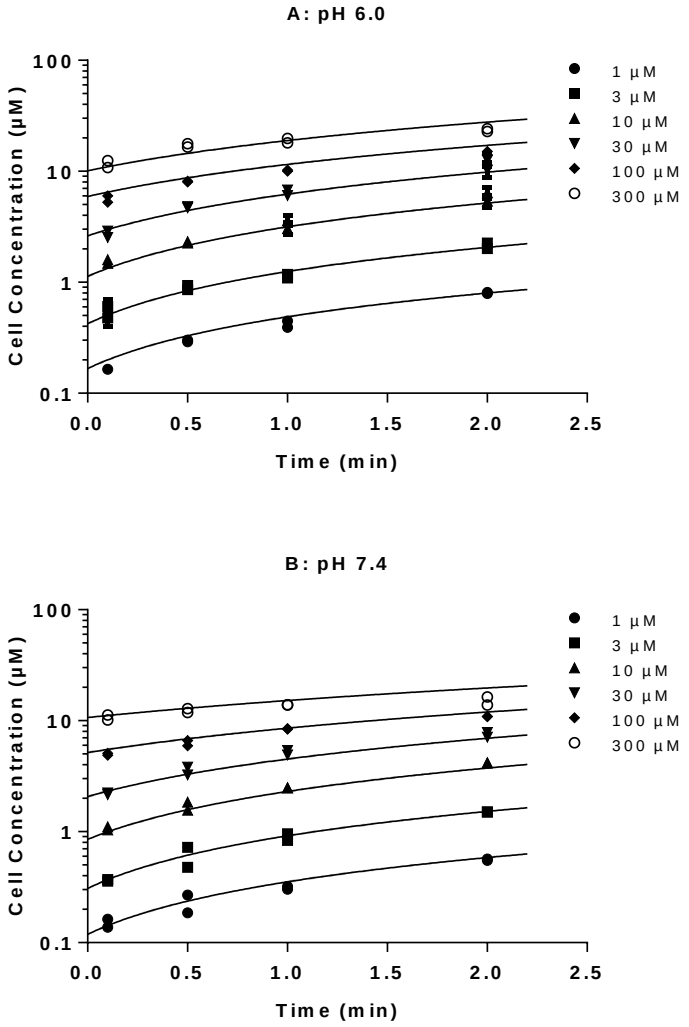

Figure 4.2 Concentration versus time profiles of DCF-AG uptake by OATP2B1. HEK-WT and HEK-OATP2B1 cells were seeded for 48 hours and incubated with increasing concentrations of DCF-AG at multiple time points in buffer titrated to either pH 6.0 or 7.4 at 37 °C. Intracellular concentrations were determined by LC/MS/MS, and the concentrations were modeled in Berkeley Madonna. (A) and (B) show the uptake of DCF-AG by HEK-OATP2B1 cells at pH 6.0 and 7.4, respectively. Fitted lines from a 2-compartment model represent the best fit. Data are the individual replicates from a typical study.

Table 4.1 Summary of DCF-AG uptake kinetics mediated by OATP2B1

Media pH	V_{max} (pmol/min/mg)	K_m (μM)	Uptake CL_{int} (μL/min/mg)	P_{dif} (μL/min/mg)
6.0	27.8 ± 4.1*	15.2 ± 0.8	1.82 ± 0.19	0.0522 ± 0.0120*
7.4	17.6 ± 1.5	14.3 ± 0.1	1.23 ± 0.11	0.0245 ± 0.0030

Table 4.1 Summary of DCF-AG uptake kinetics mediated by OATP2B1. Each value represents the mean ± standard error of the mean from 3 studies (n=2 replicates per study). * $P < 0.05$ for pH 6.0 versus pH 7.4.

Figure 4.3 Cytotoxicity of DCF and DCF-AG using HEK cells

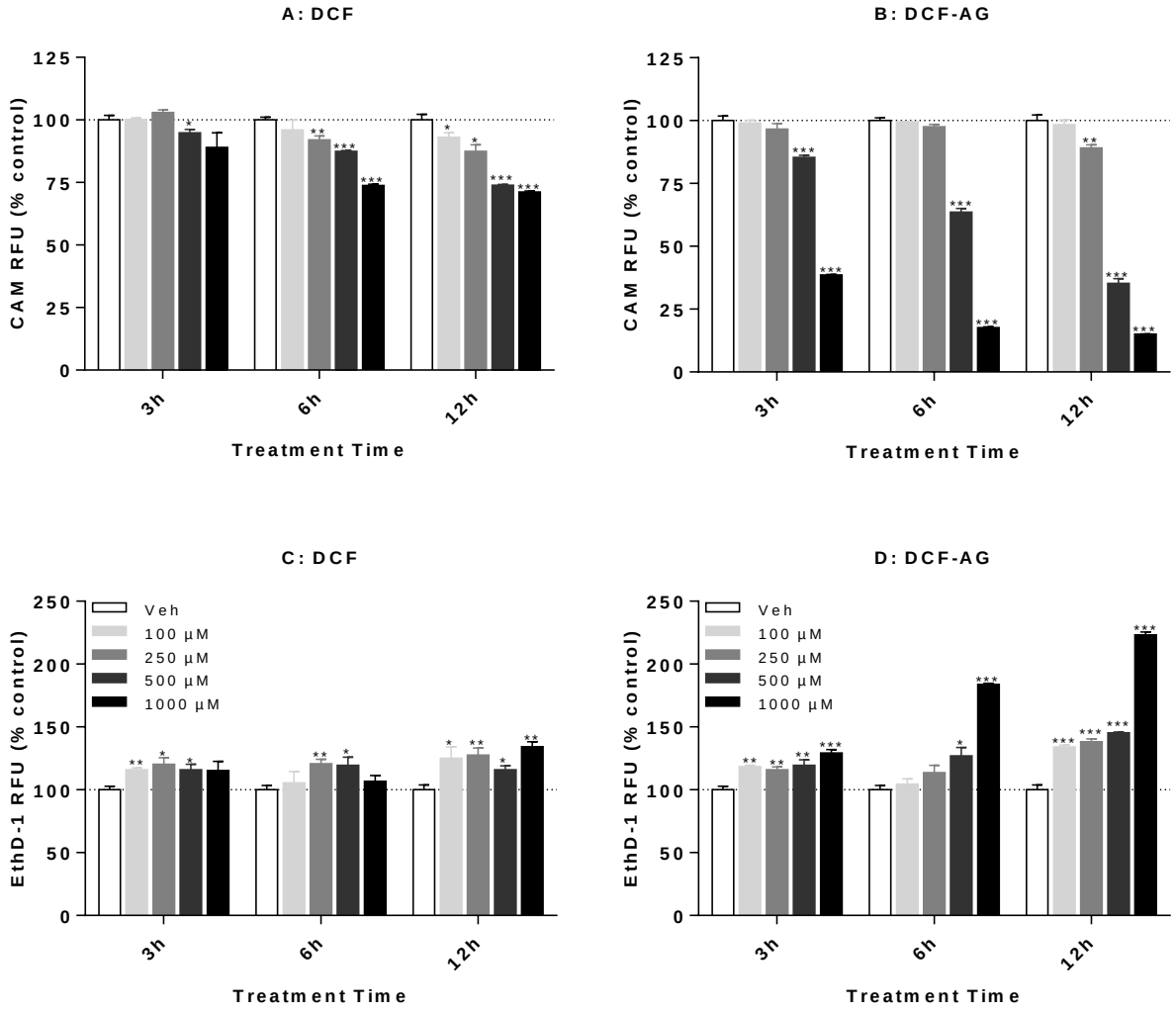

Figure 4.3 Cytotoxicity of DCF and DCF-AG using HEK cells. HEK-OATP2B1 cells were incubated in the absence or presence of increasing concentrations of compound. Incubations were conducted for 3, 6, or 12 hours at 37 °C. Cytotoxicity was assessed using Calcein AM (CAM) to determine live cells and Ethidium Homodimer-1 (EthD-1) as an indicator of dead cells. The CAM and EthD-1 responses indicate concentration-dependent cell death by DCF, and the cytotoxicity was more pronounced for DCF-AG. Each bar represents the mean ± the standard deviation of n=3 measurements per condition. * $P < 0.05$, ** $P < 0.01$; *** $P < 0.001$ compound versus its time-matched Vehicle incubation.

Figure 4.4 Generation of reactive oxygen species by in HEK cells

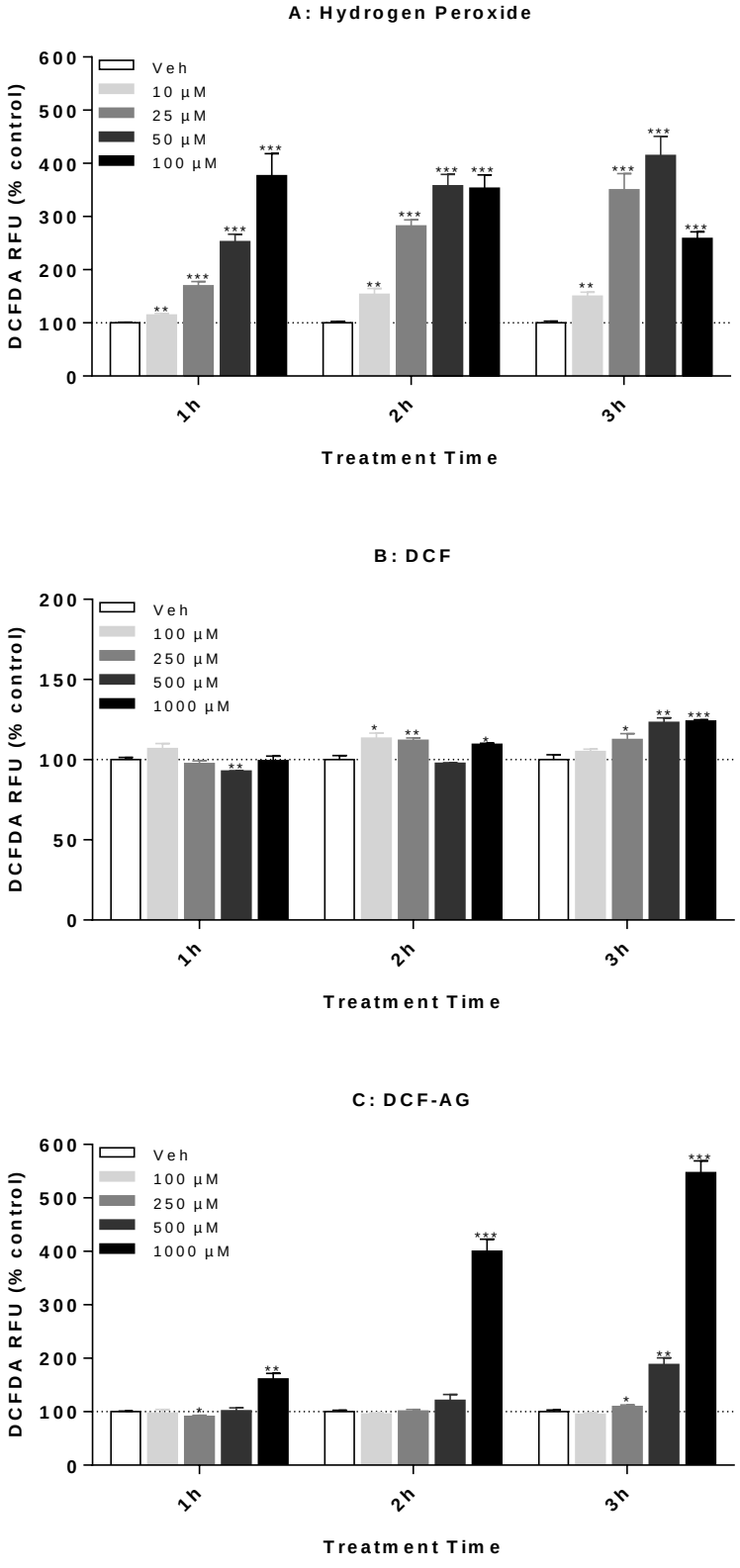

Figure 4.4 Generation of reactive oxygen species by in HEK cells. HEK-OATP2B1 cells were incubated in the absence or presence of increasing concentrations of compound. Incubations were conducted for 1, 2, or 3 hours at 37 °C after which ROS were detected with the use of DCFDA, which becomes oxidized by ROS to a fluorogenic form. Fluorescence was normalized to vehicle controls and expressed as percentage change from vehicle. Each bar represents the mean ± the standard deviation of n=3 measurements per condition. * $P < 0.05$, ** $P < 0.01$; *** $P < 0.001$ compound versus its time-matched vehicle incubation.

Figure 4.5 Inhibition of superoxide dismutase as an indication of oxidative stress

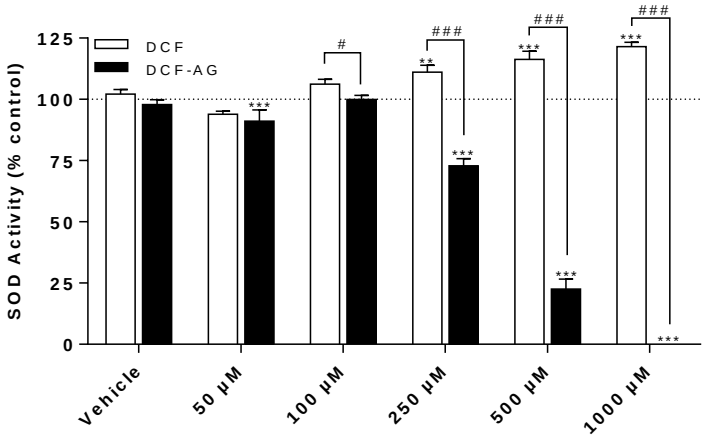

Figure 4.5 Inhibition of superoxide dismutase as an indication of oxidative stress. Copper/zinc SOD was incubated in the absence or presence of increasing concentrations of DCF (□) or DCF-AG (■) for 30 min at room temperature (ca. 25 °C). Vehicle shows assay performance in the presence of the same level of organic solvent (DMSO) used in the inhibitor incubations. Each bar reflects the mean ± standard error of the mean from 3 separate studies (n=2 replicates per study). ** $P < 0.01$; *** $P < 0.001$ inhibitor versus its Vehicle incubation. # $P < 0.05$, ### $P < 0.001$ for DCF versus DCF-AG.

Figure 4.6 COX-1 inhibition profiles of DCF, OH-DCF, and DCF-AG

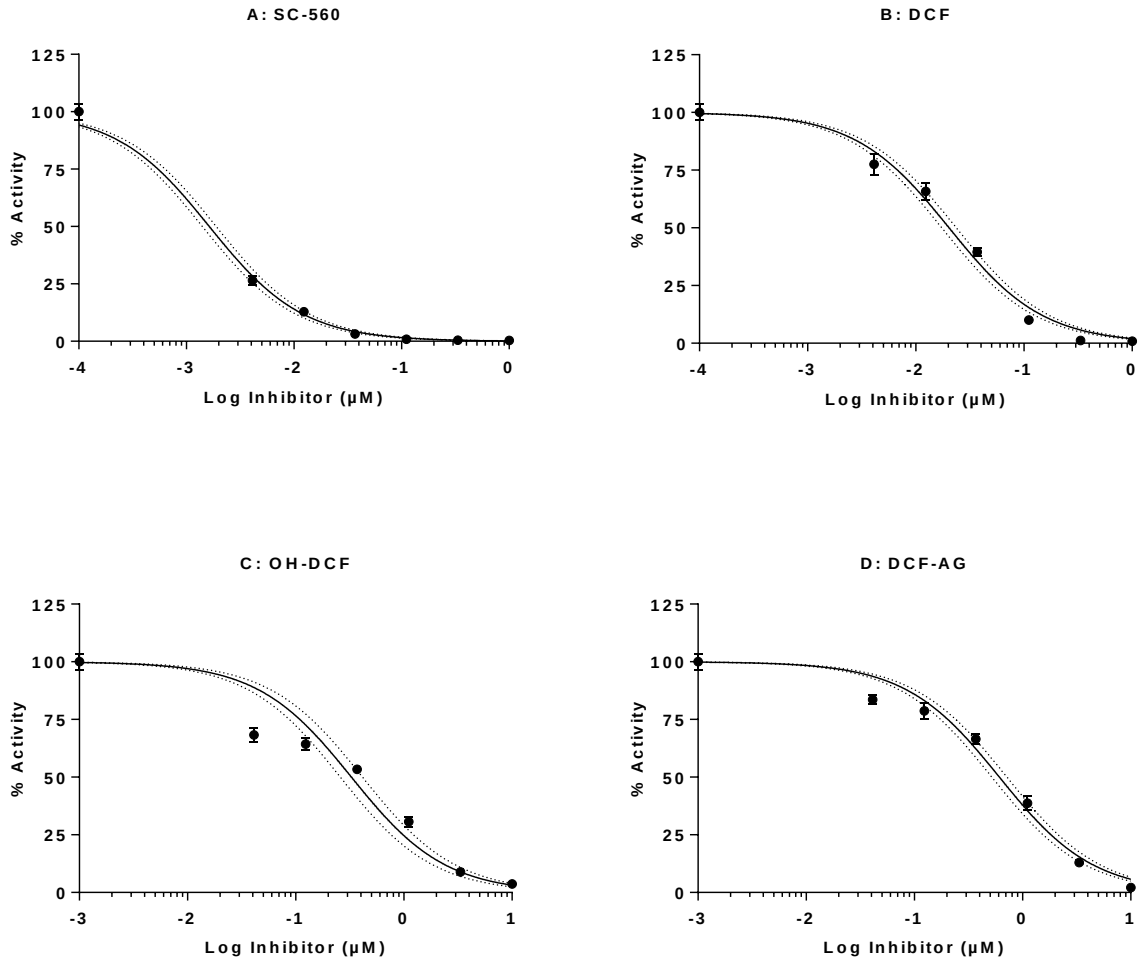

Figure 4.6 COX-1 inhibition profiles of DCF, OH-DCF, and DCF-AG. Recombinant COX-1 was incubated in the presence of inhibitors for 2 min at 37 °C, and the formation of PGE_2 from AA was monitored via LC/MS/MS. Data reflect the mean ± standard error of the mean from 3 separate studies (n=2 replicates per study). Inhibition data were fit with a three parameter model to calculate IC_{50}. Dotted lines reflect the 95% confidence intervals of the fit.

Figure 4.7 COX-2 inhibition profiles of DCF, OH-DCF, and DCF-AG

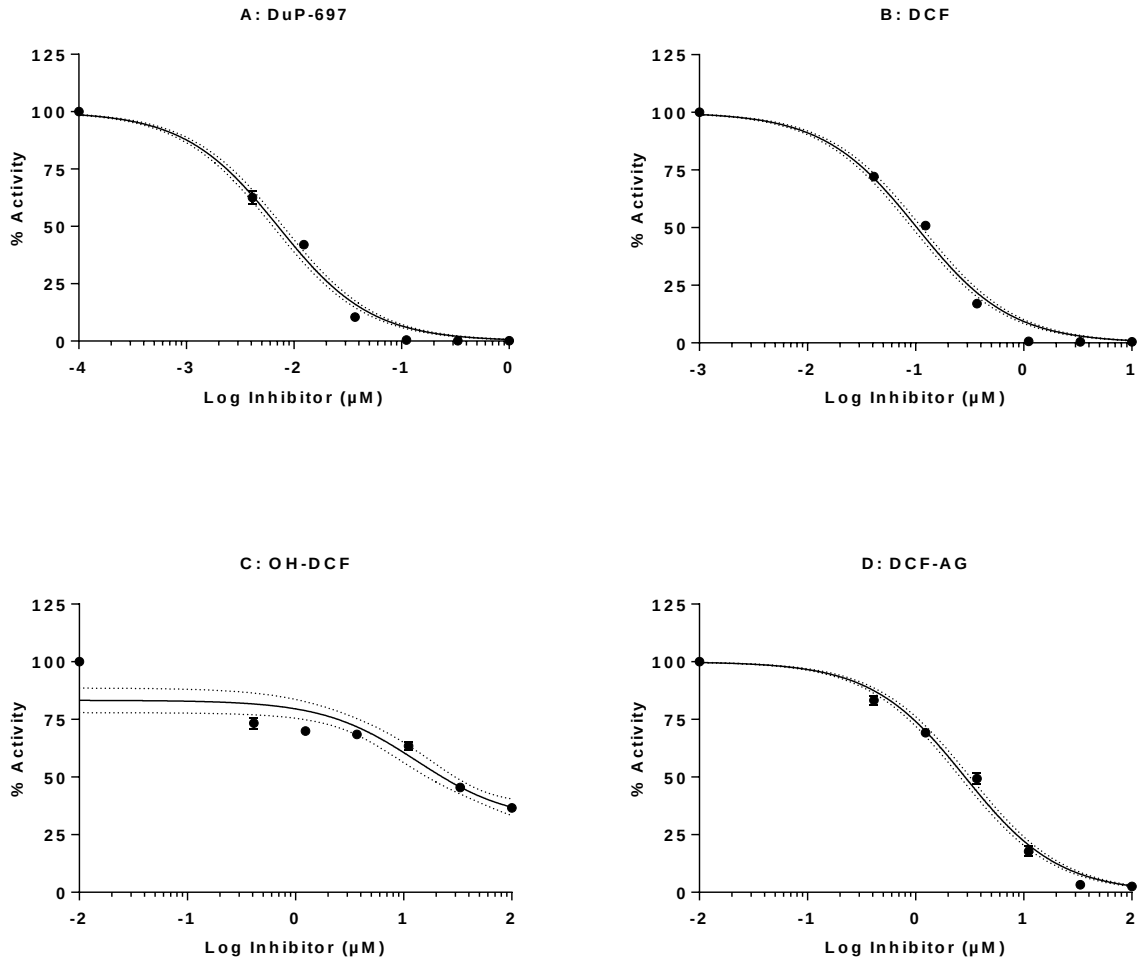

Figure 4.7 COX-2 inhibition profiles of DCF, OH-DCF, and DCF-AG. Recombinant COX-2 was incubated in the presence of inhibitors for 2 min at 37 °C, and the formation of PGE_2 from arachidonic acid was monitored via LC/MS/MS. Data reflect the mean ± standard error of the mean from 3 separate studies (n=2 replicates per study). Inhibition data were fit with a three parameter model to calculate IC_{50}. Dotted lines reflect the 95% confidence intervals of the fit.

Table 4.2 Summary of *in vitro* COX inhibition assays

Compound	COX-1 IC_{50} (μM)	COX-2 IC_{50} (μM)
SC-560 (COX-1 selective)	0.00166 ± 0.00022	N.D.
DuP-697 (COX-2 selective)	N.D.	0.00714 ± 0.0007
DCF	0.0206 ± 0.0037	0.103 ± 0.005
OH-DCF	0.375 ± 0.075	21.2 ± 0.3
DCF-AG	0.620 ± 0.105	2.91 ± 0.36

Table 4.2 Summary of *in vitro* COX inhibition assays. IC_{50} values reflect the mean ± standard error of the mean from 3 experiments (n=2 replicates per experiment). N.D.: not determined.

Figure 4.8 Proposed pathways on the disposition and mechanism of intestinal toxicity for DCF-AG

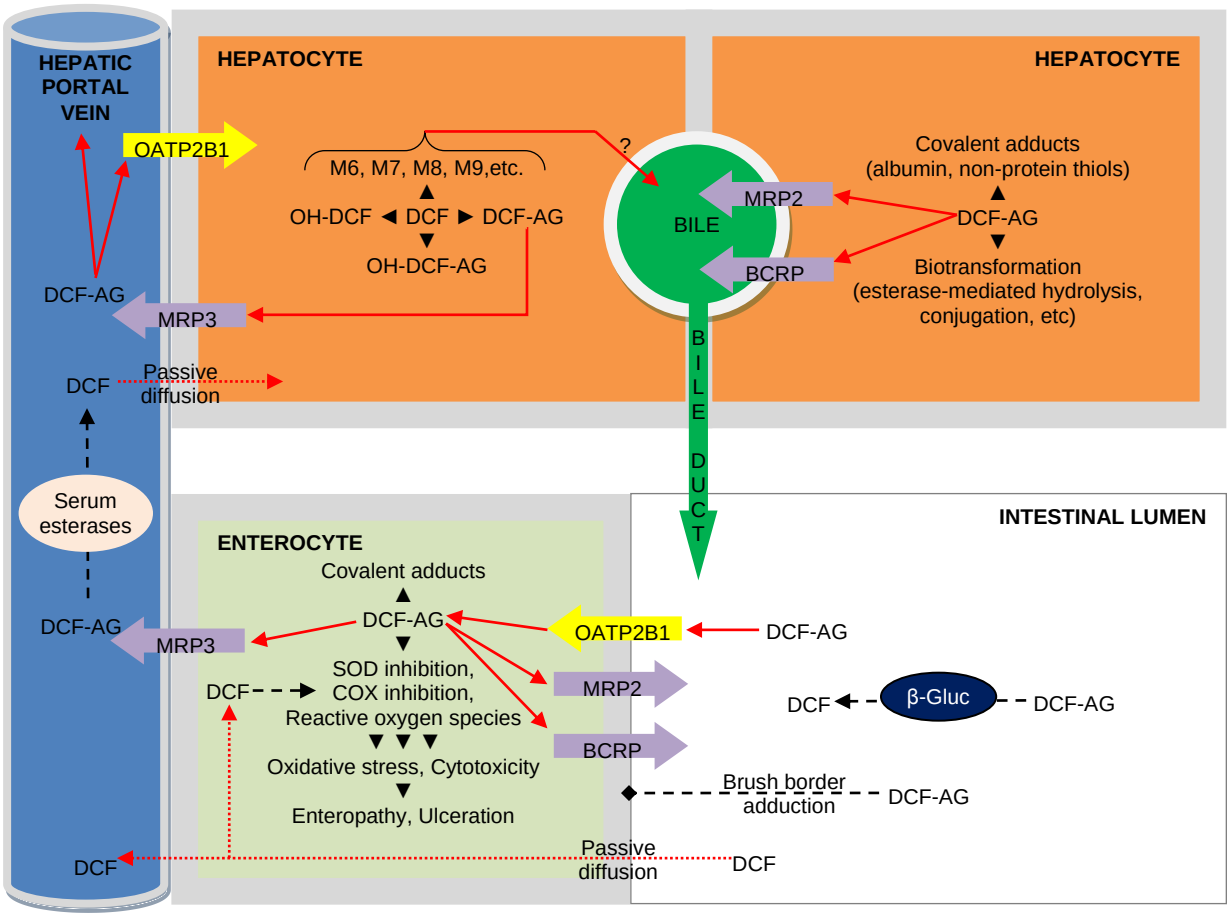

Figure 4.8 Proposed pathways on the disposition and mechanisms of toxicity for DCF-AG. DCF-AG is generated in the liver after DCF (IP or PO) administration where it undergoes excretion into bile or blood via ABC transporters. Luminal DCF-AG is taken up by OATPs where it exerts various effects that lead to intestinal injury. The absence of MRP3 exacerbates GI injury from DCF-AG due to the loss of a clearance mechanism from enterocytes. Solid arrows indicate vectorial transport via uptake or efflux transporters, or via blood flow. Dotted arrows signify transport by passive processes. Dashed lines demonstrate possible enzymatic reactions such as inhibition of COX, generation of ROS, or cleavage by bacterial β-glucuronidases. The question mark denotes uncertainty regarding the efflux pathways for the indicated metabolites.

4.5 Discussion

Our interest in exploring the toxicity attributed to DCF-AG was borne through our initial work of characterizing the role that efflux transporters have in modulating toxicity following acute administration of DCF. Our research led to the discovery that mice lacking the efflux transporter Mrp3 were more susceptible to intestinal injury compared to WT (Scialis et al., 2015). Though the intestinal toxicity differences between WT and KO were unequivocal, the mechanisms behind those differences were uncertain. Hence the research presented herein sought to elucidate the probable causes through which injury occurred.

In light of the findings that immunohistochemical staining of intestinal tissues detected covalent adducts on the brush border of enterocytes as well as deep within the villi, we postulated that DCF-AG, as a causative agent to the covalent adducts, was subjected to an active transport process. The intestines are host to an array of transporters (Drozdzik et al., 2014) some of which may be operative with respect to DCF-AG transport. One of the likely candidates for uptake of DCF-AG would be OATP2B1, a transporter known to mediate influx of glucuronide conjugates of other compounds (Gao et al., 2012; Grosser et al., 2014). Thus, OATP2B1 was investigated for affinity of DCF-AG using a stably transfected cell system. By implementing a mechanistic model (Poirier et al., 2008), we were able to define the kinetic parameters describing DCF-AG uptake by OATP2B1. Compartmental modeling is becoming more frequently used due to the versatility it offers to define multiple processes in addition to allowing simultaneous fitting of several datasets (Poirier et al., 2009; Menochet et al., 2012; De Bruyn et al., 2015). Preliminary studies with transfected cells showed that after six

minutes of incubation, OATPs were able to increase intracellular DCF-AG concentrations to levels exceeding the initial buffer conditions (Supplement 3). Based on those observations, we investigated the activity of OATP2B1 as a concentrative force for DCF-AG uptake.

We report that OATP2B1 acts an uptake transporter for DCF-AG, and that its affinity for DCF-AG varies with extracellular pH. OATP2B1 transporter clearance for DCF-AG was 1.82 µL/min/mg at pH 6.0 while the transport clearance at pH 7.4 was 1.23 µL/min/mg (Table 4.1). These findings are relevant in that they indicate OATP2B1 activity is greater at pH 6.0 which is a typical pH in the intestines (Evans et al., 1988). The differential affinity is not surprising given that pravastatin uptake by OATP2B1 was also found to be sensitive to pH. (Varma et al., 2011). The transporter clearance values at pH 7.4 would be applicable for hepatic OATP-mediated uptake of DCF-AG as several OATPs, including OATP2B1, are expressed on the basolateral membrane in the liver (Hagenbuch and Meier, 2003; Wang et al., 2015). The mechanistic modeling permitted estimation of the passive diffusion clearance for DCF-AG. We determined that DCF-AG had a passive uptake clearance that was nearly 2.1-fold greater at pH 6.0 compared to pH 7.4 (0.0522 versus 0.0242 µL/min/mg, respectively). The OATP-dependent uptake of the two positive controls that are known to be OATP2B1 substrates, estrone-3-sulfate and rosuvastatin, were similarly increased at pH 6 compared to pH 7.4 (data not shown). A study by Ming and colleagues likewise indicated that fexofenadine uptake at pH 6.0 was increased compared to pH 7.4 transport (Ming et al., 2011). The increase in DCF-AG passive permeability can be explained through analysis of its structure. The carboxylic acid moiety on the glucuronide ring of DCF-AG has an apparent pKa of 2.7

that becomes less ionized at acidic pH (ACD/Labs). Thus the increased passive diffusion at pH 6.0 was driven by increased flux of unionized DCF-AG. This rationale has been used to explain the tissue distribution of ionized and neutral species at various pH using OATP-mediated uptake (Ghosh et al., 2014). The same cells used by Ghosh and colleagues were implemented for DCF-AG uptake, hence the two findings are comparable. Despite the increased passive diffusion at pH 6.0, DCF-AG uptake would be dominated by active uptake as the intrinsic uptake clearance by OATP2B1 was 35-fold greater than passive diffusion. This categorizes DCF-AG as an ECCS class 3b compound making it dependent on active uptake to attain meaningful intracellular concentrations (Varma et al., 2015). DCF, in contrast, as a smaller molecule with high passive uptake, has no such limitations and can more freely enter cells (Huang et al., 2010). Though OATP2B1 is a human transporter, there exists a mouse homologue Oatp2b1 that has been shown to be expressed in the intestinal tract (Cheng et al., 2005). Overall, the OATP2B1 studies provide insight as to how the intracellular covalent adducts observed in our previous mouse studies (Chapter 3 Figure 3.5) may have arisen.

Having established a potential role for OATP2B1-mediated uptake of DCF-AG, we next theorized that toxicity from DCF-AG could be enhanced due to OATP2B1 transport. To that end, we conducted cytotoxicity assays with HEK-OATP2B1 cells. Our studies indicated that DCF-AG is indeed cytotoxic, and that cytotoxicity can manifest within 3 hours of exposure (Figure 4.3B). Furthermore, the cytotoxicity by DCF-AG was found to be greater than that of the parent compound. The DCF-AG concentrations chosen for the cytotoxicity assays were physiologically relevant in that they are in the same range

as the biliary concentrations detected in mice after an IA administration of 75 mg/kg DCF (Chapter 3 Figure 3.2). In our toxicodynamic studies with 90 mg/kg diclofenac, we were only able to observe intestinal injury 24-hours post-administration since that was the sole time point chosen for tissue harvesting (Chapter 3 Figure 3.4). The cytotoxicity data here indicate that injury, in terms of cell death, may occur with early onset. Cell death by DCF reached a maximum of 29% by 12 hours at 1 mM compared to nearly 62% cell death for DCF-AG by 3 hours at 1 mM with a maximal cell death of 85% reached after 12 hours. DCF can cause higher cytotoxicity than what was observed in our assays. These data substantiate the findings reported in TR- rats wherein administration of bile containing DCF-AG elicited greater intestinal injury compared to an equimolar dose of DCF (Seitz and Boelsterli, 1998). It is conceivable that Oatp-mediated uptake of DCF-AG in our mouse model, along with the cytotoxicity potential of DCF-AG, may have contributed to the increased enteropathy in Mrp3 KO mice since those mice had reduced capacity to eliminate DCF-AG compared to WT.

Oxidative stress is another means by which cell toxicity can occur. Specifically, generation of reactive oxygen species may overwhelm a cell's ability to maintain homeostatic redox levels. For instance, the pesticide rotenone is a known inducer of ROS, and exposure to rotenone results in cell death (Tamilselvam et al., 2013). Accordingly, we conducted ROS assays with DCF and DCF-AG to determine their ROS activity. The positive control in the assay, hydrogen peroxide, increased ROS in a dose-dependent manner (Figure 4.4A) verifying its role as a ROS-inducting agent (Alia et al., 2005). DCF ROS induction was relatively weak, yet ROS production was significantly increased after 2 hours of exposure (Figure 4.4B). The modest ROS

increase by DCF in our assay was less than a nearly 6-fold increase in ROS caused by DCF after a 30 hour exposure in a hepatocyte model of cytotoxicity (Lim et al., 2006). DCF-AG exhibited a dose-dependent increase in ROS with a maximal increase of 5.5-fold after 3 hours (Figure 4.4). Given that the ROS assay was carried out from 1-3 hours compared to the cytotoxicity assay time frame of 3-12 hours, an argument can be made that DCF-AG ROS production is a contributing factor to the observed cell death in our assays. As to how ROS production promotes cell death, possible pathways are through inhibition of ATPases, oxidation of DNA, perturbation of the mitochondrial permeability transition pore, or protein inactivation (Cantoni et al., 1989; Martinez-Reyes and Cuezva, 2014).

Oxidative stress can come about through means other than generation of ROS. For instance, administration of high doses of acetaminophen promotes oxidative stress in the liver through depletion of hepatic glutathione due to the formation of a reactive intermediate NAPQI that immediately reacts with glutathione (van de Straat et al., 1987). Glutathione depletion following DCF exposure has been shown to occur using an *in vitro* hepatotoxicity model (Pourahmad et al., 2011). Nonetheless, oxidative stress via other pathways remained a possibility. One such route is the inhibition of superoxide dismutase, an important part of the cell's antioxidant response system (Fukui and Zhu, 2010). Therefore, we conducted SOD inhibition assays using the same concentrations of DCF and DCF-AG as applied in the aforementioned *in vitro* assays. The SOD assay was not cell-based hence incubations were executed within a relatively short time span since inhibitor uptake was not necessary. DCF failed to yield any inhibition and surprisingly appeared to stimulate SOD activity (Figure 4.5). The nature of this

stimulation is unknown to us. A striking observation was the clear dose-dependent inhibition of SOD by DCF-AG, so much so that at the highest tested DCF-AG concentration of 1 mM, SOD activity was reduced to non-detectable levels (Figure 4.5). Prior evidence for SOD inhibition by an NSAID metabolite was reported by Chiou and colleagues (1999). In their study, 5 mM of suprofen acyl glucuronide reduced SOD activity by 88% after a 14-day treatment using a non-cell based *in vitro* model. In the same study, 5 mM suprofen decreased SOD activity by 5% after a 14-day incubation. Our data show that DCF-AG can elicit as great an inhibition but at lower doses and within a shorter time scale. Taken into context, the SOD inhibition along with ROS generation by DCF-AG may lead to sustained oxidative stress, culminating in cell death.

A last part of our research focused on the inherent pharmacology of DCF-AG. DCF was developed as a treatment for inflammation and pain, and it is through its ability to inhibit COX enzymes that pharmacologic efficacy is achieved. Hydroxylated metabolites of DCF have been tested for COX inhibition, but there has been no investigation of DCF-AG's pharmacology. Hence, we sought to identify if DCF-AG possessed COX inhibitory activity. Our inhibition assays with COX-1 and COX-2 led to a novel finding. DCF-AG had apparent COX-1 and COX-2 IC_{50} values of 0.620 ± 0.105 µM and 2.91 ± 0.36 µM, respectively (Figure 4.6, Figure 4.7, Table 4.2). The COX inhibition potency by DCF-AG was notably weaker compared to DCF for which we determined IC_{50} values of 0.0206 ± 0.0037 µM and 0.103 ± 0.005 µM for COX-1 and COX-2, respectively, values that are in line with published findings (Johnson et al., 1995).

The IC_{50} concentrations determined in the COX inhibition assays take on greater meaning when considering that the inhibition values are physiologically relevant both in

terms of circulating plasma concentrations that were observed in our mouse toxicokinetic studies as well as human plasma levels (professional communiqué, publication pending). Furthermore, the inhibition assays were performed with the intent to monitor formation of PGE_2 which has several important physiological functions such as immune system modulation (Nicolaou et al., 2014). Critically, PGE_2 is responsible for the protection of the GI mucosa, and deficiencies in PGE_2 signaling were associated with increased GI injury (Takeuchi, 2014). There is a deeper significance to the COX inhibition findings. Mere inhibition of COX-1 or COX-2 is not sufficient as a causal factor of gastrointestinal injury. As an example, administration to rats of the selective COX-1 inhibitor SC-560 or the selective COX-2 inhibitor rofecoxib, which was recalled as a marketed drug, did not induce any gastrointestinal damage (Tanaka et al., 2001). However, when SC-560 and rofecoxib were co-administered, extensive damage was observed implying that inhibition of the two isoforms of COX is essential to injury formation. Using the same model, administration of non-selective COX inhibitors (diclofenac, indomethacin, and naproxen) resulted in gastrointestinal injury. Furthermore, studies with COX-1 or COX-2 KO mice demonstrated that COX-1 activity promotes intestinal intactness while COX-2 activity is necessary for healing of ulcers (Schmassmann et al., 2006). That DCF-AG, like its parent compound, can inhibit both COX enzymes represents a novel finding and offers a possible cause during enteropathy associated with exposure to DCF-AG.

The results from the *in vitro* assays in the preceding sections can be interwoven into a mechanistic paradigm for injury directly attributable to DCF-AG. In Figure 4.8 we propose a tox model describing the multiplicity of transporters, pharmacologic, and

inhibitory activities that capture our current and past investigations. The model is predicated on the transfer of DCF into the liver after administration (the route of administration is not a defining factor at this point) whereupon it undergoes extensive biotransformation. The metabolite DCF-AG can be excreted into the blood via MRP3 or alternatively transported into the bile by BCRP or MRP2. In our toxicokinetic studies, we determined that the biliary concentration of DCF-AG were between 1.3 to 4.0 mM (Chapter 3). Any remaining DCF-AG in the liver may undergo adduct formation either to albumin or sequestration by glutathione (Grillo et al., 2003). In addition, we have characterized DCF-AG stability and determined that its half-life in the presence of S9 esterases was approximately 15 min (Supplement 1), setting up a scenario where residual hepatic DCF-AG reverts to parent compound reinitializing another round of metabolism. It is important to note that this proposed injury model does not apply to the liver since the *in vivo* studies (Chapter 3) showed no hepatotoxicity by DCF. Biliary DCF-AG traverses the common bile duct and enters the small intestine at the proximal duodenal region. The acidic environment of the intestinal lumen acts as a stabilizing force on DCF-AG decreasing the rate of non-enzymatic hydrolysis (Supplement 2). Once in the GI lumen, DCF-AG may undergo conversion back to parent compound by the activity of bacterial β-glucuronidase present in the gut microflora (Louis et al., 2014). Free DCF-AG may also take one of two steps: 1) covalent adduction to the outside of the enterocytes, or 2) active uptake by OATP2B1. Once inside the cell, DCF-AG can induce cytotoxicity either through ROS generation or SOD inhibition ultimately leading to oxidative stress. DCF-AG may be cleared from enterocytes if MRP3 is present and functional. However, lack of MRP3 (as in the null mice) may result in greater DCF-AG

retention and more aggravated damage by the aforementioned mechanisms. The tox mechanistic model also includes the inhibitory attributes of DCF-AG against COX enzymes. COX-mediated inhibition by DCF-AG may potentiate enteropathy via loss of PGE_2 protection as well as interference of COX-2 directed wound healing. Lastly, DCF is expected to contribute to intestinal injury in conjunction to DCF-AG via similar pathways of COX inhibition, oxidative stress, and ROS generation.

It may not be clear which of the proposed mechanisms are dominant and which have minor roles. Nonetheless, our results lay the foundation of a novel multifactorial process of intestinal injury attributable directly to DCF-AG. The *in vitro* assays detailed in the current work along with our previous findings offer potential explanations and insight that have not been previously explored. In conclusion, we believe we have made a rational argument of the potential for DCF-AG to directly mediate toxicity and have provided credible mechanistic leads that could explain this toxicity.

Chapter 5 THE MODULATION OF TRANSCRIPTIONAL EXPRESSION AND INHIBITION OF MULTIDRUG RESISTANCE ASSOCIATED PROTEIN 4 (MRP4) BY ANALGESICS AND THEIR PRIMARY METABOLITES

5.1 Abstract

During the course of a toxic challenge, changes in gene expression can manifest such as induction of metabolizing enzymes as a compensatory detoxification response. We currently report that a single 400 mg/kg IP APAP dose to C57BL/6J mice led to an increase in Mrp4 (*Abcc4*) mRNA 12 hours after administration. Alanine aminotransferase, as a marker of liver injury, was also elevated indicating hepatotoxicity had occurred. Therefore, induction of Mrp4 mRNA was likely attributable to APAP-induced liver injury. Mrp4 has been shown to be upregulated during oxidative stress, and it is well-established that APAP overdose causes oxidative stress due to depletion of glutathione. Given the importance of Mrp4 induction as an adaptive response during cholestatic and oxidative liver injury, we next investigated the extent by which human Mrp4 can be inhibited by the analgesics, APAP, DCF, and their metabolites. Using an *in vitro* assay with inside out human MRP4 vesicles, we determined that APAP-cysteine inhibited MRP4-mediated transport of leukotriene C_4 with an apparent IC_{50} of 125 µM. APAP-glutathione also attenuated MRP4 activity though it achieved only 28% inhibition at 300 µM. DCF-AG inhibited MRP4 transport by 34% at 300 µM. The MRP4 *in vitro* inhibition occurs at APAP-cysteine and DCF-AG concentrations seen *in vivo* after a toxic dose of APAP or DCF in mice, hence the findings are important given the role that Mrp4 serves as a compensatory response during oxidative stress following toxic challenge.

5.2 Introduction

Injury following overdose with analgesics is relatively common and can result in extensive damage to multiple organs that may ultimately lead to death in severe cases (Jones, 2002). Mild to moderate toxicity may induce changes vis-à-vis regulation of genes. Such changes involve modulation of transcription factors or induction of transporters as a compensatory response (Blazka et al., 1995a; Barnes et al., 2007). Intoxication with APAP, for example, has been demonstrated to result in upregulation of the efflux transporter Mrp4 (Campion et al., 2008) as well as the metabolic enzyme flavin containing monooxygenase 3 (Rudraiah et al., 2014a), a particularly novel finding given that Fmo3 was previously thought to be non-inducible (Cashman and Zhang, 2002). The mechanism of Mrp4 induction has been demonstrated to be linked to activation of nuclear factor erythroid 2-like 2 (Nrf2, *Nfe2l2*) as evidenced by lack of Mrp4 upregulation in Nrf2 knockout mice (Ghanem et al., 2015). Furthermore, Mrp4 induction by APAP was found to be dependent on Kupffer cell activation (Campion et al., 2008). Mrp4 expression also was induced after administration of clofibrate via activation of peroxisome proliferator-activated receptor α (Moffit et al., 2006). In a mouse model, the elevated expression of Mrp4 after an initial toxic APAP insult results in mice becoming refractory to injury following subsequent toxic doses, an effect termed autoprotection (Aleksunes et al., 2008a).

In the previously cited work by Campion and colleagues, protein induction became evident two to three days after administration of toxic doses of APAP. Measurement of ALT as an indicator of hepatocellular injury has been utilized in human and rodents (McGill et al., 2012; Singhal et al., 2012), and there is a clear relationship between ALT

and manifestations of injury. Furthermore, Rudraiah and colleagues (2014b) reported elevations in ALT and Fmo3 mRNA following toxic APAP treatment leading the authors to conclude that induction of Fmo3 was likely a protective mechanism in response to APAP-induced hepatotoxicity. To date, transporter expression as a function of ALT has not been thoroughly investigated.

As expected, administration of xenobiotics results in the generation of metabolites that can be eliminated through biliary or urinary excretion. Work from our group has previously shown that metabolites of APAP and DCF (Figure 5.1) can be generated in high concentrations, with respect to the parent compound, after toxic doses (Chen et al., 2003; Manautou et al., 2005; Scialis et al., 2015). Though metabolite disposition has been characterized, and in some instances the affinity for a transporter to mediate metabolite clearance quantified (Zelcer et al., 2003b; Zamek-Gliszczynski et al., 2006c), there has not been systematic examination as to the potential for these metabolites to interfere with normal transporter function.

Thus the goals of our current work were to first assess the relationship, if one exists, between elevations in ALT and transcriptional regulation of Mrp4. To accomplish this objective, a toxic dose of APAP will be given to C57BL/6J mice with measurement of ALT and Mrp4 mRNA at several time points post-administration. The second aspect of our inquiry focuses on the inhibition of MRP4 by APAP, DCF, and their primary metabolites. The MRP4 inhibition assays were conducted using APAP and DCF metabolite concentrations that reflect those observed during *in vivo* studies from our laboratory.

Figure 5.1 Structures of APAP, DCF, and their major metabolites

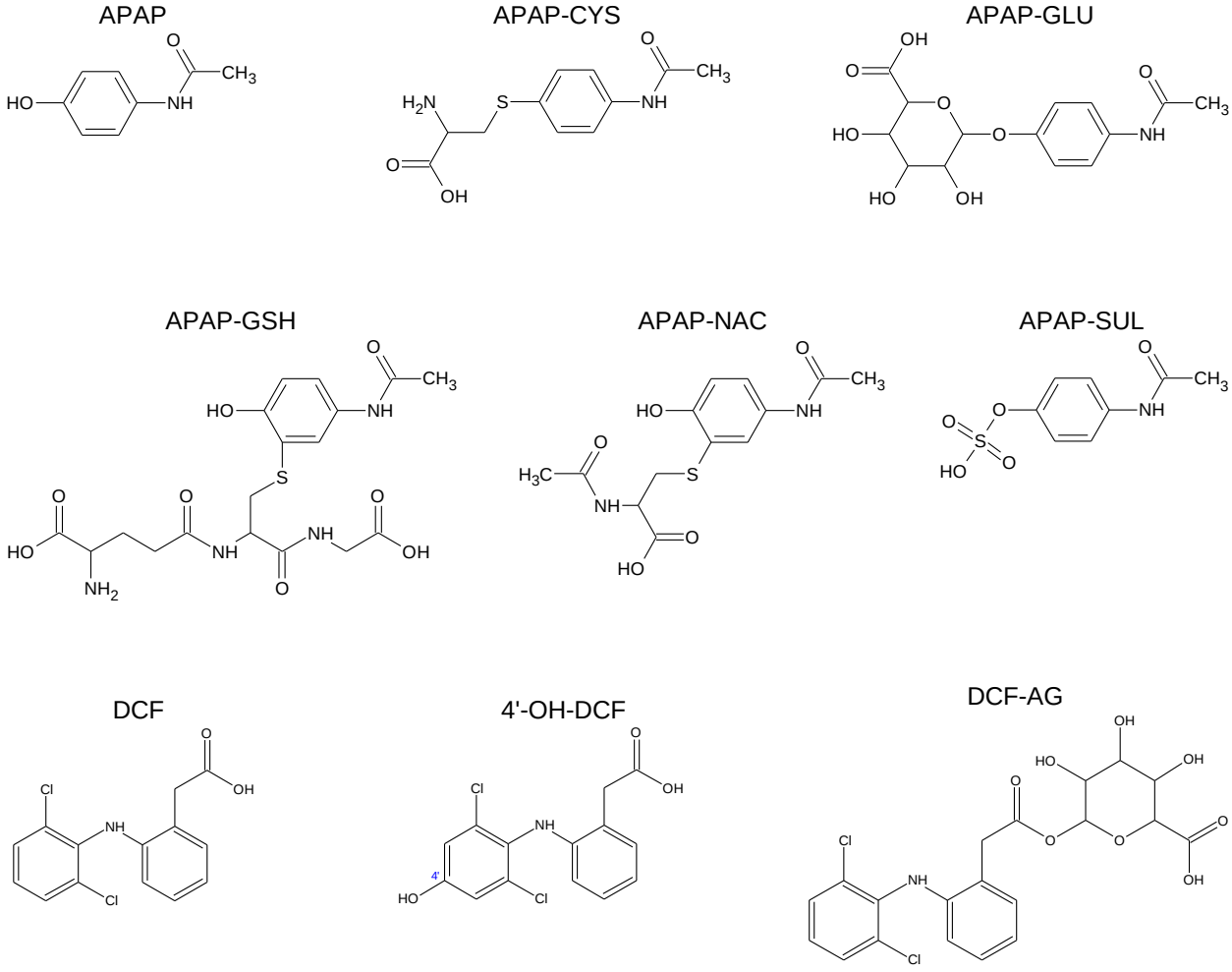

Figure 5.1 Structures of APAP, DCF, and their major metabolites. The various conjugated metabolites of APAP as the result of Phase II metabolism or spontaneous adduction to the CYP450-mediated reactive intermediate NAPQI. APAP: acetaminophen, APAP-CYS: acetaminophen cysteine, APAP-GLU: acetaminophen glucuronide, APAP-GSH: acetaminophen glucuronide, APAP-NAC: acetaminophen N-acetylcysteine, APAP-SUL: acetaminophen sulfide, DCF: diclofenac, 4'-OH-DCF: 4'-hydroxy diclofenac, DCF-AG: diclofenac acyl glucuronide.

5.3 Materials and Methods

Chemicals and Reagents. APAP, AMP, ATP, DCF, formic acid, indomethacin (used as the IS), KCl, $MgCl_2$, MOPS, OH-DCF, and Tris-HCl, were purchased from Sigma-Aldrich Corporation. (St. Louis, MO). DCF-AG was purchased from Toronto Research Chemicals Incorporated (Toronto, Canada). APAP metabolites were obtained from McNeil-PPC Incorporated (Fort Washington, PA). Leukotriene C4 and MK-571 were purchased from Santa Cruz Biotechnology (Dallas, TX). MRP4 vesicles were purchased from GenoMembrane Corporation (Kanazawa, Japan). All LC/MS/MS solvents were of high analytical grade and were purchased from Burdick & Jackson (Muskegon, MI).

Animals. Male C57BL/6J mice were purchased from Jackson Laboratories (Bar Harbor, ME). Mice were housed in an American Animal Associations Laboratory Animal Care accredited facility at the University of Connecticut under a standard temperature-, light-, and humidity-controlled environment. Mice had free access to Harlan Teklad 2018 chow (Harlan, Madison, WI) and drinking water. All animal studies were performed in accordance with the Guide for the Care and Use of Laboratory Animals using protocols reviewed and approved by the local Institutional Animal Care and Use Committee at the University of Connecticut.

***In Vivo* Studies.** Mice were used at 2-3 months of age. The mice received a single IP dose of 400 mg/kg APAP in 0.9% saline. Mice were sacrificed by decapitation at 6, 12, and 24 hours after APAP administration. Blood samples were collected and subsequently centrifuged at 1,200 × *g* for 15 min to yield plasma. Livers were harvested, rinsed in ice-cold saline, and quickly frozen in liquid nitrogen prior to storage at -80 °C.

RNA Isolation and RT-PCR. Total liver RNA was extracted using TRIzol reagent (Thermo Fisher Scientific, Waltham, MA) according to the manufacturer's protocol. The concentration of total RNA in each sample was quantified spectrophotometrically at 260 nm, and the integrity was evaluated by agarose gel electrophoresis. RNA (1 µg) was reverse transcribed to cDNA using a M-MLV Reverse Transcriptase kit (Thermo Fisher Scientific). mRNA expression of *Abcc4* and was quantified using specific primers (Table 5.1) by the ΔΔCT method and normalized to the housekeeping gene *Actb*. Primer pairs were synthesized by Integrated DNA Technologies (Coralville, IA). Amplification was performed using an Applied Biosystems 7500 Fast Real-Time PCR System (Thermo Fisher Scientific) and carried out in a 20 µL reaction volume containing diluted cDNA, Fast SYBR Green PCR Master Mix (Thermo Fisher Scientific), and 1 µM of each primer.

Clinical Chemistry. Plasma samples were analyzed for alanine aminotransferase (ALT) using a kit purchased from Thermo Fisher Scientific as per the manufacturer's recommendations. A BioTek UV/Vis microplate spectrophotometer (BioTek Instruments Incorporated, Winooski, VT) was used to measure assay endpoints.

***In Vitro* Transport.** Commercially available MRP4 inside-out vesicles from GenoMembrane were quickly thawed from storage and placed on ice. Incubation reactions consisted of uptake buffer at pH 7.0 (50 mM MOPS-Tris, 70 mM KCl, and 7.5 mM $MgCl_2$), 25 µg vesicle protein, 5 mM of AMP or ATP, and 2.5 mM GSH. After a 5 min pre-incubation period of reaction mixture, incubations were commenced by addition of increasing concentrations of LTC_4 for substrate studies. For inhibition studies, the concentration of LTC_4 was fixed while increasing concentrations of inhibitor was added. Incubations were conducted at 37 °C in a total volume of 75 µL. Reactions were

quenched by the addition of 100 µL ice-cold stopping buffer (40 mM MOPS-Tris and 70 mM KCl), and the quenched mixtures were quickly transferred to a 96-well glass-fiber filter plate (EMD Millipore, Billerica, MA). The plate was subjected to vacuum filtration followed by 5 rapid washes of 100 µL/well ice-cold stopping buffer. The filter plate was allowed to dry before extraction of samples. Once the filter plate was dry, LTC_4 was extracted by filling each well of the filter plate with 200 µL of 80:20 (v/v) methanol: water. Plates were shaken for 15 min on ice, and the filtrate was collected via centrifugation at 3,000 × *g* for 10 min and 4 °C. The filtrate was evaporated to dryness under warm N_2 at 40 °C. The resulting residue was reconstituted with 100 µL water and 100 µL IS in methanol, vigorously vortex-mixed, and injected onto the LC/MS/MS. The accumulation of LTC_4 was quantified against a standard curve, and the data were expressed as pmol uptake normalized to mg vesicle protein.

LC/MS/MS Method. Chromatographic separation of analytes was performed on a 2.6 µm Kinetex XB-C18 30 × 2 mm column (Phenomenex Incorporated, Torrance, CA). The system front end consisted of a HTC PAL Autosampler (LEAP Technologies Incorporated, Carrboro, NC), a CBM-20A system controller, two LC20ADvp pumps, and a DGU-14A degasser (Shimadzu Scientific Instruments, Columbia, MD). Analytes of interest were eluted using a gradient program that began with 10% solvent B for the first 0.5 min, which was then increased to 90% solvent B at 1.25 min using a linear gradient and held at this mixture for 0.25 min before reverting back to initial solvent conditions for 0.5 min to re-equilibrate the column. The flow rate for was 0.3 mL/min, and the column effluent was directed to waste for the initial 0.5 min before switching to the mass spectrometer. Analytes were detected using an AB Sciex API™ 4000 LC/MS/MS triple

quad mass-spectrometer with a TurboIonSpray® probe and Analyst version 1.5.2 software (AB Sciex, Framingham, MA) that was operated in multiple reaction monitoring mode. Ion spray voltage was -4250 V, and the source temperature was set to 400 °C. The mass transitions in negative ion mode for monitoring LTC_4 and IS were *m/z* 626.4→189.5 and 356.0→311.8, respectively. The retention times of LTC_4 and IS were 1.33 and 1.47 min, respectively. Concentrations of analytes in the samples were determined by comparing the peak area ratios (analyte/IS) to those in the standard curve using a linear regression model. The criterion of acceptance for standards was defined to be ±20% of nominal concentration.

Data Analysis. Where IC_{50} estimates could be determined for Mrp4 inhibition, K_i values for the inhibitors were calculated according to the following equation (Cheng and Prusoff, 1973):

Equation 5.1

$$K_i = \frac{IC_{50}}{1 + \frac{[S]}{K_m}}$$

where K_i is the affinity of the inhibitor, IC_{50} is the inhibitor concentration producing 50% inhibition, [S] is the substrate concentration in the incubation, and K_m is the Michaelis constant representing substrate affinity for the transporter.

Statistical Analysis. Data are expressed as mean ± standard error of the mean. *P* values $\leq$ 0.05 were considered as statistically significant. Statistical analysis of data was performed using R version 3.2.1 (R Core Team, 2015). Two groups were compared by Student's *t* test, and multiple groups were compared by an analysis of variance followed by Tukey's *post hoc* test. GraphPad Prism version 6.0 (GraphPad

Software Incorporated, La Jolla, CA) was used to calculate kinetic parameters (V_{max} and K_m) as well as the IC_{50} inhibition parameter.

Table 5.1 Primer sequences for quantitative RT-PCR

Gene (Protein)	Primer Sequence
Actb (β-actin)	Forward: 5′-GCA ACG AGC GGT TCCG-3′
	Reverse: 5′-GCA GAC AGC CAA GGA GCC CAA AGA CC-3′
Abcc4 (Mrp4)	Forward: 5′-ACC TCT GCT CGC GCG TGT TCT-3′
	Reverse: 5′-CCA GTA CCG TTG AAG CTC CTC TCC-3′
	Reverse: 5′-CTC AGC ATG ATG GAC TTG GA-3′

5.4 Results

***In Vivo* Study**. C57BL/6J male mice were administered a single IP dose of 400 mg/kg APAP in 0.9% saline. Animals were sacrificed 6, 12, and 24 hours post administration, and livers were harvested. Plasma was used to assess liver injury using ALT as a marker. The mean ALT values at 6, 12, and 24 hours were, 930, 1,080, and 1,750 U/L, respectively (Figure 5.2). Transcriptional changes of Mrp4 were assessed at the same time points used for ALT analysis. An increase in Mrp4 mRNA was observed at 12 hours, and this increase was statistically significant ($P < 0.05$). Taken together, the data suggest that APAP-induced liver injury, evidenced by high ALT values, resulted in the induction of Mrp4 mRNA.

LTC_4 Kinetics. Human MRP4 was characterized for transport of LTC_4 prior to conducting inhibition studies. The linearity of MRP4-mediated transport for 0.1 µM LTC_4 was evaluated and determined to be time-dependent (Figure 5.3A). The dynamic response reached a maximal value of 19-fold (ATP response divided by AMP response) by 20 minutes. Next, LTC_4 was characterized for concentration-dependent transport. Kinetic parameters of V_{max} and K_m for MRP4 LTC_4 transport were determined to be 245 pmol/min/mg and 4.25 µM, respectively (Figure 5.3B). Kinetic data were fitted using a single K_m model without assuming cooperativity.

MRP4 Inhibition. The potential for MRP4 inhibition was carried out in the presence of parent compounds and their metabolites. MK-571 was used as inhibitor control yielding an IC_{50} of 14.2 µM (Figure 5.4), a value that is close to its reported IC_{50} against other probes (Reid et al., 2003a; Rius et al., 2003). APAP, APAP-SUL, APAP-GLU, and APAP-NAC did not manifest any significant inhibition. APAP-CYS inhibited transport

with an IC_{50} of 125 µM. APAP-GSH decreased MRP4 transport, but only at the two highest doses resulting in 29% inhibition at 300 µM. DCF and its metabolites likewise inhibited MRP4, with DCF-AG showing the greatest inhibition reaching a maximal inhibition of 34% at the highest tested concentration of 300 µM. The apparent K_i values using Equation 5.1 for MK-571 and APAP-CYS were calculated to be 13.9 and 122 µM, respectively.

Figure 5.2 Relationship between ALT values and Mrp4 gene expression following acute exposure to APAP

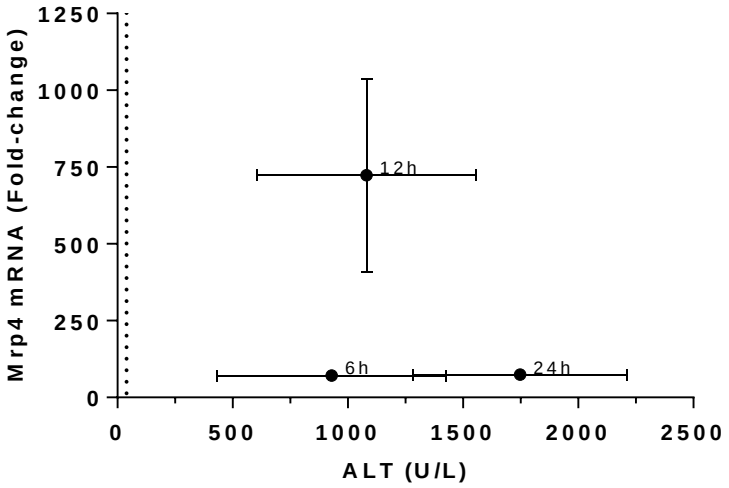

Figure 5.2 Relationship between ALT values and Mrp4 gene expression following acute exposure to APAP. Male C57BL/6J mice were administered 400 mg/kg APAP and sacrificed 6, 12, or 24 hours after administration. ALT was determined from plasma while Mrp4 mRNA expression was determined via RT-PCR using RNA extracted from whole liver homogenate. Data are expressed as the mean ± standard error of the mean for n=5-7 subjects/group. The vertical dotted line reflects the ALT upper limit of normal value of 40 U/L.

Figure 5.3 Time-dependent and concentration-dependent transporter kinetics of LTC_4 with MRP4 vesicles

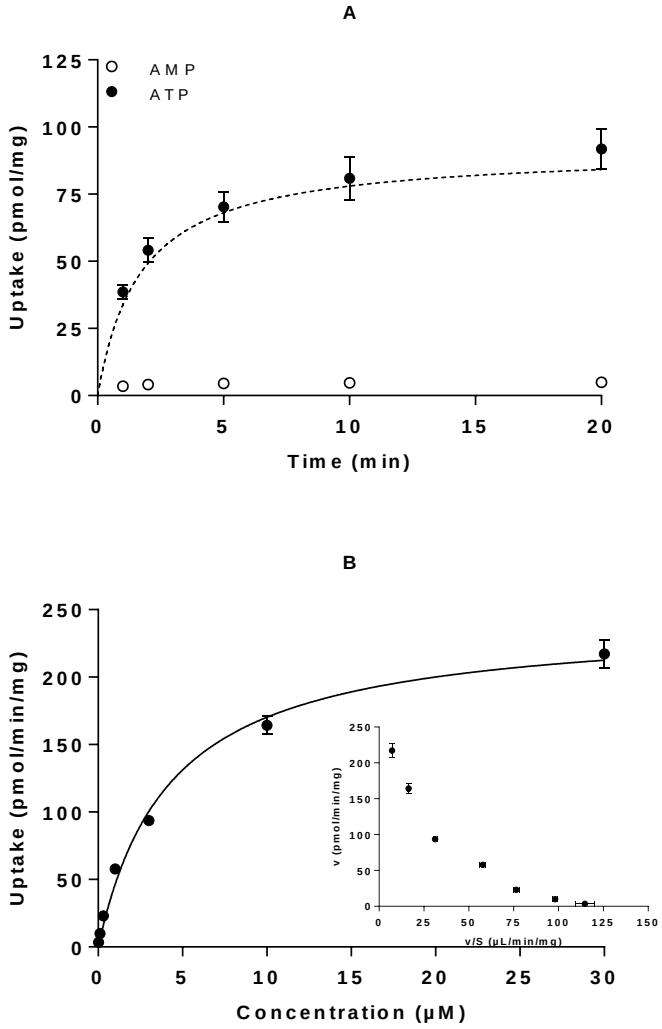

Figure 5.3 Time-dependent and concentration-dependent transporter kinetics of LTC_4 with MRP4 vesicles. MRP4 vesicles were incubated with LTC_4 in the presence of either AMP or ATP. (A) The time-dependent transport of 0.1 µM LTC_4 in the presence of 5 mM AMP (○) or 5 mM ATP (●) at 37 °C. The dotted line represents the nonlinear fit of LTC_4 active transport and was calculated by subtracting the AMP values (background and passive uptake) from the ATP response. (B) The concentration-dependent transport of LTC_4 at 37 °C. The fitted line indicates the ATP-dependent transport assuming typical Michaelis-Menten kinetics. Insert: Eadie-Hofstee plot. Each data point reflects the mean ± the standard error of the mean for n=3 measurements per time point or concentration.

Figure 5.4 Inhibition of MRP4 activity by APAP, APAP metabolites, DCF, and DCF metabolites

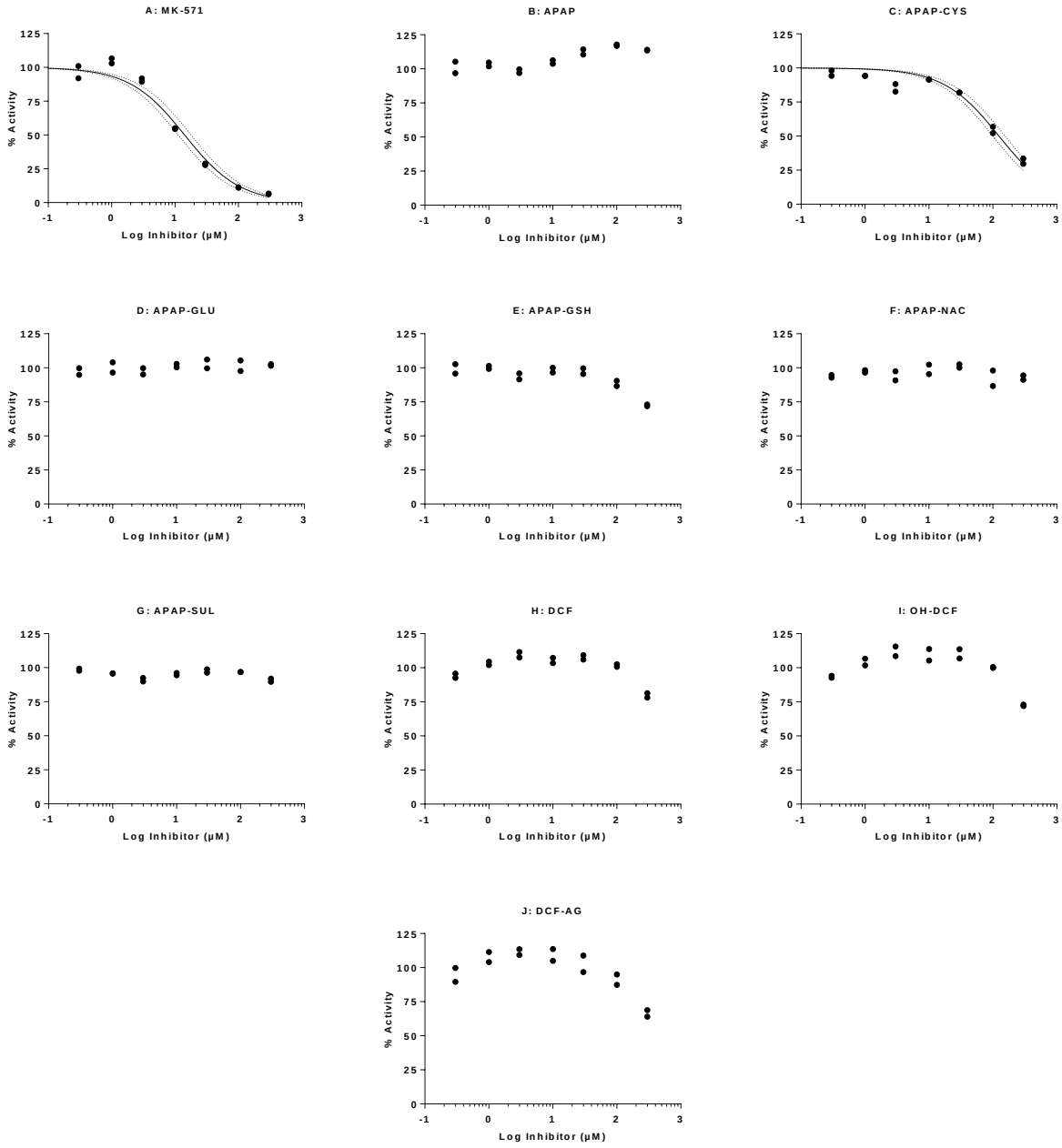

Figure 5.4 Inhibition of MRP4 activity by APAP, APAP metabolites, DCF, and DCF metabolites. *In vitro* inhibition was conducted using MRP4 vesicles with 0.1 µM LTC_4 in the presence of 5 mM ATP at 37 °C for 5 min. The ATP-dependent transport of LTC4 in the absence of inhibitor was set to 100%. Inhibition data were fit with a three parameter model to calculate IC_{50}. Dotted lines reflect the 95% confidence intervals of the fit. Each data point reflects individual values (n=2 per inhibitor concentration).

5.5 Discussion

The objective of our current work was to evaluate the regulation and function of Mrp4 following a toxic challenge by APAP. Analysis of major hepatic transporters in untreated C57BL/6J mouse livers showed that Mrp4 has one of the lowest expression levels in a comparative profile panel of uptake and efflux transporters (Supplement 4). Despite its seemingly low hepatic expression during homeostatic conditions, Mrp4 is quite inducible and plays a major role after intoxication by xenobiotics. As an example, work by Campion et al. (2008) showed that among the Mrp class of transporters, Mrp4 was the most inducible after a 500 mg/kg IP APAP dose to C57BL/6J mice, and its protein expression increased 10- and 33-fold by 48 and 72 hours, respectively. Furthermore, the mechanism of induction was shown to be dependent on the functional presence of hepatic macrophages known as Kupffer cells. Loss of Kupffer cell viability, via targeted cell death by the agent clodronate, resulted in loss of Mrp4 induction. Moreover, induction of Mrp4 following APAP challenge was found to be dependent on the transcription factor Nrf2 as mice lacking Nrf2 did not show any changes to Mrp4 mRNA or protein levels after a toxic APAP dose (Aleksunes et al., 2008b). During the course of our current study, we observed that Mrp4 mRNA was significantly upregulated 12 hours after a 400 mg/kg APAP challenge (Figure 5.2). Curiously, the Mrp4 mRNA levels were essentially the same at 6 and 24 hours. Given the prior protein expression data, we postulate that the transcriptional upregulation at 12 hours was sufficient to be the driving factor for Mrp4 protein levels to reach maximal expression at 48 hours.

We next sought to draw correlation between liver injury and Mrp4 mRNA. Serum ALT has been used a reliable indicator for liver injury, and we detected ALT levels that were

consistent with APAP toxicity (Figure 5.2). ALT levels were elevated at all the time points examined, while Mrp4 mRNA reached maximal induction 12 hours post-dose. Ghanem et al. (2015) similarly reported that ALT and Mrp4 mRNA levels were significantly increased 24 hours following toxic challenge by APAP. Rudraiah and colleagues (2014b) observed an association between ALT and flavin containing monooxygenase-3 (*Fmo3*) mRNA where both reached maximal values 48 hours after a 400 mg APAP dose. Thus the results suggest that liver injury following toxic APAP administration may have lead to the induction of Mrp4 mRNA.

Given the importance Mrp4 has as a compensatory response during APAP toxicity, we investigated the potential for Mrp4 inhibition by APAP and its metabolites. The rationale for investigating Mrp4 inhibition is based on the finding that Mrp4 is upregulated as a compensatory mechanism during oxidative stress (Xu et al., 2010). Considering APAP metabolism can cause oxidative stress that can lead to hepatotoxicity, inhibition of Mrp4 by APAP or its metabolites may further exacerbate liver injury. In lieu of mouse Mrp4, we chose to use vesicles containing human MRP4 as a surrogate. Our first course of action was to characterize the assay for performance. Among the substrates for MRP4 are estradiol-17β-glucuronide, ferosemide, and methotrexate (Chen et al., 2001; Chen et al., 2002; Hasegawa et al., 2007). The choice of estradiol-17β-glucuronide as a probe can result in potentially misleading findings as it was shown to be stimulated by several compounds that were able to inhibit the vesicular transport for other substrates (Kidron et al., 2012). Hence, we decided to use Leukotriene C_4 as our probe based on the work of Rius et al. (2008) that identified LTC_4 as a substrate for MRP4. LTC_4 as a measure of MRP4 activity is advantageous since it is a naturally occurring derivative of

arachidonic acid and plays a role during pro-inflammatory responses (Dahlen et al., 1983; Zipser et al., 1987). Using inside-out MRP4 vesicles, we determined that the transport of LTC_4 was time-dependent (Figure 5.3A). Furthermore, the transport of LTC_4 was concentration-dependent with a V_{max} and K_m of 253 pmol/min/mg and 4.25 µM, respectively (Figure 5.3B).

We next proceeded to conduct MRP4 inhibition assays, and expanded our assay to include two analgesics and their metabolites. Our results show that APAP has no effect on MRP4, and neither did APAP-SUL, APAP-GLU or APAP-NAC. However, we observed that APAP-CYS had concentration-dependent inhibition of MRP4 with an apparent IC_{50} of 125 µM. Based on the *in vitro* parameters from our assays, we calculate a K_i of 122 µM for APAP-CYS. Bearing in mind the low LTC_4 substrate concentration relative to its K_m and ratio of IC_{50} to K_i, it is likely the inhibition of MRP4 by APAP-CYS was of a competitive nature (Burlingham and Widlanski, 2003). That APAP-NAC did not manifest inhibition was surprising considering the structural resemblance it shares with APAP-CYS (Figure 5.1). Yet, APAP-GSH, which has a longer side chain compared to APAP-NAC and would potentially have greater steric hindrance, was able to inhibit LTC_4 transport by 29% inhibition at 300 µM. The results show the high specificity and discretionary recognition by MRP4 of closely related chemical entities. Inhibition by APAP-GSH is intriguing in light of the fact that it is a major metabolite stemming from sequestration of the highly reactive APAP intermediate NAPQI (Mitchell et al., 1973; Moore et al., 1985).

Akin to APAP-GSH, DCF and two of its main metabolites produced inhibition of MRP4 with DCF-AG achieving 34% inhibition. The DCF inhibition was not surprising as a

previous investigation established that DCF was able to inhibit the MRP4-mediated uptake of methotrexate (El-Sheikh et al., 2007). In that study, DCF was found to possess a two-site affinity with IC_{50} values of 326 and 0.006 µM for the high and low site, respectively. Since DCF only achieved 22% for the current study, the difference in potency is likely reflective of substrate selection. MRP4 inhibition by DCF parent and metabolites may have physiological ramifications. Studies point to MRP4 being an efflux transporter for PGE_2 (Reid et al., 2003b). In light of PGE_2's role in promoting cell survival and repair (Takeuchi, 2014), abrogation of its efflux could interfere with localized signaling in response to DCF-induced injury. It should be noted that the concentrations chosen for the *in vitro* inhibition were physiologically relevant as they reflect the *in vivo* metabolite concentrations observed in prior animal studies (Chen et al., 2003; Manautou et al., 2005; Scialis et al., 2015).

To summarize our findings, we report that Mrp4 mRNA expression was induced after a single toxic dose of APAP, and that induction was maximal at 12 hours. ALT, as a marker of hepatic injury, was also elevated. Also, we show that human MRP4 function was inhibited by APAP metabolites with APAP-CYS achieving an apparent IC_{50} that is physiologically relevant. We believe these findings demonstrate the intricate balance between compensatory transporter upregulation due to xenobiotic intoxication and the possible deleterious effects that xenobiotics continue to exert in the form of their circulating metabolites.

Chapter 6 SUMMARY

DCF is a non-steroidal anti-inflammatory drug that has been used for the past several decades to treat a variety of conditions such as arthritis, pain, and migraine (Novartis, 2011; Depomed, 2014). In the United States, DCF is available only by prescription, and it is normally tolerated by a majority of patients. However, patient compliance with DCF treatment can become problematic owing to ADRs such as gastrointestinal bleeding, perforation, and ulceration. In these cases, patients are alternatively prescribed a combination of DCF with misoprostol which can significantly lessen the occurrence of GI injury (Reyes-Garcia et al., 2007; Pfizer, 2014).

DCF has been extensively studied for its pharmacology, pharmacokinetics, and metabolism (Menasse et al., 1978; Riess et al., 1978; Tang et al., 1999; Kenny et al., 2004). DCF has nearly 100% absorption after oral dosing due to its high passive uptake (Kalgutkar and Daniels, 2010). DCF undergoes extensive first-pass hepatic metabolism resulting in approximately 50% bioavailability in humans. Among the primary metabolites generated by the liver are hydroxylated metabolites (4'-OH-DCF, 5-OH-DCF, 4',5-$(OH)_2$-DCF, 3'-OH-DCF, 3',4'-$(OH)_2$-DCF) and conjugated metabolites (acyl glucuronides, ether glucuronides, hydroxylated acyl glucuronides, sulfated conjugates, and taurine conjugates). Many of these metabolites have been characterized using animal models (Stierlin and Faigle, 1979; Stierlin et al., 1979; Pickup et al., 2012; Sarda et al., 2012). Despite the notion that metabolism serves to detoxify the body of xenobiotics, in the case of DCF, biotransformation leads to the creation of reactive metabolites that can potentially cause injury. The 4'-OH-DCF and 5-OH-DCF metabolites undergo rearrangement to form quinone imines which can adduct

proteins via covalent binding. These quinone imines can be neutralized by sequestration with glutathione that is present in millimolar concentrations in the liver (Kaplowitz, 1981). In general, depletion of hepatic glutathione without subsequent replenishment may result in oxidative stress and hepatocellular damage (Grewal and Racz, 1993; Rafeiro et al., 1994; Hinson et al., 2010). Biotransformation of DCF also results in production of the reactive metabolite diclofenac acyl glucuronide which was a major focus of the work presented herein.

The reactive nature of DCF-AG has been the subject of intense investigation. DCF-AG had been previously shown to covalently adduct to a number of hepatic proteins and enzymes such as albumin, Mg^{2+}-ATPase, and dipeptidyl peptidase IV (Hargus et al., 1995; Sallustio and Holbrook, 2001; Kenny et al., 2004), an enzyme that has emerged as a pharmacological target in the treatment of diabetes (Rohrborn et al., 2015). An early study reported that though DCF-AG can covalently bind to hepatic proteins, DCF-AG itself did not appear to contribute to hepatotoxicity *in vitro* (Kretz-Rommel and Boelsterli, 1993). In contrast, a follow-up study indicated DCF-AG could directly mediate intestinal injury *in vivo*. Specifically, rats that were administered DCF-AG exhibited greater intestinal damage, in terms of ulcer number and length, compared to rats that received an equimolar dose of DCF (Seitz and Boelsterli, 1998). In that same study, it was determined that mutant rats lacking the efflux transporter Mrp2 had less intestinal injury compared to rats that expressed Mrp2. The reduction in intestinal injury was from reduced canalicular excretion of DCF-AG from the liver into bile, a transport process mediated by Mrp2 (Seitz et al., 1998). These studies were significant as they

demonstrated that transporters were able to modulate toxicity after exposure to a single DCF dose.

Based on the earlier work with mutant Mrp2 rats, we chose to investigate if other efflux transporters were operative in the transport of DCF or its metabolites. Our preliminary studies used mouse models in which either breast cancer resistance protein (Bcrp) or Mrp3 was genetically knocked out (Chapter 2). Whereas the loss of Bcrp led to a reduction in DCF biliary excretion in KO mice compared to WT, there was no concomitant increase in KO plasma DCF concentrations. On the other hand, a marginal decrease of biliary DCF-AG excretion in KO led to increased DCF-AG plasma in KO relative to WT, and this trend was observed at two subtoxic doses of DCF (Figure 2.1 and Figure 2.2). Overall the data conclusively indicate that both DCF and DCF-AG are Bcrp substrates with perhaps OH-DCF also being a Bcrp substrate based on the results from the 10 mg/kg DCF dose. The results from the Mrp3 study were more profound. Mrp3 KO mice had reduced DCF-AG plasma concentrations compared to WT mice, yet there were no differences in the DCF-AG biliary excretions between WT and KO (Figure 2.4 and Figure 2.5). Neither DCF nor OH-DCF had any differences between WT and KO in plasma concentrations or biliary excretion signifying that neither are Mrp3 substrates. Analysis of terminal liver concentrations did not reveal any accumulation of DCF-AG in WT, Bcrp KO, or Mrp3 KO mice (Figure 2.6). Whereas loss of the canalicular efflux transporter Bcrp affected both biliary and plasma disposition of DCF-AG, the deletion of the basolateral efflux transporter Mrp3 impacted only plasma DCF-AG concentrations. Taken together, our results were consistent with the published

findings of Bcrp- and Mrp3-mediated transport of DCF-AG (Lagas et al., 2009; Lagas et al., 2010).

That Bcrp and Mrp3 were carriers of DCF-AG was not surprising given their roles in mediating the efflux of glucuronide conjugates derived from other compounds (Kawabata et al., 2001; Nakatomi et al., 2001; Manautou et al., 2005; Zamek-Gliszczynski et al., 2009). While loss of Mrp3 resulted in decreased plasma concentrations of acetaminophen glucuronide and 4-methylumbelliferyl glucuronide along with increased biliary excretion for those two respective glucuronides (Manautou et al., 2005; Zamek-Gliszczynski et al., 2006b), there was no corresponding elevation in KO biliary levels for DCF-AG despite WT mice having nearly 10-fold higher plasma concentrations compared to KO. Our data with Mrp3 implied that only basolateral excretion of DCF-AG was affected by Mrp3 deletion, and that the function or expression of Mrp3 did not affect biliary disposition of DCF-AG. Our finding is not an anomaly in light of the evidence provided for the Mrp3 substrates fexofenadine and hydeoxycholate glucuronide for which only basolateral excretion was significantly decreased in Mrp3 KO animals while biliary efflux was comparable between WT and KO for both fexofenadine and hydeoxycholate glucuronide (Zelcer et al., 2006; Tian et al., 2008).

As our studies provided evidence that Mrp3 can modulate DCF-AG disposition *in vivo* with mouse knockout models, we next sought to determine the affinity of DCF-AG for human MRP3. For these studies, we used commercially available MRP3 inside-out vesicles where substrate affinity was measured by quantifying the transport of probe into the vesicles and subsequently compared to the transport activity of human MRP2 vesicles. The comparison to MRP2 was important as MRP2 has been shown to

modulate DCF-induced toxicity as well as DCF-AG disposition in humans and rodents. For instance, human subjects with reduced MRP2 expression were associated with greater hepatotoxicity during DCF treatment while rats lacking hepatic Mrp2 were refractory to intestinal injury following treatment with DCF (Seitz and Boelsterli, 1998; Daly et al., 2007). We observed that MRP3 has an apparent high affinity and low affinity binding site for DCF-AG (Figure 2.11). The low affinity site exhibited comparable transporter kinetics as calculated for the MRP2-mediated transport of DCF-AG. The high affinity MRP3 site implies that at low DCF-AG concentrations, transport of DCF-AG is likely to be dominated by MRP3 relative to MRP2. To summarize this part of our work, the mouse *in vivo* studies and human *in vitro* experiments indicated that MRP3/Mrp3 has a major role in the disposition of DCF-AG.

With Mrp3 transport of DCF-AG firmly established, our next aim was to find out whether deletion of Mrp3 leads to increased hepatocellular or intestinal injury (Chapter 3). To accomplish our goals, we used WT and Mrp3 KO mice and administered a single toxic dose of 90 mg/kg DCF. The selected dose was the highest tolerated DCF dose that did not result in morbidity. Clinical chemistry analysis using serum markers of liver injury did not reveal any obvious damage to either WT or KO livers (Figure 3.3). In contrast to our results, Lagas et al. (2010) reported elevated ALT levels suggestive of mild hepatic injury after a 25 mg/kg DCF dose. The difference between our study and that of Lagas is likely due to the triple knockout mouse model (Bcrp/Mrp2/Mrp3) they used, which is expected to be more susceptible to injury due to a heavily compromised hepatobiliary transport capacity (Kock and Brouwer, 2012). Histopathological examination in our studies showed no gross hepatic injury despite the presence of intense covalent DCF

adducts (Figure 3.5). The lack of hepatocellular injury in our mouse *in vivo* studies may be explained by less oxidative metabolism of DCF in mouse compared to human. Our toxicokinetic experiment showed that hydroxylated metabolites accounted for a small fraction of overall DCF metabolism (Figure 3.1), with DCF-AG and other conjugates being the predominant metabolites identified in the bile (Figure 2.7 and Figure 2.8). Hepatotoxicity in human hepatocytes following DCF exposure was revealed to be dependent on CYP450-mediated generation of 5-OH-DCF and *N*,5-$(OH)_2$-DCF (Bort et al., 1999b). In addition, repeated dosing may be necessary for immune-mediated hepatic injury following DCF exposure. The rationale for this argument stems from the work by Aithal et al. (2004) in which antibodies taken from human patients presenting with hepatotoxicity as a result of DCF treatment recognized the hepatic covalent adducts in rats that received daily dosing of 30 mg/kg DCF. However, the same human antisera failed to recognize hepatic adducts in rats that were given a single 200 mg/kg DCF dose. We conclude therefore that Mrp3 deletion does not lead to increased hepatotoxicity following acute exposure to DCF.

As Mrp3 is also expressed in the mouse gastrointestinal tract (Zelcer et al., 2006), we examined the extent of GI injury after a toxic DCF dose. Compared to WT mice, the intestines of KO mice exhibited profound damage in terms of ulcer count and overall inflammation (Figure 3.4.). Interestingly, the level of covalent adduction in KO intestines determined through immunohistochemistry was not commensurate with injury. In fact, both WT and KO appeared to have the same level of intestinal covalent adducts despite the finding that KO mice had more injury compared to WT (Figure 3.5). The apparent disconnect between injury and adduct formation led us to the conclusion that covalent

adducts of xenobiotics merely indicate the presence of reactive species, and that their presence and intensity is not a direct indicator of the degree in tissue damage. In short, covalent adduction is just a byproduct of metabolism and not an overt contributor to injury on an acute basis. Disregarding the covalent adduct aspect for a moment, the functional expression of Mrp3 served to protect the GI supported by the mild injury observed in WT mice while the loss of Mrp3 was met by significant injury in KO animals. Given the preponderance of data linking DCF-AG to Mrp3-mediated transport, we believe that the increased intestinal injury in KO mice was due to altered DCF-AG disposition and that DCF-AG was contributory toward intestinal enteropathy. Since MRP3 is known to be expressed along the human GI tract (Groer et al., 2013; Drozdzik et al., 2014), the presumed protection afforded by Mrp3 in our mouse model may be applicable to humans as well. Permutation to MRP3 function or expression due to genetic polymorphisms, of which many are known to exist for MRP3 (Kobayashi et al., 2008; Sasaki et al., 2011), may render certain patient populations more susceptible to GI injury during the course of treatment with DCF.

The intense covalent adducts detected in mouse livers is understandable given that the liver was the primary site of DCF-AG synthesis. Adduct formation in the GI tract was more intriguing. Certainly brush border adduction would be likely to occur given that DCF-AG would naturally come into contact with that part of the villi during transit in the gut lumen. The brush border staining we observed was consistent with what was reported in rats that were administered DCF (Atchison et al., 2000b). We became curious how adducts could form so deep in the villi. Endocytosis of adducted plasma membrane protein was a possibility, though our investigation lead us to the belief that

active uptake of DCF-AG was also an option. To examine if this could be the case, we used stably transfected cells to characterize DCF-AG uptake by a major intestinal transporter (Chapter 4). Based on the expression of likely uptake transporter candidates, we focused our efforts on OATP2B1 which is expressed both in the human GI tract as well as mice intestines (Hagenbuch and Meier, 2004; Cheng et al., 2005).

To determine the extent of OATP2B1-mediated uptake of DCF-AG, a two-compartmental model was used. This same approach was also used to characterize OATP-mediated uptake in transfected cells and primary hepatocytes (Poirier et al., 2008; Menochet et al., 2012; Pfeifer et al., 2013). The advantage to using such a model is that it allows for estimates of active and passive processes, and the models can be adapted to utilize and fit data over a range of time rather than be limited to a single time point as used in traditional transporter kinetic studies. Our studies indicated that DCF-AG uptake by OATP2B1 was concentration-dependent and that uptake activity was higher at pH 6.0 compared to pH 7.4 (Figure 4.2). The acidic nature of the intestinal lumen would partially stabilize DCF-AG, which hydrolyzes more readily at pH 7.4 (Supplement 2), and potentially enhance its uptake by OATP2B1 at pH 6.0. With DCF-AG uptake into enterocytes plausibly explained by OATP2B1 activity, we next determined the potential for DCF-AG to directly induce injury.

Our cytotoxicity studies with DCF-AG demonstrated that not only could DCF-AG cause cell death, but that it induced greater cell death compared to an equimolar concentration of DCF (Figure 4.3). The cytotoxicity results were in line with the observations of Seitz and Boelsterli (1998) who reported that DCF-AG elicited greater GI injury than DCF *in vivo*. Furthermore, cell death was brought on fairly early and occurred within 3 hours of

exposure to DCF-AG. To resolve the mechanism of the cytotoxicity, we examined the potential for DCF-AG to induce reactive oxygen species and found that DCF-AG indeed caused ROS to increase in a dose-dependent manner with onset occurring after 1 hour (Figure 4.4). In comparison, DCF was reported to promote ROS generation at much later time points (Lim et al., 2006). The presence of ROS was important as it indicated that DCF-AG could create a state of oxidative stress. As suprofen acyl glucuronide was purported to inhibit superoxide dismutase (Chiou et al., 1999), a key cellular defense against oxidative stress, we examined if DCF-AG also inhibits SOD. We report that DCF-AG exemplified a clear dose-dependent inhibition of SOD whereas DCF showed either no effect or stimulation of SOD (Figure 4.5). Lastly, we examined if DCF-AG had inherent pharmacology against cyclooxygenases as this has not been fully explored. Our *in vitro* assays repeatedly demonstrated that DCF-AG possesses the ability to inhibit both COX-1 and COX-2, and that the inhibition leads to decreased synthesis of prostaglandin E_2 from arachidonic acid. Considering the role PGE_2 has in protecting the GI tract and that inhibition of both COX enzymes is necessary for intestinal injury to develop (Tanaka et al., 2001; Sigthorsson et al., 2002; Hoshino et al., 2003; Kotani et al., 2006), DCF-AG modulation of COX activity may have exacerbated the GI injury normally ascribed to DCF. Ostensibly, we believe our studies demonstrate that DCF-AG directly contributed to enteropathy in our *in vivo* models via active uptake by mouse Oatp2b1 resulting in enhanced cytotoxicity in Mrp3 KO animals, due to decreased basolateral excretion (and greater enterocyte retention) from the combined effects of ROS generation, SOD inhibition, and attenuation of the PGE_2-derived protection of the intestinal tract.

The last aspect of our work focused on the upregulation of Mrp4 during oxidative stress and the potential for inhibition of human MRP4 by analgesics and/or their metabolites (Chapter 5). Induction of Mrp4 was shown to occur after toxic doses of APAP were given to mice (Aleksunes et al., 2008b; Campion et al., 2008). Mrp4 transcriptional regulation appeared to be causally linked to hepatic injury, as assessed by serum ALT levels, after toxic APAP administration in mice (Figure 5.2). MRP4 activity in the presence of APAP, APAP metabolites, DCF, and DCF metabolites was characterized using human MRP4 inside-out vesicles. Our study indicated that APAP-CYS and DCF-AG were able to significantly inhibit MRP4 activity, with APAP-CYS having an IC_{50} of 125 µM and DCF-AG achieving 34% inhibition at 300 µM (Figure 5.4). The inhibition of these two metabolites is physiologically relevant in that both metabolites are present, following toxic doses of their respective parent compounds, at concentrations matching their inhibitory potencies (Chen et al., 2003; Manautou et al., 2005; Scialis et al., 2015). Since Mrp4 is upregulated in response to oxidative stress, which can occur following toxic challenge by APAP or DCF (Moore et al., 1985; Lim et al., 2006), inhibition of MRP4/Mrp4 may further promote injury by limiting the ability to excrete toxic agents.

In conclusion, our collective work offers conclusive evidence that the disposition of DCF-AG is modulated not only by MRP2/Mrp2, but also by MRP3/Mrp3, Bcrp, and OATP2B1. Furthermore, we determined that Mrp3 serves a protective role against injury by DCF-AG, and that loss of Mrp3 results in increased susceptibility to GI damage. The enteropathy observed in our mouse studies was the result of the multi-factorial mechanisms through which DCF-AG can induce harm, namely induction of oxidative stress through generation of ROS, inhibition of SOD, cell death, and the combined

effects of COX-1 and COX-2 inhibition resulting in the diminished protection by PGE_2. We also demonstrate that DCF-AG can inhibit MRP4, which is normally upregulated in response to oxidative stress and is involved in PGE_2 signaling. The results of our studies represent novel findings and offer insight into the roles that DCF-AG has in enteropathy. Subsequent studies should focus on identifying patient populations at risk of GI injury from DCF-AG as a result of diminished MRP3 function so that alternative treatment can be prescribed.

Chapter 7 APPENDIX

Supplement 1 Stability of DCF-AG in mouse S9 fraction without co-factors at 37 °C

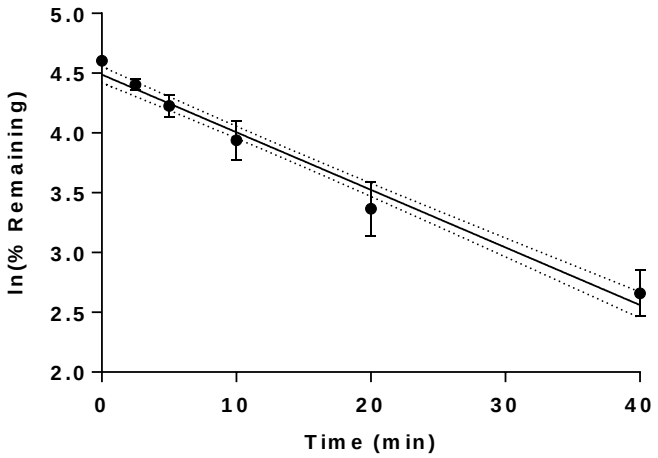

The metabolic stability of 1 µM DCF-AG in the presence of 1 mg/mL mouse S9 fraction at pH 7.4 is shown. Incubations were conducted at 37 °C using S9 without NADPH, GSH, or UDPGA. Loss of DCF-AG is reflective by spontaneous hydrolysis as well as the activity of endogenous hepatic esterases. The estimated $t_{1/2}$ was 14.5 ± 0.6 min. Dotted lines reflect the 95% confidence intervals of the fit (solid line). Each point reflects the mean ± standard error of the mean of n=4 measurements from two separate experiments.

Supplement 2 Stability of DCF-AG at various pH levels

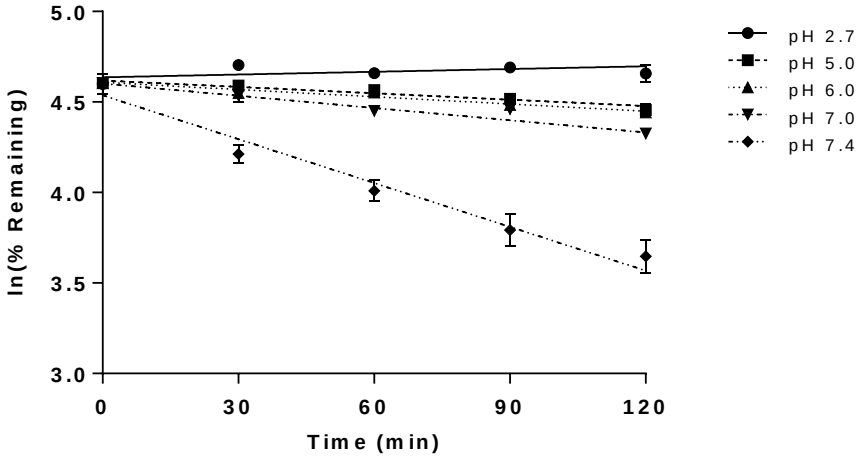

The aqueous stability of 1 µM DCF-AG at various pH levels and 37 °C is shown. The pH values reflect the conditions utilized for several of the *in vitro* assays described throughout the thesis. The pH value of 2.7 represents the acidity in 0.1% formic acid that was used for sample preparation and LC/MS/MS analysis. The lines reflect the best fit for the indicated pH. Each point reflects the mean ± standard error of the mean from n=2 measurements from two separate studies.

Supplement 3 Time-dependent uptake of DCF-AG by HEK-OATP cells

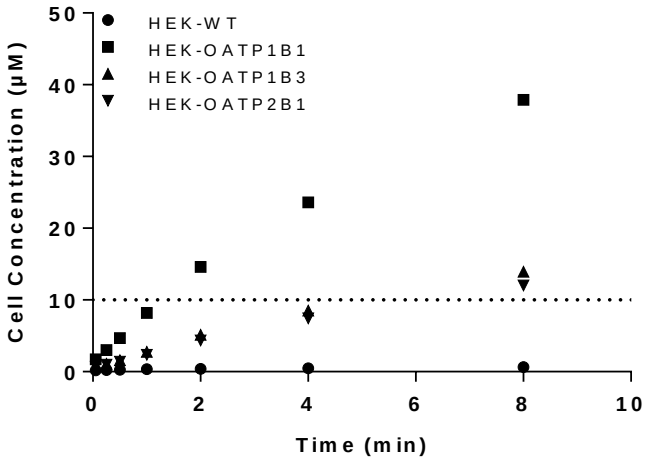

The time-dependent uptake of 10 µM DCF-AG from media by stably-transfected HEK cells is shown. The dashed line reflects the initial buffer DCF-AG concentration of 10 µM and demonstrates that OATPs can increase intracellular DCF-AG concentrations to levels greater than initial buffer conditions. Each point reflects the mean ± standard error of the mean of n=3 measurements.

Supplement 4 Basal transporter expression in C57BL/6J male mouse liver

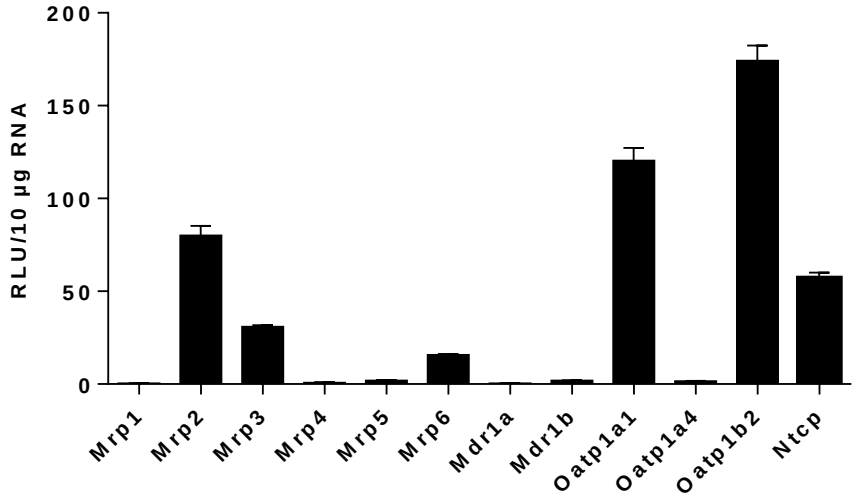

The basal transporter expression in the livers of male C57BL/6J mice is shown. Expression profiles were detected using a bDNA assay. Data are expressed as relative light units (RLU) per 10 µg RNA. Each bar reflects the mean ± standard error of the mean of n=4 subjects.

COPYRIGHT PERMISSIONS

PERMISSION LICENSE: PRINT REPUBLICATION

Request ID/Invoice Number: RON22242

Date: November 10, 2015

To: Ron Scialis
University of Connecticut
School of Pharmacy
69 North Eagleville Road
Storrs CT 06268
United States of America
"Licensee"

McGraw-Hill Education Material

Author: Reisner, Howard
Title: Pathology: A Modern Case Study
ISBN: 9780071621564
Description of material: Figure 10.2

Fee: Waived
Due date: May 10, 2016

Licensee Work:

Author: Ron Scialis
Title: Doctoral Dissertation
Publisher: The Modulation of Non-steroidal Anti-inflammatory Toxicity as a Function of the Interplay between Uptake and Efflux Transporters
Printrun: Approximately 3 printed copies
Distribution Territory: United States
Languages: English

Permission for the use described above is granted under the following conditions:

1. The permission fee of (Waived) must be received by McGraw-Hill Education on or before May 10, 2016, and MUST BE ACCOMPANIED BY A SIGNED COPY OF THIS AGREEMENT. A check should be made payable McGraw-Hill Global Education Holdings, LLC, Attn: Permissions Department, Wells Fargo Bank, Lockbox #6167, PO Box 8500, Philadelphia, Pa. 19178-6167. Please include the invoice number indicated at the top of this form on your check.

2. No adaptations, deletions, or changes will be made in the material without the prior written consent of McGraw-Hill Education.

3. This permission is non-exclusive, non-transferable, and limited to the use specified herein. McGraw-Hill Education expressly reserves all rights in this material.

4. A credit line must be printed on the first page on which the material appears. This credit must include the author, title, copyright date, and publisher, and indicate that the material is reproduced with permission of McGraw-Hill Education.

5. This permission does not allow the use of any material, including but not limited to photographs, charts, and other illustrations, which appears in a McGraw-Hill Education work copyrighted in or credited to the name of any person or entity other than McGraw-Hill Education. Should you desire permission to use such material, you must seek permission directly from the owner of that material, and if you use such material you agree to indemnify McGraw-Hill Education against any claim from the owners of that material.

Please sign and return one copy (with payment, if applicable) to the address above, as outlined in Clause 1 of this agreement.

For McGraw-Hill Education:

_____

Permissions Department
McGraw-Hill Education

For Licensee:

Name DocuSigned by: Ron Scialis 26B409BA8DC54E7 _____

Title Doctoral Candidate _____

ENCYCLOPÆDIA Britannica

digital innovation. ADVANCING EDUCATION

ONLINE SERVICES USAGE AGREEMENT ("TERMS OF USE")
For All Britannica Sites, Services and Applications
Advertising-Supported and Subscription, Consumer and Institutional

Effective as of October 16, 2015

These Terms of Use govern your use of Encyclopædia Britannica® Online and, unless other terms and conditions expressly govern, any other electronic services, including mobile application services, provided by or made available through Encyclopædia Britannica, Inc. ("Britannica"), and its affiliates Encyclopædia Britannica (UK) Ltd., Encyclopædia Britannica (India) Pvt. Ltd., Encyclopædia Britannica Australia Ltd., and Britannica Asia Pacific Pty Ltd., that may be available from time to time (collectively, the "Services").

Your use of the Services constitutes your agreement to these Terms of Use. If you do not agree with these Terms of Use, please do not use the Services. Britannica reserves the right to change, modify, add, or remove portions of these Terms of Use at any time, and the modified Terms of Use will be effective when posted on the Services. Please check this page periodically for any modifications. Your use of any of the Services following the posting of changes constitutes your acceptance of the changes.

THESE TERMS OF USE CONTAIN DISCLAIMERS OF WARRANTIES AND LIABILITY, CHOICE OF LAW AND BINDING ARBITRATIONCLAUSES, AND A CLASS ACTION WAIVER. THESE PROVISIONS AFFECT YOUR RIGHTS ABOUT HOW TO RESOLVE ANY DISPUTE WITH BRITANNICA. PLEASE READ THEM.

Britannica offers three types of access to its Services: (1) advertising-supported; (2) individual and family consumer subscriptions; and (3) institutional subscriptions. Section 1 of these Terms of Use applies to all individuals who use our Services – advertising-supported and subscription-based. Section 2 applies only to individuals with consumer subscriptions. Section 3 applies only to individuals who are Authorized Users under institutional subscriptions. Section 4 – Service-Specific Terms – applies only to users of a particular Service. Section 5 - Legal Notices – applies to everyone. These Terms of Use also incorporate the terms contained in

our Privacy Policy, so please read.

SECTION 1
Terms of Use for Everyone

Ownership. The content on the Services is the property of Britannica, its affiliated companies or licensors, and is protected by international copyright, patent, and trademark laws.

Advertising. Advertisements, promotions, and marketing messages may appear on the Services from time to time, unless you or your institution has a subscription-based Service. Please see our Privacy Policy for more information.

Use of Content. You may display, reproduce, print or download content on the Services only for your personal, non-commercial use. If you are a teacher, scholar or student, you may copy reasonable portions of the content for lesson plans, interactive whiteboards, reports, dissertations, presentations, school newspapers and for similar nonprofit educational purposes to the extent permitted by applicable law. In each case, however, you may not remove or alter any copyright, trademark, service mark or other proprietary notices or legends. You may not publish, distribute, retransmit, sell or provide access to the content on the Services, except as permitted under applicable law or as described in these Terms of Use. Britannica works to ensure that all the content on its Services is in compliance with applicable U.S. copyright laws. However, in the case of works on the Services authored by parties other than Britannica, you may wish to check on their copyright status before downloading them if you are in another country. You may not use data mining, robots, screen scraping, or similar data gathering and extraction tools on the Services, except with our express written permission. You may not decompile, reverse engineer or disassemble any software or other products or processes accessible through the Services, insert any code or product, or manipulate the content of the Services in any way that affects the user's experience.

If you want to reproduce or use content for any purpose or in any manner other than as described above, you will need Britannica's permission. Requests should be directed to this syndication form.

ASPET
Transforming Discoveries into Therapies

November 11, 2015

Ron Scialis
Department of Pharmaceutical Sciences
University of Connecticut
69 North Eagleville Rd.
Storrs, CT 06269

Dear Ron Scialis:

This is to grant you permission to include the following article in your thesis entitled "The Modulation of Non-steroidal Anti-inflammatory Toxicity as a Function of the Interplay between Uptake and Efflux Transporters" for the University of Connecticut:

> Renato J. Scialis, Iván L. Csanaky, Michael J. Goedken, and José E. Manauto, Multidrug Resistance-Associated Protein 3 Plays an Important Role in Protection against Acute Toxicity of Diclofenac, *Drug Metab Dispos* July 2015 43:944-950

On the first page of each copy of this article, please add the following:

> Reprinted with permission of the American Society for Pharmacology and Experimental Therapeutics. All rights reserved.

In addition, the original copyright line published with the paper must be shown on the copies included with your thesis.

Sincerely yours,

Richard Dodenhoff
Journals Director

9650 Rockville Pike | Bethesda | MD | 20814-3995
P: (301) 634-7060 | F: (301) 634-7061 | E: info@aspet.org | www.aspet.org

REFERENCES

Abramovitz M, Adam M, Boie Y, Carriere M, Denis D, Godbout C, Lamontagne S, Rochette C, Sawyer N, Tremblay NM, Belley M, Gallant M, Dufresne C, Gareau Y, Ruel R, Juteau H, Labelle M, Ouimet N, and Metters KM (2000) The utilization of recombinant prostanoid receptors to determine the affinities and selectivities of prostaglandins and related analogs. *Biochim Biophys Acta* **1483:**285-293.

ACD/Labs pkA DB version 4.03, Advanced Chemistry Development, Inc., Toronto, ON, Canada.

Adibi SA (2003) Regulation of expression of the intestinal oligopeptide transporter (Pept-1) in health and disease. *Am J Physiol Gastrointest Liver Physiol* **285:**G779-788.

Agrawal NM, Van Kerckhove HE, Erhardt LJ, and Geis GS (1995) Misoprostol coadministered with diclofenac for prevention of gastroduodenal ulcers. A one-year study. *Dig Dis Sci* **40:**1125-1131.

Aguilar-Bryan L, Clement JPt, Gonzalez G, Kunjilwar K, Babenko A, and Bryan J (1998) Toward understanding the assembly and structure of KATP channels. *Physiol Rev* **78:**227-245.

Ahlin G, Hilgendorf C, Karlsson J, Szigyarto CA, Uhlen M, and Artursson P (2009) Endogenous gene and protein expression of drug-transporting proteins in cell lines routinely used in drug discovery programs. *Drug Metab Dispos* **37:**2275-2283.

Aithal GP, Ramsay L, Daly AK, Sonchit N, Leathart JB, Alexander G, Kenna JG, Caldwell J, and Day CP (2004) Hepatic adducts, circulating antibodies, and cytokine polymorphisms in patients with diclofenac hepatotoxicity. *Hepatology* **39:**1430-1440.

Akabane T, Tabata K, Kadono K, Sakuda S, Terashita S, and Teramura T (2009) A Comparison of Pharmacokinetics between Humans and Monkeys. *Drug Metabolism and Disposition* **38:**308-316.

Akahira-Azuma M, Szczepanik M, Tsuji RF, Campos RA, Itakura A, Mobini N, McNiff J, Kawikova I, Lu B, Gerard C, Pober JS, and Askenase PW (2004) Early delayed-type hypersensitivity eosinophil infiltrates depend on T helper 2 cytokines and interferon-gamma via CXCR3 chemokines. *Immunology* **111:**306-317.

Akamine Y, Miura M, Sunagawa S, Kagaya H, Yasui-Furukori N, and Uno T (2010) Influence of drug-transporter polymorphisms on the pharmacokinetics of fexofenadine enantiomers. *Xenobiotica* **40:**782-789.

Aleksunes LM, Campion SN, Goedken MJ, and Manautou JE (2008a) Acquired resistance to acetaminophen hepatotoxicity is associated with induction of multidrug resistance-associated protein 4 (Mrp4) in proliferating hepatocytes. *Toxicol Sci* **104:**261-273.

Aleksunes LM, Slitt AL, Maher JM, Augustine LM, Goedken MJ, Chan JY, Cherrington NJ, Klaassen CD, and Manautou JE (2008b) Induction of Mrp3 and Mrp4 transporters during acetaminophen hepatotoxicity is dependent on Nrf2. *Toxicol Appl Pharmacol* **226:**74-83.

Alia M, Ramos S, Mateos R, Bravo L, and Goya L (2005) Response of the antioxidant defense system to tert-butyl hydroperoxide and hydrogen peroxide in a human hepatoma cell line (HepG2). *J Biochem Mol Toxicol* **19:**119-128.

Altschul SF, Madden TL, Schaffer AA, Zhang J, Zhang Z, Miller W, and Lipman DJ (1997) Gapped BLAST and PSI-BLAST: a new generation of protein database search programs. *Nucleic Acids Res* **25:**3389-3402.

Altschul SF, Wootton JC, Gertz EM, Agarwala R, Morgulis A, Schaffer AA, and Yu YK (2005) Protein database searches using compositionally adjusted substitution matrices. *FEBS J* **272:**5101-5109.

Annilo T and Dean M (2004) Degeneration of an ATP-binding cassette transporter gene, ABCC13, in different mammalian lineages. *Genomics* **84:**34-46.

Arlanov R, Porter A, Strand D, Brough R, Karpova D, Kerb R, Wojnowski L, Schwab M, and Lang T (2012) Functional characterization of protein variants of the human multidrug transporter ABCC2 by a novel targeted expression system in fibrosarcoma cells. *Hum Mutat* **33:**750-762.

Arnhold J (2004) Properties, functions, and secretion of human myeloperoxidase. *Biochemistry (Mosc)* **69:**4-9.

Atchison CR, Balakumaran A, West AB, Hoffmann WE, and Treinen-Moslen M (2000a) Aging enhances susceptibility of diclofenac-treated rats to gastric ulceration, while attenuating enteropathy. *Dig Dis Sci* **45:**614-620.

Atchison CR, West AB, Balakumaran A, Hargus SJ, Pohl LR, Daiker DH, Aronson JF, Hoffmann WE, Shipp BK, and Treinen-Moslen M (2000b) Drug enterocyte adducts: possible causal factor for diclofenac enteropathy in rats. *Gastroenterology* **119:**1537-1547.

Awtry EH and Loscalzo J (2000) Aspirin. *Circulation* **101:**1206-1218.

Aydogdu I, Erkurt MA, Ozhan O, Kaya E, Kuku I, Yitmen E, and Aydin NE (2006) Reversible bone marrow necrosis in a patient due to overdosage of diclofenac sodium. *Am J Hematol* **81:**298.

Badr MZ, Belinsky SA, Kauffman FC, and Thurman RG (1986) Mechanism of hepatotoxicity to periportal regions of the liver lobule due to allyl alcohol: role of oxygen and lipid peroxidation. *J Pharmacol Exp Ther* **238:**1138-1142.

Bailey MJ and Dickinson RG (1996) Chemical and immunochemical comparison of protein adduct formation of four carboxylate drugs in rat liver and plasma. *Chem Res Toxicol* **9:**659-666.

Bandler PE, Westlake CJ, Grant CE, Cole SP, and Deeley RG (2008) Identification of regions required for apical membrane localization of human multidrug resistance protein 2. *Mol Pharmacol* **74:**9-19.

Barnes SN, Aleksunes LM, Augustine L, Scheffer GL, Goedken MJ, Jakowski AB, Pruimboom-Brees IM, Cherrington NJ, and Manautou JE (2007) Induction of hepatobiliary efflux

transporters in acetaminophen-induced acute liver failure cases. *Drug Metab Dispos* **35:**1963-1969.

Beaumont K, Cole SM, Gibson K, and Gosset JR (2010) ADMET for the Medicinal Chemist, in: *Metabolism, Pharmacokinetics and Toxicity of Functional Groups: Impact of the Building Blocks of Medicinal Chemistry on ADMET*, pp 61-98, RSC Publishing, Cambridge, UK.

Bera TK, Iavarone C, Kumar V, Lee S, Lee B, and Pastan I (2002) MRP9, an unusual truncated member of the ABC transporter superfamily, is highly expressed in breast cancer. *Proc Natl Acad Sci U S A* **99:**6997-7002.

Berge KE, Tian H, Graf GA, Yu L, Grishin NV, Schultz J, Kwiterovich P, Shan B, Barnes R, and Hobbs HH (2000) Accumulation of dietary cholesterol in sitosterolemia caused by mutations in adjacent ABC transporters. *Science* **290:**1771-1775.

Bilzer M, Roggel F, and Gerbes AL (2006) Role of Kupffer cells in host defense and liver disease. *Liver Int* **26:**1175-1186.

Blanco FJ, Guitian R, Moreno J, de Toro FJ, and Galdo F (1999) Effect of antiinflammatory drugs on COX-1 and COX-2 activity in human articular chondrocytes. *J Rheumatol* **26:**1366-1373.

Blazka ME, Germolec DR, Simeonova P, Bruccoleri A, Pennypacker KR, and Luster MI (1995a) Acetaminophen-induced hepatotoxicity is associated with early changes in NF-kB and NF-IL6 DNA binding activity. *J Inflamm* **47:**138-150.

Blazka ME, Wilmer JL, Holladay SD, Wilson RE, and Luster MI (1995b) Role of proinflammatory cytokines in acetaminophen hepatotoxicity. *Toxicol Appl Pharmacol* **133:**43-52.

Boelsterli UA (2003) Diclofenac-induced liver injury: a paradigm of idiosyncratic drug toxicity. *Toxicol Appl Pharmacol* **192:**307-322.

Bolze S, Bromet N, Gay-Feutry C, Massiere F, Boulieu R, and Hulot T (2002) Development of an in vitro screening model for the biosynthesis of acyl glucuronide metabolites and the assessment of their reactivity toward human serum albumin. *Drug Metab Dispos* **30:**404-413.

Borne R, Levi M, and Wilson N (2013) Nonsteroidal Anti-Inflammatory Drugs, in: *Foye's Principles of Medicinal Chemistry*, pp 987-1044, Wolters Kluwer Health/Lippincott Williams & Wilkins, Philadelphia.

Bort R, Mace K, Boobis A, Gomez-Lechon MJ, Pfeifer A, and Castell J (1999a) Hepatic metabolism of diclofenac: role of human CYP in the minor oxidative pathways. *Biochem Pharmacol* **58:**787-796.

Bort R, Ponsoda X, Jover R, Gomez-Lechon MJ, and Castell JV (1999b) Diclofenac toxicity to hepatocytes: a role for drug metabolism in cell toxicity. *J Pharmacol Exp Ther* **288:**65-72.

Bouwens L, Baekeland M, De Zanger R, and Wisse E (1986) Quantitation, tissue distribution and proliferation kinetics of Kupffer cells in normal rat liver. *Hepatology* **6:**718-722.

Breen EG, McNicholl J, Cosgrove E, McCabe J, and Stevens FM (1986) Fatal hepatitis associated with diclofenac. *Gut* **27:**1390-1393.

Burlingham BT and Widlanski TS (2003) An Intuitive Look at the Relationship of Ki and IC50: A More General Use for the Dixon Plot. *Journal of Chemical Education* **80:**214.

Busch D, Groer C, Busemann A, I. PL, Heidecke CD, Siegmund W, and Oswald S (2015) Protein Abundance of Clinically Relevant Metabolizing Enzymes along the Human Intestine, in: *20th North American ISSX Meeting*, Orlando.

Campbell NA (1993) Animal Nutrition, in: *Biology*, pp 794-817, Benjamin/Cummings.

Campion SN, Johnson R, Aleksunes LM, Goedken MJ, van Rooijen N, Scheffer GL, Cherrington NJ, and Manautou JE (2008) Hepatic Mrp4 induction following acetaminophen exposure is dependent on Kupffer cell function. *Am J Physiol Gastrointest Liver Physiol* **295:**G294-304.

Cannell GR, Vesey DA, and Dickinson RG (2001) Inhibition of proliferation of HT-29 colon adenocarcinoma cells by carboxylate NSAIDs and their acyl glucuronides. *Life Sci* **70:**37-48.

Cantoni O, Brandi G, Salvaggio L, and Cattabeni F (1989) Molecular mechanisms of hydrogen peroxide cytotoxicity. *Ann Ist Super Sanita* **25:**69-73.

Cashman JR and Zhang J (2002) Interindividual differences of human flavin-containing monooxygenase 3: genetic polymorphisms and functional variation. *Drug Metab Dispos* **30:**1043-1052.

Castell JV, Gomez-Lechon MJ, Ponsoda X, and Bort R (1997) The use of cultured hepatocytes to investigate the mechanisms of drug hepatotoxicity. *Cell Biol Toxicol* **13:**331-338.

Catella-Lawson F, Reilly MP, Kapoor SC, Cucchiara AJ, DeMarco S, Tournier B, Vyas SN, and FitzGerald GA (2001) Cyclooxygenase Inhibitors and the Antiplatelet Effects of Aspirin. *New England Journal of Medicine* **345:**1809-1817.

Chalasani N, Bonkovsky HL, Fontana R, Lee W, Stolz A, Talwalkar J, Reddy KR, Watkins PB, Navarro V, Barnhart H, Gu J, and Serrano J (2015) Features and Outcomes of 899 Patients With Drug-Induced Liver Injury: The DILIN Prospective Study. *Gastroenterology* **148:**1340-1352 e1347.

Chalasani NP, Hayashi PH, Bonkovsky HL, Navarro VJ, Lee WM, and Fontana RJ (2014) ACG Clinical Guideline: the diagnosis and management of idiosyncratic drug-induced liver injury. *Am J Gastroenterol* **109:**950-966; quiz 967.

Chen C, Hennig GE, and Manautou JE (2003) Hepatobiliary excretion of acetaminophen glutathione conjugate and its derivatives in transport-deficient (TR-) hyperbilirubinemic rats. *Drug Metab Dispos* **31:**798-804.

Chen H, Rossier C, Lalioti MD, Lynn A, Chakravarti A, Perrin G, and Antonarakis SE (1996) Cloning of the cDNA for a human homologue of the Drosophila white gene and mapping to chromosome 21q22.3. *Am J Hum Genet* **59:**66-75.

Chen ZS, Guo Y, Belinsky MG, Kotova E, and Kruh GD (2005) Transport of bile acids, sulfated steroids, estradiol 17-beta-D-glucuronide, and leukotriene C4 by human multidrug resistance protein 8 (ABCC11). *Mol Pharmacol* **67:**545-557.

Chen ZS, Lee K, and Kruh GD (2001) Transport of cyclic nucleotides and estradiol 17-beta-D-glucuronide by multidrug resistance protein 4. Resistance to 6-mercaptopurine and 6-thioguanine. *J Biol Chem* **276:**33747-33754.

Chen ZS, Lee K, Walther S, Raftogianis RB, Kuwano M, Zeng H, and Kruh GD (2002) Analysis of methotrexate and folate transport by multidrug resistance protein 4 (ABCC4): MRP4 is a component of the methotrexate efflux system. *Cancer Res* **62:**3144-3150.

Chen ZS and Tiwari AK (2011) Multidrug resistance proteins (MRPs/ABCCs) in cancer chemotherapy and genetic diseases. *FEBS J* **278:**3226-3245.

Cheng X, Maher J, Chen C, and Klaassen CD (2005) Tissue distribution and ontogeny of mouse organic anion transporting polypeptides (Oatps). *Drug Metab Dispos* **33:**1062-1073.

Cheng Y and Prusoff WH (1973) Relationship between the inhibition constant (K1) and the concentration of inhibitor which causes 50 per cent inhibition (I50) of an enzymatic reaction. *Biochem Pharmacol* **22:**3099-3108.

Cherrington NJ, Hartley DP, Li N, Johnson DR, and Klaassen CD (2002) Organ distribution of multidrug resistance proteins 1, 2, and 3 (Mrp1, 2, and 3) mRNA and hepatic induction of Mrp3 by constitutive androstane receptor activators in rats. *J Pharmacol Exp Ther* **300:**97-104.

Chiou YJ, Tomer KB, and Smith PC (1999) Effect of nonenzymatic glycation of albumin and superoxide dismutase by glucuronic acid and suprofen acyl glucuronide on their functions in vitro. *Chem Biol Interact* **121:**141-159.

Christians U (2004) Transport proteins and intestinal metabolism: P-glycoprotein and cytochrome P4503A. *Ther Drug Monit* **26:**104-106.

Claudel T, Zollner G, Wagner M, and Trauner M (2011) Role of nuclear receptors for bile acid metabolism, bile secretion, cholestasis, and gallstone disease. *Biochim Biophys Acta* **1812:**867-878.

Cohn SM, Schloemann S, Tessner T, Seibert K, and Stenson WF (1997) Crypt stem cell survival in the mouse intestinal epithelium is regulated by prostaglandins synthesized through cyclooxygenase-1. *J Clin Invest* **99:**1367-1379.

Coleman RA, Smith WL, and Narumiya S (1994) International Union of Pharmacology classification of prostanoid receptors: properties, distribution, and structure of the receptors and their subtypes. *Pharmacol Rev* **46:**205-229.

Copeland RA, Williams JM, Giannaras J, Nurnberg S, Covington M, Pinto D, Pick S, and Trzaskos JM (1994) Mechanism of selective inhibition of the inducible isoform of prostaglandin G/H synthase. *Proc Natl Acad Sci U S A* **91:**11202-11206.

Coughtrie MW and Fisher MB (2003) The Role of Sulfotransferases (SULTs) and UDP-Glucuronosyltransferases (UGTs) in Human Drug Clearance and Bioactivation, in: *Drug Metabolizing Enzymes* (Lee JS, Obach RS, and Fisher MB eds), pp 541-575, CRC Press, Boca Raton.

Dahlen SE, Hansson G, Hedqvist P, Bjorck T, Granstrom E, and Dahlen B (1983) Allergen challenge of lung tissue from asthmatics elicits bronchial contraction that correlates with the release of leukotrienes C4, D4, and E4. *Proc Natl Acad Sci U S A* **80:**1712-1716.

Daly AK, Aithal GP, Leathart JB, Swainsbury RA, Dang TS, and Day CP (2007) Genetic susceptibility to diclofenac-induced hepatotoxicity: contribution of UGT2B7, CYP2C8, and ABCC2 genotypes. *Gastroenterology* **132:**272-281.

Davies NM and Anderson KE (1997) Clinical pharmacokinetics of diclofenac. Therapeutic insights and pitfalls. *Clinical Pharmacokinetics* **33:**184-213.

de Abajo FJ, Montero D, Madurga M, and Garcia Rodriguez LA (2004) Acute and clinically relevant drug-induced liver injury: a population based case-control study. *Br J Clin Pharmacol* **58:**71-80.

De Bruyn T, Stieger B, Augustijns PF, and Annaert PP (2015) Clearance Prediction of HIV Protease Inhibitors in Man: Role of Hepatic Uptake. *J Pharm Sci*.

De Castro WV, Mertens-Talcott S, Rubner A, Butterweck V, and Derendorf H (2006) Variation of flavonoids and furanocoumarins in grapefruit juices: a potential source of variability in grapefruit juice-drug interaction studies. *J Agric Food Chem* **54:**249-255.

Deeley RG, Westlake C, and Cole SP (2006) Transmembrane transport of endo- and xenobiotics by mammalian ATP-binding cassette multidrug resistance proteins. *Physiol Rev* **86:**849-899.

del Pozo MD, Lobera T, and Blasco A (2000) Selective hypersensitivity to diclofenac. *Allergy* **55:**412-413.

Depomed (2014) Cambia (Diclofenac Potassium for Oral Solution) Prescribing Information, Depomed Incorporated, Newark, California.

Dertinger SD, Nazarenko DA, Silverstone AE, and Gasiewicz TA (2001) Aryl hydrocarbon receptor signaling plays a significant role in mediating benzo[a]pyrene- and cigarette smoke condensate-induced cytogenetic damage in vivo. *Carcinogenesis* **22:**171-177.

Dewitt DL and Meade EA (1993) Serum and Glucocorticoid Regulation of Gene Transcription and Expression of the Prostaglandin H Synthase-1 and Prostaglandin H Synthase-2 Isozymes. *Arch Biochem Biophys* **306:**94-102.

DeWitt DL and Smith WL (1988) Primary structure of prostaglandin G/H synthase from sheep vesicular gland determined from the complementary DNA sequence. *Proc Natl Acad Sci U S A* **85:**1412-1416.

Dresser GK, Bailey DG, Leake BF, Schwarz UI, Dawson PA, Freeman DJ, and Kim RB (2002) Fruit juices inhibit organic anion transporting polypeptide-mediated drug uptake to decrease the oral availability of fexofenadine. *Clin Pharmacol Ther* **71:**11-20.

Drozdzik M, Groer C, Penski J, Lapczuk J, Ostrowski M, Lai Y, Prasad B, Unadkat JD, Siegmund W, and Oswald S (2014) Protein abundance of clinically relevant multidrug transporters along the entire length of the human intestine. *Mol Pharm* **11:**3547-3555.

Dubin IN and Johnson FB (1954) Chronic idiopathic jaundice with unidentified pigment in liver cells; a new clinicopathologic entity with a report of 12 cases. *Medicine (Baltimore)* **33:**155-197.

Dunk AA, Walt RP, Jenkins WJ, and Sherlock SS (1982) Diclofenac hepatitis. *Br Med J (Clin Res Ed)* **284:**1605-1606.

Eagling VA, Profit L, and Back DJ (1999) Inhibition of the CYP3A4-mediated metabolism and P-glycoprotein-mediated transport of the HIV-1 protease inhibitor saquinavir by grapefruit juice components. *Br J Clin Pharmacol* **48:**543-552.

Eberhart CE, Coffey RJ, Radhika A, Giardiello FM, Ferrenbach S, and DuBois RN (1994) Up-regulation of cyclooxygenase 2 gene expression in human colorectal adenomas and adenocarcinomas. *Gastroenterology* **107:**1183-1188.

Ebner T, Heinzel G, Prox A, Beschke K, and Wachsmuth H (1999) Disposition and chemical stability of telmisartan 1-O-acylglucuronide. *Drug Metab Dispos* **27:**1143-1149.

El-Sheikh AA, van den Heuvel JJ, Koenderink JB, and Russel FG (2007) Interaction of nonsteroidal anti-inflammatory drugs with multidrug resistance protein (MRP) 2/ABCC2- and MRP4/ABCC4-mediated methotrexate transport. *J Pharmacol Exp Ther* **320:**229-235.

Elsby R, Smith V, Fox L, Stresser D, Butters C, Sharma P, and Surry DD (2011) Validation of membrane vesicle-based breast cancer resistance protein and multidrug resistance protein 2 assays to assess drug transport and the potential for drug-drug interaction to support regulatory submissions. *Xenobiotica* **41:**764-783.

Emery P, Zeidler H, Kvien TK, Guslandi M, Naudin R, Stead H, Verburg KM, Isakson PC, Hubbard RC, and Geis GS (1999) Celecoxib versus diclofenac in long-term management of rheumatoid arthritis: randomised double-blind comparison. *Lancet* **354:**2106-2111.

Evans DF, Pye G, Bramley R, Clark AG, Dyson TJ, and Hardcastle JD (1988) Measurement of gastrointestinal pH profiles in normal ambulant human subjects. *Gut* **29:**1035-1041.

Evett GE, Xie WL, Chipman JG, Robertson DL, and Simmons DL (1993) Prostaglandin G/H Synthase Isoenzyme 2 Expression in Fibroblasts - Regulation by Dexamethasone, Mitogens, and Oncogenes. *Arch Biochem Biophys* **306:**169-177.

Fallingborg J (1999) Intraluminal pH of the human gastrointestinal tract. *Dan Med Bull* **46:**183-196.

Farinelli E, Giampaoli D, Cenciarini A, Cercado E, and Verrotti A (2015) Valproic acid and nonalcoholic fatty liver disease: A possible association? *World J Hepatol* **7:**1251-1257.

FDA (1998) List of Drug Products That Have Been Withdrawn or Removed from the Market for Reasons of Safety or Effectiveness, pp 54082-54089, Department of Heath and Human Services.

FDA (2014) Drug Development and Drug Interactions: Table of Substrates, Inhibitors and Inducers.

Ferrandez A, Prescott S, and Burt RW (2003) COX-2 and colorectal cancer. *Curr Pharm Des* **9:**2229-2251.

Ferreira SH, Moncada S, and Vane JR (1971) Indomethacin and aspirin abolish prostaglandin release from the spleen. *Nat New Biol* **231:**237-239.

Fisher MB, Campanale K, Ackermann BL, VandenBranden M, and Wrighton SA (2000) In vitro glucuronidation using human liver microsomes and the pore-forming peptide alamethicin. *Drug Metab Dispos* **28:**560-566.

Freytag A, Quinzler R, Freitag M, Bickel H, Fuchs A, Hansen H, Hoefels S, Konig HH, Mergenthal K, Riedel-Heller SG, Schon G, Weyerer S, Wegscheider K, Scherer M, van den Bussche H, Haefeli WE, and Gensichen J (2014) [Use and potential risks of over-the-counter analgesics]. *Schmerz* **28:**175-182.

Fridovich I (1978) The biology of oxygen radicals. *Science* **201:**875-880.

Fries JF, Williams CA, and Bloch DA (1991) The relative toxicity of nonsteroidal antiinflammatory drugs. *Arthritis Rheum* **34:**1353-1360.

Fujimura T, Ohta T, Oyama K, Miyashita T, and Miwa K (2007) Cyclooxygenase-2 (COX-2) in carcinogenesis and selective COX-2 inhibitors for chemoprevention in gastrointestinal cancers. *J Gastrointest Cancer* **38:**78-82.

Fukazawa I, Uchida N, Uchida E, and Yasuhara H (2004) Effects of grapefruit juice on pharmacokinetics of atorvastatin and pravastatin in Japanese. *Br J Clin Pharmacol* **57:**448-455.

Fukui M and Zhu BT (2010) Mitochondrial superoxide dismutase SOD2, but not cytosolic SOD1, plays a critical role in protection against glutamate-induced oxidative stress and cell death in HT22 neuronal cells. *Free Radic Biol Med* **48:**821-830.

Fukushima-Uesaka H, Saito Y, Maekawa K, Hasegawa R, Suzuki K, Yanagawa T, Kajio H, Kuzuya N, Noda M, Yasuda K, Tohkin M, and Sawada J (2007) Genetic variations of the ABC transporter gene ABCC3 in a Japanese population. *Drug Metab Pharmacokinet* **22:**129-135.

Funk CD, Funk LB, Kennedy ME, Pong AS, and Fitzgerald GA (1991) Human platelet/erythroleukemia cell prostaglandin G/H synthase: cDNA cloning, expression, and gene chromosomal assignment. *FASEB J* **5:**2304-2312.

Gao C, Zhang H, Guo Z, You T, Chen X, and Zhong D (2012) Mechanistic studies on the absorption and disposition of scutellarin in humans: selective OATP2B1-mediated hepatic uptake is a likely key determinant for its unique pharmacokinetic characteristics. *Drug Metab Dispos* **40:**2009-2020.

Geis GS, Stead H, Wallemark CB, and Nicholson PA (1991) Prevalence of mucosal lesions in the stomach and duodenum due to chronic use of NSAID in patients with rheumatoid arthritis or osteoarthritis, and interim report on prevention by misoprostol of diclofenac associated lesions. *J Rheumatol Suppl* **28:**11-14.

Ghanem CI, Rudraiah S, Bataille AM, Vigo MB, Goedken MJ, and Manautou JE (2015) Role of nuclear factor-erythroid 2-related factor 2 (Nrf2) in the transcriptional regulation of brain ABC transporters during acute acetaminophen (APAP) intoxication in mice. *Biochem Pharmacol* **94:**203-211.

Ghosh A, Maurer TS, Litchfield J, Varma MV, Rotter C, Scialis R, Feng B, Tu M, Guimaraes CR, and Scott DO (2014) Toward a unified model of passive drug permeation II: the physiochemical determinants of unbound tissue distribution with applications to the design of hepatoselective glucokinase activators. *Drug Metab Dispos* **42:**1599-1610.

Giacomini KM, Huang SM, Tweedie DJ, Benet LZ, Brouwer KL, Chu X, Dahlin A, Evers R, Fischer V, Hillgren KM, Hoffmaster KA, Ishikawa T, Keppler D, Kim RB, Lee CA, Niemi M, Polli JW, Sugiyama Y, Swaan PW, Ware JA, Wright SH, Yee SW, Zamek-Gliszczynski MJ, and Zhang L (2010) Membrane transporters in drug development. *Nat Rev Drug Discov* **9:**215-236.

Gindzienski A, Zwierz K, and Sarosiek J (2003) The role of mucus and its components in protection and repair within the alimentary tract mucosa: Polish experience. *J Physiol Pharmacol* **54 Suppl 3:**127-144.

Glaeser H, Bailey DG, Dresser GK, Gregor JC, Schwarz UI, McGrath JS, Jolicoeur E, Lee W, Leake BF, Tirona RG, and Kim RB (2007) Intestinal drug transporter expression and the impact of grapefruit juice in humans. *Clin Pharmacol Ther* **81:**362-370.

Gomez-Lechon MJ, Ponsoda X, O'Connor E, Donato T, Castell JV, and Jover R (2003a) Diclofenac induces apoptosis in hepatocytes by alteration of mitochondrial function and generation of ROS. *Biochem Pharmacol* **66:**2155-2167.

Gomez-Lechon MJ, Ponsoda X, O'Connor E, Donato T, Jover R, and Castell JV (2003b) Diclofenac induces apoptosis in hepatocytes. *Toxicol In Vitro* **17:**675-680.

Goosen TC, Cillie D, Bailey DG, Yu C, He K, Hollenberg PF, Woster PM, Cohen L, Williams JA, Rheeders M, and Dijkstra HP (2004) Bergamottin contribution to the grapefruit juice-felodipine interaction and disposition in humans. *Clin Pharmacol Ther* **76:**607-617.

Gottesman MM, Fojo T, and Bates SE (2002) Multidrug resistance in cancer: role of ATP-dependent transporters. *Nat Rev Cancer* **2:**48-58.

Green RM and Flamm S (2002) AGA technical review on the evaluation of liver chemistry tests. *Gastroenterology* **123:**1367-1384.

Gregory PA, Gardner-Stephen DA, Rogers A, Michael MZ, and Mackenzie PI (2006) The caudal-related homeodomain protein Cdx2 and hepatocyte nuclear factor 1alpha cooperatively regulate the UDP-glucuronosyltransferase 2B7 gene promoter. *Pharmacogenet Genomics* **16:**527-536.

Gregory PA, Lewinsky RH, Gardner-Stephen DA, and Mackenzie PI (2004) Regulation of UDP glucuronosyltransferases in the gastrointestinal tract. *Toxicol Appl Pharmacol* **199:**354-363.

Grewal KK and Racz WJ (1993) Intracellular calcium disruption as a secondary event in acetaminophen-induced hepatotoxicity. *Can J Physiol Pharmacol* **71:**26-33.

Grillo MP, Knutson CG, Sanders PE, Waldon DJ, Hua F, and Ware JA (2003) Studies on the chemical reactivity of diclofenac acyl glucuronide with glutathione: identification of diclofenac-S-acyl-glutathione in rat bile. *Drug Metab Dispos* **31:**1327-1336.

Groer C, Bruck S, Lai Y, Paulick A, Busemann A, Heidecke CD, Siegmund W, and Oswald S (2013) LC-MS/MS-based quantification of clinically relevant intestinal uptake and efflux transporter proteins. *J Pharm Biomed Anal* **85:**253-261.

Grosser G, Doring B, Ugele B, Geyer J, Kulling SE, and Soukup ST (2014) Transport of the soy isoflavone daidzein and its conjugative metabolites by the carriers SOAT, NTCP, OAT4, and OATP2B1. *Arch Toxicol*.

Hagenbuch B and Meier PJ (2003) The superfamily of organic anion transporting polypeptides. *Biochim Biophys Acta* **1609:**1-18.

Hagenbuch B and Meier PJ (2004) Organic anion transporting polypeptides of the OATP/ SLC21 family: phylogenetic classification as OATP/ SLCO superfamily, new nomenclature and molecular/functional properties. *Pflugers Arch* **447:**653-665.

Han YH, Busler D, Hong Y, Tian Y, Chen C, and Rodrigues AD (2010) Transporter studies with the 3-O-sulfate conjugate of 17alpha-ethinylestradiol: assessment of human liver drug transporters. *Drug Metab Dispos* **38:**1072-1082.

Harbourt DE, Fallon JK, Ito S, Baba T, Ritter JK, Glish GL, and Smith PC (2012) Quantification of human uridine-diphosphate glucuronosyl transferase 1A isoforms in liver, intestine, and kidney using nanobore liquid chromatography-tandem mass spectrometry. *Anal Chem* **84:**98-105.

Hargus SJ, Martin BM, George JW, and Pohl LR (1995) Covalent modification of rat liver dipeptidyl peptidase IV (CD26) by the nonsteroidal anti-inflammatory drug diclofenac. *Chem Res Toxicol* **8:**993-996.

Harisch G and Meyer W (1985) Studies on tissue distribution of glutathione and on activities of glutathione-related enzymes after carbon tetrachloride-induced liver injury. *Res Commun Chem Pathol Pharmacol* **47:**399-314.

Hasegawa M, Kusuhara H, Adachi M, Schuetz JD, Takeuchi K, and Sugiyama Y (2007) Multidrug resistance-associated protein 4 is involved in the urinary excretion of hydrochlorothiazide and furosemide. *J Am Soc Nephrol* **18:**37-45.

Hassan S, Kinoshita Y, Min D, Nakata H, Kishi K, Matsushima Y, Asahara M, Wang HY, Okada A, Maekawa T, Matsui H, and Chiba T (1996) Presence of prostaglandin EP4 receptor gene expression in a rat gastric mucosal cell line. *Digestion* **57:**196-200.

Hatazawa R, Tanaka A, Tanigami M, Amagase K, Kato S, Ashida Y, and Takeuchi K (2007) Cyclooxygenase-2/prostaglandin E2 accelerates the healing of gastric ulcers via EP4 receptors. *Am J Physiol Gastrointest Liver Physiol* **293:**G788-797.

He J, Nishida S, Xu M, Makishima M, and Xie W (2011) PXR prevents cholesterol gallstone disease by regulating biosynthesis and transport of bile salts. *Gastroenterology* **140:**2095-2106.

Heaton KW (1969) The importance of keeping bile salts in their place. *Gut* **10:**857-863.

Helander HF and Fandriks L (2014) Surface area of the digestive tract - revisited. *Scand J Gastroenterol* **49:**681-689.

Helfgott SM, Sandberg-Cook J, Zakim D, and Nestler J (1990) Diclofenac-associated hepatotoxicity. *JAMA* **264:**2660-2662.

Hess DT, Matsumoto A, Kim SO, Marshall HE, and Stamler JS (2005) Protein S-nitrosylation: purview and parameters. *Nat Rev Mol Cell Biol* **6:**150-166.

Hickey EJ, Raje RR, Reid VE, Gross SM, and Ray SD (2001) Diclofenac induced in vivo nephrotoxicity may involve oxidative stress-mediated massive genomic DNA fragmentation and apoptotic cell death. *Free Radic Biol Med* **31:**139-152.

Hinson JA, Roberts DW, and James LP (2010) Mechanisms of acetaminophen-induced liver necrosis. *Handb Exp Pharmacol***:**369-405.

Hinz B, Chevts J, Renner B, Wuttke H, Rau T, Schmidt A, Szelenyi I, Brune K, and Werner U (2005) Bioavailability of diclofenac potassium at low doses. *Br J Clin Pharmacol* **59:**80-84.

Hirohashi T, Suzuki H, and Sugiyama Y (1999) Characterization of the transport properties of cloned rat multidrug resistance-associated protein 3 (MRP3). *J Biol Chem* **274:**15181-15185.

Hla T and Neilson K (1992) Human cyclooxygenase-2 cDNA. *Proc Natl Acad Sci U S A* **89:**7384-7388.

Hoffmann K and Loscher W (2007) Upregulation of brain expression of P-glycoprotein in MRP2-deficient TR(-) rats resembles seizure-induced up-regulation of this drug efflux transporter in normal rats. *Epilepsia* **48:**631-645.

Hoshino T, Takano T, Tsutsumi S, Tomisato W, Tsuchiya T, and Mizushima T (2002) Effects of prostaglandin E2 on gastric irritant-induced apoptosis. *Dig Dis Sci* **47:**2370-2379.

Hoshino T, Tsutsumi S, Tomisato W, Hwang HJ, Tsuchiya T, and Mizushima T (2003) Prostaglandin E2 protects gastric mucosal cells from apoptosis via EP2 and EP4 receptor activation. *J Biol Chem* **278:**12752-12758.

Hounnou G, Destrieux C, Desme J, Bertrand P, and Velut S (2002) Anatomical study of the length of the human intestine. *Surg Radiol Anat* **24:**290-294.

Hu DG, Meech R, McKinnon RA, and Mackenzie PI (2014) Transcriptional regulation of human UDP-glucuronosyltransferase genes. *Drug Metab Rev* **46:**421-458.

Huang L, Berry L, Ganga S, Janosky B, Chen A, Roberts J, Colletti AE, and Lin MH (2010) Relationship between passive permeability, efflux, and predictability of clearance from in vitro metabolic intrinsic clearance. *Drug Metab Dispos* **38:**223-231.

Hulot JS, Villard E, Maguy A, Morel V, Mir L, Tostivint I, William-Faltaos D, Fernandez C, Hatem S, Deray G, Komajda M, Leblond V, and Lechat P (2005) A mutation in the drug transporter gene ABCC2 associated with impaired methotrexate elimination. *Pharmacogenet Genomics* **15:**277-285.

Hutzler JM and Tracy TS (2002) Atypical kinetic profiles in drug metabolism reactions. *Drug Metab Dispos* **30:**355-362.

Ieiri I, Fukae M, Maeda K, Ando Y, Kimura M, Hirota T, Nakamura T, Iwasaki K, Matsuki S, Matsuguma K, Kanda E, Deguchi M, Irie S, and Sugiyama Y (2012) Pharmacogenomic/pharmacokinetic assessment of a four-probe cocktail for CYPs and OATPs following oral microdosing. *Int J Clin Pharmacol Ther* **50:**689-700.

Ishiguro N, Maeda K, Saito A, Kishimoto W, Matsushima S, Ebner T, Roth W, Igarashi T, and Sugiyama Y (2008) Establishment of a set of double transfectants coexpressing organic anion transporting polypeptide 1B3 and hepatic efflux transporters for the characterization of the hepatobiliary transport of telmisartan acylglucuronide. *Drug Metab Dispos* **36:**796-805.

Ito K, Suzuki H, Hirohashi T, Kume K, Shimizu T, and Sugiyama Y (1997) Molecular cloning of canalicular multispecific organic anion transporter defective in EHBR. *Am J Physiol* **272:**G16-22.

Jakobsson PJ, Thoren S, Morgenstern R, and Samuelsson B (1999) Identification of human prostaglandin E synthase: a microsomal, glutathione-dependent, inducible enzyme, constituting a potential novel drug target. *Proc Natl Acad Sci U S A* **96:**7220-7225.

Jin W and Dong C (2013) IL-17 cytokines in immunity and inflammation. *Emerg Microbes Infect* **2:**e60.

Johnson BM, Zhang P, Schuetz JD, and Brouwer KL (2006) Characterization of transport protein expression in multidrug resistance-associated protein (Mrp) 2-deficient rats. *Drug Metab Dispos* **34:**556-562.

Johnson JL, Wimsatt J, Buckel SD, Dyer RD, and Maddipati KR (1995) Purification and characterization of prostaglandin H synthase-2 from sheep placental cotyledons. *Arch Biochem Biophys* **324:**26-34.

Jones A (2002) Over-the-counter analgesics: a toxicology perspective. *Am J Ther* **9:**245-257.

Jungermann K and Katz N (1989) Functional specialization of different hepatocyte populations. *Physiol Rev* **69:**708-764.

Juni P, Rutjes AW, and Dieppe PA (2002) Are selective COX 2 inhibitors superior to traditional non steroidal anti-inflammatory drugs? *BMJ* **324:**1287-1288.

Kakkar P, Das B, and Viswanathan PN (1984) A modified spectrophotometric assay of superoxide dismutase. *Indian J Biochem Biophys* **21:**130-132.

Kalgutkar AS, Chen D, Varma MV, Feng B, Terra SG, Scialis RJ, Rotter CJ, Frederick KS, West MA, Goosen TC, Gosset JR, Walsky RL, and Francone OL (2013) Elucidation of the biochemical basis for a clinical drug-drug interaction between atorvastatin and 5-(N-(4-((4-ethylbenzyl)thio)phenyl)sulfamoyl)-2-methyl benzoic acid (CP-778875), a subtype selective agonist of the peroxisome proliferator-activated receptor alpha. *Xenobiotica* **43:**963-972.

Kalgutkar AS and Daniels JS (2010) Carboxylic Acids and their Bioiosoteres, in: *Metabolism, Pharmacokinetics and Toxicity of Functional Groups: Impact of the Building Blocks of Medicinal Chemistry on ADMET*, pp 99-167, RSC Publishing, Cambridge, UK.

Kalinski P (2011) Regulation of Immune Responses by Prostaglandin E2. *The Journal of Immunology* **188:**21-28.

Kantola T, Kivisto KT, and Neuvonen PJ (1998) Grapefruit juice greatly increases serum concentrations of lovastatin and lovastatin acid. *Clin Pharmacol Ther* **63:**397-402.

Kaplowitz N (1981) The importance and regulation of hepatic glutathione. *Yale J Biol Med* **54:**497-502.

Karim A and Gels S (1995) Clinical Development of an NSAID Combined with a Prostaglandin E1 Analogue, in: *Advances in Anti Rheumatic Therapy* (Rainsford KD ed), pp 113-128, Taylor & Francis, New York.

Kawabata S, Oka M, Shiozawa K, Tsukamoto K, Nakatomi K, Soda H, Fukuda M, Ikegami Y, Sugahara K, Yamada Y, Kamihira S, Doyle LA, Ross DD, and Kohno S (2001) Breast cancer resistance protein directly confers SN-38 resistance of lung cancer cells. *Biochem Biophys Res Commun* **280:**1216-1223.

Kawamori T, Uchiya N, Sugimura T, and Wakabayashi K (2003) Enhancement of colon carcinogenesis by prostaglandin E2 administration. *Carcinogenesis* **24:**985-990.

Kellstein DE, Waksman JA, Furey SA, Binstok G, and Cooper SA (1999) The safety profile of nonprescription ibuprofen in multiple-dose use: a meta-analysis. *J Clin Pharmacol* **39:**520-532.

Kenny JR, Maggs JL, Meng X, Sinnott D, Clarke SE, Park BK, and Stachulski AV (2004) Syntheses and characterization of the acyl glucuronide and hydroxy metabolites of diclofenac. *J Med Chem* **47:**2816-2825.

Kidron H, Wissel G, Manevski N, Hakli M, Ketola RA, Finel M, Yliperttula M, Xhaard H, and Urtti A (2012) Impact of probe compound in MRP2 vesicular transport assays. *Eur J Pharm Sci* **46:**100-105.

Kim SF, Huri DA, and Snyder SH (2005) Inducible nitric oxide synthase binds, S-nitrosylates, and activates cyclooxygenase-2. *Science* **310:**1966-1970.

Kimoto E, Li R, Scialis RJ, Lai Y, and Varma MV (2015) Hepatic Disposition of Gemfibrozil and Its Major Metabolite, Gemfibrozil 1-O-beta-Glucuronide. *Mol Pharm*.

King C, Tang W, Ngui J, Tephly T, and Braun M (2001) Characterization of rat and human UDP-glucuronosyltransferases responsible for the in vitro glucuronidation of diclofenac. *Toxicol Sci* **61:**49-53.

Kitamura T, Jansen P, Hardenbrook C, Kamimoto Y, Gatmaitan Z, and Arias IM (1990) Defective ATP-dependent bile canalicular transport of organic anions in mutant (TR-) rats with conjugated hyperbilirubinemia. *Proc Natl Acad Sci U S A* **87:**3557-3561.

Kivisto KT, Lilja JJ, Backman JT, and Neuvonen PJ (1999) Repeated consumption of grapefruit juice considerably increases plasma concentrations of cisapride. *Clin Pharmacol Ther* **66:**448-453.

Kliewer SA, Moore JT, Wade L, Staudinger JL, Watson MA, Jones SA, McKee DD, Oliver BB, Willson TM, Zetterstrom RH, Perlmann T, and Lehmann JM (1998) An orphan nuclear receptor activated by pregnanes defines a novel steroid signaling pathway. *Cell* **92:**73-82.

Knauer MJ, Urquhart BL, Meyer zu Schwabedissen HE, Schwarz UI, Lemke CJ, Leake BF, Kim RB, and Tirona RG (2010) Human skeletal muscle drug transporters determine local exposure and toxicity of statins. *Circ Res* **106:**297-306.

Kneer W, Rother I, Rother M, and Seidel E (2009) A multiple-dose, open-label, safety, compliance, and usage evaluation study of epicutaneously applied Diractin (ketoprofen in Transfersome) in joint/musculoskeletal pain or soft tissue inflammation. *Curr Drug Saf* **4:**5-10.

Kobayashi K, Ito K, Takada T, Sugiyama Y, and Suzuki H (2008) Functional analysis of nonsynonymous single nucleotide polymorphism type ATP-binding cassette transmembrane transporter subfamily C member 3. *Pharmacogenet Genomics* **18:**823-833.

Kock K and Brouwer KL (2012) A perspective on efflux transport proteins in the liver. *Clin Pharmacol Ther* **92:**599-612.

Koehne CH and Dubois RN (2004) COX-2 inhibition and colorectal cancer. *Semin Oncol* **31:**12-21.

Kotani T, Kobata A, Nakamura E, Amagase K, and Takeuchi K (2006) Roles of cyclooxygenase-2 and prostacyclin/IP receptors in mucosal defense against ischemia/reperfusion injury in mouse stomach. *J Pharmacol Exp Ther* **316:**547-555.

Kretz-Rommel A and Boelsterli UA (1993) Diclofenac covalent protein binding is dependent on acyl glucuronide formation and is inversely related to P450-mediated acute cell injury in cultured rat hepatocytes. *Toxicol Appl Pharmacol* **120:**155-161.

Krieglstein CF, Anthoni C, Cerwinka WH, Stokes KY, Russell J, Grisham MB, and Granger DN (2007) Role of blood- and tissue-associated inducible nitric-oxide synthase in colonic inflammation. *Am J Pathol* **170:**490-496.

Kullak-Ublick GA, Stieger B, Hagenbuch B, and Meier PJ (2000) Hepatic transport of bile salts. *Semin Liver Dis* **20:**273-292.

Kulling PE, Backman EA, Skagius AS, and Beckman EA (1995) Renal impairment after acute diclofenac, naproxen, and sulindac overdoses. *J Toxicol Clin Toxicol* **33:**173-177.

Kutchai HC (2004a) Digestion and Absorption, in: *Physiology* (Berne RM, Levy MN, Koeppen BM, and Stanton BA eds), pp 595-620, Mosby, St. Louis.

Kutchai HC (2004b) Gastrointestinal Secretions, in: *Physiology* (Berne RM, Levy MN, Koeppen BM, and Stanton BA eds), pp 566-594, Mosby, St. Louis.

Lagas JS, Sparidans RW, Wagenaar E, Beijnen JH, and Schinkel AH (2010) Hepatic clearance of reactive glucuronide metabolites of diclofenac in the mouse is dependent on multiple ATP-binding cassette efflux transporters. *Mol Pharmacol* **77:**687-694.

Lagas JS, van der Kruijssen CM, van de Wetering K, Beijnen JH, and Schinkel AH (2009) Transport of diclofenac by breast cancer resistance protein (ABCG2) and stimulation of multidrug resistance protein 2 (ABCC2)-mediated drug transport by diclofenac and benzbromarone. *Drug Metab Dispos* **37:**129-136.

Lang T, Hitzl M, Burk O, Mornhinweg E, Keil A, Kerb R, Klein K, Zanger UM, Eichelbaum M, and Fromm MF (2004) Genetic polymorphisms in the multidrug resistance-associated protein 3 (ABCC3, MRP3) gene and relationship to its mRNA and protein expression in human liver. *Pharmacogenetics* **14:**155-164.

Lang T, Justenhoven C, Winter S, Baisch C, Hamann U, Harth V, Ko YD, Rabstein S, Spickenheuer A, Pesch B, Bruning T, Schwab M, and Brauch H (2011) The earwax-associated SNP c.538G>A (G180R) in ABCC11 is not associated with breast cancer risk in Europeans. *Breast Cancer Res Treat* **129:**993-999.

Larson AM, Polson J, Fontana RJ, Davern TJ, Lalani E, Hynan LS, Reisch JS, Schiodt FV, Ostapowicz G, Shakil AO, and Lee WM (2005) Acetaminophen-induced acute liver failure: results of a United States multicenter, prospective study. *Hepatology* **42:**1364-1372.

Lascar G, Grippon P, and Levy VG (1984) [Acute fatal hepatitis during treatment with diclofenac (Voltarene)]. *Gastroenterol Clin Biol* **8:**881-882.

Lecomte M, Laneuville O, Ji C, DeWitt DL, and Smith WL (1994) Acetylation of human prostaglandin endoperoxide synthase-2 (cyclooxygenase-2) by aspirin. *J Biol Chem* **269:**13207-13215.

Lee M (2013) Nondrug Reference Ranges for Common Laboratory Tests in Traditional and SI Units, in: *Basic Skills in Interpreting Laboratory Data*, American Society of Health-System Pharmacists, Bethesda.

Levesque E, Benoit-Biancamano MO, Delage R, Couture F, and Guillemette C (2008) Pharmacokinetics of mycophenolate mofetil and its glucuronide metabolites in healthy volunteers. *Pharmacogenomics* **9:**869-879.

Lewis DF (1999) Homology modelling of human cytochromes P450 involved in xenobiotic metabolism and rationalization of substrate selectivity. *Exp Toxicol Pathol* **51:**369-374.

Li N, Parikh SN, Xiao D, Stresser D, Crespi CL, and Patten CJ (2011) Application of Inside-out Vesicle Uptake Assay to Characterize ABC Transporters Substrates and Inhibitors, in: *17th North American Regional ISSX Meeting*, Atlanta, GA.

Lim MS, Lim PL, Gupta R, and Boelsterli UA (2006) Critical role of free cytosolic calcium, but not uncoupling, in mitochondrial permeability transition and cell death induced by diclofenac oxidative metabolites in immortalized human hepatocytes. *Toxicol Appl Pharmacol* **217:**322-331.

Lim SP, Andrews FJ, and O'Brien PE (1995) Acetaminophen-induced microvascular injury in the rat liver: protection with misoprostol. *Hepatology* **22:**1776-1781.

Linton KJ (2007) Structure and function of ABC transporters. *Physiology (Bethesda)* **22:**122-130.

LiverTox (2015) Diclofenac: Summary of Case 82, National Institute of Diabetes and Digestive and Kidney Diseases.

LoGuidice A, Wallace BD, Bendel L, Redinbo MR, and Boelsterli UA (2012) Pharmacologic targeting of bacterial beta-glucuronidase alleviates nonsteroidal anti-inflammatory drug-induced enteropathy in mice. *J Pharmacol Exp Ther* **341:**447-454.

Louis P, Hold GL, and Flint HJ (2014) The gut microbiota, bacterial metabolites and colorectal cancer. *Nat Rev Microbiol* **12:**661-672.

Lu C (2014) Metabolic Stability Screen in Drug Discovery, in: *Handbook of Metabolic Pathways of Xenobiotics*, John Wiley & Sons, Ltd.

Lu K, Lee MH, Hazard S, Brooks-Wilson A, Hidaka H, Kojima H, Ose L, Stalenhoef AF, Mietinnen T, Bjorkhem I, Bruckert E, Pandya A, Brewer HB, Jr., Salen G, Dean M, Srivastava A, and Patel SB (2001) Two genes that map to the STSL locus cause sitosterolemia: genomic structure and spectrum of mutations involving sterolin-1 and sterolin-2, encoded by ABCG5 and ABCG8, respectively. *Am J Hum Genet* **69:**278-290.

Ma L, del Soldato P, and Wallace JL (2002) Divergent effects of new cyclooxygenase inhibitors on gastric ulcer healing: Shifting the angiogenic balance. *Proc Natl Acad Sci U S A* **99:**13243-13247.

Macey R, Oster G, and Zahley T (2000) Berkeley Madonna, Berkely, CA.

Magrane M and Consortium U (2011) UniProt Knowledgebase: a hub of integrated protein data. *Database (Oxford)* **2011:**bar009.

Malarkey DE, Johnson K, Ryan L, Boorman G, and Maronpot RR (2005) New insights into functional aspects of liver morphology. *Toxicol Pathol* **33:**27-34.

Manautou JE, de Waart DR, Kunne C, Zelcer N, Goedken M, Borst P, and Elferink RO (2005) Altered disposition of acetaminophen in mice with a disruption of the Mrp3 gene. *Hepatology* **42:**1091-1098.

Mancini JA, Riendeau D, Falgueyret JP, Vickers PJ, and O'Neill GP (1995) Arginine 120 of prostaglandin G/H synthase-1 is required for the inhibition by nonsteroidal anti-inflammatory drugs containing a carboxylic acid moiety. *J Biol Chem* **270:**29372-29377.

Marino AM, Yarde M, Patel H, Chong S, and Balimane PV (2005) Validation of the 96 well Caco-2 cell culture model for high throughput permeability assessment of discovery compounds. *Int J Pharm* **297:**235-241.

Marnett LJ, Rowlinson SW, Goodwin DC, Kalgutkar AS, and Lanzo CA (1999) Arachidonic Acid Oxygenation by COX-1 and COX-2: MECHANISMS OF CATALYSIS AND INHIBITION. *Journal of Biological Chemistry* **274:**22903-22906.

Martinez-Reyes I and Cuezva JM (2014) The H(+)-ATP synthase: a gate to ROS-mediated cell death or cell survival. *Biochim Biophys Acta* **1837:**1099-1112.

Maslak E, Gregorius A, and Chlopicki S (2015) Liver sinusoidal endothelial cells (LSECs) function and NAFLD; NO-based therapy targeted to the liver. *Pharmacol Rep* **67:**689-694.

Mbonye UR, Wada M, Rieke CJ, Tang HY, DeWitt DL, and Smith WL (2006) The 19-amino Acid Cassette of Cyclooxygenase-2 Mediates Entry of the Protein into the Endoplasmic Reticulum-associated Degradation System. *Journal of Biological Chemistry* **281:**35770-35778.

McGill MR, Sharpe MR, Williams CD, Taha M, Curry SC, and Jaeschke H (2012) The mechanism underlying acetaminophen-induced hepatotoxicity in humans and mice involves mitochondrial damage and nuclear DNA fragmentation. *J Clin Invest* **122:**1574-1583.

McIlwain DR, Berger T, and Mak TW (2013) Caspase functions in cell death and disease. *Cold Spring Harb Perspect Biol* **5:**a008656.

McNeely W and Goa KL (1999) Diclofenac-potassium in migraine: a review. *Drugs* **57:**991-1003.

Menasse R, Hedwall PR, Kraetz J, Pericin C, Riesterer L, Sallmann A, Ziel R, and Jaques R (1978) Pharmacological properties of diclofenac sodium and its metabolites. *Scand J Rheumatol Suppl***:**5-16.

Menochet K, Kenworthy KE, Houston JB, and Galetin A (2012) Use of mechanistic modeling to assess interindividual variability and interspecies differences in active uptake in human and rat hepatocytes. *Drug Metab Dispos* **40:**1744-1756.

MHRA (2015) Oral diclofenac presentations with legal status 'P' – reclassified to POM.

Ming X, Knight BM, and Thakker DR (2011) Vectorial transport of fexofenadine across Caco-2 cells: involvement of apical uptake and basolateral efflux transporters. *Mol Pharm* **8:**1677-1686.

Mitchell JA, Belvisi MG, Akarasereenont P, Robbins RA, Kwon OJ, Croxtall J, Barnes PJ, and Vane JR (1994) Induction of cyclo-oxygenase-2 by cytokines in human pulmonary epithelial cells: regulation by dexamethasone. *Br J Pharmacol* **113:**1008-1014.

Mitchell JR, Jollow DJ, Potter WZ, Gillette JR, and Brodie BB (1973) Acetaminophen-induced hepatic necrosis. IV. Protective role of glutathione. *J Pharmacol Exp Ther* **187:**211-217.

Miyamoto G, Zahid N, and Uetrecht JP (1997) Oxidation of diclofenac to reactive intermediates by neutrophils, myeloperoxidase, and hypochlorous acid. *Chem Res Toxicol* **10:**414-419.

Mizuno H, Sakamoto C, Matsuda K, Wada K, Uchida T, Noguchi H, Akamatsu T, and Kasuga M (1997) Induction of cyclooxygenase 2 in gastric mucosal lesions and its inhibition by the specific antagonist delays healing in mice. *Gastroenterology* **112:**387-397.

Moffit JS, Aleksunes LM, Maher JM, Scheffer GL, Klaassen CD, and Manautou JE (2006) Induction of hepatic transporters multidrug resistance-associated proteins (Mrp) 3 and 4 by clofibrate is regulated by peroxisome proliferator-activated receptor alpha. *J Pharmacol Exp Ther* **317:**537-545.

Mohan S, Ahmad AS, Glushakov AV, Chambers C, and Dore S (2012) Putative role of prostaglandin receptor in intracerebral hemorrhage. *Front Neurol* **3:**145.

Molina DK and DiMaio VJ (2012) Normal organ weights in men: part II-the brain, lungs, liver, spleen, and kidneys. *Am J Forensic Med Pathol* **33:**368-372.

Moncada S, Gryglewski R, Bunting S, and Vane JR (1976) An enzyme isolated from arteries transforms prostaglandin endoperoxides to an unstable substance that inhibits platelet aggregation. *Nature* **263:**663-665.

Montalbetti CAGN and Falque V (2005) Amide bond formation and peptide coupling. *Tetrahedron* **61:**10827-10852.

Monteseirin J, Bonilla I, Camacho J, Conde J, and Sobrino F (2001) Elevated secretion of myeloperoxidase by neutrophils from asthmatic patients: the effect of immunotherapy. *J Allergy Clin Immunol* **107:**623-626.

Montiel V, Huberlant V, Vincent MF, Bonbled F, and Hantson P (2010) Multiple organ failure after an overdose of less than 0.4 mg/kg of colchicine: role of coingestants and drugs during intensive care management. *Clin Toxicol (Phila)* **48:**845-848.

Moolenbeek C and Ruitenberg EJ (1981) The "Swiss roll": a simple technique for histological studies of the rodent intestine. *Lab Anim* **15:**57-59.

Moore M, Thor H, Moore G, Nelson S, Moldeus P, and Orrenius S (1985) The toxicity of acetaminophen and N-acetyl-p-benzoquinone imine in isolated hepatocytes is

associated with thiol depletion and increased cytosolic Ca2+. *J Biol Chem* **260:**13035-13040.

Mor-Cohen R, Zivelin A, Rosenberg N, Shani M, Muallem S, and Seligsohn U (2001) Identification and functional analysis of two novel mutations in the multidrug resistance protein 2 gene in Israeli patients with Dubin-Johnson syndrome. *J Biol Chem* **276:**36923-36930.

Morrissey KM, Wen CC, Johns SJ, Zhang L, Huang SM, and Giacomini KM (2012) The UCSF-FDA TransPortal: a public drug transporter database. *Clin Pharmacol Ther* **92:**545-546.

Nakamori F, Naritomi Y, Hosoya Ki, Moriguchi H, Tetsuka K, Furukawa T, Kadono K, Yamano K, Terashita S, and Teramura T (2012) Quantitative Prediction of Human Intestinal Glucuronidation Effects on Intestinal Availability of UDP-Glucuronosyltransferase Substrates Using In Vitro Data. *Drug Metabolism and Disposition* **40:**1771-1777.

Nakatomi K, Yoshikawa M, Oka M, Ikegami Y, Hayasaka S, Sano K, Shiozawa K, Kawabata S, Soda H, Ishikawa T, Tanabe S, and Kohno S (2001) Transport of 7-ethyl-10-hydroxycamptothecin (SN-38) by breast cancer resistance protein ABCG2 in human lung cancer cells. *Biochem Biophys Res Commun* **288:**827-832.

Nebert DW, Dalton TP, Okey AB, and Gonzalez FJ (2004) Role of aryl hydrocarbon receptor-mediated induction of the CYP1 enzymes in environmental toxicity and cancer. *J Biol Chem* **279:**23847-23850.

Netter P, Lambert H, Larcan A, Godbillon J, and Gosset G (1984) Diclofenac sodium-chlormezanone poisoning. *Eur J Clin Pharmacol* **26:**535-536.

Nezic L, Krahenbuhl S, and Ratz Bravo AE (2012) [Diclofenac induced liver injuries]. *Praxis (Bern 1994)* **101:**371-379.

Nicolaou A, Mauro C, Urquhart P, and Marelli-Berg F (2014) Polyunsaturated Fatty Acid-derived lipid mediators and T cell function. *Front Immunol* **5:**75.

Niemi M, Pasanen MK, and Neuvonen PJ (2011) Organic anion transporting polypeptide 1B1: a genetically polymorphic transporter of major importance for hepatic drug uptake. *Pharmacol Rev* **63:**157-181.

Novartis (2011) Voltaren-XR (Diclofenac Sodium Extended Release) Prescribing Information, Novartis Pharmaceuticals Corporation, East Hanover, New Jersey.

Novartis (2014) Voltaren (Diclofenac Sodium Gel) Prescribing Information, Novartis Pharmaceuticals Corporation, Parsippany, New Jersey.

Nozawa T, Imai K, Nezu J, Tsuji A, and Tamai I (2004) Functional characterization of pH-sensitive organic anion transporting polypeptide OATP-B in human. *J Pharmacol Exp Ther* **308:**438-445.

Nozawa T, Nakajima M, Tamai I, Noda K, Nezu J, Sai Y, Tsuji A, and Yokoi T (2002) Genetic polymorphisms of human organic anion transporters OATP-C (SLC21A6) and OATP-B

(SLC21A9): allele frequencies in the Japanese population and functional analysis. *J Pharmacol Exp Ther* **302:**804-813.

Oda S, Matsuo K, Nakajima A, and Yokoi T (2015) A novel cell-based assay for the evaluation of immune- and inflammatory-related gene expression as biomarkers for the risk assessment of drug-induced liver injury. *Toxicol Lett*.

Ohno S and Nakajin S (2009) Determination of mRNA expression of human UDP-glucuronosyltransferases and application for localization in various human tissues by real-time reverse transcriptase-polymerase chain reaction. *Drug Metab Dispos* **37:**32-40.

Osborne R, Thompson P, Joel S, Trew D, Patel N, and Slevin M (1992) The analgesic activity of morphine-6-glucuronide. *Br J Clin Pharmacol* **34:**130-138.

Ota I, Sakurai A, Toyoda Y, Morita S, Sasaki T, Chishima T, Yamakado M, Kawai Y, Ishidao T, Lezhava A, Yoshiura K, Togo S, Hayashizaki Y, Ishikawa T, Endo I, and Shimada H (2010) Association between breast cancer risk and the wild-type allele of human ABC transporter ABCC11. *Anticancer Res* **30:**5189-5194.

Ozvegy C, Litman T, Szakacs G, Nagy Z, Bates S, Varadi A, and Sarkadi B (2001) Functional characterization of the human multidrug transporter, ABCG2, expressed in insect cells. *Biochem Biophys Res Commun* **285:**111-117.

Paine MF, Hart HL, Ludington SS, Haining RL, Rettie AE, and Zeldin DC (2006) The human intestinal cytochrome P450 "pie". *Drug Metab Dispos* **34:**880-886.

Paine MF, Shen DD, Kunze KL, Perkins JD, Marsh CL, McVicar JP, Barr DM, Gillies BS, and Thummel KE (1996) First-pass metabolism of midazolam by the human intestine. *Clin Pharmacol Ther* **60:**14-24.

Paine MF and Thummel KE (2003) Role of Intestinal Cytochrome P450 in Drug Disposition, in: *Drug Metabolizing Enzymes* (Lee JS, Obach RS, and Fisher MB eds), pp 421-451, CRC Press, Boca Raton.

Parkinson A (2001) Biotransformations of Xenobiotics, in: *Casarett and Doull's Toxicology: The Basic Science of Poisons*, pp 133-224, McGraw-Hill, New York.

Patel CG, Ogasawara K, and Akhlaghi F (2013) Mycophenolic acid glucuronide is transported by multidrug resistance-associated protein 2 and this transport is not inhibited by cyclosporine, tacrolimus or sirolimus. *Xenobiotica* **43:**229-235.

Pfeifer ND, Yang K, and Brouwer KL (2013) Hepatic basolateral efflux contributes significantly to rosuvastatin disposition I: characterization of basolateral versus biliary clearance using a novel protocol in sandwich-cultured hepatocytes. *J Pharmacol Exp Ther* **347:**727-736.

Pfizer (2014) Arthrotec (Diclofenac Sodium/Misoprostol) Prescribing Information, Pfizer Inc., New York, New York.

Picaud J, Beaudouin E, Renaudin JM, Pirson F, Metz-Favre C, Dron-Gonzalvez M, and Moneret-Vautrin DA (2014) Anaphylaxis to diclofenac: nine cases reported to the Allergy Vigilance Network in France. *Allergy* **69:**1420-1423.

Pickup K, Gavin A, Jones HB, Karlsson E, Page C, Ratcliffe K, Sarda S, Schulz-Utermoehl T, and Wilson I (2012) The hepatic reductase null mouse as a model for exploring hepatic conjugation of xenobiotics: application to the metabolism of diclofenac. *Xenobiotica* **42:**195-205.

Pillai U, Muzaffar J, Sen S, and Yancey A (2009) Grapefruit juice and verapamil: a toxic cocktail. *South Med J* **102:**308-309.

Poirier A, Cascais AC, Funk C, and Lave T (2009) Prediction of pharmacokinetic profile of valsartan in human based on in vitro uptake transport data. *J Pharmacokinet Pharmacodyn* **36:**585-611.

Poirier A, Lave T, Portmann R, Brun ME, Senner F, Kansy M, Grimm HP, and Funk C (2008) Design, data analysis, and simulation of in vitro drug transport kinetic experiments using a mechanistic in vitro model. *Drug Metab Dispos* **36:**2434-2444.

Polderman KH (2004) Acute renal failure and rhabdomyolysis. *Int J Artif Organs* **27:**1030-1033.

Pourahmad J, Mortada Y, Eskandari MR, and Shahraki J (2011) Involvement of Lysosomal Labilisation and Lysosomal/mitochondrial Cross-Talk in Diclofenac Induced Hepatotoxicity. *Iran J Pharm Res* **10:**877-887.

Powell CJ, Charles SJ, and Mullervy J (1994) Cocaine hepatotoxicity: a study on the pathogenesis of periportal necrosis. *Int J Exp Pathol* **75:**415-424.

Prueksaritanont T, Gorham LM, Hochman JH, Tran LO, and Vyas KP (1996) Comparative studies of drug-metabolizing enzymes in dog, monkey, and human small intestines, and in Caco-2 cells. *Drug Metab Dispos* **24:**634-642.

Prusakiewicz JJ, Duggan KC, Rouzer CA, and Marnett LJ (2009) Differential Sensitivity and Mechanism of Inhibition of COX-2 Oxygenation of Arachidonic Acid and 2-Arachidonoylglycerol by Ibuprofen and Mefenamic Acid. *Biochemistry* **48:**7353-7355.

Pussegoda K, Ross CJ, Visscher H, Yazdanpanah M, Brooks B, Rassekh SR, Zada YF, Dube MP, Carleton BC, and Hayden MR (2013) Replication of TPMT and ABCC3 genetic variants highly associated with cisplatin-induced hearing loss in children. *Clin Pharmacol Ther* **94:**243-251.

Qian YM, Song WC, Cui H, Cole SP, and Deeley RG (2001) Glutathione stimulates sulfated estrogen transport by multidrug resistance protein 1. *J Biol Chem* **276:**6404-6411.

R Core Team (2015) R: A language and environment for statistical computing. R Foundation for Statistical Computing, Vienna, Austria.

Rafeiro E, Barr SG, Harrison JJ, and Racz WJ (1994) Effects of N-acetylcysteine and dithiothreitol on glutathione and protein thiol replenishment during acetaminophen-induced toxicity in isolated mouse hepatocytes. *Toxicology* **93:**209-224.

Ramírez-Alcántara V, Castañeda-Hernández G, Alan Rampy B, Aronson JF, and Treinen-Moslen M (2005) Attenuated gastropathy but not enteropathy of diclofenac–cholestyramine complex in rats. *Drug Development Research* **64:**19-27.

Ramirez-Alcantara V, LoGuidice A, and Boelsterli UA (2009) Protection from diclofenac-induced small intestinal injury by the JNK inhibitor SP600125 in a mouse model of NSAID-associated enteropathy. *Am J Physiol Gastrointest Liver Physiol* **297:**G990-998.

Reid G, Wielinga P, Zelcer N, De Haas M, Van Deemter L, Wijnholds J, Balzarini J, and Borst P (2003a) Characterization of the transport of nucleoside analog drugs by the human multidrug resistance proteins MRP4 and MRP5. *Mol Pharmacol* **63:**1094-1103.

Reid G, Wielinga P, Zelcer N, van der Heijden I, Kuil A, de Haas M, Wijnholds J, and Borst P (2003b) The human multidrug resistance protein MRP4 functions as a prostaglandin efflux transporter and is inhibited by nonsteroidal antiinflammatory drugs. *Proc Natl Acad Sci U S A* **100:**9244-9249.

Reyes-Garcia G, Deciga-Campos M, Medina-Santillan R, and Granados-Soto V (2007) Comparison of antinociceptive efficacy and gastroprotection between celecoxib and diclofenac plus misoprostol in rats. *Proc West Pharmacol Soc* **50:**69-71.

Richardson PD and Withrington PG (1982) Physiological regulation of the hepatic circulation. *Annu Rev Physiol* **44:**57-69.

Riess W, Stierlin H, Degen P, Faigle JW, Gerardin A, Moppert J, Sallmann A, Schmid K, Schweizer A, Sulc M, Theobald W, and Wagner J (1978) Pharmacokinetics and metabolism of the anti-inflammatory agent Voltaren. *Scand J Rheumatol Suppl***:**17-29.

Ritter JK (2007) Intestinal UGTs as potential modifiers of pharmacokinetics and biological responses to drugs and xenobiotics. *Expert Opin Drug Metab Toxicol* **3:**93-107.

Rius M, Hummel-Eisenbeiss J, and Keppler D (2008) ATP-dependent transport of leukotrienes B4 and C4 by the multidrug resistance protein ABCC4 (MRP4). *J Pharmacol Exp Ther* **324:**86-94.

Rius M, Nies AT, Hummel-Eisenbeiss J, Jedlitschky G, and Keppler D (2003) Cotransport of reduced glutathione with bile salts by MRP4 (ABCC4) localized to the basolateral hepatocyte membrane. *Hepatology* **38:**374-384.

Roberts M, Magnusson B, Burczynski F, and Weiss M (2002) Enterohepatic Circulation. *Clinical Pharmacokinetics* **41:**751-790.

Robey RW, Polgar O, Deeken J, To KKW, and Bates SE (2007) Breast Cancer Resistance Protein, in: *Drug Transporters: Molecular Characterization and Role in Drug Disposition* (You G and Morris ME eds), pp 319-358, John Wiley & Sons, New Jersey.

Rodrigues AD (1999) Integrated cytochrome P450 reaction phenotyping: attempting to bridge the gap between cDNA-expressed cytochromes P450 and native human liver microsomes. *Biochem Pharmacol* **57:**465-480.

Rohrborn D, Wronkowitz N, and Eckel J (2015) DPP4 in Diabetes. *Front Immunol* **6:**386.

Rome LH and Lands WE (1975) Structural requirements for time-dependent inhibition of prostaglandin biosynthesis by anti-inflammatory drugs. *Proc Natl Acad Sci U S A* **72:**4863-4865.

Rommens JM, Iannuzzi MC, Kerem B, Drumm ML, Melmer G, Dean M, Rozmahel R, Cole JL, Kennedy D, Hidaka N, and et al. (1989) Identification of the cystic fibrosis gene: chromosome walking and jumping. *Science* **245:**1059-1065.

Ross SA, Ziska DS, Zhao K, and ElSohly MA (2000) Variance of common flavonoids by brand of grapefruit juice. *Fitoterapia* **71:**154-161.

Roth M, Obaidat A, and Hagenbuch B (2012) OATPs, OATs and OCTs: the organic anion and cation transporters of the SLCO and SLC22A gene superfamilies. *Br J Pharmacol* **165:**1260-1287.

Roth SH and Fuller P (2011) Diclofenac topical solution compared with oral diclofenac: a pooled safety analysis. *J Pain Res* **4:**159-167.

Rudraiah S, Moscovitz JE, Donepudi AC, Campion SN, Slitt AL, Aleksunes LM, and Manautou JE (2014a) Differential Fmo3 gene expression in various liver injury models involving hepatic oxidative stress in mice. *Toxicology* **325:**85-95.

Rudraiah S, Rohrer PR, Gurevich I, Goedken MJ, Rasmussen T, Hines RN, and Manautou JE (2014b) Tolerance to acetaminophen hepatotoxicity in the mouse model of autoprotection is associated with induction of flavin-containing monooxygenase-3 (FMO3) in hepatocytes. *Toxicol Sci* **141:**263-277.

Russel FG, Koenderink JB, and Masereeuw R (2008) Multidrug resistance protein 4 (MRP4/ABCC4): a versatile efflux transporter for drugs and signalling molecules. *Trends Pharmacol Sci* **29:**200-207.

Sai Y, Kaneko Y, Ito S, Mitsuoka K, Kato Y, Tamai I, Artursson P, and Tsuji A (2006) Predominant contribution of organic anion transporting polypeptide OATP-B (OATP2B1) to apical uptake of estrone-3-sulfate by human intestinal Caco-2 cells. *Drug Metab Dispos* **34:**1423-1431.

Saito S, Iida A, Sekine A, Miura Y, Ogawa C, Kawauchi S, Higuchi S, and Nakamura Y (2002) Identification of 779 genetic variations in eight genes encoding members of the ATP-binding cassette, subfamily C (ABCC/MRP/CFTR. *J Hum Genet* **47:**147-171.

Sallmann A and Pfister R (1971) Substituted Derivatives of 2-Anilinophenylacetic Acids and a Process of Preparation, Ciba-Geigy Chemical Company, U.S.A.

Sallustio BC and Holbrook FL (2001) In vivo perturbation of rat hepatocyte canalicular membrane function by diclofenac. *Drug Metab Dispos* **29:**1535-1538.

Sallustio BC, Sabordo L, Evans AM, and Nation RL (2000) Hepatic disposition of electrophilic acyl glucuronide conjugates. *Curr Drug Metab* **1:**163-180.

Sarda S, Page C, Pickup K, Schulz-Utermoehl T, and Wilson I (2012) Diclofenac metabolism in the mouse: novel in vivo metabolites identified by high performance liquid chromatography coupled to linear ion trap mass spectrometry. *Xenobiotica* **42:**179-194.

Sasaki T, Hirota T, Ryokai Y, Kobayashi D, Kimura M, Irie S, Higuchi S, and Ieiri I (2011) Systematic screening of human ABCC3 polymorphisms and their effects on MRP3 expression and function. *Drug Metab Pharmacokinet* **26:**374-386.

Sauret JM, Marinides G, and Wang GK (2002) Rhabdomyolysis. *Am Fam Physician* **65:**907-912.

Sawamura R, Okudaira N, Watanabe K, Murai T, Kobayashi Y, Tachibana M, Ohnuki T, Masuda K, Honma H, Kurihara A, and Okazaki O (2010) Predictability of idiosyncratic drug toxicity risk for carboxylic acid-containing drugs based on the chemical stability of acyl glucuronide. *Drug Metab Dispos* **38:**1857-1864.

Schmassmann A, Zoidl G, Peskar BM, Waser B, Schmassmann-Suhijar D, Gebbers JO, and Reubi JC (2006) Role of the different isoforms of cyclooxygenase and nitric oxide synthase during gastric ulcer healing in cyclooxygenase-1 and -2 knockout mice. *Am J Physiol Gastrointest Liver Physiol* **290:**G747-756.

Schror K (1997) Aspirin and platelets: the antiplatelet action of aspirin and its role in thrombosis treatment and prophylaxis. *Semin Thromb Hemost* **23:**349-356.

Schutz E, Shipkova M, Armstrong VW, Wieland E, and Oellerich M (1999) Identification of a pharmacologically active metabolite of mycophenolic acid in plasma of transplant recipients treated with mycophenolate mofetil. *Clin Chem* **45:**419-422.

Scialis R, Feng B, Kimoto E, Lai Y, Whalen K, and El-Kattan A (2011) The Impact of Grapefruit Juice on the Active Uptake of Drugs by Hepatic Transporters, in: *17th North American Regional ISSX Meeting*, Atlanta, Georgia.

Scialis RJ, Csanaky IL, Goedken MJ, and Manautou JE (2015) Multidrug Resistance-Associated Protein 3 Plays an Important Role in Protection against Acute Toxicity of Diclofenac. *Drug Metab Dispos* **43:**944-950.

Seibert K, Masferrer JL, Needleman P, and Salvemini D (1996) Pharmacological manipulation of cyclo-oxygenase-2 in the inflamed hydronephrotic kidney. *Br J Pharmacol* **117:**1016-1020.

Seitz S and Boelsterli UA (1998) Diclofenac acyl glucuronide, a major biliary metabolite, is directly involved in small intestinal injury in rats. *Gastroenterology* **115:**1476-1482.

Seitz S, Kretz-Rommel A, Oude Elferink RP, and Boelsterli UA (1998) Selective protein adduct formation of diclofenac glucuronide is critically dependent on the rat canalicular conjugate export pump (Mrp2). *Chem Res Toxicol* **11:**513-519.

Sekine S, Ito K, and Horie T (2006) Oxidative stress and Mrp2 internalization. *Free Radic Biol Med* **40:**2166-2174.

Sell S, Teschner M, Gaissmaier C, Martini F, Weidner SA, and Kusswetter W (1999) [Effect of diclofenac on human osteoblasts and their stromal precursors in vitro in relation to arthroplasty]. *Z Rheumatol* **58:**13-20.

Shackleford DM, Evans AM, Milne RW, and Nation RL (2006) Loading-washout studies of the stereoselective sinusoidal uptake of (R)- and (s)-2-phenylpropionyl acyl glucuronide. *Curr Drug Metab* **7:**817-826.

Shani M, Seligsohn U, Gilon E, Sheba C, and Adam A (1970) Dubin-Johnson syndrome in Israel. I. Clinical, laboratory, and genetic aspects of 101 cases. *Q J Med* **39:**549-567.

Sheen CL, Dillon JF, Bateman DN, Simpson KJ, and Macdonald TM (2002) Paracetamol toxicity: epidemiology, prevention and costs to the health-care system. *QJM* **95:**609-619.

Shen S, Marchick MR, Davis MR, Doss GA, and Pohl LR (1999) Metabolic activation of diclofenac by human cytochrome P450 3A4: role of 5-hydroxydiclofenac. *Chem Res Toxicol* **12:**214-222.

Shimada T, Yamazaki H, Mimura M, Inui Y, and Guengerich FP (1994) Interindividual variations in human liver cytochrome P-450 enzymes involved in the oxidation of drugs, carcinogens and toxic chemicals: studies with liver microsomes of 30 Japanese and 30 Caucasians. *J Pharmacol Exp Ther* **270:**414-423.

Shimokawa T and Smith WL (1992) Prostaglandin endoperoxide synthase. The aspirin acetylation region. *J Biol Chem* **267:**12387-12392.

Shinde DD, Kim KB, Oh KS, Abdalla N, Liu KH, Bae SK, Shon JH, Kim HS, Kim DH, and Shin JG (2012) LC-MS/MS for the simultaneous analysis of arachidonic acid and 32 related metabolites in human plasma: Basal plasma concentrations and aspirin-induced changes of eicosanoids. *J Chromatogr B Analyt Technol Biomed Life Sci* **911:**113-121.

Shipkova M, Armstrong VW, Weber L, Niedmann PD, Wieland E, Haley J, Tonshoff B, and Oellerich M (2002) Pharmacokinetics and protein adduct formation of the pharmacologically active acyl glucuronide metabolite of mycophenolic acid in pediatric renal transplant recipients. *Ther Drug Monit* **24:**390-399.

Shukla SJ, Sakamuru S, Huang R, Moeller TA, Shinn P, Vanleer D, Auld DS, Austin CP, and Xia M (2011) Identification of clinically used drugs that activate pregnane X receptors. *Drug Metab Dispos* **39:**151-159.

Sigthorsson G, Simpson RJ, Walley M, Anthony A, Foster R, Hotz-Behoftsitz C, Palizban A, Pombo J, Watts J, Morham SG, and Bjarnason I (2002) COX-1 and 2, intestinal integrity, and pathogenesis of nonsteroidal anti-inflammatory drug enteropathy in mice. *Gastroenterology* **122:**1913-1923.

Silverstein FE, Faich G, Goldstein JL, Simon LS, Pincus T, Whelton A, Makuch R, Eisen G, Agrawal NM, Stenson WF, Burr AM, Zhao WW, Kent JD, Lefkowith JB, Verburg KM, and Geis GS (2000) Gastrointestinal toxicity with celecoxib vs nonsteroidal anti-inflammatory drugs for osteoarthritis and rheumatoid arthritis: the CLASS study: A randomized controlled trial. Celecoxib Long-term Arthritis Safety Study. *JAMA* **284:**1247-1255.

Singhal R, Ganey PE, and Roth RA (2012) Complement activation in acetaminophen-induced liver injury in mice. *J Pharmacol Exp Ther* **341:**377-385.

Smith CJ, Zhang Y, Koboldt CM, Muhammad J, Zweifel BS, Shaffer A, Talley JJ, Masferrer JL, Seibert K, and Isakson PC (1998a) Pharmacological analysis of cyclooxygenase-1 in inflammation. *Proc Natl Acad Sci U S A* **95:**13313-13318.

Smith D (2003) Cytochrome P450 and its Place in Drug Discovery and Development, in: *Drug Metabolizing Enzymes* (Lee JS, Obach RS, and Fisher MB eds), pp 155-177, CRC Press, Boca Raton.

Smith G, Modi S, Pillai I, Lian LY, Sutcliffe MJ, Pritchard MP, Friedberg T, Roberts GC, and Wolf CR (1998b) Determinants of the substrate specificity of human cytochrome P-450 CYP2D6: design and construction of a mutant with testosterone hydroxylase activity. *Biochem J* **331 (Pt 3):**783-792.

Smith WL and Dewitt DL (1996) Prostaglandin Endoperoxide H Synthases-1 and -2. **62:**167-215.

Smith WL, Garavito RM, and DeWitt DL (1996) Prostaglandin Endoperoxide H Synthases (Cyclooxygenases)-1 and -2. *Journal of Biological Chemistry* **271:**33157-33160.

Snijder RJ, Dinant HJ, and Stricker BH (1987) [Fatal liver damage during use of diclofenac]. *Ned Tijdschr Geneeskd* **131:**2088-2090.

Sohlenius-Sternbeck AK (2006) Determination of the hepatocellularity number for human, dog, rabbit, rat and mouse livers from protein concentration measurements. *Toxicol In Vitro* **20:**1582-1586.

Sperker B, Backman JT, and Kroemer HK (1997) The role of beta-glucuronidase in drug disposition and drug targeting in humans. *Clinical Pharmacokinetics* **33:**18-31.

Sravan Kumar G and Das UN (1994) Effect of prostaglandins and their precursors on the proliferation of human lymphocytes and their secretion of tumor necrosis factor and various interleukins. *Prostaglandins, Leukotrienes and Essential Fatty Acids* **50:**331-334.

Stanciu A, Cotutiu C, and Amalinei C (2002) [New data about ITO cells]. *Rev Med Chir Soc Med Nat Iasi* **107:**235-239.

Staudinger JL, Goodwin B, Jones SA, Hawkins-Brown D, MacKenzie KI, LaTour A, Liu Y, Klaassen CD, Brown KK, Reinhard J, Willson TM, Koller BH, and Kliewer SA (2001) The nuclear receptor PXR is a lithocholic acid sensor that protects against liver toxicity. *Proc Natl Acad Sci U S A* **98:**3369-3374.

Stierlin H and Faigle JW (1979) Biotransformation of diclofenac sodium (Voltaren) in animals and in man. II. Quantitative determination of the unchanged drug and principal phenolic metabolites, in urine and bile. *Xenobiotica* **9:**611-621.

Stierlin H, Faigle JW, Sallmann A, Kung W, Richter WJ, Kriemler HP, Alt KO, and Winkler T (1979) Biotransformation of diclofenac sodium (Voltaren) in animals and in man. I. Isolation and identification of principal metabolites. *Xenobiotica* **9:**601-610.

Takeuchi K (2014) Gastric cytoprotection by prostaglandin E(2) and prostacyclin: relationship to EP1 and IP receptors. *J Physiol Pharmacol* **65:**3-14.

Takeuchi K, Yagi K, Kato S, and Ukawa H (1997) Roles of prostaglandin E-receptor subtypes in gastric and duodenal bicarbonate secretion in rats. *Gastroenterology* **113:**1553-1559.

Tamilselvam K, Braidy N, Manivasagam T, Essa MM, Prasad NR, Karthikeyan S, Thenmozhi AJ, Selvaraju S, and Guillemin GJ (2013) Neuroprotective effects of hesperidin, a plant flavanone, on rotenone-induced oxidative stress and apoptosis in a cellular model for Parkinson's disease. *Oxid Med Cell Longev* **2013:**102741.

Tammur J, Prades C, Arnould I, Rzhetsky A, Hutchinson A, Adachi M, Schuetz JD, Swoboda KJ, Ptacek LJ, Rosier M, Dean M, and Allikmets R (2001) Two new genes from the human ATP-binding cassette transporter superfamily, ABCC11 and ABCC12, tandemly duplicated on chromosome 16q12. *Gene* **273:**89-96.

Tanaka A, Araki H, Komoike Y, Hase S, and Takeuchi K (2001) Inhibition of both COX-1 and COX-2 is required for development of gastric damage in response to nonsteroidal antiinflammatory drugs. *J Physiol Paris* **95:**21-27.

Tang W, Stearns RA, Bandiera SM, Zhang Y, Raab C, Braun MP, Dean DC, Pang J, Leung KH, Doss GA, Strauss JR, Kwei GY, Rushmore TH, Chiu SH, and Baillie TA (1999) Studies on cytochrome P-450-mediated bioactivation of diclofenac in rats and in human hepatocytes: identification of glutathione conjugated metabolites. *Drug Metab Dispos* **27:**365-372.

Tapaninen T, Karonen T, Backman JT, Neuvonen PJ, and Niemi M (2013) SLCO2B1 c.935G>A single nucleotide polymorphism has no effect on the pharmacokinetics of montelukast and aliskiren. *Pharmacogenet Genomics* **23:**19-24.

Teng S, Jekerle V, and Piquette-Miller M (2003) Induction of ABCC3 (MRP3) by pregnane X receptor activators. *Drug Metab Dispos* **31:**1296-1299.

Terrier N, Benoit E, Senay C, Lapicque F, Radominska-Pandya A, Magdalou J, and Fournel-Gigleux S (1999) Human and rat liver UDP-glucuronosyltransferases are targets of ketoprofen acylglucuronide. *Mol Pharmacol* **56:**226-234.

Thomas D, Mathew M, Raghavan CV, Mohanta GP, and Reddy YP (2012) Days lost due to disability of diclofenac-induced adverse drug reactions. *Pharm Pract (Granada)* **10:**40-44.

Thomas PM, Cote GJ, Wohllk N, Haddad B, Mathew PM, Rabl W, Aguilar-Bryan L, Gagel RF, and Bryan J (1995) Mutations in the sulfonylurea receptor gene in familial persistent hyperinsulinemic hypoglycemia of infancy. *Science* **268:**426-429.

Thummel KE, O'Shea D, Paine MF, Shen DD, Kunze KL, Perkins JD, and Wilkinson GR (1996) Oral first-pass elimination of midazolam involves both gastrointestinal and hepatic CYP3A-mediated metabolism. *Clin Pharmacol Ther* **59:**491-502.

Tian X, Swift B, Zamek-Gliszczynski MJ, Belinsky MG, Kruh GD, and Brouwer KL (2008) Impact of basolateral multidrug resistance-associated protein (Mrp) 3 and Mrp4 on the

hepatobiliary disposition of fexofenadine in perfused mouse livers. *Drug Metab Dispos* **36:**911-915.

Tirona RG and Kim RB (2007) Organic Anion-Transporting Polypeptides, in: *Drug Transporters: Molecular Characterization and Role in Drug Disposition* (You G and Morris ME eds), pp 75-104, John Wiley & Sons, New Jersey.

Treinen-Moslen M (2001) Toxic Responses of the Liver, in: *Casarett and Doull's Toxicology: The Basic Science of Poisons*, pp 471-489, McGraw-Hill, New York.

Trelle S, Reichenbach S, Wandel S, Hildebrand P, Tschannen B, Villiger PM, Egger M, and Juni P (2011) Cardiovascular safety of non-steroidal anti-inflammatory drugs: network meta-analysis. *BMJ* **342:**c7086.

Tsujii H, Konig J, Rost D, Stockel B, Leuschner U, and Keppler D (1999) Exon-intron organization of the human multidrug-resistance protein 2 (MRP2) gene mutated in Dubin-Johnson syndrome. *Gastroenterology* **117:**653-660.

UniProt (2015) UniProt: a hub for protein information. *Nucleic Acids Res* **43:**D204-212.

UW (1999-2015) Metabolism and Transport Drug Interaction Database (accessed October 22, 2015), University of Washington.

van de Straat R, de Vries J, Debets AJ, and Vermeulen NP (1987) The mechanism of prevention of paracetamol-induced hepatotoxicity by 3,5-dialkyl substitution. The roles of glutathione depletion and oxidative stress. *Biochem Pharmacol* **36:**2065-2070.

van Der Kolk DM, Vellenga E, van Der Veen AY, Noordhoek L, Timmer-Bosscha H, Ossenkoppele GJ, Raymakers RA, Muller M, van Den Berg E, and de Vries EG (2000) Deletion of the multidrug resistance protein MRP1 gene in acute myeloid leukemia: the impact on MRP activity. *Blood* **95:**3514-3519.

Vane JR (1971) Inhibition of prostaglandin synthesis as a mechanism of action for aspirin-like drugs. *Nat New Biol* **231:**232-235.

Varma MV, Obach RS, Rotter C, Miller HR, Chang G, Steyn SJ, El-Kattan A, and Troutman MD (2010) Physicochemical space for optimum oral bioavailability: contribution of human intestinal absorption and first-pass elimination. *J Med Chem* **53:**1098-1108.

Varma MV, Rotter CJ, Chupka J, Whalen KM, Duignan DB, Feng B, Litchfield J, Goosen TC, and El-Kattan AF (2011) pH-sensitive interaction of HMG-CoA reductase inhibitors (statins) with organic anion transporting polypeptide 2B1. *Mol Pharm* **8:**1303-1313.

Varma MV, Steyn SJ, Allerton C, and El-Kattan AF (2015) Predicting Clearance Mechanism in Drug Discovery: Extended Clearance Classification System (ECCS). *Pharm Res*.

Verdickt W, Moran C, Hantzschel H, Fraga AM, Stead H, and Geis GS (1992) A double-blind comparison of the gastroduodenal safety and efficacy of diclofenac and a fixed dose combination of diclofenac and misoprostol in the treatment of rheumatoid arthritis. *Scand J Rheumatol* **21:**85-91.

Vlaming ML, Pala Z, van Esch A, Wagenaar E, de Waart DR, van de Wetering K, van der Kruijssen CM, Oude Elferink RP, van Tellingen O, and Schinkel AH (2009a) Functionally overlapping roles of Abcg2 (Bcrp1) and Abcc2 (Mrp2) in the elimination of methotrexate and its main toxic metabolite 7-hydroxymethotrexate in vivo. *Clin Cancer Res* **15:**3084-3093.

Vlaming ML, van Esch A, Pala Z, Wagenaar E, van de Wetering K, van Tellingen O, and Schinkel AH (2009b) Abcc2 (Mrp2), Abcc3 (Mrp3), and Abcg2 (Bcrp1) are the main determinants for rapid elimination of methotrexate and its toxic metabolite 7-hydroxymethotrexate in vivo. *Mol Cancer Ther* **8:**3350-3359.

Vojdani A, Kharrazian D, and Mukherjee PS (2015) Elevated levels of antibodies against xenobiotics in a subgroup of healthy subjects. *J Appl Toxicol* **35:**383-397.

Wallace JL (2008) Prostaglandins, NSAIDs, and gastric mucosal protection: why doesn't the stomach digest itself? *Physiol Rev* **88:**1547-1565.

Wang L, Prasad B, Salphati L, Chu X, Gupta A, Hop CE, Evers R, and Unadkat JD (2015) Interspecies variability in expression of hepatobiliary transporters across human, dog, monkey, and rat as determined by quantitative proteomics. *Drug Metab Dispos* **43:**367-374.

Wang N, Yvan-Charvet L, Lutjohann D, Mulder M, Vanmierlo T, Kim TW, and Tall AR (2008) ATP-binding cassette transporters G1 and G4 mediate cholesterol and desmosterol efflux to HDL and regulate sterol accumulation in the brain. *FASEB J* **22:**1073-1082.

Ware JA, Graf ML, Martin BM, Lustberg LR, and Pohl LR (1998) Immunochemical detection and identification of protein adducts of diclofenac in the small intestine of rats: possible role in allergic reactions. *Chem Res Toxicol* **11:**164-171.

Westlake CJ, Cole SP, and Deeley RG (2005) Role of the NH2-terminal membrane spanning domain of multidrug resistance protein 1/ABCC1 in protein processing and trafficking. *Mol Biol Cell* **16:**2483-2492.

Williams AM, Worrall S, de Jersey J, and Dickinson RG (1992) Studies on the reactivity of acyl glucuronides--III. Glucuronide-derived adducts of valproic acid and plasma protein and anti-adduct antibodies in humans. *Biochem Pharmacol* **43:**745-755.

Williams JA, Hyland R, Jones BC, Smith DA, Hurst S, Goosen TC, Peterkin V, Koup JR, and Ball SE (2004) Drug-drug interactions for UDP-glucuronosyltransferase substrates: a pharmacokinetic explanation for typically observed low exposure (AUCi/AUC) ratios. *Drug Metab Dispos* **32:**1201-1208.

Williams JA, Ring BJ, Cantrell VE, Jones DR, Eckstein J, Ruterbories K, Hamman MA, Hall SD, and Wrighton SA (2002) Comparative metabolic capabilities of CYP3A4, CYP3A5, and CYP3A7. *Drug Metab Dispos* **30:**883-891.

Willis JV, Kendall MJ, Flinn RM, Thornhill DP, and Welling PG (1979) The pharmacokinetics of diclofenac sodium following intravenous and oral administration. *Eur J Clin Pharmacol* **16:**405-410.

Willis JV, Kendall MJ, and Jack DB (1981) The influence of food on the absorption of diclofenac after single and multiple oral doses. *Eur J Clin Pharmacol* **19:**33-37.

Wu W-N and McKown L (2004) In Vitro Drug Metabolite Profiling Using Hepatic S9 and Human Liver Microsomes, in: *Optimization in Drug Discovery* (Yan Z and Caldwell G eds), pp 163-184, Humana Press.

Xu S, Weerachayaphorn J, Cai SY, Soroka CJ, and Boyer JL (2010) Aryl hydrocarbon receptor and NF-E2-related factor 2 are key regulators of human MRP4 expression. *Am J Physiol Gastrointest Liver Physiol* **299:**G126-135.

Yang J, Tucker G, and Rostamihodjegan A (2004) Cytochrome P450 3A expression and activity in the human small intestine. *Clinical Pharmacology & Therapeutics* **76:**391-391.

Yano A, Higuchi S, Tsuneyama K, Fukami T, Nakajima M, and Yokoi T (2012) Involvement of immune-related factors in diclofenac-induced acute liver injury in mice. *Toxicology* **293:**107-114.

Yazdanian M, Briggs K, Jankovsky C, and Hawi A (2004) The "high solubility" definition of the current FDA Guidance on Biopharmaceutical Classification System may be too strict for acidic drugs. *Pharm Res* **21:**293-299.

Yokotani K, Okuma Y, and Osumi Y (1996) Inhibition of vagally mediated gastric acid secretion by activation of central prostanoid EP3 receptors in urethane-anaesthetized rats. *Br J Pharmacol* **117:**653-656.

Yokoyama C and Tanabe T (1989) Cloning of human gene encoding prostaglandin endoperoxide synthase and primary structure of the enzyme. *Biochem Biophys Res Commun* **165:**888-894.

Yoshiura K, Kinoshita A, Ishida T, Ninokata A, Ishikawa T, Kaname T, Bannai M, Tokunaga K, Sonoda S, Komaki R, Ihara M, Saenko VA, Alipov GK, Sekine I, Komatsu K, Takahashi H, Nakashima M, Sosonkina N, Mapendano CK, Ghadami M, Nomura M, Liang DS, Miwa N, Kim DK, Garidkhuu A, Natsume N, Ohta T, Tomita H, Kaneko A, Kikuchi M, Russomando G, Hirayama K, Ishibashi M, Takahashi A, Saitou N, Murray JC, Saito S, Nakamura Y, and Niikawa N (2006) A SNP in the ABCC11 gene is the determinant of human earwax type. *Nat Genet* **38:**324-330.

Yu LJ, Chen Y, Deninno MP, O'Connell TN, and Hop CE (2005) Identification of a novel glutathione adduct of diclofenac, 4'-hydroxy-2'-glutathion-deschloro-diclofenac, upon incubation with human liver microsomes. *Drug Metab Dispos* **33:**484-488.

Zamek-Gliszczynski MJ, Hoffmaster KA, Humphreys JE, Tian X, Nezasa K, and Brouwer KL (2006a) Differential involvement of Mrp2 (Abcc2) and Bcrp (Abcg2) in biliary excretion of 4-methylumbelliferyl glucuronide and sulfate in the rat. *J Pharmacol Exp Ther* **319:**459-467.

Zamek-Gliszczynski MJ, Hoffmaster KA, Tweedie DJ, Giacomini KM, and Hillgren KM (2012) Highlights from the International Transporter Consortium second workshop. *Clin Pharmacol Ther* **92:**553-556.

Zamek-Gliszczynski MJ, Kalvass JC, Pollack GM, and Brouwer KL (2009) Relationship between drug/metabolite exposure and impairment of excretory transport function. *Drug Metab Dispos* **37:**386-390.

Zamek-Gliszczynski MJ, Nezasa K, Tian X, Bridges AS, Lee K, Belinsky MG, Kruh GD, and Brouwer KL (2006b) Evaluation of the role of multidrug resistance-associated protein (Mrp) 3 and Mrp4 in hepatic basolateral excretion of sulfate and glucuronide metabolites of acetaminophen, 4-methylumbelliferone, and harmol in Abcc3-/- and Abcc4-/- mice. *J Pharmacol Exp Ther* **319:**1485-1491.

Zamek-Gliszczynski MJ, Nezasa K, Tian X, Kalvass JC, Patel NJ, Raub TJ, and Brouwer KL (2006c) The important role of Bcrp (Abcg2) in the biliary excretion of sulfate and glucuronide metabolites of acetaminophen, 4-methylumbelliferone, and harmol in mice. *Mol Pharmacol* **70:**2127-2133.

Zarghi A and Arfaei S (2011) Selective COX-2 Inhibitors: A Review of Their Structure-Activity Relationships. *Iran J Pharm Res* **10:**655-683.

Zelcer N, Huisman MT, Reid G, Wielinga P, Breedveld P, Kuil A, Knipscheer P, Schellens JH, Schinkel AH, and Borst P (2003a) Evidence for two interacting ligand binding sites in human multidrug resistance protein 2 (ATP binding cassette C2). *J Biol Chem* **278:**23538-23544.

Zelcer N, Reid G, Wielinga P, Kuil A, van der Heijden I, Schuetz JD, and Borst P (2003b) Steroid and bile acid conjugates are substrates of human multidrug-resistance protein (MRP) 4 (ATP-binding cassette C4). *Biochem J* **371:**361-367.

Zelcer N, Saeki T, Bot I, Kuil A, and Borst P (2003c) Transport of bile acids in multidrug-resistance-protein 3-overexpressing cells co-transfected with the ileal Na+-dependent bile-acid transporter. *Biochem J* **369:**23-30.

Zelcer N, Saeki T, Reid G, Beijnen JH, and Borst P (2001) Characterization of drug transport by the human multidrug resistance protein 3 (ABCC3). *J Biol Chem* **276:**46400-46407.

Zelcer N, van de Wetering K, de Waart R, Scheffer GL, Marschall HU, Wielinga PR, Kuil A, Kunne C, Smith A, van der Valk M, Wijnholds J, Elferink RO, and Borst P (2006) Mice lacking Mrp3 (Abcc3) have normal bile salt transport, but altered hepatic transport of endogenous glucuronides. *J Hepatol* **44:**768-775.

Zelcer N, van de Wetering K, Hillebrand M, Sarton E, Kuil A, Wielinga PR, Tephly T, Dahan A, Beijnen JH, and Borst P (2005) Mice lacking multidrug resistance protein 3 show altered morphine pharmacokinetics and morphine-6-glucuronide antinociception. *Proc Natl Acad Sci U S A* **102:**7274-7279.

Zhang X, Scialis RJ, Feng B, and Leach K (2013) Detection of statin cytotoxicity is increased in cells expressing the OATP1B1 transporter. *Toxicol Sci* **134:**73-82.

Zhou S, Feng X, Kestell P, Paxton JW, Baguley BC, and Chan E (2005) Transport of the investigational anti-cancer drug 5,6-dimethylxanthenone-4-acetic acid and its acyl glucuronide by human intestinal Caco-2 cells. *Eur J Pharm Sci* **24:**513-524.

Zhou SF, Yang LP, Zhou ZW, Liu YH, and Chan E (2009) Insights into the substrate specificity, inhibitors, regulation, and polymorphisms and the clinical impact of human cytochrome P450 1A2. *AAPS J* **11:**481-494.

Zhou W, Hashimoto K, Goleniewska K, O'Neal JF, Ji S, Blackwell TS, Fitzgerald GA, Egan KM, Geraci MW, and Peebles RS, Jr. (2007) Prostaglandin I2 analogs inhibit proinflammatory cytokine production and T cell stimulatory function of dendritic cells. *J Immunol* **178:**702-710.

Zipser RD, Nast CC, Lee M, Kao HW, and Duke R (1987) In vivo production of leukotriene B4 and leukotriene C4 in rabbit colitis. Relationship to inflammation. *Gastroenterology* **92:**33-39.

Zollner G, Marschall HU, Wagner M, and Trauner M (2006) Role of nuclear receptors in the adaptive response to bile acids and cholestasis: pathogenetic and therapeutic considerations. *Mol Pharm* **3:**231-251.